

**Epigenetic control of transcription in the African  
Trypanosome *Trypanosoma brucei*.**

by

Louise Elizabeth Kerry

Thesis submitted in partial fulfillment of the requirements for the degree of  
Doctor of Philosophy (Ph. D.) in Molecular and Cellular Biosciences.

Department of Life Sciences, Division of Cell and Molecular Biology,

Imperial College London

**Declaration of originality**

I declare that all of the work presented in this thesis is my own, and that all else, information, data, results, figures and ideas from another source or from collaborations have been appropriately referenced or acknowledged.

Louise Elizabeth Kerry

November 2017

**Copyright declaration**

The copyright of this thesis rests with the author and is made available under a Creative Commons Attribution Non-Commercial No Derivatives license. Researches are free to copy, distribute or transmit the thesis on the condition that they attribute it, that they do not use it for commercial purposes and that they do not alter, transform or build upon it. For any reuse or redistribution, researchers must make clear to others the license terms of this work.

## Abstract

*Trypanosoma brucei* relies on an essential Variant Surface Glycoprotein (VSG) coat for survival in the mammalian bloodstream. A single VSG gene is transcribed by RNA polymerase I (Pol I) in a strictly monoallelic fashion from one of multiple telomeric VSG expression sites (ES). The epigenetic mechanisms that maintain monoallelic expression of a single VSG remain unclear. The goal of this research was to advance our understanding of the epigenetic factors that contribute to regulation of Pol I transcription in *T. brucei* and to evaluate epigenetic drug targets as novel anti-parasitic agents.

The distribution of the histone H3K4me3 modification at Pol I transcribed loci was determined by ChIP-qPCR. The H3K4me3 modification was not enriched within the VSG ESs or the Pol I rDNA transcription unit, suggesting that this modification does not correlate with active Pol I promoters, as is the case in higher eukaryotes. ChIP-qPCR was also used to ascertain the epigenetic state of the pre-active ESs present in *T. brucei* DDR cells that express two VSGs from two active ESs. Characterisation of the DDR parasites showed that both ESs appear to be in a pre-active state, and that the singularity of expression site body contributes to monoallelic expression of the VSG genes.

As VSG ESs are appealing targets for anti-trypanosomal chemotherapies, I evaluated the potential of histone methyltransferase inhibitors (HKMTI) and Pol I inhibitors as novel trypanocidal agents. The HKMTI and Pol I inhibitors cause parasite cell death in a time- and dose-dependant manner with favourable selectivity compared with mammalian cells. The Pol I inhibitors are toxic to trypanosomes as a result of specifically blocking *T. brucei* Pol I transcription. Whereas, cell death in the HKMTI treated parasites appears to be due to off-target effects. Ultimately, this research could contribute to the development of novel treatments for Human African Trypanosomiasis.

---

## Contents

### Table of Contents

<b>Declaration of originality</b> .....	<b>1</b>
<b>Copyright declaration</b> .....	<b>1</b>
<b>Abstract</b> .....	<b>2</b>
<b>Table of Contents</b> .....	<b>3</b>
<b>List of Tables</b> .....	<b>5</b>
<b>List of Figures</b> .....	<b>5</b>
<b>Acknowledgements</b> .....	<b>8</b>
<b>Abbreviations</b> .....	<b>9</b>
<b>Chapter One</b> .....	<b>11</b>
<b>Introduction</b> .....	<b>11</b>
1.1 - Introduction to Human African Trypanosomiasis.....	11
1.2 - Current treatments for Human African Trypanosomiasis .....	13
1.3 – Biology of the African Trypanosomes <i>Trypanosoma brucei</i> .....	16
1.4 - <i>Trypanosoma brucei</i> life cycle .....	17
1.5 - Antigenic Variation in <i>Trypanosome brucei</i> .....	18
1.6 - Genome organisation and polycistronic transcription in <i>Trypanosoma brucei</i> .....	22
1.7- Introduction to chromatin and epigenetics.....	24
1.8- Chromatin structure and epigenetic marks of RNA Polymerase II transcription units in <i>T. brucei</i> .....	25
1.9 - Monoallelic expression of <i>VSG</i> and the role of RNA Polymerase I .....	28
1.10 - Epigenetics and transcriptional control of the <i>VSG</i> ES in bloodstream form <i>T. brucei</i> .....	31
1.11 - The role of the Expression Site Body in monoallelic expression.....	33
1.12 - Repurposing of drugs and target classes for treatment of neglected tropical diseases....	35
1.13 - Thesis aims .....	37
<b>Chapter Two</b> .....	<b>38</b>
<b>Material and Methods</b> .....	<b>38</b>
2.1 - Trypanosome culturing and strains .....	38
2.2 - Cloning and constructs .....	45
2.3 - Transfection of BSF <i>T. brucei</i> .....	47
2.4 - Chemical inhibitors .....	47
2.5 - Reverse Transcription Quantitative Polymerase Chain Reaction (RT-qPCR) .....	47
2.6 - Chromatin Immunoprecipitation (ChIP) and quantitative PCR (qPCR).....	48
2.7 - Trypanosome proliferation assay .....	49
2.8 - Wash out assay .....	49
2.9 - ESB reassembly assay .....	49
2.10 - <i>In vitro</i> cytotoxicity assay .....	50
2.11 - Flow cytometry of endogenous fluorescence and antibody stained <i>T. brucei</i> .....	50
2.12 - Dilution assay.....	52
2.13 - Immunofluorescence microscopy .....	52



2.14 - Immunoblot analysis .....	53
2.15 - Peptide Competition assay .....	54
<b>Chapter Three.....</b>	<b>55</b>
<b>Distribution of the H3K4me3 epigenetic mark in bloodstream form <i>Trypanosoma brucei</i> polymerase I transcribed loci. ....</b>	<b>55</b>
3.1 - Introduction.....	55
3.2 - Aims and experimental outline.....	58
3.3 - Validation of the VSG surface coat expressed in HNI 221+ and HNI VO2+ BSF <i>T. brucei</i> cell lines.....	59
3.4 - Evaluation of specificity of two commercially available anti-H3K4me3 antibodies .....	61
3.5 - Viability of ChIP-qPCR to discern the distribution of trimethylated H3K4 in <i>T. brucei</i> . .....	63
3.6 - Distribution of H3K4me3 within rDNA transcription units in <i>T. brucei</i> .....	65
3.7 - Trimethylation of H3K4 in the VSG expression sites.....	67
3.8 - Discussion .....	70
<b>Chapter Four.....</b>	<b>74</b>
<b>Small-molecule histone methyltransferase inhibitors as potential anti-kinetoplastid agents .....</b>	<b>74</b>
4.1 - Introduction .....	74
4.2 –Aims and experimental outline.....	77
4.3 - Efficacy of BIX-01294 derived histone lysine methyltransferase inhibitors (HKMTI) against kinetoplastid parasites <i>in vitro</i> . .....	80
4.4 - Analysis of H3K4 trimethylation in inhibitor treated BSF <i>T. brucei</i> .....	85
4.5 - Discussion .....	86
<b>Chapter Five .....</b>	<b>89</b>
<b>Evaluation of RNA polymerase I inhibitors as potential anti-trypanosomal agents and as tools to investigate ESB assembly in BSF <i>T. brucei</i>. ....</b>	<b>89</b>
5.1 - Introduction.....	89
5.2 - Aims and experimental outline.....	92
5.3 - Efficacy of Pol I inhibitors against BSF <i>T. brucei in vitro</i> .....	93
5.4 – Specificity of Pol I inhibitors in BSF <i>T. brucei</i> .....	98
5.5 - Effect of CX-5461 on parasitaemia in <i>T. brucei</i> infected mice. ....	101
5.6 - Effect of Pol I inhibitors on the ESB and nucleolus.....	104
5.7 - Discussion .....	119
<b>Chapter Six .....</b>	<b>123</b>
<b>The role of epigenetics and the ESB in the transcriptional control and monoallelic exclusion of ESs. ....</b>	<b>123</b>
6.1 - Introduction.....	123
6.2 - Aims and experimental outline.....	126
6.3 - Characterisation of Double Drug Resistant (DDR) BSF <i>T. brucei</i> that express two VSGs from two VSG ESs. ....	127
6.4 - Heterogeneous DDR population or rapid switching phenotype?.....	134
6.5 - Stability of the KW01 and BH03 cell lines.....	137
6.6 - Epigenetic state of the pre-active VSG ESs in the KW01 and BH03 <i>T. brucei</i> cell lines.....	141

6.7 - Optimisation and troubleshooting of chromatin immunoprecipitation using antisera against base J in BSF <i>T. brucei</i> .....	147
6.8 - Number of ESBs present in the DDR <i>T. brucei</i> cell line KW01.....	149
6.9 - Discussion .....	151
<b>Chapter Seven .....</b>	<b>155</b>
<b>Final discussion and conclusions.....</b>	<b>155</b>
7.1 - Scope and goals of this thesis.....	155
7.2 - Distribution of H3K4me3 in Pol I transcribed loci in BSF <i>T. brucei</i> .....	156
7.3 - Repurposing of chemical inhibitors, originally developed against cancer, as potential anti-kinetoplastid agents. ....	157
7.4 - The ESB and nucleolus are transcription nucleated in BSF <i>T. brucei</i> . ....	160
7.5 - Epigenetic status and the ESB play a role in the monoallelic exclusion of <i>VSG</i> ESs.....	161
<b>Chapter Eight.....</b>	<b>164</b>
<b>References .....</b>	<b>164</b>
<b>Chapter Nine .....</b>	<b>177</b>
<b>Appendices .....</b>	<b>177</b>
9.1 - Supplementary material .....	177
9.2 - Publication.....	182
9.3 - Conference presentations .....	182
9.4 - Awards.....	182

## List of Tables

Table 2.1. Transgenic bloodstream form <i>T. brucei</i> generated or used during this study. ....	41
Table 2.2. Quantitative PCR primers.....	43
Table 2.3. Primary and Secondary antibodies. ....	44
Table S.1. Library of small molecules derived from BIX-01294 screened for anti-trypanosomal activity. ....	181

## List of Figures

Figure 1.1. Distribution of Human African Trypanosomiasis cases reported between 2010-2014. ....	12
Figure 1.2. Morphology of the African Trypanosome, <i>Trypanosoma brucei</i> . ....	16
Figure 1.3. Life cycle of <i>Trypanosoma brucei</i> .....	18
Figure 1.4. Antigenic variation in <i>Trypanosoma brucei</i> . ....	19
Figure 1.5. A single active <i>VSG</i> ES is transcribed by RNA Pol I in bloodstream form <i>T. brucei</i> . ...	20
Figure 1.6. Mechanisms of antigenic switching in <i>T. brucei</i> . ....	22
Figure 1.7. Organisation of <i>T. brucei</i> genome.....	23
Figure 1.8. Chromatin structure in eukaryotic cells.....	25
Figure 1.9. Distribution of post-translational modifications within <i>T. brucei</i> Pol II transcribed polycistronic transcription units. ....	28
Figure 1.10. Organisation of Pol I transcribed rDNA and <i>VSG</i> ESs in <i>T. brucei</i> .....	30

---

Figure 1.11. Distribution of epigenetic factors at the active and silent VSG ESs in <i>T. brucei</i> .....	32
Figure 2.1. pEnt5B-3xHA:RPA2 construct.....	46
Figure 2.2. Flow cytometry percentile gated populations.....	51
Figure 3.1. Trypanosomatids and eukaryotic histone H3 N-terminus is conserved. ....	57
Figure 3.2. VSG surface coat expression in the HNI 221+ and HNI VO2+ BSF <i>T. brucei</i> cell lines. 60	
Figure 3.3. Anti-H3K4me3 antibodies recognise trimethylation of <i>T. brucei</i> histone 3 lysine 4.. 62	
Figure 3.4. H3K4me3 is enriched within the strand switch regions (SSRs) of <i>T. brucei</i> transcriptional start sites.....	64
Figure 3.5. <i>T. brucei</i> Pol I transcribed rDNA transcription units are depleted of the H3K4me3 chromatin modification. ....	66
Figure 3.6. The histone modification H3K4me3 is only detectable at very low levels at <i>T. brucei</i> ESs.....	69
Figure 4.1. Screening algorithm used for identification of BIX-01294 derived HKMTI with potential anti-trypanosomal activity. ....	79
Figure 4.2. Time- and dose-dependant trypanocidal activity of HKMTI compounds on BSF <i>T. brucei in vitro</i> . ....	81
Figure 4.3. Toxicity of HKMTI compounds in <i>T. brucei</i> compared with mammalian L-6 rat myoblasts.....	82
Figure 4.4. H3K4me3 levels in HKMTI treated <i>T. brucei</i> . ....	86
Figure 5.1. RNA Polymerase I transcription inhibitors kill BSF <i>T. brucei</i> in a time- and dose-dependant manner.....	94
Figure 5.2. Pol I inhibitors are potent and selective inhibitors of BSF <i>T. brucei</i> compared with human cells.....	95
Figure 5.3. Washout assay to determine the reversibility of Pol I inhibitors in <i>T. brucei</i> . ....	97
Figure 5.4. Pol I inhibitors cause rapid and specific inhibition of BSF <i>T. brucei</i> Pol I transcription. ....	100
Figure 5.5. Efficacy of CX-5461 in a stage I mouse model of Human African Trypanosomiasis and corresponding pharmacokinetic data.....	103
Figure 5.6. Pol I inhibition causes disassembly of the nucleolus and loss of the ESB.....	105
Figure 5.7. Pol I inhibition in <i>T. brucei</i> results in rapid disassembly of the nucleolus.....	108
Figure 5.8. Time- and dose-dependant decrease in the number of <i>T. brucei</i> with an ESB after Pol I inhibition.....	109
Figure 5.9. Incubation of BSF <i>T. brucei</i> with Pol I inhibitors results in a striking loss of VEX1 foci. ....	110
Figure 5.10. The Pol I subunit RPA2 is not significantly degraded after Pol I inhibition caused by exposure to BMH-21 in BSF <i>T. brucei</i> . ....	112
Figure 5.11. Transcription reinitiation within the rDNA and nucleolar reassembly after removal of Pol I inhibitors in <i>T. brucei</i> . ....	117
Figure 5.12. Nucleolar reassembly after removal of BMH-21 from <i>T. brucei</i> media. ....	117
Figure 5.13. Reinitiation of Pol I ES transcription and reappearance of an ESB in <i>T. brucei</i> after removal of the BMH-21 Pol I inhibitor.....	118
Figure 6.1. Pre-active state model.....	126
Figure 6.2. Schematic representation of the Double Drug Resistant (DDR) <i>T. brucei</i> cell lines. 128	
Figure 6.3. Growth curves of KW01, BH03 and the parental cell lines.....	129

---

Figure 6.4. Immunofluorescence images and flow cytometry capturing the endogenous fluorescence in the parental and DDR <i>T. brucei</i> cell lines.....	130
Figure 6.5. <i>T. brucei</i> cell lines KW01 and BH03 simultaneously express VSG 221 and VSG VO2 surface coats.....	132
Figure 6.6. Flow cytometry analysis of endogenous fluorescence in the DDR cell lines. ....	133
Figure 6.7. Flow cytometry analysis of DDR clones obtained using a limiting dilution assay....	135
Figure 6.8. Flow cytometry analysis of 221PG_VHC and VHC_221PG limiting dilution assay clones.....	136
Figure 6.9. Stability of the DDR subpopulation upon removal of drug selection. ....	139
Figure 6.10. Monitoring ESs in DDR cells maintained either on or off of drug selection.....	140
Figure 6.11. Distribution of histone H3 in the Pol I transcribed VSG ESs, rDNA transcription units and Pol II transcribed gene loci in DDR parasites. ....	144
Figure 6.12. Distribution of histone H1 in the Pol I transcribed VSG ESs, rDNA transcription unit and Pol II transcribed gene loci in DDR parasites. ....	145
Figure 6.13. Distribution of TDP1 in the Pol I transcribed VSG ESs, rDNA transcription unit and Pol II transcribed gene loci in DDR parasites. ....	146
Figure 6.14. Optimisation of CHIP using an antibody against the DNA modification base J.....	148
Figure 6.15. Representative immunofluorescence microscopy panels of a KW01 cell containing two ESBs. ....	150
Figure S.1. Native H3K4me3 and Histone H3 CHIP signal normalised to percentage input.....	178
Figure S.2. Exposure to 300 nM and 1 $\mu$ M of Pol I inhibitors results in disintegration of the nucleolus in BSF <i>T. brucei</i> . ....	179

## Acknowledgements

I would like to express my sincere gratitude to my PhD supervisors, Professor Gloria Rudenko and Dr Matthew Fuchter, and the Biotechnology and Biological Science Research Council (BBSRC) for the opportunity and funding to do a PhD at Imperial College London. I am grateful to Professor Gloria Rudenko for the opportunity to undertake my research in the Rudenko laboratory, and for helping me develop my knowledge, independence and confidence as a scientist. I would also like to acknowledge and thank my collaborators, Professor Ross Hannan and Donald Cameron (Australian National University), Kevin Read (Drug Discovery Unit, University of Dundee), Kirsten Gillingwater and Marcel Kaiser (Swiss Tropical and Public Health Institute), and Rose Peter (Global Alliance for Livestock Veterinary Medicine) for sharing their resources, expertise and data.

A big thank you to past and present members of the Rudenko Lab, particularly Jackie Cheung and Sophie Ridewood for helping me through the early part of my PhD, Carys Davis for her support through my final year, and James Budzak and Elaine Pegg for their help with the Pol I inhibitor research. A special thank you to CP Ooi for his support, scientific acumen and calm guidance during the challenges of the past three years. To my awesome trypanosome friend, Amber Lynch, and my amazing friends, Harriet Steel and Kiki, your support and humour has been invaluable.

To my wonderful parents, Katherine and Roger, your passion for science is clearly contagious! I would like to thank you for your support over the past few years and for the five star tea, biscuit and pep talk service provided during my thesis write-up. A huge thank you to my siblings Emma and Sarah. Together we have laughed, cried, encouraged and supported each other through our postgraduate degrees. Finally, I would like to thank my partner Oliver, who has been supportive, loving, understanding and encouraging through the ups and downs of my research. I consider myself truly privileged to be a part of team Kerry/Douglas.

---

## Abbreviations

Base J	$\beta$ -D-glucosyl-hydroxymethyldeoxyuridine
BiP	Binding protein
BSF	Bloodstream form
ChIP	Chromatin immunoprecipitation
COMPASS	Complex Proteins Associated with Set1
DDR	Double drug resistant
DIC	Differential interference contrast
DMSO	Dimethyl sulfoxide
DOT1	Disruptor of Telomeric Silencing
eGFP	Enhanced Green fluorescent protein
ES(s)	Expression site(s)
ESAG	Expression site associated protein
ESB	Expression Site Body
eYFP	Enhanced Yellow fluorescent protein
GALVmed	Global Alliance for Livestock Veterinary Medicines
GLP	G9a-like protein
HAT	Human African Trypanosomiasis
HDACi	Histone deacetylases inhibitors
HDMT	Histone demethyltransferase
HKMT	Histone lysine methyltransferase
HKMTI	Histone lysine methyltransferase inhibitor
Hyg	Hygromycin
IP	Immunoprecipitated
ISG	Invariant surface glycoproteins

ISWI	Imitation-Switch protein
MNase	Micrococcal nuclease
NECT	Nifurtimox-Eflornithine Combination Therapy
Neo	Neomycin
NLP	Nucleoplasmin-like protein
NTD	Neglected tropical disease
PCF	Procyclic form
PFA	Paraformaldehyde
Pol I	RNA polymerase I
Pol II	RNA polymerase II
PTMs	Post-translational modifications
PTU	Polycistronic transcription unit
Puro	Puromycin
RT-qPCR	Quantitative Reverse Transcriptase Polymerase Chain Reaction
SAH	S-adenosylhomocysteine
SAM	S-adenosylmethionine
SET	Su(var)3-9, Enhancer of zeste, Trithorax
SI	Selectivity Index
SL	Spliced leader
SSR	Strand switch region
Swiss TPH	Swiss Tropical and Public Health Institute
TSS	Transcriptional start site
TTS	Transcriptional termination sites
VSG $\Psi$	VSG pseudogene
VSG	Variant Surface Glycoprotein

# Chapter One

## Introduction

### 1.1 - Introduction to Human African Trypanosomiasis

Human African Trypanosomiasis (HAT) and nagana (Animal Trypanosomiasis) are vector-borne diseases prevalent in more than 20 sub-Saharan Africa countries (Büscher et al. 2017). The geographical distribution of HAT is determined by the prevalence of the tsetse fly vector (Malvy & Chappuis 2011) (Figure 1.1). The protozoan parasite *Trypanosoma brucei* and related subspecies are the causative agents of HAT and Nagana. The parasites are transmitted between humans and reservoir hosts by the bite of an infected tsetse fly (genus *Glossina*) during a blood meal. Several thousand new cases of HAT are reported each year (Büscher et al. 2017) and an estimated 70 million people are at risk of infection (Simarro et al. 2012).

There are three subspecies of the African trypanosome: *T. brucei gambiense*, *T. brucei rhodesiense* and *T. brucei brucei*. The subspecies *T. b. rhodesiense* and *T. b. gambiense* are the etiological agents of the acute and chronic form of HAT, respectively. *T. b. rhodesiense* is endemic to eastern Africa and accounts for 3% of HAT cases (WHO 2017c) (Figure 1.1). This acute form of the disease progresses rapidly, and without treatment *T. b. rhodesiense* infection is often fatal within 6 months (Büscher et al. 2017). The remaining 97% of HAT cases are caused by infection with *T. b. gambiense*, which is prevalent in western and central Africa (WHO 2017c) (Figure 1.1). An individual may be infected with *T. b. gambiense* for many years or even decades before presenting evident symptoms (Sudarshi et al. 2014). Unfortunately, this often results in a poor prognosis, as the infected individual has already progressed to the later stage of the disease before diagnosis occurs. *T. b. gambiense* can also persist in the skin of asymptomatic individuals and act as reservoirs for infection (Capewell et al. 2016). The third subspecies of African trypanosome, *T. b. brucei*, causes the disease nagana and infects a broad range of native mammals, as well as, various species of domestic livestock including cattle, dogs, camels and horses (Giordani et al. 2016).



Co-ordinated disease surveillance and vector control efforts, as well as, improved access to diagnostic and medical care has drastically reduced the number of reported HAT cases by 89-90% since 1999. However, this devastating human and animal pathogen still causes considerable human mortality and socio-economic hardship in sub-Saharan Africa (Büscher et al. 2017). Additionally, civil unrest, ecological changes, complex treatment regimes and the emergence of drug resistant parasites are just some of the issues that need to be overcome to achieve the World Health Organisations (WHO) aim of eliminating HAT as a public health problem by 2020 (WHO 2017c).

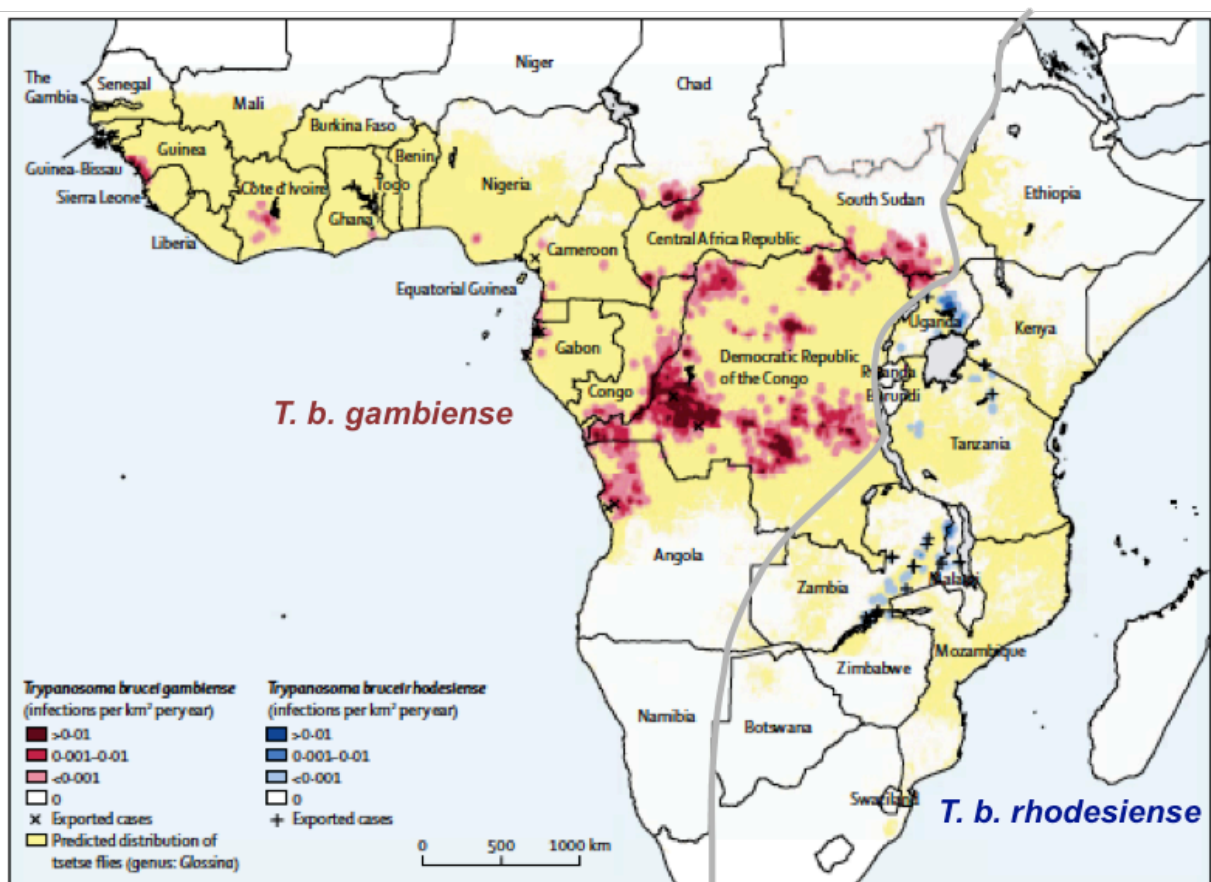


**Figure 1.1. Distribution of Human African Trypanosomiasis cases reported between 2010-2014.**

HAT is caused by African Trypanosome subspecies, *Trypanosoma brucei gambiense* found in west and central Africa and *Trypanosoma brucei rhodesiense* found in eastern Africa. The density of reported *T. b. gambiense* (red) and *T. b. rhodesiense* (blue) infections are shown as infections per square kilometre per year. The geographical distribution of tsetse flies is shown in yellow and the grey line indicates the boundary between *T. b. gambiense* and *T. b. rhodesiense* endemic regions. The map and data was adapted from (Büscher et al. 2017) and (Fèvre et al. 2006).

HAT disease progression occurs in two stages, the haemolympathic stage and the meningoencephalitic stage. The haemolympathic stage (first stage) occurs within one to three weeks of infection, as the parasites multiply in the subcutaneous tissue and peripheral circulatory system of the host. This is followed by the meningoencephalitic stage (second stage) that occurs once the trypanosomes have crossed the blood-brain barrier and invaded the central nervous system (Kennedy 2013; Büscher et al. 2017). Patients in the first stage of the disease present with headaches, muscle and joint pain, lymphadenopathy and intermittent fever as a result of the fluctuating levels of parasitaemia. Once the parasites have crossed the blood-brain barrier fever becomes less frequent, however neuropsychiatric changes including sensory disturbances, tremors, speech disorders and behavioural changes occur. Patients also present with daytime somnolence and night time insomnia, symptoms from which HAT derives its historic name of “sleeping sickness” (Brun et al. 2010; WHO 2017c). If an infected individual is not treated, HAT typically results in coma and death (Büscher et al. 2017), but some cases of asymptomatic carriers and spontaneous resolution of *T. b. gambiense* infection have been reported (Jamonneau et al. 2012; Capewell et al. 2016). Although the period for disease progression differs, the clinical features of the two stages of HAT are similar for both *T. b. gambiense* and *T. b. rhodesiense* infection.

## **1.2 - Current treatments for Human African Trypanosomiasis**

Vaccine development against African trypanosomes has proven problematic due to the lack of viable target proteins. African trypanosomes evade the host immune response through antigenic variation of the major surface coat protein reducing potential vaccine targets. Despite numerous attempts, no anti-trypanosomal vaccines have proven to be effective in a field setting (La Greca & Magez 2011). This has resulted in increased pressure for the development of effective anti-trypanosomal chemotherapies. Currently, the chemotherapy administered to treat HAT depends on the infective agent (*T. b. gambiense* or *T. b. rhodesiense*) and the stage of the disease (first or second stage). Five drugs are commonly used to treat HAT; Pentamidine, Suramin, Melarsoprol, Eflornithine

and Nifurtimox with the latter two often administered as Nifurtimox-Eflornithine Combination Therapy (NECT).

Pentamidine and Suramin are used in the treatment of the first stage of *T. b. gambiense* and *T. b. rhodesiense* infection, respectively. Although both treatments are effective with up to 98% efficacy, the treatment regimes are complex, requiring intramuscular or intravenous drug administration daily for seven days to one month (Büscher et al. 2017). Pentamidine is generally well tolerated with minor and reversible side effects including hypotension, abdominal pain and gastrointestinal problems. Ingestion of sugar (10-20 g) is required prior to Pentamidine administration in order to reduce the likelihood of hypoglycaemia normally observed in 5-40% of patients (Pohlig et al. 2016). Suramin side effects are frequent and include fever, nephrotoxicity (kidney damage) and peripheral neuropathy (nerve damage). Less frequently, Suramin administration can induce acute hypersensitivity reactions (Büscher et al. 2017).

Once *T. b. gambiense* has crossed the blood brain barrier, NECT is used as the first line treatment as it has a higher cure rate (95-98 %), low fatality (<1 %) and reduced adverse reactions compared to Eflornithine monotherapy. However, the treatment regime is still complex, requiring three daily doses of Nifurtimox for seven days and daily intravenous doses of Eflornithine for ten days (Franco et al. 2012; Priotto et al. 2009). Eflornithine monotherapy is administered in the absence of Nifurtimox but this has adverse side effects (vomiting, diarrhoea, fever and seizures) and a fatality rate of ~2 % (Balasegaram et al. 2006). Additionally, Eflornithine is trypanostatic and therefore requires an active immune response to clear infection, which is problematic for the ~13% of HAT patients coinfecting with HIV (Kagira et al. 2011). Second stage HAT caused by *T. b. rhodesiense* or Eflornithine resistant *T. b. gambiense* is treated with Melarsoprol (Babokhov et al. 2013). Melarsoprol is a highly toxic melaminophenyl arsenical that has treatment related mortality rates of approximately 10%, primarily as a result of Melarsoprol induced encephalopathy in 5-18% of HAT patients (Chappuis et al. 2005; Büscher et al. 2017).

Drug resistance is always a concern when a limited repertoire of chemotherapies is available to treat an infectious disease. Mutations in *T. brucei* subspecies that confer resistance to Pentamidine and Melarsoprol have been identified, as have some of the trypanosome transporters and channels believed to be responsible for Melarsoprol-Pentamidine cross-resistance (Baker et al. 2013). A rise in Melarsoprol treatment failure in the late 1990s sparked concern of an increase in prevalence of Melarsoprol resistant trypanosomes in several sub-Saharan countries. The increase in Melarsoprol resistant HAT cases was successfully overcome by switching to NECT as the first line treatment (Barrett et al. 2011). This highlights the importance of having a range of alternative chemotherapies with diverse mechanisms of action available to treat drug resistant trypanosome populations and prevent HAT epidemics.

There are currently only a few new HAT chemotherapies in the drug pipeline including Fexinidazole and SCYX-7158 (Field et al. 2017). Importantly, these chemotherapies treat both the first and second stage of HAT and can be administered orally. This eliminates the need to diagnose the stage of the disease prior to commencing treatment and negates the need for intravenous or intramuscular administration (Büscher et al. 2017). Fexinidazole is currently recruiting for a phase III clinical trial (Clinicaltrial.gov NCT03025789) and SCYX-7158 is recruiting for a phase II/III safety and efficacy trial (Clinicaltrial.gov NCT03087955). Although the development of Fexinidazole and SCYX-7158 as anti-trypanosomal agents looks promising, continuing research and drug screening efforts will be required to ensure the development of affordable, safe, effective treatments for HAT, which can be easily stored and administered under field conditions (Field et al. 2017; Büscher et al. 2017). A deeper understanding of *T. brucei* biology would therefore facilitate the development of better treatments against this lethal parasite.

### 1.3 – Biology of the African Trypanosomes *Trypanosoma brucei*

The *T. brucei* subspecies (*T. b. gambiense*, *T. b. rhodesiense* and *T. b. brucei*) are unicellular, flagellated protozoan parasites, which are morphologically indistinguishable from one another (Gibson 2003). The cell body of *T. brucei* tapers toward the anterior end, a single flagellum emerges from the cell body near the posterior end and is attached lengthwise extending beyond the anterior tip of the cell (Figure 1.2) (Leung et al. 2014). *T. brucei* contains a number of single copy organelles and structures including a nucleus, a nucleolus within the nuclear matrix and a kinetoplast (mitochondrion DNA organised into a network of interlocking rings) within the mitochondrion matrix (Hammarton 2007).

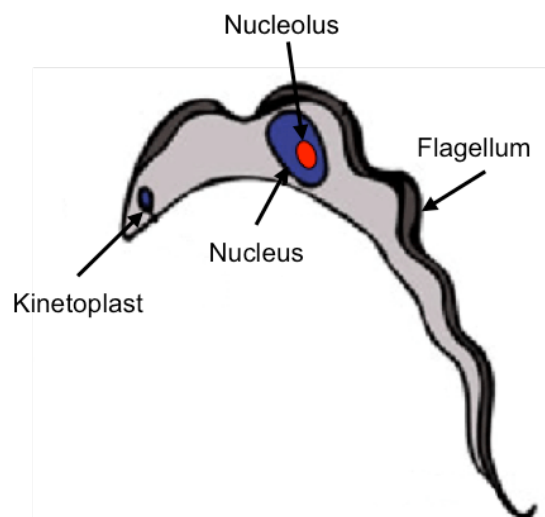


**Figure 1.2. Morphology of the African Trypanosome, *Trypanosoma brucei*.**

Bloodstream form *Trypanosoma brucei* are approximately 20  $\mu\text{m}$  in length and 2-4  $\mu\text{m}$  in width. The parasites have a cylindrical shape cell body tapering towards the anterior end. A single flagellum extends the length of the cell body beyond the anterior tip. *T. brucei* contains several single copy organelles including a nucleus, nucleolus, kinetoplast (Mitochondrial DNA). Adapted from (Giordani et al. 2016).

#### 1.4 - *Trypanosoma brucei* life cycle

As a digenetic parasite, *T. brucei* has a complex life cycle to cope with transmission and colonisation of both the mammalian host and tsetse fly vector (Figure 1.3). Metacyclic trypomastigotes are injected into the mammalian host tissue by an infected tsetse fly during a blood meal (Barrett et al. 2003). These non-replicating metacyclic trypomastigotes transform into bloodstream form trypomastigotes, which proliferate by binary fusion in the blood, lymph and spinal fluid (Matthews et al. 2004). Bloodstream form (BSF) *T. brucei* are extracellular and are therefore vulnerable to the host immune response, and in particular to complement mediated lysis. *T. brucei* can evade the host immune system by masking the invariant trypanosome proteins with a dense surface coat comprised of Variant Surface Glycoprotein (VSG) (Barry & McCulloch 2001). Only one VSG is expressed at a time, and switching between a repertoire of hundreds of VSG genes provides the trypanosome with sufficient antigen variation to prolong host infection (Borst 2002; Pays et al. 2001; Vanhamme et al. 2001; Berriman 2005).

Over the course of a host infection non-replicating trypomastigotes appear that are pre-adapted for transmission to the tsetse fly. Once ingested during the insect blood meal the trypomastigotes differentiate into the procyclic form (PCF) stage in the tsetse fly midgut (Fenn & Matthews 2007). During differentiation, the VSG coat is replaced with a new set of glycoproteins called procyclin, containing GPEET (Gly-Pro-Glu-Glu-Thr) or EP (Glu-Pro) repeats (Acosta-Serrano et al. 2001). PCF trypomastigotes differentiate into epimastigotes and migrate to the tsetse fly salivary glands, where they multiply and ultimately transform back into the metacyclic form ready for transmission to the mammalian host (Matthews 2005).

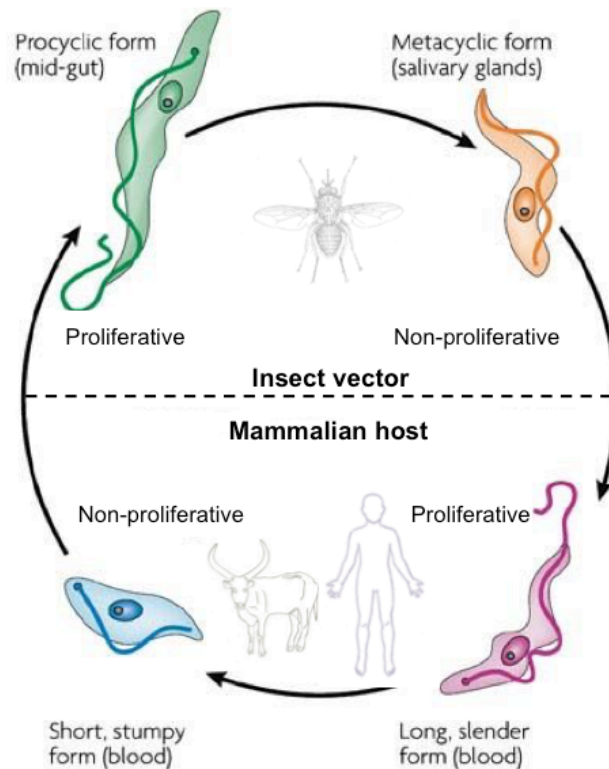


**Figure 1.3. Life cycle of *Trypanosoma brucei*.**

*T. brucei* is a digenetic parasite transmitted from the tsetse fly vector to the mammalian hosts and back during its life cycle. Metacyclic trypomastigotes are transmitted to the mammalian host by the tsetse fly during a blood meal. In the mammalian host the trypanosome morphology assumes a more slender form and the parasites proliferate in the blood, lymph and spinal fluid. These bloodstream form (BSF) trypanosomes are covered in a dense coat of Variant Surface Glycoprotein (VSG). As parasitaemia increases, the BSF *T. brucei* differentiate into the non-proliferative short stumpy form, which are ingested by the tsetse fly. Once in the tsetse fly midgut, *T. brucei* differentiates into the procyclic form and the VSG coat is lost and replaced with procyclin. Eventually, the procyclic form (PCF) migrates to the tsetse fly salivary glands ready for transmission into the mammalian host. Figure adapted from (Hee Lee et al. 2007; Büscher et al. 2017).

### 1.5 - Antigenic Variation in *Trypanosome brucei*

As an extracellular pathogen, *T. brucei* is vulnerable to the host immune response and specifically to complement and antibody mediated lysis. To evade the host immune system BSF trypanosomes have evolved an elegant strategy of antigenic variation (Figure 1.4). BSF *T. brucei* express a dense surface coat of approximately  $10^7$  VSG molecules, which are densely packed into

homodimers covering the trypanosome cell surface (Cross 1975; Cross 1990). These VSG homodimers shield the invariant trypanosome molecules, such as the transferrin receptors (Steverding 2000) and Invariant Surface Glycoproteins (ISGs), from recognition by the host immune system (Ziegelbauer & Overath 1993).

The VSGs are highly immunogenic, and the host rapidly mounts an immune response against the predominant VSG variant leading to antibody mediated cell lysis (Magez et al. 2008) (Figure 1.4). However, within the trypanosome population VSG switch variants arise, which have switched to express an antigenically different VSG. As the VSG surface coat of the switched *T. brucei* population is not recognised by the host antibodies against the predominant variant, the parasitic infection persists (Taylor & Rudenko 2006). It is these undulating levels of parasitaemia, which cause the intermittent fever observed in HAT patients (Ponte-Sucre 2016).

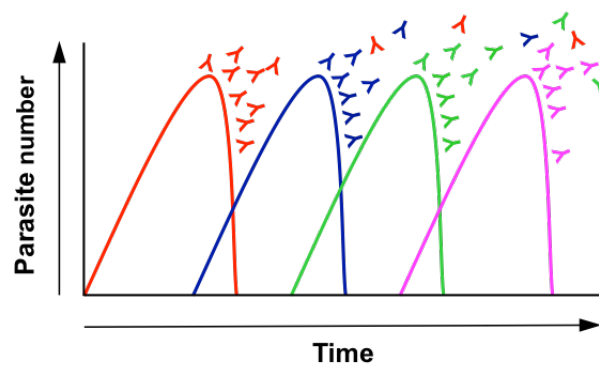


**Figure 1.4. Antigenic variation in *Trypanosoma brucei*.**

Schematic representation of the undulating levels of parasitaemia within the host over the course of infection. *T. brucei* express a given VSG variant (red line) upon initial infection and proliferate in the bloodstream of the host. The host immune system generates antibodies (red Y) against this VSG coat resulting in a reduction in the number of parasites. Switch variants have arisen within the parasite population that express an antigenically different VSG (blue Y). This new population proliferates thereby prolonging infection.

Monoallelic expression of a single VSG and periodic switching to express a different VSG are required for successful antigenic variation. The trypanosome genome encodes a vast repertoire of ~2000 VSG genes and pseudogenes (Berriman 2005). This library of VSG genes is predominately



located in the chromosome subtelomeric arrays but some *VSG* genes are also found at the telomeres of the minichromosomes (Berriman 2005; Williams et al. 1982; Cross et al. 2014). Expression sites (ESs) are polycistronic transcription units located at telomeres that encode a number of ES-associated genes (ESAGs) as well as the telomeric *VSG*. A single *VSG* gene is transcribed by RNA polymerase I (Pol I) in a strictly monoallelic fashion from one of the telomeric *VSG* ESs (Figure 1.5) (Taylor & Rudenko 2006). While transcriptional initiation occurs at the other 14 ESs, the loss of transcriptional elongation ensures these ESs are essentially inactive (Vanhamme et al. 2000).

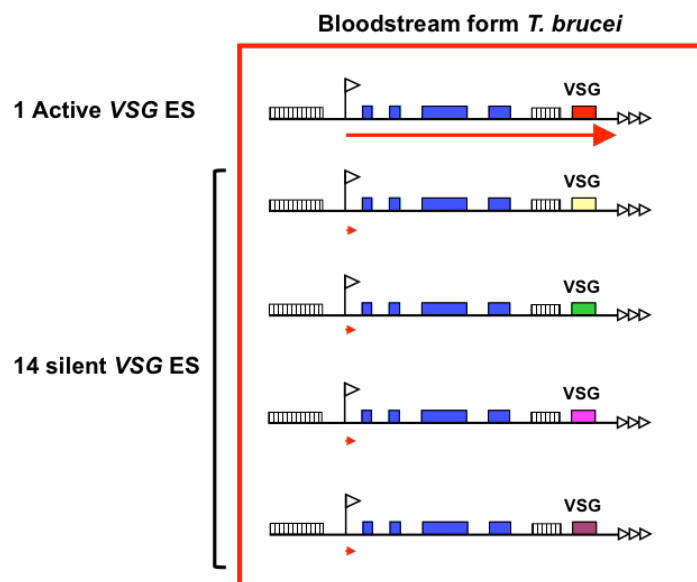


**Figure 1.5. A single active *VSG* ES is transcribed by RNA Pol I in bloodstream form *T. brucei*.**

Each *VSG* ES contains two types of repeats (striped boxes), the 50bp repeats upstream of the ES promoter (flag) and the 70bp repeats upstream of the *VSG* gene, which are represented as coloured boxes. The Expression site associated genes (ESAGs) are shown as lilac boxes and the chromosome telomeres are represented as arrowheads. The long red arrow indicates transcriptional initiation and elongation at the single active *VSG* ES. The shorter red arrows indicate the low level of transcription that occurs at the 14 “silent” *VSG* ESs. The outer box is representative of the *VSG* coat being expressed by a single BSF trypanosome.

VSG switching occurs via three different molecular mechanisms; gene conversion, telomere exchange and *in situ* (transcriptional) switching (Figure 1.6) (Pena et al. 2016). *T. brucei* accesses the vast repertoire of silent VSG genes and pseudogenes by homologous recombination into the single active ES. The 70bp repeats upstream of the VSG gene and conserved region at the 3' end of the VSG gene provide sufficient homology for gene conversion to occur (Bernards et al. 1981; Pays et al. 1983). VSG switching by gene conversion can be duplicative or segmental. Duplicative gene conversion involves a silent VSG gene being replicated and exchanged for the VSG gene currently present within the active ES (Figure 1.6). Alternatively, a chimeric VSG is generated in the active ES by gene conversions between segments of old VSG and segments of the functional or non-functional pseudogenes (Robinson et al. 1999). Homologous recombination can also occur between two telomeres. Unlike gene conversion, telomere exchange does not result in the loss of the VSG gene, which previously occupied the active ES (Figure 1.6). *In situ* (transcriptional) switching does not involve homologous recombination but refers to the silencing of the active ES and activation of one of the other 14 ESs (Figure 1.6) (Taylor & Rudenko 2006; Horn & McCulloch 2010).

Interestingly, VSG switching still occurs *in vitro* and in immune-deficient mice, which suggests switching is a stochastic process that occurs in the absence of immune selection (Doyle et al. 1980; Myler et al. 1985). Another interesting characteristic of trypanosomes is that VSG expression is essential even *in vitro*. Blocking VSG synthesis results in a rapid growth arrest and a precise pre-cytokinesis cell cycle arrest (Shedder et al. 2005), presumably as a protective mechanism to maintain the integrity of the VSG surface coat (Smith et al. 2009). *In vivo* ablation of VSG transcript results in rapid clearance of parasitaemia in mice within 12 hours presumably due to clearance by mice macrophages (Shedder et al. 2005).

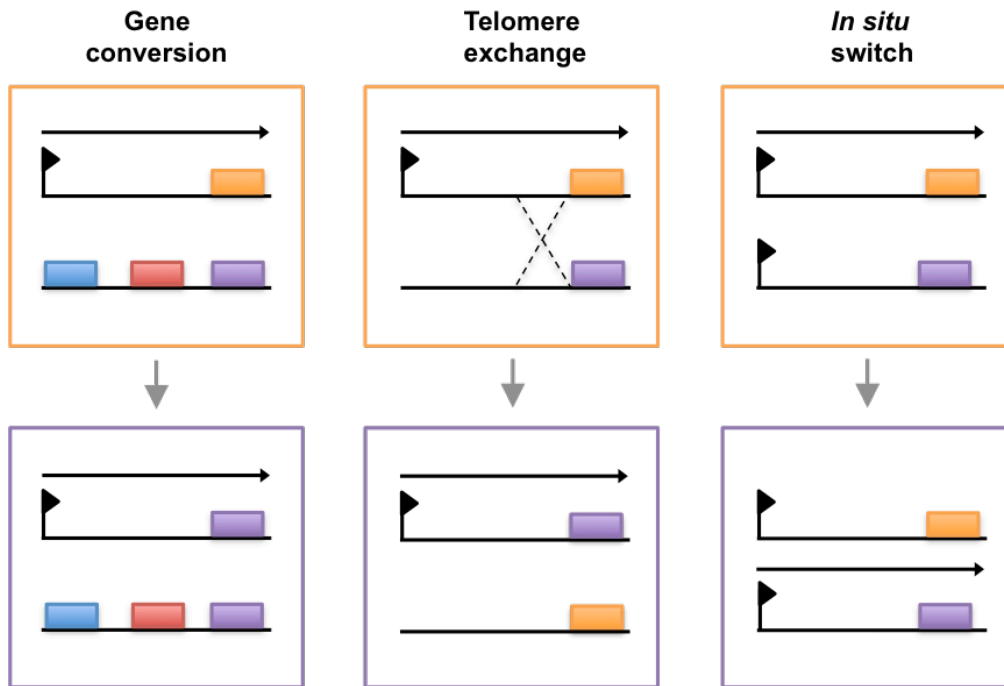


**Figure 1.6. Mechanisms of antigenic switching in *T. brucei*.**

VSG switching occurs via three main mechanisms. Gene conversion, results in a VSG gene from the silent arrays being inserted into the active ES with concurrent loss of the previously active VSG gene. Switching can result from homologous recombination between telomeres termed telomeric exchange. Alternatively, a silent ES can be activated and the active ES silenced resulting in an *in situ* switch. The flags indicate the ES promoters. The coloured boxes represent the different VSG genes with active transcription shown as a black arrow. The orange and purple box outlines represent the VSG being expressed on the trypanosome surface. Adapted from (Taylor & Rudenko 2006).

### 1.6 - Genome organisation and polycistronic transcription in *Trypanosoma brucei*

The genome of *T. brucei* is composed of eleven diploid megabase chromosomes, intermediate chromosomes and approximately 100 minichromosomes of 50-100Kb each that contain the silent VSG genes and pseudogenes (Ersfeld 2011). Kinetoplastids branched early in evolution resulting in some striking divergences in the regulation of gene expression compared with other eukaryotes (Embley & Martin 2006). For example, the megabase chromosomes are organised into long, non-overlapping, polycistronic transcription units (PTUs) (Dunbar et al. 2000). Constitutive transcription of the PTUs by RNA polymerase II (Pol II) occurs from putative transcriptional start sites (TSS) at strand switch regions (SSRs), which can be divergent or convergent

(Figure 1.7). Although superficially reminiscent of bacterial operons, there is no evidence that adjacent genes within the trypanosome PTUs are cotranscribed or involved in the same biochemical pathways (Berriman 2005).

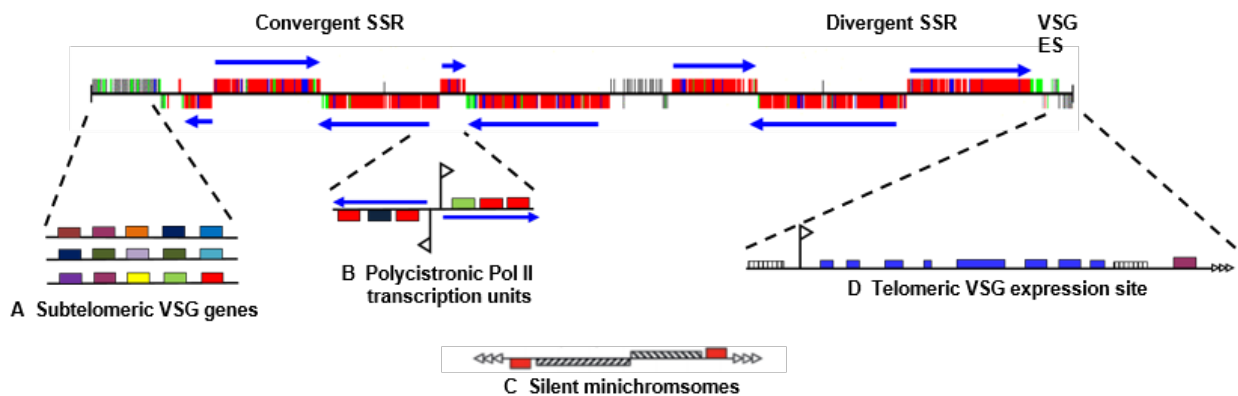


**Figure 1.7. Organisation of *T. brucei* genome.**

A schematic of a megabase chromosome is shown with the open reading frames indicated in red. The convergent and divergent strand switch regions (SSRs) of the polycistronic transcription units are shown with transcription indicated by blue arrows. **(A)** The subtelomeric VSG genes and pseudogenes are arranged in tandem repeats indicated by coloured boxes. **(B)** The majority of the trypanosome protein coding genes are organised into polycistronic transcription units constitutively transcribed by Pol II. Flags indicate the putative promoters and the blue arrows indicate transcription. **(C)** A representation of one of the approximately 100 transcriptionally silent minichromosomes. These are comprised predominantly of large palindromes of 177bp repeat sequences (striped boxes) with VSG genes (red boxes) located upstream of the telomeric repeats (arrowheads). **(D)** A single active VSG gene is transcribed by Pol I from one of approximately 15 telomeric VSG ES transcription units. The expression site associated genes (ESAGs) are shown as blue boxes downstream of the ES promoter (flag). The telomere repeats are indicated with arrowheads downstream of the VSG gene shown as a maroon box. The ES simple sequence repeats located upstream of the ES promoter are shown as striped boxes. Adapted from (Rudenko 2010).

There is no evidence for transcriptional control of trypanosome Pol II, and bioinformatics analyses have shown that trypanosomes lack homologues of classic eukaryote Pol II promoters and transcription factors (Ivens et al. 2005; Iyer et al. 2008). It is evident that the Pol II promoters must be present within the TSS but mapping of Pol II promoters within the SSRs using strand-specific

nuclear run-ons has proven to be problematic (Rudenko 2010). To date the Pol II spliced leader promoter is the only well characterised Pol II promoter in trypanosomes (Schimanski et al. 2005).

Polyguanine stretches have been identified 1-5 kilobase pairs upstream of putative TSSs in *T. brucei* (Siegel et al. 2009). The role of these polyguanine tracts in *T. brucei* has not yet been elucidated but polyguanine motifs are capable of forming G-quadruplexes, which recruit transcription initiation factors in humans (Etzioni et al. 2005). Alternatively, the polyguanine stretches may ensure the unidirectionality of Pol II transcription in *T. brucei*, as stretches of guanines can hinder progression of Pol II when located on the mRNA sense strand (Tornaletti et al. 2008). In *T. brucei* levels of mRNA are predominately regulated post-transcriptionally. Individual mRNAs are stabilised by cleavage of the polycistronic precursor RNAs through trans-splicing of a capped spliced leader transcript to the 5' end as well as polyadenylation of the 3' end (Liang et al. 2003).

### **1.7- Introduction to chromatin and epigenetics**

The eukaryotic genome is packaged into chromatin, whereby nucleosomes are the basic repetitive unit. Nucleosomes are comprised of an octamer of four core histones (H2A, H2B, H3 and H4) around which is wrapped ~146bp of DNA. A linker histone, H1, binds the DNA between adjacent nucleosomes and plays a role in chromatin condensation (Figure 1.8) (Alsford & Horn 2004). In addition to the four canonical histones, trypanosomes have four histone variants (H2AZ, H2BV, H3V and H4V) (Lowell et al. 2005; Lowell & Cross 2004). Trypanosome DNA is generally less compact compared to the chromatin observed in higher eukaryotes and does not visibly compact during metaphase (Hecker & Gander 1985). However, BSF *T. brucei* appear to have more compact chromatin than the PCF parasites, which is believed to contribute to the alteration in gene expression as the parasites progress through the life cycle (Hecker et al. 1994; Schlimme et al. 1993).

Histones are subject to post-translational modifications (PTMs) that occur predominately on the exposed histone N-terminal tails, which protrude from the nucleosomes. These PTMs form a

histone code, which is written and erased by the histone modifying enzymes, and read by histone binding proteins (Jenuwein & Allis 2001). These epigenetic regulators dictate the dynamic transition between transcriptionally active (euchromatic) and repressed (heterochromatic) chromatin states.

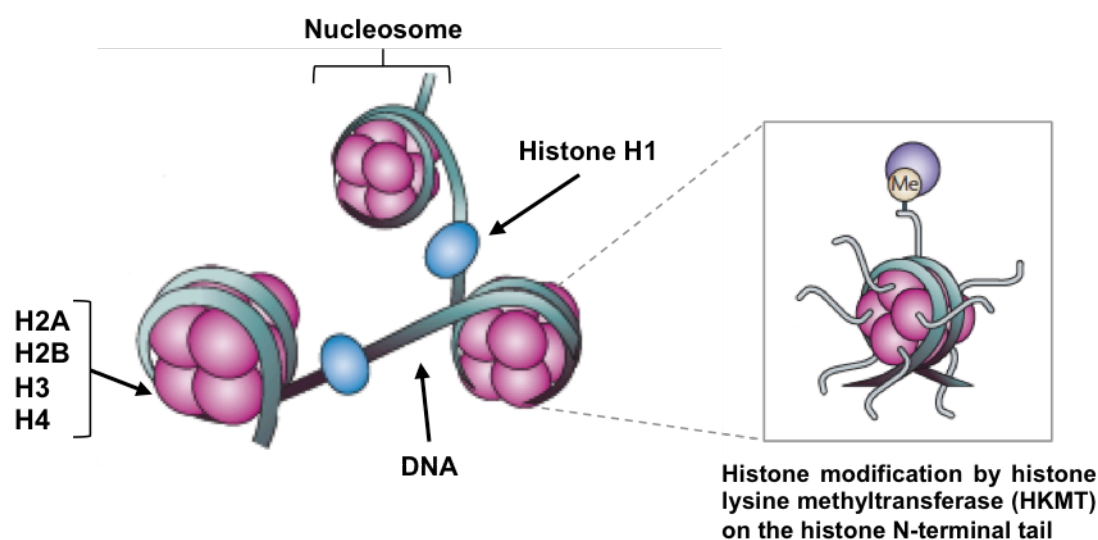


**Figure 1.8. Chromatin structure in eukaryotic cells.**

Eukaryotic genomes are compacted into chromatin. DNA is wrapped around an octamer of four core histones to form nucleosomes. Linker histones (histone H1) bind to DNA between nucleosomes generating a heterochromatic state. The histone N-terminal tails that protrude from the nucleosome are often subject to post-translational modifications, such as methylation or acetylation (insert). Adapted from (Figueiredo et al. 2009).

### 1.8- Chromatin structure and epigenetic marks of RNA Polymerase II transcription units in *T. brucei*

The *T. brucei* genome encodes a number of putative histone modifying proteins as well as characterised genes encoding histone methyltransferases, acetyltransferases and deacetylases (Janzen et al. 2006a; Siegel et al. 2008; Ingram & Horn 2002). Trypanosomes have two classes of histone lysine methyltransferases (HKMT) responsible for adding methyl groups to lysine residues; the DOT1 (Disruptor of Telomeric Silencing) homologues and the SET (Su(var)3-9, Enhancer of zeste, Trithorax) domain containing proteins (Horn 2007). The latter class is named after its evolutionary conserved SET domain, which consists of a ~130 amino acid sequence responsible for histone lysine

methylation. In this process the histone lysine is methylated in an  $S_N2$  reaction with the activated co-factor S-adenosylmethionine (SAM) resulting in S-adenosylhomocysteine (SAH) and N-methylation of the lysine residue (Helin & Dhanak 2013). The role of the *T. brucei* DOT1 homologues, DOT1A and DOT1B, has been described but none of the 20-27 SET domain-containing proteins encoded in the *T. brucei* genome have yet been characterised (Figueiredo et al. 2009).

The sequences of canonical core histones are relatively conserved in eukaryotes, however as an early branching eukaryote trypanosome histones are less conserved than those of higher eukaryotes, particularly with regard to the N-terminal tails (Thatcher & Gorovsky 1994; Alsford & Horn 2004). Edman degradation and mass spectrometry of the *T. brucei* PTMs identified some conserved PTMs (e.g. H4K20ac), as well as a number of trypanosome specific modifications (e.g. H4A1me1) (Mandava et al. 2007; Janzen et al. 2006b). Identification of histone H3 modifications in *T. brucei* proved challenging as Edman degradation is blocked by the acetylated N-terminal serine, however mass spectrometry analyses revealed K4, K32 and K76 were methylated (Janzen et al. 2006b). Sequence alignment of *T. brucei* histone H3 and canonical eukaryotic histone H3 suggests that *T. brucei* H3K4, H3K23 and H3K76 correspond to H3K4, H3K27 and H3K79 in other eukaryotes (Maree & Patterson 2014).

The importance of epigenetics in the regulation of gene expression in trypanosomes was initially disputed (Rudenko 2010). However, more robust studies have helped elucidate the important role chromatin remodelling plays in the regulation of Pol II transcribed gene expression in *T. brucei*. Siegel and colleagues (2009) conducted an extensive genome wide analysis of several *T. brucei* histone variants and histone modifications to identify the epigenetic marks present at transcription initiation and termination sites. Their analysis using chromatin immunoprecipitation and sequencing (ChIP-Seq) showed a 300-fold enrichment of the bromodomain factor BDF3, H4K10ac, H2AZ and H2BV at putative Pol II TSSs with the H3V and H4V histone variants enriched at probable transcriptional termination sites (Figure 1.9) (Siegel et al. 2009).

Nucleosomes containing the histone variants H2AZ and H2BV are less stable than those containing the canonical core histone counterparts (H2A and H2B). This enrichment of unstable histone variants within nucleosomes at the TSS probably aids nucleosome eviction leading to a more open chromatin structure predisposed for transcription initiation. Enrichment of BDF3 is thought to aid recruitment of chromatin remodelling complexes to the trypanosome Pol II TSSs in a similar fashion as BDF1 in yeast (Korber & Hörz 2004). Acetylation of lysine 10 of histone H4 (H4K10ac) is markedly enriched at the putative TSSs in *T. brucei* (Siegel et al. 2009). Additional ChIP-Seq data showed the H4K10ac histone mark co-localise with H3K4me3 (Figure 1.9) (Wright et al. 2010).

In higher eukaryotes the H3K4 trimethylation state is strongly associated with the TSSs of active Pol II transcribed genes (Barski et al. 2007), and actively transcribed rDNA transcription unit promoters (McStay & Grummt 2008), and it is thought that H3K4me3 may be required for histone tail acetylation (Pillus 2008). In *Saccharomyces cerevisiae*, Set1 is the sole HKMT responsible for H3K4 methylation and the catalytic activity of Set1 is modulated through the Complex Proteins Associated with Set1 (COMPASS) (Miller et al. 2001). Trimethylation of H3K4 in higher metazoans is more convoluted as several SET domain-containing complexes with H3K4me3 activity have been identified. The *T. brucei* genome contains 20-27 SET-domain encoding genes however the methyltransferase(s) responsible for the H3K4me3 epigenetic mark has not yet been identified (Figueiredo et al. 2009; Ruthenburg et al. 2007). It is evident from these genome wide studies, that although trypanosomes lack classic Pol II promoters, epigenetics plays an important role in the regulation of Pol II transcription initiation and termination.



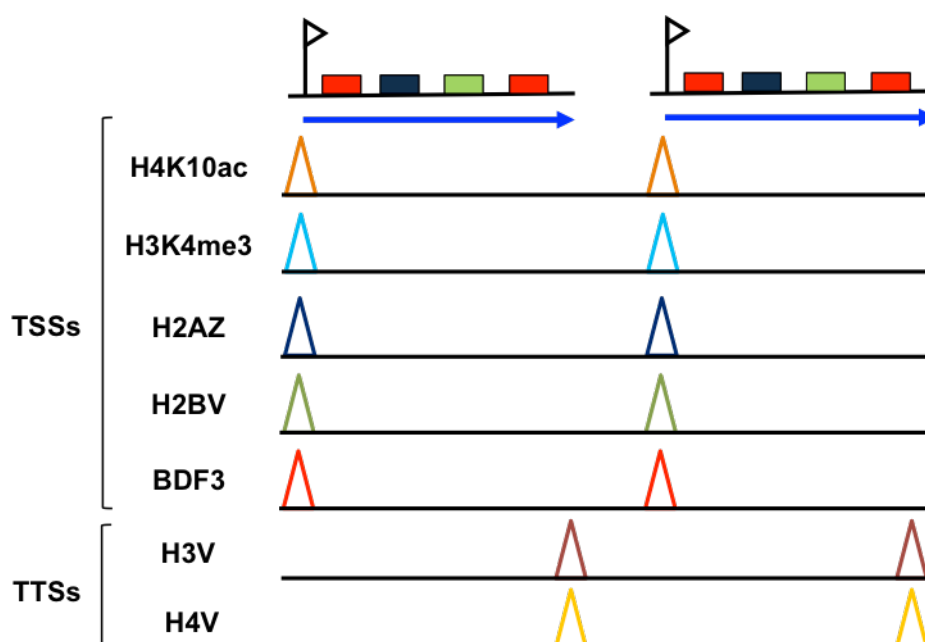


**Figure 1.9. Distribution of post-translational modifications within *T. brucei* Pol II transcribed polycistronic transcription units.**

Schematic of the epigenetic marks known to be enriched at the Pol II transcriptional start and termination sites in *T. brucei*. The putative Pol II promoters (flags) and genes (coloured boxes) of two transcription units are shown. The blue arrows indicate gene transcription. The histone modifications H4K10ac and H3K4me3, histone variants H2AZ and H2BV and bromodomain factor BDF3 are enriched at Pol II transcriptional start sites (TSSs). The histone variants H3V and H4V are enriched at transcriptional termination sites (TTSs). This is a simplified schematic of the data presented in (Wright et al. 2010; Siegel et al. 2009) adapted from (Rudenko 2010)

### 1.9 - Monoallelic expression of *VSG* and the role of RNA Polymerase I

Although there is no transcriptional control of the constitutively transcribed Pol II polycistronic transcription units in *T. brucei*, large segments of the genome containing the vast repertoire of *VSG* genes and pseudogenes are kept transcriptionally silent. Silent *VSG* genes are located within the nucleus at the telomeres of minichromosomes, in large subtelomeric arrays, and in the approximately 14 silent ESs (Figure 1.10) (Berriman 2005; Williams et al. 1982; Cross et al. 2014). In trypanosomes and other eukaryotes Pol I transcription of rDNA transcription units occurs within the subnuclear compartment of the nucleolus (Figure 1.10) (Günzl et al. 2003). However, in BSF trypanosomes Pol I also localises to an extranucleolar body, termed the expression site body

(ESB), where it transcribes the active *VSG* ES (Figure 1.10) (Navarro & Gull 2001). Generally, eukaryotic Pol I transcription units generate uncapped and therefore unstable mRNAs (Lo et al. 1998; Rudenko 2010). However, trypanosomes have evolved to add a 39-nucleotide sequence, termed the spliced leader (SL) sequence to the 5' end of *VSG* mRNAs (Liang et al. 2003). This SL adds a cap to the mRNAs allowing the parasites to use Pol I to transcribe the protein coding *VSG* genes and procyclin loci, in addition to the rDNA genes (Liang et al. 2003; Günzl et al. 2003).

There are several possible reasons as to why trypanosomes evolved to use Pol I to transcribe certain protein coding genes. First, as *VSG* accounts for approximately 10% of *T. brucei* total cell protein, the parasite requires an abundance of *VSG* transcript (Böhme & Cross 2002). This may provide an explanation for the use of Pol I in trypanosomes to transcribe protein coding genes, as Pol I transcription units are transcribed at an approximately 10-fold higher rate than the *T. brucei* polycistronic Pol II transcription units (Biebinger et al. 1996; Rudenko 2010). Second, both the *VSG* genes and *procyclin* genes are regulated in a life-cycle specific manner, and Pol I transcription occurs where transcriptional control is required (Rudenko 2010). *VSG* transcription is downregulated in the PCF within the tsetse fly vector, while the procyclin loci are downregulated in BSF *T. brucei* (Rudenko et al. 1994). Transcriptional control is also observed in the BSF parasite, with regards to the monoallelic expression of a single active *VSG* ES and repression of the other ESs during host infection (Borst 2002). The *VSG* ESs are regulated at the level of transcriptional initiation, as well as the level of transcriptional elongation. Although some transcriptional initiation occurs at the promoters of the silent *VSG* ESs, the high level of fully processive Pol I transcription only extends down to the telomeres in the active ES in BSF *T. brucei* (Rudenko et al. 1994; Vanhamme et al. 2000).

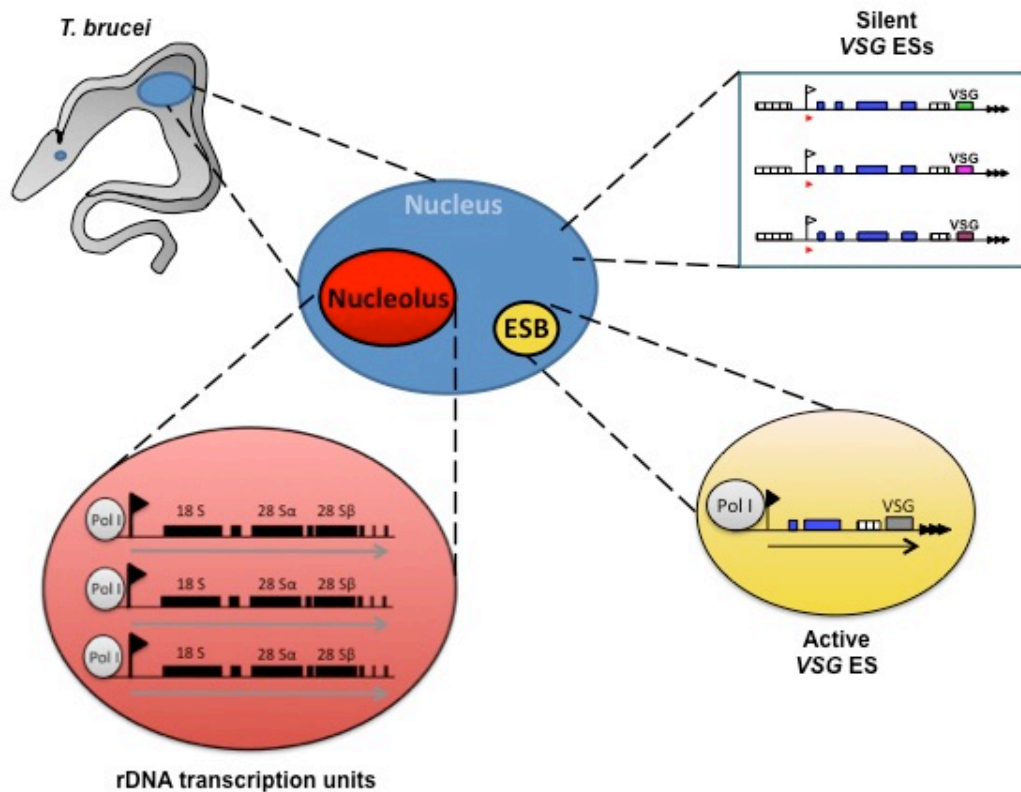


**Figure 1.10. Organisation of Pol I transcribed rDNA and VSG ESs in *T. brucei*.**

A schematic of the BSF *T. brucei* is shown in the top left, within which the small blue dot represents the kinetoplast (mitochondrial DNA) and the large blue dot represents the nucleus. The silent VSG ESs (top right box) and Pol II transcribed genes (not shown) are located within the nucleus. Pol I transcribes the rDNA transcription units within the subnuclear compartment of the nucleolus (red dot). The single active VSG ES is transcribed by Pol I in an extranucleolar body called the expression site body (ESB) (yellow dot). Dotted lines indicated a more detailed view of the denoted structure. Promoters are shown as flags and active transcription is shown as an arrow.

The epigenetic mechanisms that maintain maximal activation of a single VSG ES are not fully understood, and it has proven impossible to select for BSF trypanosomes, which stably express two VSGs from two transcriptionally active VSG ES at the same time. However, double drug resistant (DDR) parasites that unstably express two VSGs from two ESs tagged with different drug resistant genes have been generated to analyse the switching mechanism (Chaves et al. 1999). The DDR parasites were believed to rapidly switch between the two tagged ESs, but appeared unable to simultaneously activate a third ES under drug selection (Chaves et al. 1999; Ulbert et al. 2002). This

data provided evidence for a pre-active ES state model in which a single silent ES is poised in a pre-active state from which it can be more rapidly activated than the rest of the silent ESs. This may be advantageous, allowing the trypanosome to rapidly revert to a previously active ES if the newly activated VSG ES is defective (Chaves et al. 1999). The stable pre-active ES state is thought to be due to epigenetic factors rather than mutation and is discussed in more detail in chapter six.

### **1.10 - Epigenetics and transcriptional control of the VSG ES in bloodstream form *T. brucei***

The stringent monoallelic expression of a single VSG is essential for the parasite to elude the host immune system and cause prolonged infections (Taylor & Rudenko 2006). However, this monoallelic expression requires that a single Pol I transcribed VSG ES, which is highly similar to the other ES transcription units (Hertz-Fowler et al. 2008), be reversibly activated and its transcriptional state be heritable. There is now an increasing body of evidence that chromatin structure; chromatin-remodelling proteins and a kinetoplastid specific DNA modification may be required for the regulation of the VSG ESs (Povelones et al. 2012; Stanne & Rudenko 2010; Figueiredo & Cross 2010; Narayanan & Rudenko 2013; van Leeuwen et al. 1997).

ChIP analysis of the core histones and micrococcal nuclease (MNase) digestion of chromatin has shown that nucleosomes are depleted at the active VSG ES and at the promoter regions of actively Pol I transcribed loci including the rDNA transcription units in BSF *T. brucei* (Stanne & Rudenko 2010; Figueiredo & Cross 2010). Depletion of histone H3 has been shown to result in derepression of the silent VSG ES (Figure 1.11) (Alsford & Horn 2012). Similarly, ablation of the linker histone H1 in trypanosomes resulted in 6 to 8-fold derepression of silent ES promoters and a 10-fold more open chromatin structure compared to the control cell line (Povelones et al. 2012; Pena et al. 2014). Collectively, this provides strong evidence that chromatin structure plays an important role in ES silencing.

Several chromatin-remodelling proteins and epigenetic factors involved in ES control have been identified in *T. brucei* (Figure 1.11). ISWI (Imitation-Switch protein) is an essential chromatin remodelling protein found in PCF and BSF *T. brucei*. ISWI occupies both active and silent ES as well as SSRs. Depletion of ISWI leads to 30 to 60-fold derepression of the VSG ES in BSF *T. brucei* and 10 to 17-fold derepression of the VSG ESs in the PCF *T. brucei* (Hughes et al. 2007). A recent study identified several ISWI-associated proteins. This includes the nucleoplasmin-like protein (NLP) that has previously been shown to be important for ES regulation in *T. brucei* (Stanne et al. 2015). While NLP is associated with all genomic DNA, depletion resulted in a 45 to 65-fold derepression of silent VSG ESs leading the authors to conclude NLP has a role in the down regulation of ESs (Narayanan et al. 2011). The telomere-binding protein RAP1 has been shown to be essential for ES silencing and appears to aid repression at the telomeric end of the ES preventing transcription elongation from silenced ES promoters (Yang et al. 2009).

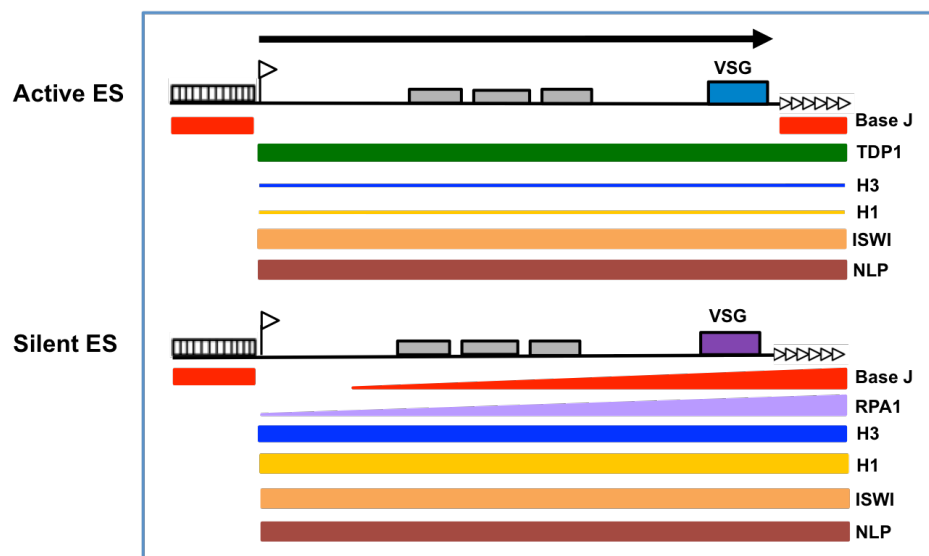


**Figure 1.11. Distribution of epigenetic factors at the active and silent VSG ESs in *T. brucei*.**

Schematic of VSG ESs in BSF *T. brucei*. The DNA modification Base J ( $\beta$ -D-glucosyl-hydroxymethyldeoxyuridine) is present in the 50bp repeats (striped boxes) and at the telomeres (arrowheads) of both the active and silent VSG ESs. A decreasing gradient of base J and RAP1 extends from the telomeres into the silent VSG ES towards the ES promoter (flag). TDP1 has an inverse occupancy pattern to the histones and is enriched at the active VSG ES. Histones H1 and H3 (thin blue and yellow line) are depleted at the active ES compared to the silent ESs (thick lines). ISWI and NLP interact with all ES.

The novel DNA modification  $\beta$ -D-glucosyl-hydroxymethyldeoxyuridine (Base J) is unique to Kinetoplastids and some unicellular flagellates. Base J is present in bloodstream form but not procyclic trypanosomes (Gommers-Ampt et al. 1993). In the BSF trypanosome an increasing gradient of base J extends towards the telomeres at the silent *VSG* ESs (Figure 1.11) Base J is also present in multiple repeat sequences including the 50bp repeats upstream of the ES promoters (van Leeuwen et al. 1996; van Leeuwen et al. 1997). The distribution of base J initially led to a hypothesis that it was important for *VSG* ES silencing, however depletion of base J synthesising proteins (JBP1 and JBP2) did not derepress silent telomeric *VSG* genes (Cliffe et al. 2009).

The epigenetic factors DOT1B and TDP1 function in *VSG* ES silencing. DOT1B is a histone methyltransferase responsible for trimethylation of H3K76 in *T. brucei*. DOT1B is non-essential but causes de-repression of silent *VSG* ESs, and an increase in the time taken to switch between *VSG* ESs is observed in DOT1B null mutants (Janzen et al. 2006a). TDP1 belongs to a family of architectural chromatin proteins and shows an inverse occupancy pattern to that of histone H3, being enriched at Pol I transcribed rDNA transcription units and *VSG* ESs (Figure 1.11). This led the authors to propose a model in which TDP1 replaces histones to maintain an euchromatic state at Pol I transcribed loci in *T. brucei* (Narayanan & Rudenko 2013). Collectively, these studies highlight the important role played by chromatin remodelling proteins and epigenetic factors in regulating transcription in trypanosomes.

### **1.11 - The role of the Expression Site Body in monoallelic expression**

The expression site body (ESB) is a discrete extranucleolar Pol I focus that harbours the active *VSG* ES and is thought to be necessary for monoallelic exclusion. The ESB is present in all cell cycle stages of BSF *T. brucei* and remains as a single focus into the G2 phase, with replication occurring late during mitosis (Navarro & Gull 2001). Curiously, an ESB can only be visualised in approximately 60-70 % of BSF trypanosomes in the G1 stage of the cell cycle when analysed by immunofluorescence microscopy. The authors proposed the absence of a visible ESB in some cells

may be the result of the extranucleolar Pol I focus being obscured by the Pol I signal from the nucleolus (Navarro & Gull 2001). An important feature of antigenic variation in *T. brucei* is the inheritance of a single active ES into each daughter cell. Cohesin is essential for this inheritance as both alleles of the active ES must be associated with the single ESB until late mitosis. Knockdown of cohesin results in early disassociation of the active ES alleles leading to the premature formation of two ESBs, resulting in an increased frequency of VSG switching (Landeira et al. 2009). This suggests association with the ESB is required for epigenetic inheritance of the active transcriptional status of the ES.

The procyclin loci and the rDNA transcription units are transcribed within the nucleolus and are not subject to monoallelic exclusion (Günzl et al. 2003). The nucleolar location, in conjunction with the loss of the ESB during differentiation to the procyclic form supports the argument that the ESB contributes to monoallelic expression of the active VSG ES in BSF *T. brucei* (Landeira & Navarro 2007). In addition to aiding allelic exclusion, the ESB is potentially important in ensuring sufficient expression of the VSG. The ESB is enriched for TDP1 and SUMOylated proteins, as well as containing an abundance of Pol I (Narayanan & Rudenko 2013; López-Farfán et al. 2014). This has led to the proposal that the ESB ensures the availability of all the components required for full processing the ES, including pre-mRNA processing factors and elongation factors not required for rDNA transcription (Daniels et al. 2010).

How trypanosomes maintain the singularity of the ESB remains unclear. It has been proposed that the ESB is a prebuilt structure that can interact with only a single ES at a time (Navarro & Gull 2001). Alternatively, the ESB may be transcription nucleated, similar to the nucleolus (Názer et al. 2011), and the singularity maintained by limited availability of one or more ESB components (Kerry et al. 2017). Efforts to identify ESB specific factors using proteomic and bioinformatic approaches have not proven successful (Daniels et al. 2010). However, characterisation of the ESB associated protein VEX1 may be the first step in identifying additional

factors required for maintenance of monoallelic expression of the ES in BSF *T. brucei* (Glover et al. 2016).

### **1.12 - Repurposing of drugs and target classes for treatment of neglected tropical diseases**

Drug repurposing is the utilisation of an existing compound or drug to treat new indications, such as a communicable disease. Whereas, target repurposing is the use of compounds or drugs with a known target as the basis for developing compounds specific to the target homologue in another species (Klug et al. 2016). Although slightly different, these repurposing approaches both exploit drugs or molecular targets validated for one disease in order to develop treatments for another disease (Andrews et al. 2014). A famous example of successful repurposing was Sildenafil, which was originally developed to treat angina but later repurposed to treat erectile dysfunction under the brand name Viagra® and to treat pulmonary arterial hypertension as REVATIO® (Barratt & Frail 2012).

Drug repurposing relies on the availability of existing compounds and target data. Although thousands of approved or registered compounds appropriate for drug repurposing exists, access to these compounds can be problematic due to commercial concerns of the pharmaceutical company, such as issues surrounding intellectual property (Huang et al. 2011). Despite these concerns, repurposing of existing drugs, compounds and targets are appealing options for pharmaceutical companies as safety, pharmacokinetic, toxicity and clinical study data are often available. This increases the success rate of drug development, reduces the time frame by half, and costs a quarter of *de novo* drug development (Nosengo 2016). Additionally, repurposing of an existing drug extends the patent life, and previously failed compounds can be recovered and repurposed for an alternative indication (e.g. Sildenafil), which are financially beneficial to a pharmaceutical company (Andrews et al. 2014; Pollastri & Campbell 2011). These factors are particularly important when developing drugs for neglected diseases, as these maladies disproportionately affect less economically developed countries and new chemotherapies are predominately developed by for-profit companies.



The target market for pharmaceutical companies is predominately the more economically developed countries, where tropical neglected diseases are not endemic but diseases such as cancer are an increasing problem. It is therefore unsurprising that several drugs, which have been successfully repurposed to treat neglected diseases, were originally developed as anti-cancer therapies. Eflornithine is currently used to treat stage two of HAT caused by *T. b. gambiense* but was originally studied as a human cancer therapeutic. Eflornithine acts as a suicide inhibitor of ornithine decarboxylase, which is part of the polyamine biosynthesis pathway. Although Eflornithine had poor efficacy against cancer cells, a homologue of ornithine decarboxylase was identified in *T. brucei*, leading to its repurposing as an anti-trypanosomal agent (Sekhar et al. 2014). Tamoxifen is another example of an anti-cancer therapy being redeveloped to target the causative agent of the tropical neglected disease, leishmaniasis (Miguel et al. 2008a; Miguel et al. 2008b). Not all repurposed treatments for HAT have originated as anti-cancer therapies. Nifurtimox, which is used in conjunction with Eflornithine (NECT) to treat HAT, was originally used for the treatment of Chagas disease (American Trypanosomiasis). Interestingly, Nifurtimox is now being studied to evaluate its potential as an anti-cancer treatment for neuroblastoma (Saulnier Sholler et al. 2011).

Collaborations between academic institutes, non-profit organisation and pharmaceutical companies are boosting the number of drug candidates under development and have resulted in the delivery of six new treatments for neglected tropical diseases (DNDi 2017). *De novo* drug development will be required to ensure a portfolio of safe, effective and easily administered compounds are available to treat HAT. However, drug repurposing remains an important branch of drug development for neglected tropical disease, primarily due to the low development costs, reduced risk of failure and expedited delivery time (Andrews et al. 2014).

### 1.13 - Thesis aims

The overall focus of my PhD research is to investigate the epigenetic factors that play a role in regulation of Pol I transcription in *Trypanosoma brucei* and to evaluate epigenetic drug targets with novel anti-trypanosomal agents.

The main aims are:

1. Determine the distribution of trimethylation of lysine 4 of histone H3 across the Pol I transcribed loci in BSF *T. brucei*.
2. Investigate the potential for histone methyltransferase chemical inhibitors derived from BIX-01294, previously found to cause parasite cell death and a reduction in the levels of H3K4me3 in *Plasmodium falciparum*, as an on-target anti-parasitic chemotherapy.
3. Evaluate the use of RNA polymerase I chemical inhibitors as an anti-trypanosomal agent and characterise the mechanism of action.
4. To investigate the chromatin state, DNA modification and chromatin remodelers required for the strict monoallelic expression of a single *VSG* ES in *Trypanosoma brucei* using trypanosomes that unstably expression two *VSGs* from two *VSG* ESs as a result of drug selection.

---

## Chapter Two

### Material and Methods

#### Material

##### 2.1 - Trypanosome culturing and strains

Derivatives of the BSF *Trypanosoma brucei brucei* strain 427 were used in all experiments. BSF *T. brucei* were grown at 37°C with 5% CO<sub>2</sub> in HMI-9 medium (Hirumi & Hirumi 1989) containing 15% foetal bovine serum (Gibco®). Trypanosomes were regularly sub-cultured to maintain log phase growth. Strain details for each cell line are outlined in table 2.1 including the concentration of drug required to maintain the transgenic lines.

The two isogenic BSF *T. brucei* cell lines, HNI VO2+ and HNI 221+, were used for the H3K4me3 CHIP-qPCR experiments. The constructs in this cell line contain a neomycin resistant gene and hygromycin resistant gene downstream of the expression site promoters as previously published (Rudenko 1998). The HNI VO2+ line has an active *VSG VO2* ES maintained on neomycin selection and, the *VSG 221* ES is selected on hygromycin resistance in the HNI 221+ cell line.

Excluding the HNI 221+ and HNI VO2+ lines, all the cell lines in this study are derived from the *T. brucei* 'single marker' S16 BSF line (Wirtz et al. 1999) and contain a construct encoding a T7 RNA Polymerase and a tetracycline repressor in the tubulin array under neomycin selection (2µg/ml, Invitrogen). This construct allows for tetracycline inducible transcription. The *T. brucei* S16 line (Wirtz et al. 1999) and derivative, S16\_221Pur that contains a puromycin resistance gene downstream of the *VSG 221* promoter, were used for *in vitro* cytotoxicity assay, inhibitor cell proliferation assays and wash out assays. These cell lines were cultured in drug free media for at least 48 hours prior to inhibitor treatment. The S16 and S16\_221Pur lines were also used as non-fluorescent and Alexa-647 positive controls for flow cytometry experiments. The S16 derivative, S16\_221PureGFP (Shedden et al. 2004), has a puromycin resistance gene and an *eGFP* reporter gene

in the active *VSG 221* ES. The S16\_221PureGFP cell line was used for HKMTI immunoblot analysis and analysis of RNA precursor transcript after treatment with Pol I inhibitors.

For immunofluorescence analyses of the ESB, and RPA2 immunoblot analyses the TY-YFP-RPA2 BSF *T. brucei* line (Kerry et al. 2017) was generated by transfection of XhoI linearized pENT5H-Y:NLS:RPA2 (gift from Gull lab, Daniels et al. 2012) into the S16 cell line (Wirtz et al. 1999). The TY-YFP-RPA2 cell line has a single RPA2 allele endogenously tagged with a TY epitope (Bastin et al. 1996) and enhanced Yellow Fluorescent Protein (eYFP) at the N-terminus (cell line transfected by James Budzak). The *T. brucei* cell line S16\_221PurVEX1myc (Kerry et al. 2017) was used for the quantification of VEX1 foci in Pol I inhibitor treated cells. The *T. brucei* S16\_221Pur cell line was transfected with pNATVEX1<sup>x12myc</sup> construct (gift from Horn lab, Glover et al. 2016) linearized with SphI and stable transformants selected by resistance to blasticidin (5 µg/ml, Invitrogen). This resulted in S16\_221Pur cells with a 12xc-myc C-terminal epitope tag at the native loci.

The KW01 and 221PG\_VHC cell lines were transfected with the pEnt5B-3xHA:RPA2 construct to triple HA epitope tag the N-terminus of the RPA2 gene. This transfection generated the KW01-3xHA:RPA2 and 221PG\_VHC-3xHA:RPA2 cell lines; used to quantify the number of extra-nucleolar RPA2 foci in cells expressing two *VSGs* from two ESs. The double drug resistant BSF *T. brucei* KW01 and BH03 cell lines were derived from 221PG\_VHC and VHC\_221PG, respectively. The cells contain a puromycin resistance gene (Pur) fused to TY1 (TY) and herpes simplex virus Thymidine Kinase gene (TK) in a single open reading frame, and an enhanced Green Fluorescent Protein (eGFP) reporter gene upstream of the *VSG 221* gene at the telomere end of the *VSG 221* ES. A hygromycin resistance gene and *mCherry* reporter gene are present at a comparable telomere locus on the *VSG VO2* ES.

*VSG 221* expression is selected for in the 221PG\_VHC cell line with puromycin (0.2 µg/ml, Sigma) and negative selection with ganciclovir (4 µg/ml, Sigma) was used to switch to the *VSG VO2* ES, which is maintained in the VHC\_221PG line with hygromycin (5 µg/ml, Roche) (lines made by Manish Kushwaha). Higher concentrations of puromycin (0.8 µg/ml) and hygromycin (50 µg/ml) are

required to select for both the *VSG 221* and *VSG VO2* ESs in the DDR lines. The BH03 line was isolated from the VHC\_221PG cells that had activated the *VSG 221* ES in addition to the *VSG VO2* ES under puromycin and hygromycin selection (line generated by Belinda Hall). Cells isolated from the 221PG\_VHC line that had activated the *VSG VO2* ES while maintaining an active *VSG 221* ES under double drug selection became the KW01 line (line generated by Kathrin Witmer).

<i>T. brucei</i> Cell line	VSG surface coat	Drug resistance genes	Drug selection ( $\mu\text{g/ml}$ )	Reference
HNI VO2+	VO2	Neomycin (G418) Hygromycin	2 -	(Rudenko 1998)
HNI 221+	221	Neomycin (G418) Hygromycin	- 5	(Rudenko 1998)
221PG_VHC	221	Neomycin (G418) Puromycin Hygromycin	2 0.2 -	Rudenko Laboratory
VHC_221PG	VO2	Neomycin (G418) Puromycin Hygromycin	2 - 5	Rudenko Laboratory
KW01	VO2 & 221	Neomycin (G418) Puromycin Hygromycin	2 0.8 50	Rudenko Laboratory
BH03	VO2 & 221	Neomycin (G418) Puromycin Hygromycin	2 0.8 50	Rudenko Laboratory
S16	Predominantly 221	Neomycin (G418)	2	(Wirtz et al. 1999)
S16_221Pur	221	Neomycin (G418) Puromycin	2 0.2	Rudenko Laboratory
S16_221PureGFP	221	Neomycin (G418) Puromycin	2 0.2	(Shedder et al. 2004)
TY-YFP-RPA2	221	Neomycin (G418) Puromycin Hygromycin	2 0.2 5	(Kerry et al. 2017)
S16_221Pur- VEX1:12xmyc	221	Neomycin (G418) Puromycin Blasticidin	2 0.2 5	(Kerry et al. 2017)
221PG_VHC- 3xHA:RPA2	221	Neomycin (G418) Puromycin Hygromycin Blasticidin	2 0.2 - 5	Rudenko Laboratory
KW01- 3xHA:RPA2	221	Neomycin (G418) Puromycin Hygromycin Blasticidin	2 0.8 50 5	Rudenko Laboratory

**Table 2.1. Transgenic bloodstream form *T. brucei* generated or used during this study.**

All transgenic cell lines are derived from the *T. brucei brucei* 427 strain. The cell line name and VSG surface coat expressed are shown for all the transgenic cell lines used in this study. The final drug concentration in the medium required to maintain the transgenic cell lines is noted. In some instances drug resistance genes are present in the genome but are not selected for, these are indicated with a –.

<b>Gene/Location</b>	<b>Primer name</b>	<b>Sequence (5'-3')</b>
Upstream Of ES	ES_UP_652s	TATTATGGATCAGGTCAGAG
	ES_UP_776as	AACATACTGCAACAACAATC
Upstream of ES	ES_UP_1116s	ATACCTTATTTCCCATTTGT
	ES_UP_1197as	AAGACCTTCATTATCACG
ES promoter	ES_1s	ATATCCCTATTACCACACCA
	ESP_CorePro_61as	TTGCAGAAATCTCGGATA
ESAG 7	ESAG6_281s	AACAGTATTGAGGAATGAG
	ESAG6_524as	ATTTTGTAAAGGGTTTCAG
ESAG 5	ESAG5_236s	GTGTGAGTGTAGAAGAGAC
	ESAG5_391as	ACAGGTAACACCAAAAC
ESAG 8	ESAG8_1193s	TGTATCTTCGTGATGTTAAGTC
	ESAG8_1299as	ACTCAGGCTTGTTATTCTCTC
ESAG 2	ESAG2_1060s	GTCAGTTACAAGCACACACTT
	ESAG2_1321as	GAGTAAGCCCATCATTATCTAC
VSG 221	VSG221_s2	CCGCTGAAAGCCAACAACAA
	VSG221_as2	TGCATGGGGATTTGCACTCA
Neomycin resistance gene	Neomycin_302s	ATCTCCTGTCATCTCACCTTG
	Neomycin_489as	CTGATGCTCTTCGTCCAG
rDNA spacer	rDNAspacer_178s	ATTTTCTCTACCCCTCTCTT
	rDNAspacer_323as	ATCATCGTATCATTTCATC
rDNA promoter	rDNAprom_s	GTACGGAGCAGGAGAGCAAC
	rDNAprom_as	GCATTGCGCAAAGTTTACAG
18s subunit	18s_177s	GCATTACTGGATAACTTGG
	18S_250as	GTTCTAATTTCAATTCATTCG
5.8s subunit	5.8s_36s	GGATGACTTGGCTTCTAT
	5.8S_95as	ATTGATACCACTTATCGCACT
28S alpha subunit	28Salpha_226s	ACACATTTACAACCCTTCAT
	28Salpha_410as	CTATCGGTCTTCTACTCTAT
rDNA spacer	rDNASp_3303s	TTACGAACGTGAAGTGTAGAT
	rDNASp_3499as	CATTTGGAACACGGTAACTAT
Upstream of SSR	C3DN_185s	CAGACAACCCATTCTACTACAG
	C3DN_300as	CAGCAGGGTGATGTTAAAGTA
Within SSR	Dive2_SSR_3108s	GAACACCAAACCTCACTTC
	Dive2_SSR_3229as	CTCCATCTCTTATCCTTATTC
Y-Tubulin	GammaTub_491s	AATCACCGTATTTGGACACAAG
	GammaTub_583as	GTTTGAGTGTTGCTGAAAGAG
Pol I	poll-349s	ATTCACCGTATTTGGACACAAG
	poll-486as	GTTTGAGTGTTGCTGAAAGAG
Actin	Actin_1031s	GTTCCATCCTCTCATCACTA
	Actin_486as	TCGTATCACTCTTCGTTATC
VSG 800	VSG800_99s	GAAGGTCTGGGAACCTCTAT
	VSG800_295aS	GGCTGTAATATGCTCGTAGA
VSG 14	VSG14_959s	CACTAGACTCAAATCACAAATC
	VSG14_1090as	GGTTTATCACTAGGTTGTCTT
mCherry	mCherry_528s	CACTACGACGCTGAGGTCAA
	mCherry_627s	GTGGGAGGTGATGTCCAAC
eGFP	eGFP_184s	GTGACCACCCTGACCTAC
	eGFP_324as	CTTGTAGTTGCCGTCGTC
Hygromycin resistance gene	Hygro_419s	GAATCGGTCAATACACTACAT

	Hygro_492as	AGTTTGCCAGTGATACACAT
VSG 221	VSG221_s4	GCGACAACCAGCCAACCAAG
	VSG221_as4	TCAGCGGGCTTGTGCTTCTG
Puromycin resistance gene	Puromycin_288s	CGAGTTGAGCGGTTCC
	Puromycin_333as	GCCTCCATCTGTTGCT
VSG VO2	VSGVO2_94s	CTAGTAGCCTCACAACGATG
	VSGVO2_199as	ACAGCCGCTGTATCTCTTGC
rDNA precursor transcript 1	18S_UP_377s	CCATGCTCTCTCGTGTGTGTA
	18S_UP_52as	TTCCTCAAGGCGTCACTCTATC
rDNA precursor transcript 2	28Sa_UP_136s	AAAGAGGCGGCGGATAGTG
	28Sa_UP_52as	ACGAAAGAAGCACAAGCACATA
rDNA precursor transcript 2 & 3	70srRNA_UP_182s	TTGAAGGGAATGCAAAAAGTGTA
	70srRNA_UP_68as	AACTGGAAGAGACGGAGGTA
rDNA precursor transcript 2 & 3	140srRNA_UP_89s	TTGTGTTTCTATGTGTGTGTGTAAG
	140srRNA_1as	CGTTTGGAGAGGGACAAAATAT
VSG 221 precursor	Pre_221CTR_F2	TGGAGCGTACACACAAGTGA
	Pre_221CTR_R2	ATGCATTGGCACACTTTCCG
VSG pseudo gene precursor	Pseudo_221_f_kw	GCAGGCAAGCATTACCAGAG
	Pseudo_221_r_kw	CTGTTCCGAATAGCGCGTC
Tubulin precursor	$\alpha$ Tub_up331s	GAGGAGGTGGGAAGGGTATATG
	$\alpha$ Tub_up205as	GAAGGCGTGTGATGAGTTGTA
Actin	Actin_1031s	GTTCCATCCTCTCATCACTA
	Actin_1091as	TCGTATTCACTCTTCGTTATC

**Table 2.2. Quantitative PCR primers.**

List of primer pairs used for RT-qPCR to determine transcript or precursor transcript abundance in total cell RNA and for CHIP-qPCR to amplify regions of interest from immunoprecipitated material.



Primary antibodies	Organism	Origin	ChIP	Immunoblot analysis	Microscopy	Flow cytometry
Anti-H3K4me3 (ab8580)	Rabbit	Abcam	-	1:125	-	-
Anti-H3K4me3 (M04-745)	Rabbit	Millipore	10µg	-	-	-
Anti-TY (BB2)	Mouse	A gift from Keith Gull	-	1:9000	-	-
Anti-L1C6	Mouse	A gift from Keith Gull	-	-	1:200	-
Anti-VSG221 (-CRD)	Rabbit	A gift from Jay Bangs	-	-	1:1000	1:4000
Anti-VSG221	Rabbit	Eurogentec	-	1:10000	-	-
Anti-VSGVO2	Rabbit	A gift from Piet Borst	-	1:1000	1:1000	1:2000
Anti-BiP	Rabbit	A gift from Jay Bangs	-	1:10000	-	-
Anti-H1	Rabbit	Eurogentec	10µg	1:1000	-	-
Anti-H3 (ab1791)	Rabbit	Abcam	2µg	-	-	-
Anti-TDP1	Rabbit	A gift from Klaus Ersfeld	10µl	1:500	-	-
Anti-Base J	Rabbit	A gift from Piet Borst	2.5-20µl	-	1:250	-

Secondary antibodies	Organism	Origin	ChIP	Immunoblot analysis	Microscopy	Flow cytometry
Alexa Fluor 488 Anti-rabbit IgG (H+L)	Goat	ThermoFisher Scientific	-	-	1:500	-
Alexa Fluor 594 Anti-rabbit IgG (H+L)	Goat	ThermoFisher Scientific	-	-	1:500	-
Alexa Fluor 647 Anti-rabbit IgG (H+L)	Goat	ThermoFisher Scientific	-	-	-	1:1000
AlexaFluor 647 Anti-mouse IgG (H+L)	Goat	ThermoFisher Scientific	-	-	1:500	-
Amersham ECL anti-rabbit HRP conjugate	Donkey	GE Healthcare Life Sciences	-	1:10000	-	-

**Table 2.3. Primary and Secondary antibodies.**

The experimental details for all primary and secondary antibodies used in this study are stated under the appropriate assay. – Indicates the antibody was not used in the assay.

## Methods

### 2.2 - Cloning and constructs

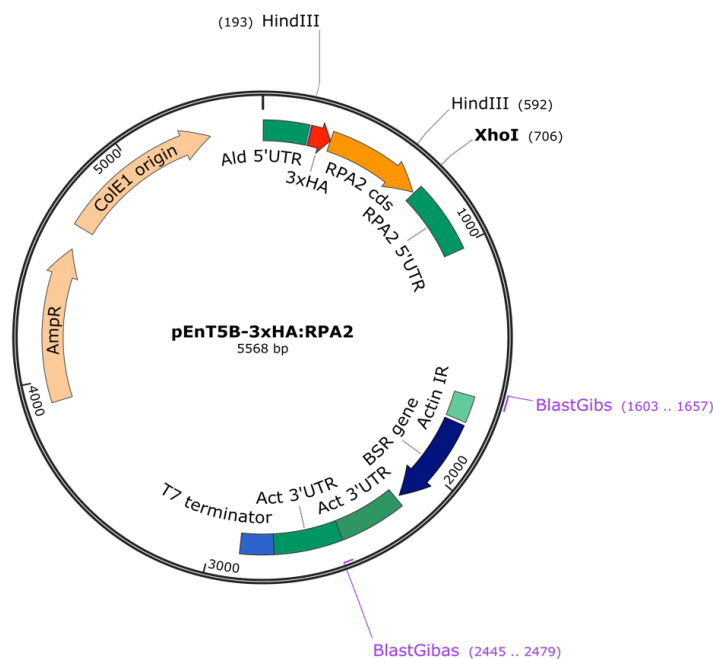
The pEnT5B-3xHA:RPA2 construct used to N-terminally tag the RPA2 gene is shown in figure 2.1A. The pENT5H-Y:NLS:RPA2 construct (gift from the Gull laboratory) was digested with *StuI* to remove the hygromycin resistance gene and associated Actin UTRs. Q5 polymerase (NEB) was used as per the manufactures instructions to amplify a blasticidin drug resistance gene and replacement Actin UTRs. The primers used for amplification were BlastGibs 5'-ATACTGACGAAATCAAAGAGTTGGAGGATGGATAGGGAGGGCACAGCAAGGTCTTCTGAA-3' and BlastGibas 5'-ACAATTTTGGCCACACAACCCGGTGTAGGATCTCCGAGGAATACTGCATAGATAACAAA-3'. The resulting PCR fragment was purified using the QIAquick PCR Purification kit (Qiagen) as per the manufactures guidelines. A 1:1 ratio of linearized vector (0.05 pmol) and PCR fragment, with 20bp overhangs of desired homology to the flanking region, were combined with Gibson Assembly Master Mix (320  $\mu$ l 5x Isothermal reaction mix (500 mM Tris-HCL, pH 7.5, 50 mM MgCl<sub>2</sub>, 1 mM dGTP, 1 mM dATP, 1 mM dTTP, 1 mM dCTP, 50 mM DTT, 25% PEG-800, 5 mM NAD), 700  $\mu$ l ddH<sub>2</sub>O, 0.64  $\mu$ l T5 exonuclease (NEB), 20  $\mu$ l Phusion DNA Polymerase (NEB), 160  $\mu$ l Taq DNA ligase (NEB)) and incubated at 50° C for 1 hour. The mixture was transformed into DH5-alpha cells and pENT5B-Y:NLS:RPA2 plasmid DNA isolated using the Qiagen Miniprep kit (Qiagen).

The TY:eYFP tag and part of the RPA2 targeted coding region was excised from the pEnTB5-Y:NLS:RPA2 construct (Daniels et al. 2012) by digesting with *HindIII*. Treated with Shrimp Alkaline Phosphatase (rSAP, NEB) to prevent religation of the linearized plasmid. The linearized plasmid was then gel purified using the QIAquick Gel Extraction kit (Qiagen) as per the manufacturers guidelines.

To N-terminally tag the RPA2 gene (Tb11.03.0450), a sequencing encoding the excised 5' end of the RPA2 targeted coding region (300bp) and a codon optimized triple HA tag was synthesized by Genewiz (Figure 2.1B). The 417bp fragment was excised from the pUC57 holding vector using *HindIII* restriction enzyme sites flanking the synthesized insert. T4 DNA Ligase (NEB) was used to ligate the

synthesized insert into the pEntTB5 plasmid, which was subsequently transformed into DH5-alpha cells and DNA isolated using Qiagen Miniprep kit (Qiagen). The correct orientation of the insert was confirmed by diagnostic digest. The pEnt5B-3xHA:RPA2 construct was sequenced using sanger sequencing (Genewiz).

A



B

Tyr	Pro	Tyr	Asp	Val	Pro	Asp	Tyr	Ala	Tyr	Pro	Tyr	Asp	Val	Pro	Asp	Tyr	Ala	Tyr	Pro	Tyr	Asp	Val	Pro	Asp	Tyr	Ala
TACCC	TTACG	ATG	TGC	CTGA	TTACG	CGTAC	CCATAC	GACG	TGCCA	GACTA	CGCATA	CCCG	TACGAT	GTGC	CCGATT	ACGC	A									
ATGGG	AATGC	TACAC	GACT	AATGC	GCAIG	GGTAT	GCTGC	ACGGT	CTGAT	GCGTAT	GGGC	ATGCT	ACAC	GGCTA	AATGC	T										

**Figure 2.1. pEnt5B-3xHA:RPA2 construct.**

(A) Plasmid used to N-terminally tag the RPA2 gene with a triple HA epitope in BSF *T. brucei* 221PG\_VHC and KW01 cell lines. Primers used for Gibson assembly are shown in purple. The synthesized DNA fragment, encoding the 300bp of the RPA2 cds and 3xHA tag, was inserted using HindIII restriction enzyme sites. The construct was linearized for transfection by XhoI digestion. (B) Codon optimized 3xHA epitope tag synthesized by Genewiz.

### 2.3 - Transfection of BSF *T. brucei*

For all transfections, the sequenced DNA was isolated using the HiSpeed Plasmid Midi Kit (Qiagen). DNA constructs were linearised with the appropriate enzyme and the sterile DNA prepared using phenol:chloroform extraction and ethanol precipitation.  $3 \times 10^7$  BSF *T. brucei* cells were mixed with 10 µg DNA re-suspended in transfection buffer (90 mM NaH<sub>2</sub>PO<sub>4</sub>, 5 mM KCL, 0.15 mM CaCl<sub>2</sub>, 50 mM HEPES, pH 7.3) and subjected to nucleofection using the Amaxa Nuclofactor® II (Lonza) X-001 setting. Transfected cells were plated at 1x, 10x, 100x and 1000x dilutions and recovered for a minimum of 6 hours in HMI-9 media, under normal culturing conditions, prior to appropriate drug selection. Clonal transformants were selected 5-7 days post transfection.

### 2.4 - Chemical inhibitors

Stock solution of (10 mM) CX-5461 (gift from Prof Hannan, Australian National University) in 50 mM NaH<sub>2</sub>PO<sub>4</sub> (pH 7) (Haddach et al. 2012), (1 mM) Quarfloxin (AdooQ Bioscience) (Drygin et al. 2009) and (1 mM) BMH-21 (Sigma) (Peltonen et al. 2010) in ≥99.9% dimethyl sulfoxide (DMSO, Sigma) were protected from light and stored at -20°C. Stock solutions of (40 mM) HKMTI-1-014, HKMTI-1-017 and HKMTI-1-251 (gift from Dr Fuchter, Imperial College London, Department of Chemistry) in ≥99.9% dimethyl sulfoxide (DMSO, Sigma) were stored at -80°C. A 10 mM stock of Suramin (Sigma) was made with nuclease free water immediately prior to use. All compound stock solutions were diluted in HMI-9 media directly prior to treatment.

### 2.5 - Reverse Transcription Quantitative Polymerase Chain Reaction (RT-qPCR)

Precursor transcript analysis was performed using quantitative Reverse Transcriptase Polymerase Chain Reaction (RT-qPCR). Total RNA was isolated from treated or control *T. brucei* using the RNeasy kit (Qiagen) then DNase treated with the TURBO DNA-free kit (Invitrogen). The 100 ng of the resulting RNA was used as a template for cDNA synthesis with 5 mM random hexamer primers (Promega) and the Omniscript RT kit (Qiagen) as per the manufactures instructions. Reverse

transcriptase negative control reactions were run in parallel as a control. The reaction components were incubated at 37°C for 1 hour and the synthesised cDNA diluted 10-fold.

All RT-qPCRs were performed on the 7500 Fast Real-Time PCR system (Life technologies) using Brilliant II SYBR® Green QPCR Low ROX Master Mix (Agilent technologies). DNase-treated RNA without RT was used as a control for residual gDNA at each time point. Transcript levels were normalised to actin and plotted as percentage of relative expression compared to time zero. The amplification conditions for each primer pair used for RT-qPCR were optimised, and the primers listed in table 2.2.

## **2.6 - Chromatin Immunoprecipitation (ChIP) and quantitative PCR (qPCR)**

Parasites were fixed in 1% formaldehyde for 1 hour at room temperature. The crosslinking reaction was terminated by the addition of glycine to a final concentration of 125 mM. Chromatin from  $3 \times 10^8$  cell equivalents per cell line was sonicated to an average DNA size of 200 bp and the sonicated extract clarified by centrifugation. Immunoprecipitations (IPs) were performed for 18 hours at 4°C with an anti-histone H3 antibody (Ab1791), a monoclonal anti-H3K4me3 antibody (Millipore 04-745), anti-H1 antibody (Povelones et al. 2012), anti-TDP1 antibody (Narayanan & Rudenko 2013), anti-Base J antibody (Van Leeuwen et al. 1998) and no antibody (negative control) coupled to Dynabeads® Protein G magnetic beads (Novex, Life technologies). Immunoprecipitated DNA was washed once in TSE-150 (0.1% SDS, 1% triton X-100, 2 mM EDTA, 20 mM TrisHCl (pH 8.0), 150 mM NaCl with 1 mM protease inhibitors), TSE-500 (0.1% SDS, 1% triton X-100, 2 mM EDTA, 20 mM TrisHCl (pH 8.0), 500 mM NaCl), LiCl wash (0.25 M LiCl, 1% NP-40, 1% Na-Deoxycholate, 1 mM EDTA, 10 mM trisHCl (pH 8.0)) and twice in TE buffer (10 mM TrisHCl (pH 8.0), 1 mM EDTA) on ice. DNA/protein complexes were eluted from the beads in 1% SDS-0.1 M NaHCO<sub>3</sub>. Cross-links were reversed by the addition of NaCl to a final concentration of 327 mM and incubation at 65°C for 4 hours. DNA was treated with RNase A (10 µg/µl) for 1 hour at 37°C and proteinase K (20 µg/µl) for 2.5 hours at 56°C, prior to purification using the QIAquick PCR purification kit (Qiagen).

Quantitative PCR was used to amplify regions of interest using the 7500 Fast Real-Time PCR system (Life technologies). Input chromatin (10% of total chromatin input), immunoprecipitated material, standard gDNA template and the relevant controls were amplified using SYBR® Green QPCR Low ROX Master Mix (Agilent technologies) and primers (Table 2.2). IP quantification was calculated as the percentage of input immunoprecipitated after subtraction of the no antibody control value. The H3K4me3 ChIP data was then calculated relative to nucleosome density (% IP of histone H3). The number of replicates is indicated in each figure legend. Statistical analyses are Student's *t*-test (unpaired, two-tailed) (GraphPad Prism V5). Data was considered 'significant' where  $P = 0.01-0.05$ , 'very significant' where  $P = 0.001-0.01$  or 'extremely significant' where  $P = <0.001$ .

### **2.7 - Trypanosome proliferation assay**

Proliferation assays were established with a starting density of  $1 \times 10^4$ - $1 \times 10^5$  cells/ml *T. brucei* S16 or derived cell lines. Treated parasites were incubated in HMI-9 media containing the various concentrations of chemical inhibitors or appropriate controls. Parasite culture densities were determined at the indicated time points by counting with a Neubauer haemocytometer. Cell counts were repeated minimally in triplicate and plotted using GraphPad Prism version 5.

### **2.8 - Wash out assay**

*T. brucei* S16 cells were exposed to various concentration of the Pol I chemical inhibitors. After 2 hours incubation under normal culturing conditions, the parasites were washed and resuspended in pre-warmed HMI-9. Cell proliferation was monitored as described above.

### **2.9 - ESB reassembly assay**

*T. brucei* TY-YFP-RPA2 cells were exposed to 1  $\mu$ M BMH-21 or HMI-9 media (untreated control) for 2 hours. Cells were then washed and resuspended in pre-warmed HMI-9. Samples for fluorescence microscopy and RT-qPCR were collected pre-incubation, directly after removal of BMH-21 (0 hour), 15 minutes, 30 minutes, 1 hour and 2 hours post wash. RT-qPCR was performed as

previously described and the primers shown in table 2.2. Cells were stained with L1C6 and the number of extra-nucleolar YFP positive foci quantified as described below. Student's *t*-test (unpaired, two-tailed) was calculated using GraphPad Prism V5. Data was considered 'significant' where  $P = 0.01-0.05$ , 'very significant' where  $P = 0.001-0.01$  or 'extremely significant' where  $P = <0.001$ .

### **2.10 - *In vitro* cytotoxicity assay**

S16 BSF *T. brucei* ( $2 \times 10^3$  cells/ml) were plated on 96 well-plates and incubated under normal culturing conditions with two fold serial dilutions of the chemical compounds for 72 hours. At 72 hours, 20  $\mu$ l of 0.125 mg/ml Resazurin (Sigma) was added and the parasites cultured for a further 18 hours under normal conditions. The fluorescence was measured using a Tecan infinite plate reader (excitation at 530 nm, emission at 585 nm). The percentage of untreated cells was calculated by subtracting the fluorescence of the treated cells at each concentration of inhibitor from the untreated control then multiplying by 100. The percentage of untreated cells was plotted as a function of the chemical compound concentration using the sigmoidal dose-response (variable slope) algorithm in GraphPad Prism version 5.  $IC_{50}$  was defined as the amount of compound or inhibitor required to decrease cell viability by 50% compared to an untreated control culture. The EC99 as calculated from *in vitro* data using the ECanything algorithm in GraphPad Prism version 5 assuming a slope factor of 1.

### **2.11 - Flow cytometry of endogenous fluorescence and antibody stained *T. brucei***

Parasites were centrifuged, washed once in PSG, and fixed in 2% paraformaldehyde (PFA) for 20 minutes in the dark at room temperature. Cells probed with anti-VSG antibodies were blocked in 0.5% BSA for 30 minutes, prior to being coated in the required primary antibody (Table 2.3) for 1 hour. The cells were then washed once in PBS (137 mM NaCl, 2.7 mM KCL and 10 mM phosphate

buffer solution (pH 7.4), Sigma) and probed with the Goat anti-Rabbit IgG Alexa Fluor 647 secondary antibody (Table 2.3) for 1 hour. All incubations were carried out at room temperature in the dark.

All cells were then washed once and resuspended in PBS and analysed by flow cytometry using a BD Bioscience LSRFortessa. 10 000 events were recorded for each sample as well as the compensation controls. Quantification of endogenous fluorescence (eGFP and mCherry) and *T. brucei* probed with anti-221 or anti-VO2 (Alexa-647) was analysed using FlowJo V7 software (FlowJo, LLC). Quad gates were calculated using the 98<sup>th</sup> percentile of relevant control cell lines and a representative sample of the gated populations is shown in figure 2.2. The appropriate compensation controls were used and compensation applied using the FlowJo V7 software.

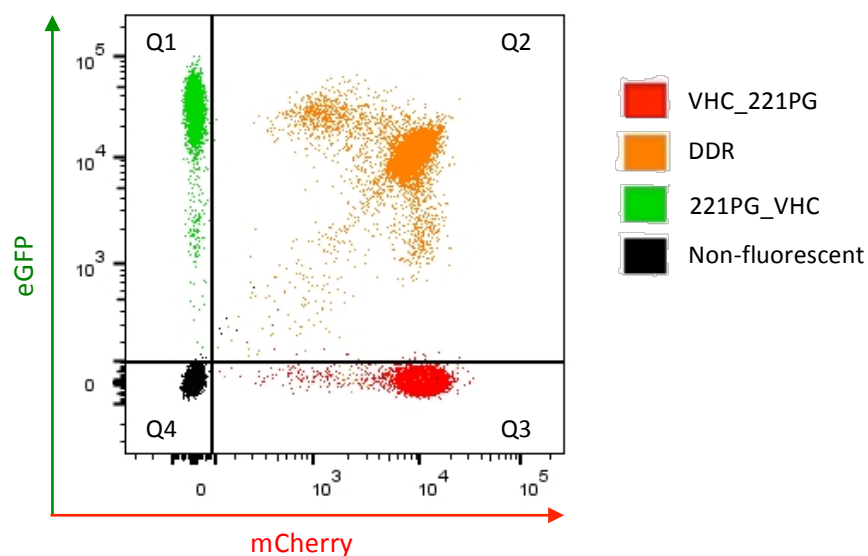


**Figure 2.2. Flow cytometry percentile gated populations.**

Overlaid flow cytometry traces of eGFP and mCherry expression from 221PG\_VHC (green), VHC\_221PG (red), KW01 (orange) and a non-fluorescent (black) cell lines are shown. Percentile intensity of the parental cell lines was used to determine the gate parameters. The quadrants define the eGFP positive (Q1), mCherry positive (Q3), Double Drug Resistant (DDR) (Q2) and non-fluorescent (Q4) cell populations.



### 2.12 - Dilution assay

Three fold serial dilution of the 221PG\_VHC, VHC\_221PG, KW01 and BH03 cell lines were diluted in HMI-9 and plated in 96-well plates to give a final concentration of 1, 0.33, 0.11 cells/well. Cultures were then incubated for 7 days under normal culturing conditions. Five clonal cultures were selected from the 0.33 or 0.11 cells/well 96-well plates for each cell line. The endogenous eGFP and mCherry expression for all five clones and the parental population of each cell line were analysed by flow cytometry as previously described.

### 2.13 - Immunofluorescence microscopy

Parasites were centrifuged and washed once in PSG (60 mM Na<sub>2</sub>HPO<sub>4</sub>, 3 mM NaH<sub>2</sub>PO<sub>4</sub>, 44 mM NaCl and 56 mM glucose) prior to fixing cells in a final concentration of 2% PFA for 20 minutes. Antibody stained cells were washed in PBS and permeabilised with 0.1% NP-40 (ThermoFisher Scientific) for 5 minutes at room temperature. Permeabilised cells were then blocked in 1% w/v BSA block (PBS with Bovine serum Albumin, Sigma) prior to being incubated with an antibody against the uncharacterised nucleolar marker L1C6 (Devaux et al. 2007), anti-myc tag antibody (clone 4A6, EMD Millipore), anti-HA tag antibody (ab18181, AbCam) or the anti-Base J antibody (Van Leeuwen et al. 1998). The probed cells were visualised using the appropriate secondary antibody coupled to either Alexa-594 (Molecular probes) or Alexa-647 (ThermoFisher) (Table 2.3).

All fixed cells were mounted in Vectashield containing the DNA stain, DAPI (Vector Laboratories). Microscopy was performed using a Zeiss Imager.M1 microscope equipped with a Zeiss AxioCam MRm camera and Axio Vision Rel 4.8 software. All images were processed using Image J software 1.47v, and the exposure time and contrast was uniformly adjusted across all samples. For quantification of the extra-nucleolar RPA2 endogenous eYFP signal and detection of VEX1:myc tagged protein, a Z-stack of images was taken at 200 nm intervals for each field, and the data from each channel reassembled using Image J software 1.47v.

### 2.14 - Immunoblot analysis

Parasites were pelleted by centrifugation then washed twice in ice cold PSG. They were re-suspended in lysis buffer (50 mM HEPES pH 7.5, 10% v/v glycerol, 1% v/v Triton X-100, 1.5 mM MgCl<sub>2</sub>, 1 mM EGTA and Protease inhibitors (Roche)) at either 10<sup>5</sup> cells/ml or 10<sup>6</sup> cells/ml depending on the final number of cell equivalents required for analysis. Lysed samples were incubated for 20 minutes on ice before storage at -80°C. Prior to fractionation, protein lysate was diluted in sample loading buffer containing DTT (250 mM Tris-HCL pH 6.8, 8% w/v SDS, 40% v/v glycerol, 0.01% w/v bromophenol blue, 50 mM DTT and ddH<sub>2</sub>O) and boiled at 100°C for 10 minutes.

Total protein extract of 5x10<sup>5</sup> - 1x10<sup>7</sup> cell equivalents per lane (uniform number of cell equivalents loaded for each experiment) was fractionated on a Tris-Glycine SDS-PAGE gel (Sambrook et al. 1989) at 100 Volts for 1.5 hours. Protein was transferred to an Amersham Hybond-P PVDF membrane (GE Healthcare) at 100 Volts for 1 hour then the membrane was incubated in 5% w/v milk block (PBS with Skim Milk Powder, Sigma) overnight at 4°C. The blots were washed three times in PBST (PBS with 0.02% v/v Tween-20) for 5 minutes each. The blots were then probed by incubating for 1 hour with the primary antibody diluted in 2% w/v milk block. Post incubation the membrane was washed a further three times in PBST. To allow for the antibody to be visualised, the membrane was incubated for 1 hour with the appropriate secondary antibody (Table 2.3) conjugated to horseradish peroxidase (HRP) diluted in 2% w/v milk block. Signal was detected using SuperSignal West Pico Chemiluminescent Substrate (Thermo Scientific) on the ChemiDoc XRS+ Imager (BioRad) Chemi application.

Membranes were incubated in Stripping Buffer (100 mM β-mercaptoethanol, 2% SDS, 62.5 mM Tris-HCL (pH 6.7)) for 30 minutes at 65°C, washed in PBST, and incubated overnight in 5% w/v milk block at 4°C ready for re-probing. Alternatively, the blocked membrane was stained with Ponceau S (0.1% w/v Ponceau S, 5% w/v glacial acetic acid and ddH<sub>2</sub>O) until the Ponceau S had bound to the amino acid group of the protein. The saturated membrane was then rinsed in ddH<sub>2</sub>O

until the background became clear and protein bands were visible. The stained membrane was imaged using the ChemiDoc XRS+ Imager (BioRad) Colourmetric application.

Densitometry quantification of H3K4me3 protein levels was performed using Image J software and the relative levels of signal were normalized to the signal of the loading control. Values obtained were then normalized to the untreated control sample for each time point.

### **2.15 - Peptide Competition assay**

The specificity of two commercial ChIP-grade antibodies, a polyclonal anti-H3K4me3 antibody (AbCam 8580) and a monoclonal anti-H3K4me3 antibody (Millipore 04-745) (raised against the human H3K4me3 modification), for *T. brucei* H3K4me3 was determined by peptide competition assay. Total protein extract of  $1.5 \times 10^7$  cell equivalents per lane was fractionated on a Tris-Glycine SDS-PAGE gel (Sambrook et al. 1989) at 100 Volts for 1.5 hours. Protein was transferred to an Amersham Hybond-P PVDF membrane (GE Healthcare) at 100 Volts for 1 hour then incubated in blocking buffer (5% w/v Milk block) overnight at 4°C. Prior to hybridisation the antibodies were pre-incubated for 20 minutes at room temperature with either the H3K4 (RTKETARTC) or H3K4me3 (RT{LYS(Me3)}ETARTC) peptides (GenScript) at a concentration range of 0.2-10 µg/ml. Membranes were then hybridised for 1 hour at room temperature with either the monoclonal or polyclonal anti-H3K4me3 primary antibody using the MiniBlotter® (Immunetics) apparatus. Secondary antibody incubation, protein detection, stripping and re-probing of the membrane with a loading control antibody was all performed as described above.

## Chapter Three

### Distribution of the H3K4me3 epigenetic mark in bloodstream form *Trypanosoma brucei* polymerase I transcribed loci.

#### 3.1 - Introduction

Histone modifications play an important role in the regulation of gene transcription in *T. brucei* (Wright et al. 2010; Siegel et al. 2009). The trypanosome genome is organised into long polycistronic transcription units that are constitutively transcribed by Pol II (Berriman 2005). *T. brucei* lacks the transcriptional regulatory elements present at the promoters of higher eukaryotes (Siegel et al. 2009). However, modified histones and histone variants demarcate putative promoters at TSS in these parasites (Talbert & Henikoff 2009). Unlike Pol II transcription, the Pol I transcribed *VSG* genes are transcribed in a strictly monoallelic fashion from one of approximately 15-20 *VSG* ESs (Günzl et al. 2003, Hertz-Fowler et al. 2008). Monoallelic expression of a single *VSG* from the repertoire of hundreds of *VSG* genes is essential to ensure sufficient antigenic variation to prolong host infection. Chromatin structure, chromatin-remodelling proteins and a DNA modification are known to contribute to the transcriptional state of both active and silent *VSG* ESs (Povelones et al. 2012; Figueiredo & Cross 2010; Narayanan & Rudenko 2013; van Leeuwen et al. 1997).

The N-terminal trimethylation of lysine four of histone H3 is widely conserved in eukaryotes and is predominately associated with transcriptionally active genes (Ruthenburg et al. 2007). Chromatin immunoprecipitation experiments have determined the genomic distribution of the H3K4me3 epigenetic mark. These studies have shown it to be enriched at the promoters and the 5' region of active Pol II transcribed genes in eukaryotes (Santos-Rosa et al. 2002; Li et al. 2008; Liu et al. 2005). Given the striking correlation between the H3K4me3 modification and transcriptionally active genes it was widely accepted that trimethylated H3K4 played a role in transcription initiation.

Interestingly, gene activation by H3K4me3 lacks a clearly defined mechanism, and this has since cast doubt on its role as an activator of gene expression (Howe et al. 2017). Recent

experiments examining trimethylation and transcription over a time course showed the majority of H3K4 trimethylation was observed after transcription initiation of zebrafish embryonic genomes post fertilisation (Vastenhouw et al. 2010). Similarly, transcriptional initiation prior to H3K4me3 deposition was noted in yeast and mice (Sollier et al. 2004, Le Martelot et al. 2012). Collectively, these studies suggest that the H3K4me3 modification may be enriched as a result of active transcription rather than driving transcription. Based on the meta-analysis of published and unpublished H3K4me3 data, Howe and colleagues (2017) have postulated that trimethylation of H3K4 in actively transcribed sites may be required for transcriptional consistency or to preserve the memory of a previous activation state.

In addition to Pol II promoter regions, the H3K4me3 modification is also deposited at the 5' end of actively transcribed Pol I rDNA transcription units distinguishing them from the silent rDNA repeats in vertebrates (McStay & Grummt 2008). Intriguingly, mutation of Set1, the sole HKMT responsible for methylation of H3K4 in *S. cerevisiae* (Briggs et al. 2001), results in defective telomere and rDNA silencing. This suggests that the H3K4me3 modification may be directly required for rDNA silencing in yeast (Fingerman et al. 2005). However, recent indirect immunofluorescence experiments using tagged-Set1 in *S. cerevisiae* showed low occupancy of Set1 in the nucleolus, leading the authors to conclude that rDNA silencing is likely to be an indirect effect of the methyltransferase activity of Set1 (Dehé & Géli 2006).

The sequences of canonical core histones are relatively conserved in eukaryotes but as trypanosomes branched early in evolution their histones are among the most divergent (Thatcher & Gorovsky 1994). This divergence is particularly evident with regard to the N-terminal tails (Alsford & Horn 2004). With the exception of the histone H3 N-terminal sequence surrounding lysine 4 that is conserved in trypanosomatid species and higher eukaryotes (Figure 3.1) (Wright et al. 2010).

H3 N-terminus	
<b>Trypanosomatids</b>	
<i>T. brucei</i>	S R T K E T A R T K K T I T S
<i>T. cruzi</i>	S R S K E T A R S K R T I T S
<i>T. viva</i>	S R T K E T A R T K K T V T S
<i>L. donovani</i>	S R T K E T A R A K R T I T S
<b>Eukaryotes</b>	
<i>S. cerevisiae</i>	A R T K Q T A R K S T G G K A
<i>D. melanogaster</i>	A R T K Q T A R K S T G G K A
<i>H. sapiens</i>	A R T K Q T A R K S T G G K A

**Figure 3.1. Trypanosomatids and eukaryotic histone H3 N-terminus is conserved.**

Alignment of the N-terminal sequence of *T. brucei* histone H3 with corresponding histone H3 sequences of closely related trypanosomatids and higher eukaryotes. Conserved amino acids (green text) around H3 lysine 4 (highlighted in yellow) are as shown. Alignment produced using CLUSTAL multiple sequence alignment by MUSCLE v3.8.

In 2008 a chromatin immunoprecipitation study showed a marginal enrichment of the H3K4me3 modification at putative Pol II promoters in the SSRs of *Trypanosoma cruzi* genome. This lead the authors to speculate that the H3K4me3 modification may potentially play a role in transcriptional regulation (Respuela et al. 2008). A more recent study, using a mass spectrometry-based proteomics approach to map PTMs in *T. cruzi*, did not detect trimethylation of H3K4. However, the authors suggested the discrepancy in detection of the H3K4me3 PTM maybe due to either difference in the *T. cruzi* strain analysed or the experimental technique employed (Picchi et al. 2017).

In 2010 Wright and colleagues, generated an antibody to target the trimethylated and unmethylated form of *T. brucei* H3K4. Although the antibody showed specific selectivity for the trimethylated H3K4 peptide it cross-reacted with the H3K76me3 modification. Histone H3K76 is trimethylated by the HKMT DOT1B but is not essential for *T. brucei* survival (Janzen et al. 2006a). To overcome the cross-reactivity issue, ChIP-Sequencing was performed using a *DOT1B* null strain of *T. brucei*. Sequencing showed the H3K4me3 modification to be enriched at probable Pol II TSSs and regions flanking the Pol III transcribed tRNA genes (Wright et al. 2010). ChIP-Seq data was not

mapped to the *VSG* ESs as the ES are extremely similar, and the *T. brucei* strain used did not contain any unique genes to distinguish the active and silent ESs.

In addition to the H3K76 methyltransferase (DOT1B), chromatin structure, chromatin-remodelling proteins and DNA modification that have been shown to be required for the regulation of Pol I transcribed *VSG* ESs (Stanne & Rudenko 2010; Figueiredo & Cross 2010; Figueiredo et al. 2008; Narayanan & Rudenko 2013). ChIP-Seq analysis in *T. brucei* has established enrichment of both trimethylated H3K4 and acetylated H4K10 at putative Pol II TSSs, arguing that trypanosomes could utilise histone modifications to regulate transcription (Wright et al. 2010). The localisation of the H3K4me3 mark in various species has led to the general consensus that H3K4me3 is associated with the 5' end of genes actively transcribed by Pol II (Howe et al. 2017) and Pol I transcribed rDNA transcription units (McStay & Grummt 2008). Trypanosomes use Pol I to transcribe not only the active rDNA transcription units but also the active *VSG* ES (Günzl et al. 2003). Monoallelic expression of a single *VSG* ES is paramount for *T. brucei* survival within the host, as it allows for antigenic variation within the switched population to prolong host infection (Taylor & Rudenko 2006). Identification of the histone modifications that contribute to the activation or repression of *VSG* ESs may not only give further insight into ES regulation in *T. brucei* but also identify potential drug targets. In this chapter, I investigated the distribution of the H3K4me3 modification at the Pol I transcribed loci in BSF *T. brucei*.

### **3.2 - Aims and experimental outline**

The aim of the experiments in this chapter were to determine the distribution of trimethylated H3K4 within the Pol I transcribed rDNA transcription units and *VSG* ESs. To achieve this, I performed a peptide competition assay to ensure specificity of commercially available anti-H3K4me3 antibodies for the histone modification in *T. brucei*. The anti-H3K4me3 antibody and a histone H3 antibody were used for chromatin immunoprecipitation (ChIP) experiments in the isogenic *T. brucei* cell lines HNI 221+ and HNI VO2+. The drug resistance genes present in the *VSG*

---

VO2 and VSG 221 ESs provided single-copy marker genes, which were amplified by primers used for qPCR. qPCR Analysis of the immunoprecipitated material revealed the distribution of the H3K4me3 modification within the Pol I transcribed loci in BSF *T. brucei*.

### **3.3 - Validation of the VSG surface coat expressed in HNI 221+ and HNI VO2+ BSF *T. brucei* cell lines.**

The genome of the HNI *T. brucei* cell line encodes a hygromycin resistance gene (*hyg*) downstream of the VSG 221 ES promoter and a neomycin resistance gene (*neo*) in a corresponding position within the VSG VO2 ES (Figure 3.2A). Active transcription of the VSG 221 ES in HNI 221+ line and the VSG VO2 ES in HNI VO2+ cell line is maintained by positive selection for hygromycin and neomycin resistant parasites, respectively (Rudenko 1998). The selection for a specific VSG ES and the presence of the single copy marker genes enables the determination of H3K4me3 distribution within either active or silent ESs.

I established the surface coat being expressed by the HNI 221+ and HNI VO2+ parasites by immunoblot analysis and immunofluorescence microscopy using anti-221 and anti-VO2 antibodies. The immunoblot data (Figure 3.2B) showed that the HNI 221+ parasites express the VSG 221 surface coat and the HNI VO2+ cell line express the VSG VO2 surface coat. Immunofluorescence analysis of the VSG surface coat in individual cells affirmed that the HNI 221+ and HNI VO2+ cell lines are clonal (Figure 3.2C). Therefore, I can verify that the HNI 221+ and HNI VO2+ cell lines are clonal populations that express the desired VSG coat.



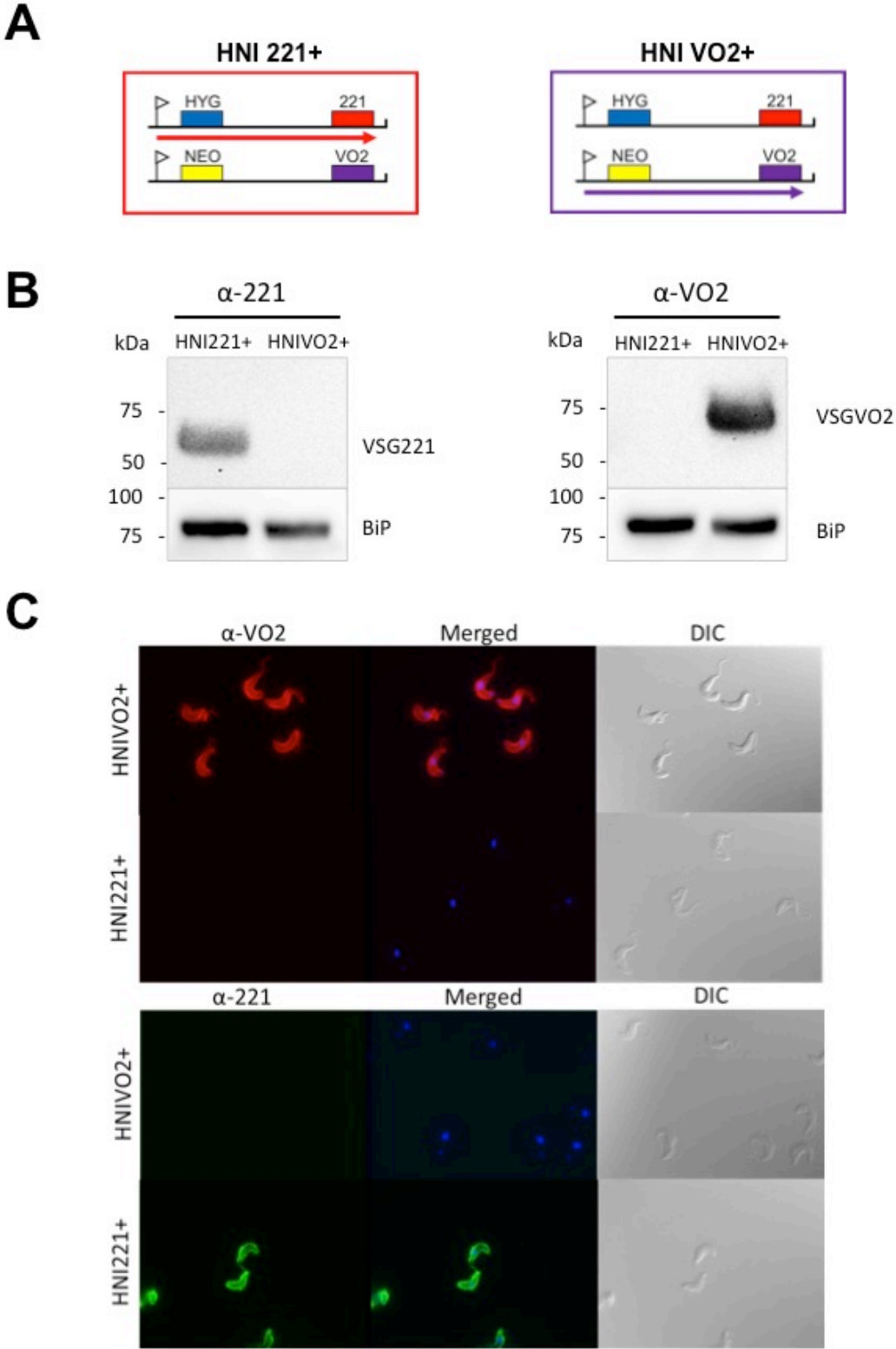


**Figure 3.2. VSG surface coat expression in the HNI 221+ and HNI VO2+ BSF *T. brucei* cell lines.**  
(A) Schematic of the HNI 221+ and HNI VO2+ cell lines. The hygromycin (*HYG*) and Neomycin (*NEO*) drug resistance genes are located downstream of the ES promoter (flag). The *VSG 221* gene and *VSG VO2* gene are shown as red and purple boxes, respectively. Active transcription of ESs is shown by the coloured arrows and the VSG surface coat being expressed is represented by the coloured

outline. (B) Immunoblot analysis of VSG surface coats expressed by HNI 221+ and HNI VO2+ cell lines. The blots loaded with lysate from  $1 \times 10^6$  cell equivalents were probed with anti-221 and anti-VO2 antibodies then stripped and probed with the anti-BiP antibody as a loading control. The size markers are indicated in kilodaltons (kDa). (C) Panels show HNI 221+ and HNI VO2+ cells stained with either anti-VO2 primary antibody conjugated to Alexa-594 secondary antibody (top panel) or anti-221(-CRD) primary antibody and Alexa-488 secondary antibody (bottom panel) visualised by Immunofluorescence microscopy. The DNA was visualised by DAPI staining and cells visualised using differential interference contrast (DIC).

### 3.4 - Evaluation of specificity of two commercially available anti-H3K4me3 antibodies

Wright and colleagues (2010) previously generated a ChIP-grade antibody specific for *T. brucei* H3K4me3. Unfortunately, the affinity purified antibody cross-reacted with the H3K76me3 modification introduced by the HKMT, DOT1B. Consequently, use of this antibody would require both alleles of DOT1B to be knocked out in the HNI 221+ and HNI VO2+ cell lines.

Given the relatively high degree of H3 N-terminal sequence conservation in trypanosomatids compared with higher eukaryotes (Figure 3.1), and the successful use of a commercial anti-H3K4me3 antibody for ChIP-qPCR experiments in *T. cruzi* (Respuela et al. 2008), I performed peptide competition assays to assess the specificity of two commercial ChIP-grade anti-H3K4me3 antibodies. A monoclonal anti-H3K4me3 antibody M04-745 (Millipore) and a polyclonal anti-H3K4me3 antibody ab8580 (Abcam) raised against the human H3K4me3 modification were assayed, using peptides synthesised to correspond to the *T. brucei* histone H3 N-terminal sequence in both the trimethylated and non-methylated states.

The results of the peptide competition experiments are shown in figure 3.3. If specific for the trimethylated H3K4 modification the anti-H3K4me3 antibodies will bind to the trimethylated peptide (H3K4me3) during the pre-incubated step of the assay. Once bound to the H3K4me3 peptide, the antibody cannot bind to the trimethylated H3K4 protein in the immunoblot, resulting in a reduction or loss of detectable signal upon immunoblot imaging. Unmodified H3K4 peptide was used as a control; antibodies specific for H3K4me3 should bind the H3K4me3 protein in the

immunoblot not the unmodified peptide resulting in detection of a clear band on the immunoblot. A decreased signal is observed in the immunoblot probed with M04-745 antibody pre-incubated with  $>3.2 \mu\text{g/ml}$  of the trimethylated peptide (Figure 3.3A) and the signal is undetectable in the blot probed with Ab8580 pre-incubated with  $10 \mu\text{g/ml}$  of modified peptide (Figure 3.3B). Thus indicating that the trimethylated peptide was recognised by the commercial anti-H3K4me3 antibodies. A comparable signal was observed in the lanes probed with the anti-H3K4me3 antibodies pre-incubated with no peptide and the unmodified H3K4 peptide (Figure 3.3), with the exception of the M04-745 antibody pre-exposed to  $3.2\text{-}10 \mu\text{g/ml}$  unmodified peptide in which a marginal reduction in signal was observed (Figure 3.3A). Collectively, these data show that the antibodies are specific for the trimethylated H3K4 in *T. brucei* but not the unmodified state (H3K4).

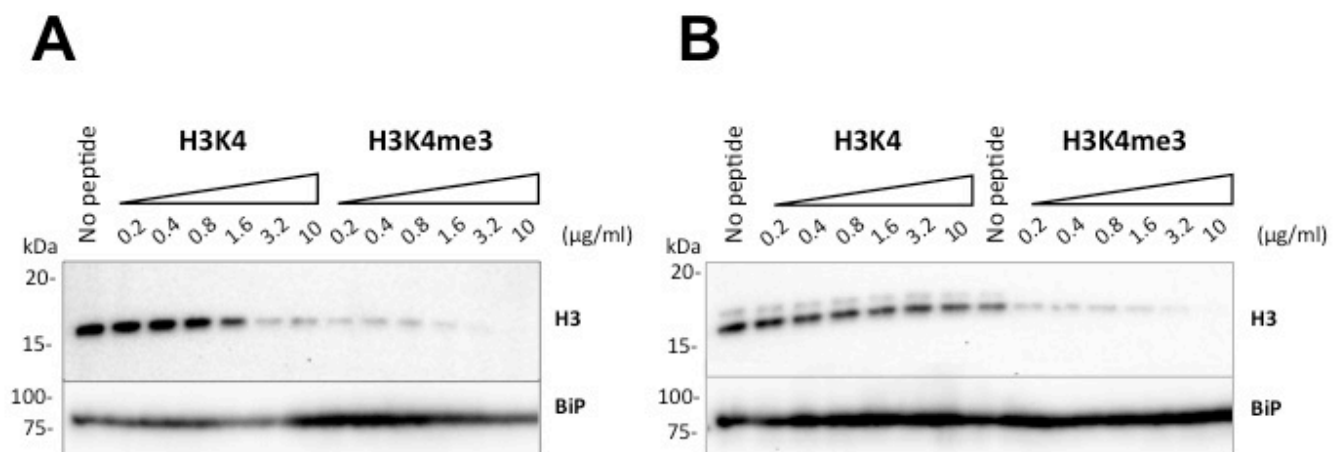


**Figure 3.3. Anti-H3K4me3 antibodies recognise trimethylation of *T. brucei* histone 3 lysine 4.**

The total cell extract from  $1.5 \times 10^7$  S16\_221PureGFP BSF *T. brucei* cells was electrophoresed and probed with either (A) the anti-H3K4me3 (M04-745) antibody or (B) the anti-H3K4me3 (Ab8580) antibody pre-incubated for 20 minutes at room temperature with either the H3K4 or H3K4me3 peptide at the concentrations indicated. Peptide sequences: H3K4me3 RT{LYS(Me3)}ETARTC; H3K4 RTKETARTC. The endoplasmic reticulum chaperone protein BiP was probed for a loading control.

### 3.5 - Viability of ChIP-qPCR to discern the distribution of trimethylated H3K4 in *T. brucei*.

In order to discern the distribution of the H3K4me3 epigenetic mark in BSF *T. brucei* Pol I transcribed rDNA transcription units and the VSG ESs, I performed ChIP using the anti-H3K4me3 antibody with the isogenic *T. brucei* cell lines, HNI 221+ and HNI VO2+. Immunoprecipitation using an anti-H3 antibody and no antibody were conducted in tandem as controls. qPCR was then used to analyse the immunoprecipitated material. As the nucleosome density varies within the genome the H3K4me3 ChIP signal was normalised relative to histone H3 allowing, for the differences in histone modification levels to be differentiated from the differences in nucleosome density.

The viability of this approach was confirmed using qPCR primers to amplify two regions of *T. brucei* chromosome 10 (Figure 3.4A); the strand switch region (SSR) is known to be enriched for the H3K4me3 modification (primer B) as well as a region approximately 1 kb outside of the SSR (primer A) (Wright et al. 2010). Analysis of the ChIP-qPCR data revealed an enrichment of trimethylated H3K4 at the SSR (~4.3% input/H3) compared with the transcription unit internal region (~0.01% input/H3) in both HNI 221+ and HNI VO2+ parasites (Figure 3.4B). The observed enrichment is in agreement with previously published data (Wright et al. 2010).

Native ChIP data, in which H3K4me3 is not normalised to histone H3 but instead both ChIP data sets are presented, as percentage immunoprecipitated minus the no-antibody control, are shown in Supplementary figure S1A. Native ChIP analysis of histone H3 showed relatively similar levels were immunoprecipitated at the SSR (~1.2% input) and internal region of chromosome 10 (~1.4% input) in both cell lines (Supplementary figure S1A). This is in agreement with the uniform histone H3 distribution over the same regions of chromosome 10 previously published by Stanne & Rudenko (2010). Therefore, ChIP-qPCR using the commercially available anti-H3K4me3 antibody (M04-745) is a viable approach to determine the H3K4me3 distribution in BSF *T. brucei*.

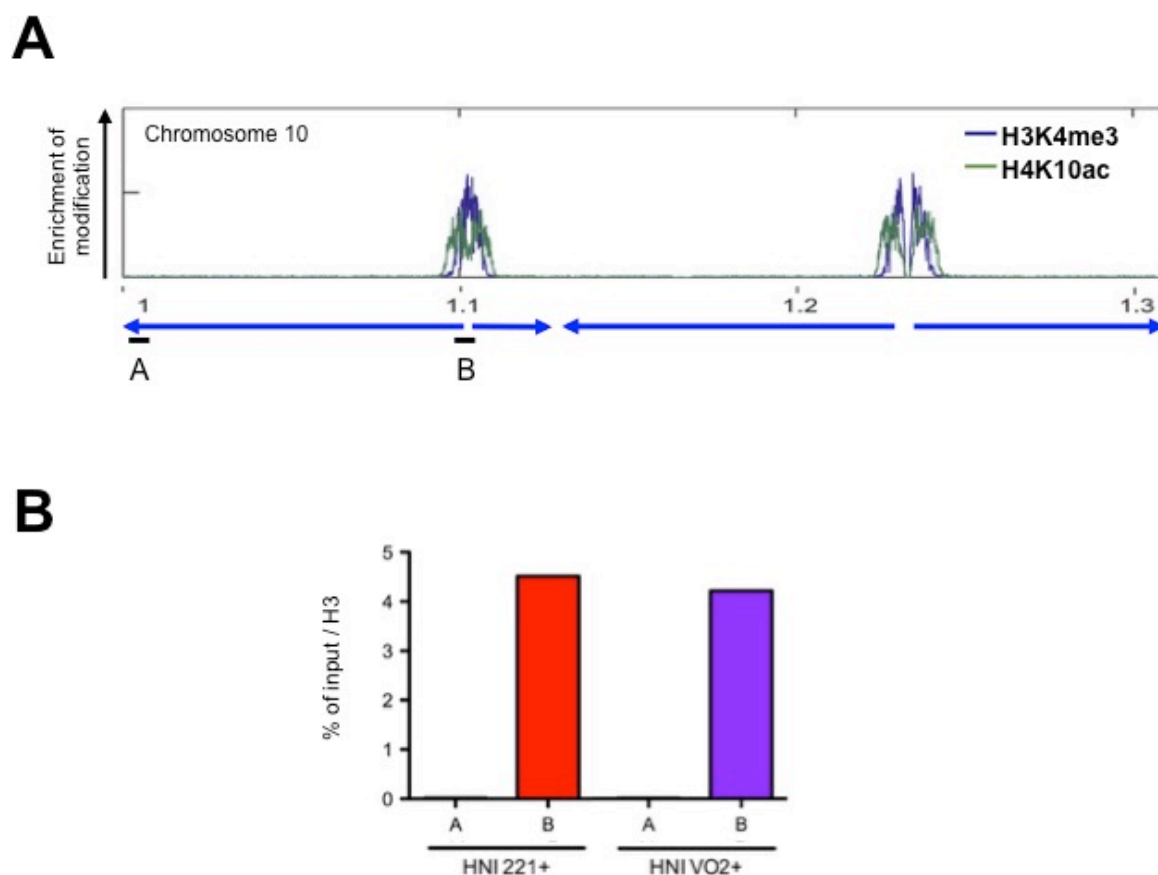


**Figure 3.4. H3K4me3 is enriched within the strand switch regions (SSRs) of *T. brucei* transcriptional start sites.**

(A) ChIP-Seq data showing enriched peaks of H3K4me3 and H4K10ac at SSRs of *T. brucei* chromosome 10 (adapted from Wright et al. 2010). Blue arrows indicate the direction of transcription. The regions amplified by qPCR primer A (C3DN\_185s/C3DN\_300as) and primer B (Dive2\_SSR\_3108s/Dive2\_SSR\_3229as) are annotated (not to scale). (B) Levels of trimethylated H3K4 normalised to histone H3 as determined by ChIP using anti-H3K4me3 and anti-H3 antibodies. qPCR primers were used to amplify the regions shown in panel A. Data is shown as the percentage of H3K4me3 input immunoprecipitated after normalisation to histone H3. Results are from qPCR analysis of ChIP material from a single immunoprecipitation experiment.

### 3.6 - Distribution of H3K4me3 within rDNA transcription units in *T. brucei*

The H3K4me3 epigenetic mark has been found to be present at the active Pol I transcribed rDNA transcription units of multiple eukaryotes (McStay & Grummt 2008). The *T. brucei* genome encodes 11-12 rDNA transcription units spread over 6-7 chromosomes (Berriman 2005). In light of this, I investigated the distribution of H3K4me3 in Pol I transcribed genes, to determine if this modification may play a role in *T. brucei* gene regulation, as has been shown in other eukaryotes. CHIP-qPCR analysis was performed using a range of primers targeting regions that span the length of the rDNA transcription unit and non-transcribed rDNA spacer of *T. brucei* (Figure 3.5A).

Both isogenic cell lines showed a 2 to 8-fold enrichment of the H3K4me3 mark in the non-transcribed rDNA spacer (~0.1-0.4% input normalised to histone H3) compared to the Pol I transcribed rDNA transcription unit (<0.06% input normalised to histone H3) (Figure 3.5B). The rDNA spacer has more trimethylated H3K4 (H3K4me3) than unmodified H3K4 within the rDNA transcription unit relative to the nucleosome density determined by histone H3 (Figure 3.5B primers A&F). However, The level of detectable H3K4me3 in the rDNA transcription unit and rDNA spacer is very low compared to the H3K4me3 enrichment observed at the SSRs (Figure 3.4B). Consequently, these data suggest trimethylation of histone H3K4 is not enriched at the Pol I transcribed rDNA transcription unit or the rDNA spacer in BSF *T. brucei*.

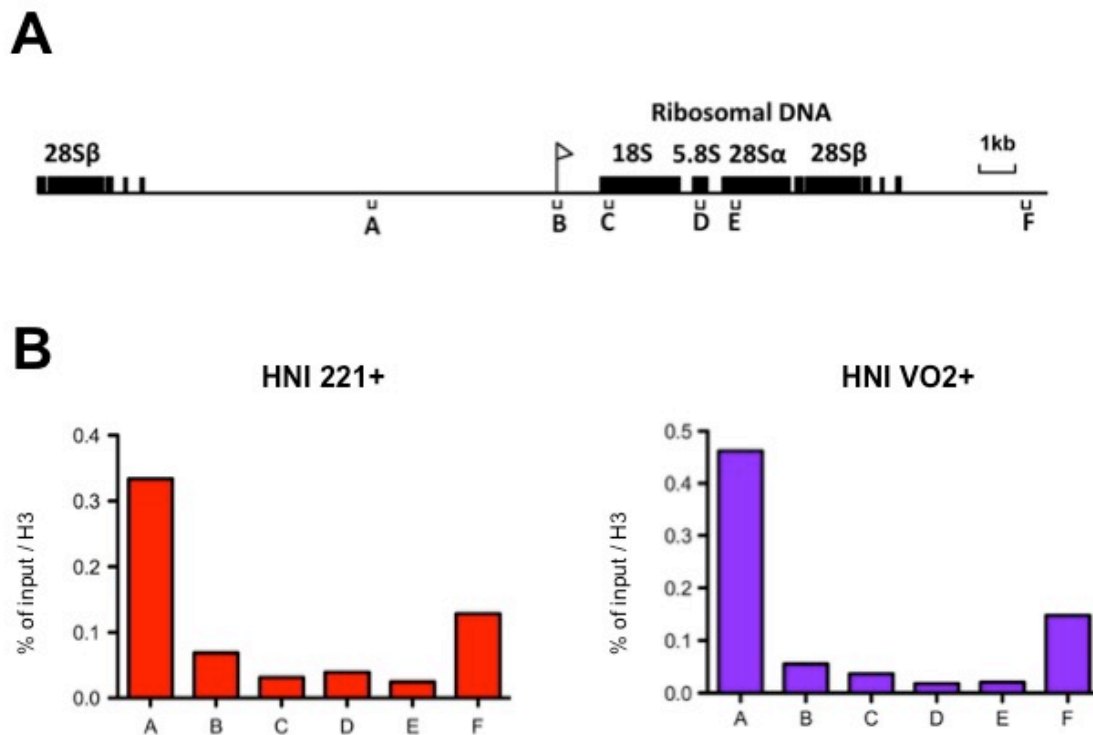


**Figure 3.5. *T. brucei* Pol I transcribed rDNA transcription units are depleted of the H3K4me3 chromatin modification.**

(A) Schematic of the *T. brucei* rDNA transcription unit (adapted from Stanne & Rudenko 2010). The rDNA genes are shown as black boxes, the flag denotes the rDNA promoter, and the regions amplified by the qPCR primers are indicated with letters. (B) The abundance of trimethylated H3K4 was determined by ChIP using an anti-H3K4me3 antibody in the isogenic HNI 221+ (red) and HNI VO2+ (purple) BSF *T. brucei*. Primers within the rDNA spacer and rDNA transcription unit were used to amplify regions of interest by qPCR. The H3K4me3 data shows the percentage of H3K4me3 input Immunoprecipitated normalised to histone H3, after subtraction of the no antibody control. The qPCR was performed using material obtained from a single ChIP experiment.

### 3.7 - Trimethylation of H3K4 in the VSG expression sites.

Unusually, trypanosomes utilise Pol I to transcribe not only the rDNA transcription units but also a single active *VSG* gene from one of approximately 15 ESs (Günzl et al. 2003; Hertz-Fowler et al. 2008). Multiple epigenetic factors have previously been shown to contribute to the monoallelic expression of the active *VSG* ES, and the H3K4me3 PTM is known to be enriched at the promoter and 5' region of active Pol I transcribed genes in other eukaryotes (Rudenko 2010; Howe et al. 2017). Therefore I investigated the distribution of the H3K4me3 modification across the ESs of the HNI 221+ and HNI VO2+ BSF *T. brucei* cell lines. The single marker genes within the ESs of these cell lines provide a unique tool to map epigenetic modifications to known active and silent ESs.

To investigate the distribution of the trimethylated H3K4 at active and silent *VSG* ESs, I performed ChIP-qPCR analysis on the marker genes and conserved ES sequences present in the HNI 221+ and HNI VO2+ cell lines (Figure 3.6A-B). Native ChIP-qPCR of histone H3 (Supplementary figure S1C right hand panel) confirmed a reduced level was observed over the “core” ES promoter (Figueiredo & Cross 2010; Stanne & Rudenko 2010) and histone H3 was depleted in the active BSF *VSG* ESs in both isogenic cell lines. The exception to this was histone H3 at the *VO2* gene in the HNI VO2+ cell line, where the percentage of histone H3 immunoprecipitated was almost half the level of histone H3 in the HNI 221+ parasites (Supplementary figure S1C primer K). However, *T. brucei* encodes two copies of the *VO2* *VSG* gene, and the qPCR primer pair K is most likely also amplifying the second *VO2* gene, located in a non-ES locus.

As the nucleosome density differs in active and silent ESs, the H3K4me3 ChIP signal was normalised to total histone H3 that was immunoprecipitated in parallel. The normalised ChIP-qPCR data, shown in figure 3.6, revealed trimethylated H3K4 within the silent *VSG* ES marker genes in HNI 221+ (Figure 3.6C primers J-K) and HNI VO2+ (Figure 3.6D primers H-I), but only at low levels. Higher levels of H3K4me3 were detected within the active 221 *VSG* ESs (Figure 3.6C primers H-I) compared to the silent *VO2* *VSG* ES in the HNI 221+ cell line (Figure 3.6C primers J-K). However, this



enrichment of H3K4me3 in the active versus silent ESs was not mirrored in the HNI VO2+ cell line data (Figure 3.6D primers H-K).

Additional ChIP-qPCR analysis was conducted using qPCR primers that recognise conserved sequences present in the majority of the ~15 known VSG ESs (Figure 3.6A) (Hertz-Fowler et al. 2008). Less than 0.08% of H3K4me3 input normalised to histone H3 was immunoprecipitated from the isogenic cell line VSG ESs (Figure 3.6C-D primers A-G). Collectively, these data indicate that the H3K4me3 epigenetic mark is detectable, but only at very levels within the Pol I transcribed VSG ESs and no consistent increase in the level of this modification was observed in either the active or silent VSG ESs in BSF *T. brucei*.

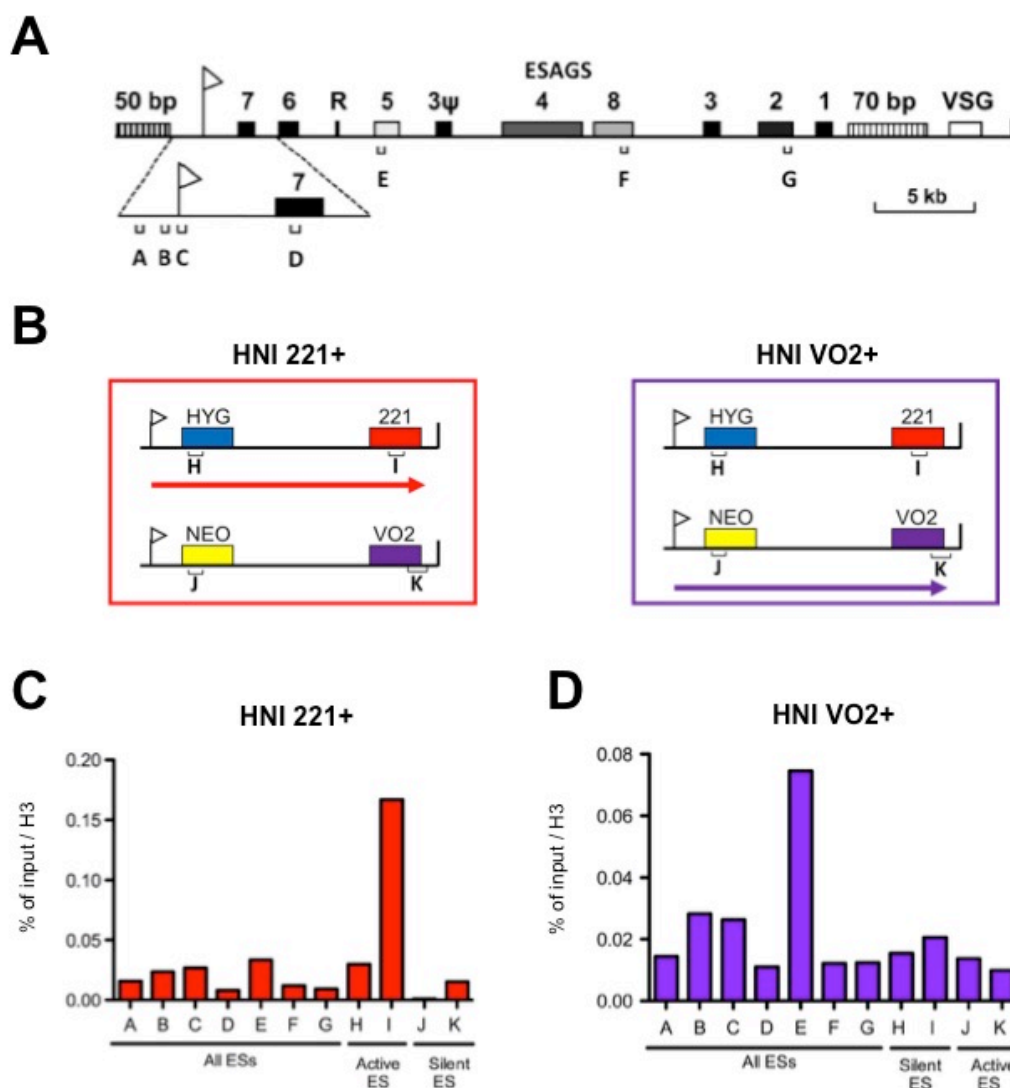


**Figure 3.6. The histone modification H3K4me3 is only detectable at very low levels at *T. brucei* ESs.** (A) A schematic of a BSF *T. brucei* expression site adapted from AnTat 1.3A (Lips et al. 1993). A flag denotes the promoter, numbered boxes indicate the expression site associated genes (ESAGS) and characteristic 50 and 70 bp repeat arrays are shown with striped boxes. Letters show primers used to amplify all ESs. The area around the ES promoter is shown in the magnified section. (Adapted from (Stanne & Rudenko 2010)). (B) HNI 221+ and HNI VO2+ cell lines, that express VSG 221 or VSG VO2 respectively, from an active ES were used to investigate the levels of H3K4me3 at active and silent ESs. The single copy *hygromycin* (HYG) and *neomycin* (NEO) resistance genes are indicated, as are the VSGs. The flag marks the ES promoter and an arrow indicates active transcription. The level of H3K4me3 normalised to nucleosome density was determined across all the ESs, including active and silent ESs, in the (C) HNI 221+ and (D) HNI VO2+ parasites by ChIP using an anti-H3K4me3 and anti-H3 antibody. The no antibody control was subtracted from the H3K4me3 and histone H3 signals and the data plotted as a percentage of H3K4me3 input immunoprecipitated divided by percentage of H3 immunoprecipitated (% of input/H3). All ES data is from qPCR of ChIP material from a single immunoprecipitation experiment.

### 3.8 - Discussion

It has been previously shown that the H3K4me3 PTM is enriched at putative Pol II TSSs in *T. brucei* (Wright et al. 2010). However, Wright and colleagues were unable to map the distribution of the H3K4me3 modification within the *VSG* ESs as the ES are extremely similar, and the *T. brucei* strain used did not contain any unique genes to distinguish the active and silent ESs. The CHIP-qPCR experiments presented in this chapter used the isogenic HNI 221+ and HNI VO2+ *T. brucei* cell lines, which contain single marker genes in known active and silent ESs. These unique sequences enabled me to performed qPCR analysis of CHIP material to determine the distribution of trimethylated lysine 4 of histone H3 at Pol I transcribed loci in BSF *T. brucei*, specifically the active and silent *VSG* ESs. Additionally, I assayed two commercial anti-H3K4me3 antibodies, which I have shown to be specific for the trimethylated form of *T. brucei* H3K4. Use of the commercial monoclonal CHIP grade H3K4me3 antibody circumvented the need to generate *DOT1B* null mutant trypanosomes; required in the previous study to overcome cross-reactivity issues of a non-commercial *T. brucei* anti-H3K4me3 antibody (Wright et al. 2010).

Nucleosomes are not equally distributed throughout the genome but are depleted at the Pol I transcribed rDNA transcription units and active *VSG* ES compared with non-transcribed genomic loci (Stanne & Rudenko 2010). As H3K4me3 is a histone modification found on the N-terminal tail of histone H3, the variability in nucleosome density must be accounted for when analysing the distribution of this epigenetic mark. This was achieved by normalising the H3K4me3 CHIP-qPCR signal to histone H3 to highlight differences in the level of the histone modification relative to nucleosome density.

All normalisation methods have drawbacks; in this instance differences in the two antibodies, such as their epitope binding kinetics, can make it complicated to quantitatively compare the qPCR signals (Haring et al. 2007). To ensure normalisation relative to nucleosome density did not distort the data; I also plotted the native CHIP data (Supplementary figure S1). Both native and

normalised ChIP data are the ChIP-qPCR signals from the histone H3 and H3K4me3 antibodies minus the signal from the no antibody control. For normalised ChIP data the H3K4me3 signal is then normalised to histone H3 and plotted as a percentage of input/H3. The data from both normalisation methods showed similar trends with regards to the distribution of H3K4me3, arguing that normalisation relative to nucleosomes was a viable method of analysing these data.

The ChIP-qPCR data presented in this chapter showed an apparent lack of detectable H3K4me3 at Pol I promoters in BSF *T. brucei*. This was unexpected as enrichment of H3K4me3 correlates with the promoter regions of transcriptionally active rDNA in other eukaryotes (McStay & Grummt 2008). When interpreting this data several factors must be taken into account. First, the qPCR primers used in this study detect most if not all of the 11-12 highly similar rDNA transcription units encoded in *T. brucei* genome (Stanne & Rudenko 2010). Second, analysis of the chromatin structure in eukaryotes suggests that only about 50% of the rDNA transcription units are actively transcribed (Conconi et al. 1989). Similar observations with regard to transcriptionally active and silent rDNA transcription units have been noted in *T. brucei* (Rudenko lab, unpublished). Third, the ChIP material is obtained from a population of ( $\sim 3 \times 10^8$ ) parasites, not a single cell. The H3K4me3 distribution is an average of multiple rDNA transcription units, which may be in an active or inactive transcriptional state, across a population of trypanosomes. Collectively, these factors limit the clarity of the interpretation of the rDNA ChIP-qPCR data. However, given the extremely low abundance of trimethylated H3K4 within the rDNA transcription unit compared to the enriched SSR, I would postulate that H3K4me3 is not enriched at rDNA loci in BSF *T. brucei*.

Uniquely, BSF *T. brucei* utilises Pol I to transcribe not only the rDNA genes but also a single VSG ES in a strictly monoallelic manner (Günzl et al. 2003). Use of isogenic *T. brucei* encoding single copy marker genes in the VSG VO2 and VSG 221 ESs, allowed the distribution of H3K4me3 at known active and silent Pol I transcribed regions to be investigated. Although H3K4me3 and H3 bound DNA is immunoprecipitated from a population of parasites, drug selection ensures that all cells within the

population express the same *VSG* ES. CHIP-qPCR analysis of the H3K4me3 modification normalised to histone H3 density showed no enrichment of the H3K4me3 modification in either the active or silent ESs of the isogenic BSF parasites.

In other eukaryotes trimethylation of H3K4 is enriched approximately 0-1kb downstream of the promoters of genes that are actively transcribed (Mikkelsen et al. 2007; Guenther et al. 2007; Kratochwil & Meyer 2015). This distribution of the H3K4me3 modification does not appear to be conserved in BSF *T. brucei*. The unique *hyg* and *neo* drug resistance genes in the isogenic *T. brucei* cell lines are present at 0.7-1kb and 0.6-1kb downstream of the *VSG 221* and *VSG VO2* ESs, respectively. The low levels of detectable H3K4me3 within the marker genes strongly suggests the H3K4me3 PTM is not enriched within this region at the 5' end of active or silent Pol I transcribed *VSG* ESs (Figure 3.6). Although marginally elevated levels of H3K4me3 were observed at the actively transcribed *VSG 221* gene in the HNI 221+ parasites (Figure 3.6), the histone modification is still diminished compared to trimethylated H3K4 at the enriched SSR (Figure 3.3).

In higher eukaryotes, the H3K4me3 modification is also enriched at the promoters of genes that are not actively transcribed but at which transcriptional initiation occurs (Guenther et al. 2007). Interestingly, some low level of transcriptional initiation occur at the promoters of all 15 silent *VSG* ESs (Vanhamme et al. 2000). To determine if the trimethylated H3K4 is enriched at sites of Pol I transcriptional initiation but not elongation; CHIP-qPCR material was analysed using qPCR primers that recognise sequences present in the majority of the *VSG* ESs. The H3K4me3 modification was only detectable at very low levels at the Pol I *VSG* ES promoter and 3.4kb downstream (Figure 3.6 primers A-D). An approximate 2.5-fold increase in the amount of H3K4me3 immunoprecipitated (0.074% of input/H3) was observed 10kb downstream of the ES promoters compared to the promoter region (Figure 3.6D primer E) but this increase is marginal compared to the enrichment of H3K4me3 at the SSR (~4.3% of input/H3). As this data is from a single biological replicate I cannot rule out the possibility that the elevated levels observed within the *VSG 221* gene in the HNI 221+

parasites (Figure 3.6C primer I) and ESAG 5 in the HNI VO2+ (Figure 3.6D primer E) are not the result of experimental variability. However, due to the apparent lack of H3K4me3 within Pol I transcribed loci in BSF *T. brucei* and the high cost of the reagents required for these experiments, no further CHIP-qPCR replicates were performed.

If accurate, the apparent lack of trimethylation of H3K4 at BSF *T. brucei* Pol I transcribed promoters is unexpected, as this epigenetic modification is associated with active transcription of Pol I and Pol II transcribed genes in eukaryotes (Howe et al. 2017). Furthermore, enrichment of the H3K4me3 modification correlates with putative Pol II transcriptional starts sites in *T. brucei*, suggesting this epigenetic mark could play a role in transcriptional initiation in trypanosomes (Wright et al. 2010). However, trypanosomes branched early in evolution and consequently some features of the epigenome that are well conserved in other eukaryotes, are divergent in *T. brucei* (Janzen et al. 2006a). Unconventionally, trypanosomes employ Pol I to transcribe surface coat protein coding genes (Günzl et al. 2003) and it is therefore plausible these parasites have also evolved an unorthodox mechanism to regulate Pol I gene expression. Although several epigenetic modifications have been identified in *T. brucei* not all have been mapped at the genome level (Mandava et al. 2007; Janzen et al. 2006b). It is therefore possible that another, potentially unidentified, alternative epigenetic mark may be correlated with Pol I TSSs in *T. brucei*.

## Chapter Four

### Small-molecule histone methyltransferase inhibitors as potential anti-kinetoplastid agents

#### 4.1 - Introduction

Human African Trypanosomiasis (HAT) is one of three kinetoplastid diseases regarded as neglected tropical diseases (NTD). HAT is endemic to Sub-Saharan Africa, several thousand new cases are reported each year (Büscher et al. 2017) and a further 70 million people are at risk of infection (Simarro et al. 2012). There are a number of drugs currently available for the treatment of both the first (hemolymphatic) and second (meningoencephalitic) stages of HAT including Suramin and Eflornithine, respectively. However, the issues associated with these commonly used treatments, include increased incidences of parasite resistance, complex administration regimes and significant side effects (Horn & Duraisingh 2014; Ferrins et al. 2013). This highlights the need for novel anti-trypanosomal chemotherapies.

In order to elude the host immune responses *T. brucei* subspecies rely on antigenic variation to prolong infection within the mammalian host. Epigenetic regulators and chromatin structure has been shown to be important in maintaining the monoallelic expression of a single *VSG* ES in *T. brucei*, a critical feature for survival through antigenic variation (Rudenko 2010). One such type of epigenetic regulator are the bromodomain proteins, which govern gene expression by binding acetylated histone lysine residues (Zhou et al. 1999). Ablation of the *T. brucei* bromodomain proteins, TbBDF2 and TbBDF3, results in upregulation of silent *VSG* genes and disruption of life cycle specific gene expression (Schulz et al. 2015). Successful reduction of parasite virulence was observed in mice infected with trypanosomes pre-treated with the bromodomain inhibitor (I-BET151). Unfortunately, I-BET151 has unfavourable affinity for the host bromodomains compared with parasite bromodomains, which has limited its *in vivo* success (Schulz et al. 2015). Nonetheless, this does demonstrate the viability of epigenetic inhibitors as a new target class of anti-trypanosomal drugs.

Aside from the *T. brucei* subspecies, two other kinetoplastid protozoan parasites are the causative agents of NTDs. *Trypanosoma cruzi* is an intracellular protozoan parasite that causes Chagas disease (American Trypanosomiasis) and is endemic to 21 countries in Latin America, with an estimated 6-7 million people believed to be infected (WHO 2017a). Cutaneous leishmaniasis and visceral leishmaniasis are the two most common disease manifestations caused by *Leishmania* parasites; the latter form of the disease is fatal without treatment. An estimated one million people are infected each year with up to 30,000 deaths occurring annually (WHO 2017b). Available treatments can be difficult to administer, cause toxicity, or are no longer effective due to parasite resistance. With only 1% of all new therapeutic agents approved over a 10-year period being recommended for treatment of these NTDs, it is evident there is a pressing need for new anti-kinetoplastid agents (Pedrique et al. 2013).

As intracellular pathogens, *T. cruzi* and *Leishmania* parasites do not undergo antigenic variation of their surface proteins to evade the host immune response. However, the surface proteins are linked to parasite virulence and pathogenicity, and epigenetic factors have a role in regulating their expression (Lopez-Rubio et al. 2007). Consequently, small molecules that inhibit epigenetic regulators and histone modifying enzymes are intriguing drug targets, such as histone deacetylase inhibitors (HDACi). Several aryltriazolylhydroxamates HDACis have anti-leishmanial activity *in vitro* comparable to the only current oral medication available to treat the visceral form of the disease, Miltefosine (Patil et al. 2010). Another potential anti-trypanosomal agent being investigated is the nonspecific HKMT inhibitor Chaetocin (Cherblanc et al. 2013). Exposure to >1  $\mu\text{M}$  Chaetocin caused impaired cell proliferation and reduced viability of *T. cruzi* epimastigotes *in vitro* (Zuma et al. 2017). These examples illustrate the possibility of developing epigenetic inhibitors to broadly target kinetoplastid disease.

There are a multitude of small molecules currently being screened as possible epigenetic targets against a plethora of human diseases. Intriguingly, Chaetocin has also been investigated as



an anti-cancer agent (Marks & Xu 2009). The anti-cancer drug Belinostat® was originally identified from a library of HDACi developed as anti-cancer therapies (O'Connor et al. 2015), however screening of the same library of HDACi led to the identification of several lead anti-trypanosomal agents. This is an interesting example of target repurposing to identify compounds with potential anti-parasitic properties avoiding the cost and time of *de novo* drug development.

The HKMT inhibitor BIX-01294 is another example of target repurposing. BIX-01294 was shown to selectively inhibit the G9a and G9a-like protein (GLP) responsible for methylation of H3K9 in humans (Kubicek et al. 2007). The BIX-01294 compound was identified by high-throughput target based screening using recombinant human G9a enzyme. Structural analysis exploring the mode of action of these inhibitors showed that the BIX-01294 inhibitor binds the peptide groove normally occupied by H3K9 and adjacent residues, thus preventing G9 methylation of the histone N-terminus (Chang et al. 2009). A study in prostate cancer cells determined that the G9a methyltransferase regulates chromatin structure and uncontrolled H3K9 methylation may promote malignancy (Kondo et al. 2008). Therefore G9a is considered an important target for anti-cancer therapies.

In addition to being a viable anti-cancer compound, the BIX-01294 inhibitor and derivatives synthesised by Dr Fuchter and colleagues (Department of Chemistry, Imperial College London) have proven to be an intriguing drug lead against an apicomplexan parasite. Trimethylation of H3K9 is known to play a role in the virulence of *Plasmodium falciparum*, leading to the investigation of BIX-01294 as a potential anti-malarial chemotherapy. The BIX-01294 compound and several derivatives of it caused rapid parasite cell death *in vivo* and *in vitro*. Predictably, treated parasites exhibited a decrease in H3K9 trimethylation, but interestingly reduced levels of H3K4me3 were also recorded in *P. falciparum* (Sundriyal et al. 2014; Malmquist et al. 2012). Additional synthetic chemistry optimisation of the BIX-01294 derived inhibitors has resulted in analogues with improved selectivity for plasmodium HKMT(s) compared to human G9a (Sundriyal et al. 2017).

Trimethylation of H3K9 has not been observed in trypanosomes but acetylated H3K9 is enriched at the origins of polycistronic transcription in *L. major* and divergent strand switch regions (SSRs) in *T. cruzi* (Thomas et al. 2009; Respuela et al. 2008). The SSRs are also enriched for methylated H3K4 in *T. brucei* and *T. cruzi*, resulting in the speculation that this modification has an important role in Pol II transcription initiation (Wright et al. 2010; Respuela et al. 2008). The anti-parasitic activity of BIX-01294 and derived compounds, as well as the observed reduction in H3K4me3 histone modification made this an interesting topic to investigate further. Therefore a collaboration between the Fuchter Group and the Rudenko laboratory (Imperial College London) was established to investigate the potential anti-trypanosomal activity of these suspected histone lysine methyltransferase inhibitors (HKMTI).

A compound library of 38 small molecules derived from BIX-01294 was synthesised by the Fuchter laboratory (Supplementary Table S1). Dr Mani Narayanan and Rudenko laboratory colleagues screened inhibitors for potential anti-trypanosomal activity against BSF *T. brucei in vitro*. The screening algorithm used is outlined in figure 4.1 (Grey boxes) and resulted in the identification of two compounds (HKMTI-1-016 and HKMTI-1-014) that show potential anti-trypanosomal activity at nanomolar concentrations. In this chapter, I conducted further characterisation of the previously identified HKMTI-1-014 compound, as well as two newly synthesised analogues HKMTI-1-017 and HKMTI-1-251 (Figure 4.1). Unfortunately, the HKMTI-1-016 compound degraded after storage at -80°C and was therefore excluded from further characterisation.

#### **4.2 –Aims and experimental outline**

The experiments presented in this chapter had two aims; first, to further characterise the HKMTI compounds previously identified to have anti-trypanosomal properties as part of a small molecule library screen. Second, to assess the anti-parasitic potential of these HKMTI compounds against other causative agents of neglected tropical diseases. To achieve this I conducted cell

proliferation and cytotoxicity assays to determine the potency of the three HKMTI compounds in BSF *T. brucei*. I investigated the effect of the inhibitors on trimethylation of histone H3 lysine 4 levels in BSF *T. brucei* using densitometry analysis of H3K4me3 specific immunoblots of treated parasites. In collaboration with colleagues at the Swiss Tropical and Public Health Institute (Swiss TPH) and Global Alliance for Livestock Veterinary Medicines (GALVmed), the potency of the three HKMTI compounds against other disease causing kinetoplastids (*T. congolense*, *T. vivax*, *T. b. rhodesiense*, *T. cruzi* and *L. donovani*) and Rat skeletal myoblasts were determined.

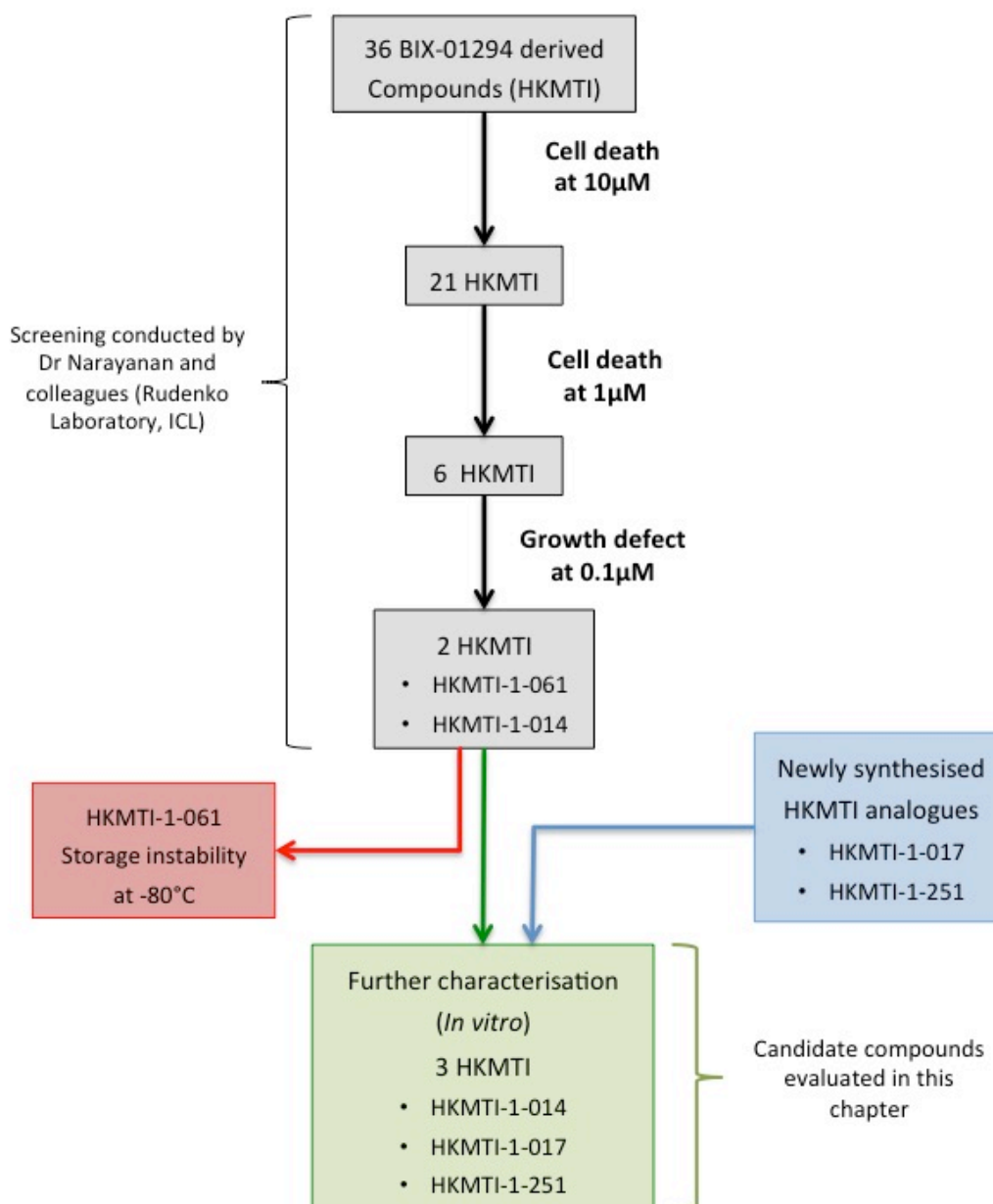


**Figure 4.1. Screening algorithm used for identification of BIX-01294 derived HKMTI with potential anti-trypanosomal activity.**

The stages of screening a 38 small molecule library synthesised by the Fuchter laboratory. Compounds were screened for BSF *T. brucei* cell death after 24 hours of exposure to 10  $\mu\text{M}$  and 1  $\mu\text{M}$  of the small molecule compounds. Further screening by Dr Mani Narayanan and Rudenko laboratory colleagues identified two HKMTI compounds that caused a growth defect after 24 hours exposure to 0.1  $\mu\text{M}$  (grey boxes). HKMTI-1-061 was discarded from further study due to storage instability (red box) and two new HKMTI analogues synthesised by members of the Fuchter laboratory (blue box) were included for further *in vitro* characterisation (green box).

### 4.3 - Efficacy of BIX-01294 derived histone lysine methyltransferase inhibitors (HKMTI) against kinetoplastid parasites *in vitro*.

In order to investigate the effect of the HKMTI-1-014 compound and the two related compounds (HKMTI-1-017 and HKMTI-1-251) on parasite growth, I monitored cell proliferation of BSF *T. brucei* exposed to a range of concentrations of the HKMTI compounds over a 48-hour period (Figure 4.2A-C). Cell proliferation of untreated *T. brucei* cultures was monitored in parallel, with parasites cultured in media containing the compound vehicle (final concentration of 0.8% DMSO) as a negative control. The anti-trypanosomal agent Suramin was used as a positive control (Figure 4.2D).

*T. brucei* proliferation was affected by exposure to HKMTI-1-014 as well as the analogues, HKMTI-1-017 and HKMTI-1-251. Parasite proliferation was reduced after incubation with 150 nM HKMTI-1-014 (Figure 4.2A) or  $\geq 50$  nM of HKMTI-1-017 (Figure 4.2B) and  $\geq 80$  nM of HKMTI-1-251 (Figure 4.2C). After 24 hours exposure to 200 nM of HKMTI-1-017 and 400 nM of HKMTI-1-251 no viable trypanosomes were observed (Figure 4.2B-C). A shorter period of 17 hours was required to kill BSF *T. brucei* cultured in media containing 200 nM of HKMTI-1-014 (Figure 4.2A). The untreated parasites and those exposed to the vehicle (DMSO) proliferated over the 48 hour period and had a doubling time of approximately 8 hours, thus indicating the compound vehicle does not have a negative effect on parasite proliferation. The proliferation assay data suggests that the HKMTI compounds kill BSF *T. brucei* in a time- and dose-dependent manner.

To assess the efficacy of the HKMTI compounds against BSF *T. brucei* I generated dose response curves using an AlamarBlue® cytotoxicity assay (Figure 4.3A-C), with the anti-trypanosomal agent Suramin as a reference compound (Figure 4.3D). Parasites were treated with two fold serial dilutions of the chemical compounds for 72 hours under standard culturing conditions and cell viability was determined after addition of the indicator resazurin to the cultures. The IC<sub>50</sub> values showed all the HKMTI compounds to be effective within the nanomolar range (Figure 4.3E), with

HKMTI-1-014 (146 nM) marginally less effective than HKMTI-1-017 (122 nM) or HKMTI-1-251 (127 nM). The Suramin  $IC_{50}$  value of 34nM was comparable to previously published data (Kibona et al. 2006).

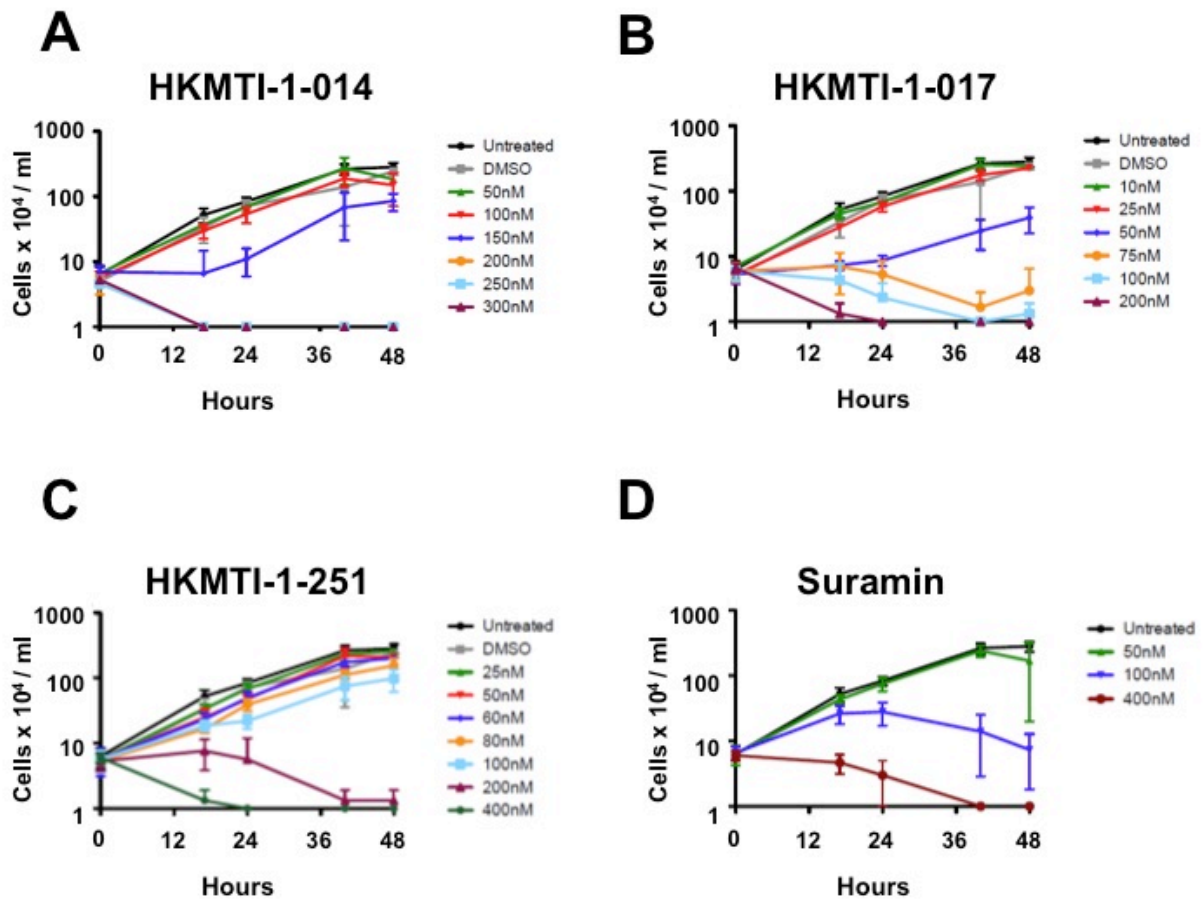
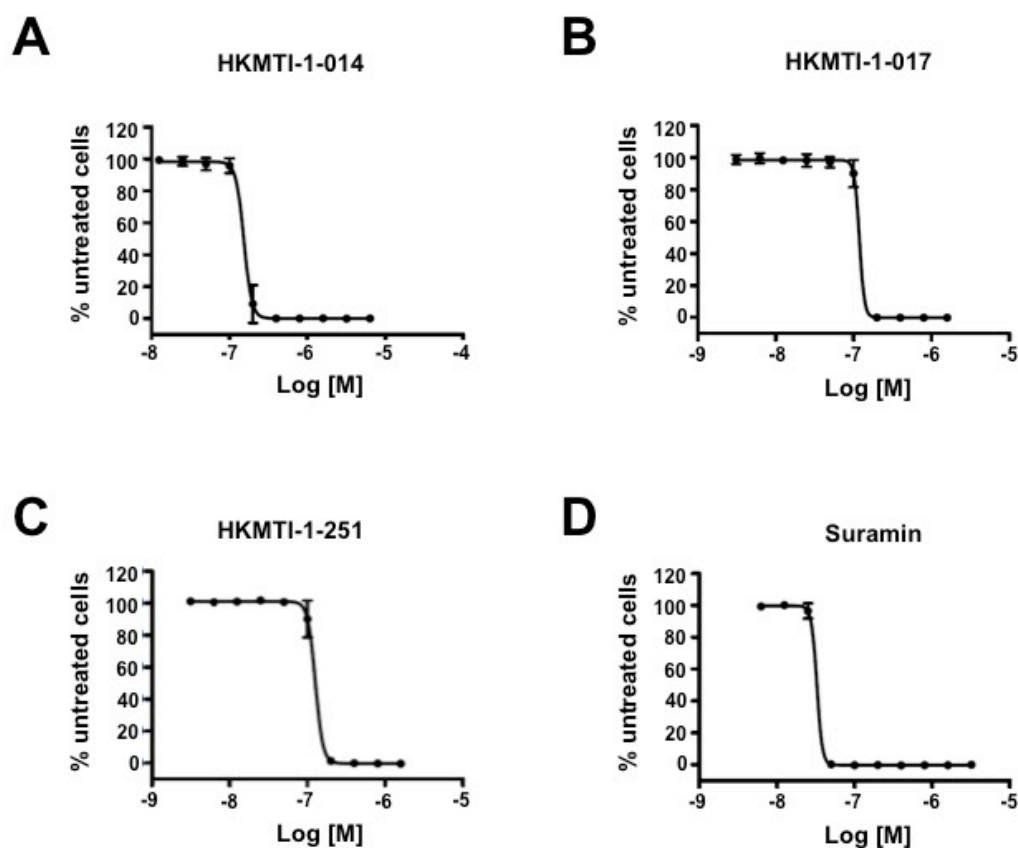


**Figure 4.2. Time- and dose-dependant trypanocidal activity of HKMTI compounds on BSF *T. brucei* *in vitro*.**

Cell proliferation assays were performed in which BSF (S16\_221PureGFP) *T. brucei* were incubated with (A) HKMTI-1-014, (B) HKMTI-1-017, (C) HKMTI-1-251 and the anti-trypanosomal agent Suramin (D) at a range of concentrations. As controls, the cell density of untreated parasites and *T. brucei* exposed to 0.8% DMSO were also monitored over a 48-hour period. The mean of three biological replicates is plotted with standard deviation indicated with error bars.



Compound	IC <sub>50</sub>		
	<i>T. brucei</i> S16 (nM ± SD)	Rat myoblast L-6 (nM ± SD)	SI
HKMTI-1-014	146 ± 26.2	948.3 ± 34.8	6.5x
HKMTI-1-017	122 ± 8.1	1070 ± 35.1	8.8x
HKMTI-1-251	127 ± 12.9	941 ± 325.9	7.4x
Suramin	34 ± 8.4	-	-
Podophyllotoxin	-	9.65 ± 1.4	-

**Figure 4.3. Toxicity of HKMTI compounds in *T. brucei* compared with mammalian L-6 rat myoblasts.**

*In vitro* cytotoxicity was assessed using an AlamarBlue® assay to determine the sigmoidal dose response curves of (A) HKMTI-0-014, (B) HKMTI-1-017, (C) HKMTI-1-251 and (D) Suramin for *T. brucei*. (E) The IC<sub>50</sub> values are the mean amount of HKMTI (nM) required to reduce cell viability by half compared to an untreated control. The L-6 rat myoblast data was obtained from collaborators at the Swiss Tropical and Public Health Institute. Toxicity of the HKMTI compounds in L-6 rat myoblast cell was determined using an AlamarBlue® assay. The mean and standard deviation from three biological replicates is shown. – Indicates data is not available. SI is selectivity index.

In collaboration with the Swiss Tropical and Public Health Institute, the toxicity of the three HKMTI compounds to the mammalian L-6 (rat skeletal myoblast) cell line was determined using an AlamarBlue® assay (Ioset et al. 2009). Podophyllotoxin was used in parallel as the reference compound for the L-6 cells. The IC<sub>50</sub> values for mammalian L-6 cell viability were approximately 6.5 to 9-fold higher than those achieved when BSF *T. brucei* were exposed to the HKMTI compounds (Figure 4.3E). Collectively, these data suggests that all three HKMTI compounds are cell permeable potent inhibitors of BSF *T. brucei in vitro*, and display favourable selectivity for trypanosomes over mammalian cells.

In light of the trypanocidal activity of the HKMTI compounds on *T. brucei*, the efficacy of these inhibitors was assessed in other kinetoplastids by our collaborators at GALVmed and the Swiss Tropical and Public Health Institute. Cytotoxicity assays were performed in accordance with the Pan-Asian Screening Network drug screening for kinetoplastid diseases guidelines (Ioset et al. 2009) and the IC<sub>50</sub> values shown in table 4.1.

	HKMTI-1-014			HKMTI-1-017			HKMTI-1-251		
	IC <sub>50</sub>		SI	IC <sub>50</sub>		SI	IC <sub>50</sub>		SI
	nM	µg/ml		nM	µg/ml		nM	µg/ml	
<i>T. brucei</i>	146	0.084	6.5x	122	0.072	8.8x	127	0.073	7.4x
<i>T. rhodesiense</i> <sup>1</sup>	31	0.018	30.9x	25	0.015	43.0x	24	0.014	38.7x
<i>T. congolense</i> <sup>1</sup>	40	0.023	24.0x	8	0.005	123.5x	12	0.007	76.3x
<i>T. vivax</i> <sup>2</sup>	88	0.051	10.8x	20	0.012	52.3x	64	0.037	14.7x
<i>L. donovani</i> <sup>2</sup>	17290	9.975	0.05x	15790	9.300	0.07x	10840	6.230	0.09x
<i>T. cruzi</i> <sup>2</sup>	3130	1.805	0.3x	3030	1.785	0.4x	3080	1.770	0.3x
Rat myoblast <sup>2</sup>	948	0.547	-	1070	0.630	-	941	0.541	-

**Table 4.1. Efficacy and toxicity of HKMTI compounds against Kinetoplastids and mammalian cells.** Our collaborators at GALVmed<sup>1</sup> and Swiss TPH<sup>2</sup> calculated the IC<sub>50</sub> values of the HKMTI compounds in several disease-causing kinetoplastids and L-6 rat myoblast cells. The IC<sub>50</sub> values are shown as both nM and µg/ml. Selectivity Index (SI) = IC<sub>50</sub> for mammalian cell lines / IC<sub>50</sub> for parasite. Standard reference compounds were used as positive controls for every assay (data not shown). Data shown is the mean of a minimum of two biological replicates.



Our collaborators at GALVmed tested the HKMTI compounds against *T. congolense* and *T. vivax*, which are the causative agent of nagana (Animal Trypanosomiasis). HKMTI-1-017 was the most potent compound, with an IC<sub>50</sub> of either 8 nM or 20 nM in *T. congolense* or *T. vivax*, respectively. However, both HKMTI-1-014 and HKMTI-1-251 had IC<sub>50</sub>s within the nanomolar range, and a favourable selectivity index (SI) of  $\geq 10$ -fold compared to L-6 rat myoblasts (Table 4.1).

The HKMTI compounds showed potent trypanosomal activity against the etiological agent of HAT, *T.b. rhodesiense* (Table 4.1). HKMTI-1-251 and HKMTI-1-017 had very similar IC<sub>50</sub> values of 24 nM and 25 nM, and HKMTI-1-014 had an IC<sub>50</sub> value of 31 nM. Consequently, all the HKMTI compounds are considered to be active based on the drug screening for kinetoplastids diseases guidelines, which suggest a compound is active if it has an IC<sub>50</sub> of  $<0.5 \mu\text{g/ml}$  (Ioset et al. 2009) (see table 4.1 for conversion of nM to  $\mu\text{g/ml}$ ). Additionally, all three HKMTI compounds had favourable selectivity for parasites (SI  $\geq 30$ -fold), well above the minimum SI of  $\geq 10$ -fold advised by the drug screening guidelines (Ioset et al. 2009).

The HKMTI compounds appear to be potent anti-trypanosomal agents against *T. brucei* and *T.b.rhodesiense*, but were only moderately active (IC<sub>50</sub> is 0.5-5  $\mu\text{g/ml}$ ) against the intracellular trypanosome, *T. cruzi* (Table 4.1). The HKMTI compounds also appear to be considerably more toxic to the L-6 rat myoblast than the *T. cruzi* cells. Our collaborators at the Swiss TPH also tested the HKMTI compounds against the axenic form of *L. donovani* (Table 4.1). All three of the tested compounds were classed as inactive against *L. donovani*, as the IC<sub>50</sub> values were  $>5 \mu\text{g/ml}$ . These HKMT compounds had poor efficacy against Leishmania parasites, and were far more toxic to the L-6 rat myoblasts than the *L. donovani* cell line.

These data show that the HKMTI compounds are potent agents against *T. brucei*, *T.b.rhodesiense*, *T. congolense* and *T. vivax*, but are not effective against *L. donovani* or *T. cruzi*. The cytotoxicity assays reveal favourable selectivity against trypanosome species that cause HAT and nagana compared to L-6 rat myoblasts (Table 4.1). However, the L-6 rat myoblast IC<sub>50</sub> values are  $<2$

µg/ml for all three HKMTI compounds, and therefore the compounds are classified as cytotoxic under the criteria developed for drug screening for kinetoplastids diseases (Ioset et al. 2009). Ultimately, the HKMTI compounds would require further synthetic chemistry optimisation to reduce their toxicity in mammalian cells.

#### **4.4 - Analysis of H3K4 trimethylation in inhibitor treated BSF *T. brucei*.**

The BIX-01294 inhibitor from which the HKMTI compounds were derived, was originally designed to target the histone methyltransferase responsible for H3K9 methylation in humans (Kubicek et al. 2007). In *P. falciparum*, BIX-01294 and derivatives cause cell death both *in vitro* and *in vivo*, which is correlated with a reduction in the levels of H3K4 and H3K9 trimethylation detected in exposed parasites (Malmquist et al. 2012). Methylation of H3K9 has not been detected in *T. brucei*, however lysine 4 of histone H3 is trimethylated by an uncharacterised histone methyltransferase(s) (Wright et al. 2010).

To determine the effect of the HKMTI compounds on trimethylation of H3K4 in BSF *T. brucei*, parasites were exposed to inhibitory concentrations of the HKMTI compounds. I collected whole cell protein lysate samples over a 24-hour period in order to assess the H3K4me3 modification using immunoblotting. The endoplasmic reticulum chaperon protein BiP was used as a loading control. The H3K4me3 signal was detected by immunoblot analysis, and then quantified by densitometry. This was normalised to the loading control, and the resulting values normalised to the untreated control for each time point (Figure 4.4). Densitometry analysis showed no time-dependent decrease in the level of detectable H3K4me3 over the 24-hour period, suggesting that the HKMTI compounds do not target the histone methyltransferase responsible for the H3K4me3 modification or related pathways.

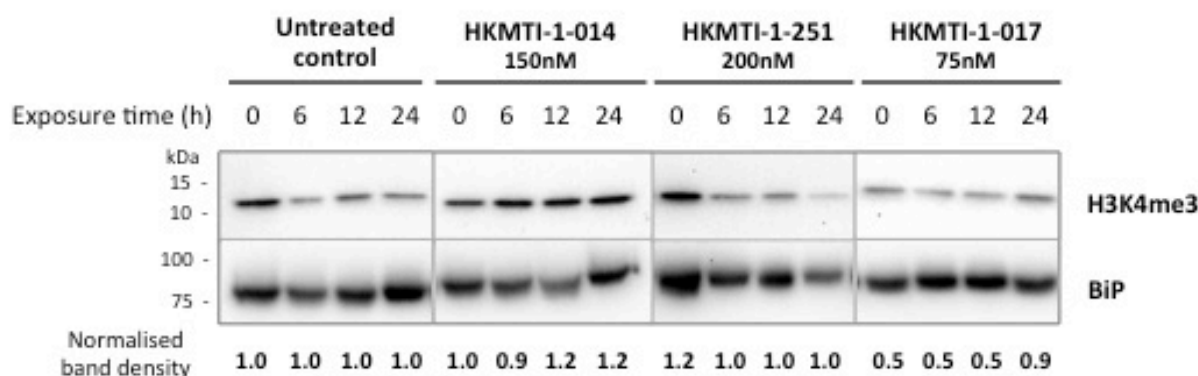


**Figure 4.4. H3K4me3 levels in HKMTI treated *T. brucei*.**

Whole cell protein lysate samples were harvested at 0, 6, 12 and 24 hours (h) after BSF *T. brucei* were exposed to the concentrations of the HKMTI compounds indicated. H3K4me3 and BiP were detected by immunoblot analysis and the band density normalised to the signal of the loading control (BiP). The resulting values were then normalised to the corresponding untreated control sample and annotated in bold under the immunoblot.

#### 4.5 - Discussion

Here, I have investigated several derivatives of the BIX-01294 compound, originally designed as an anti-cancer therapy, as potential anti-kinetoplastid agents. The BIX-01294 chemical inhibitor and derivatives were originally designed to selectively inhibit the human G9a histone methyltransferase responsible for methylation of H3K9, an important anti-cancer target (Kubicek et al. 2007). More recently these compounds were shown to cause a reduction of the H3K4me3 modification in *P. falciparum* (Malmquist et al. 2012).

In this chapter, I have shown these compounds are lethal to BSF *T. brucei* in a time- and dose-dependent manner and selectively inhibit parasite proliferation compared to a mammalian cell line. Data provided by our collaborators at GALVmed and the Swiss Tropical and Public Health Institute shows that all three of the HKMTI compounds are active against *T.b.rhodesiense*, *T. congolense* and *T. vivax*, with  $IC_{50}$  values of  $<0.5 \mu\text{g/ml}$  *in vitro*. Similar to our *T. brucei* data, these data also showed that the HKMTI compounds are more toxic to trypanosomes species compared with mammalian cells. This favourable selectivity was not observed in *T. cruzi* or *L. donovani*

cultures exposed to the HKMTI compounds. Instead the HKMTI compounds were more toxic to the mammalian cells and classed as inactive against *L. donovani* ( $IC_{50} = <0.5 \mu\text{g/ml}$ ) and only moderately active against *T. cruzi* ( $IC_{50} = 0.5\text{-}5 \mu\text{g/ml}$ ).

Interestingly, *L. donovani* and *T. cruzi* are intracellular protozoan parasites whereas the other Kinetoplastids are extracellular. However, the lack of efficacy of the HKMTI compounds against *L. donovani* and *T. cruzi* cannot simply be caused by membrane impermeability as the axenic form of *L. donovani* was used for the *in vitro* cytotoxicity assay. It is therefore more plausible that the differences in HKMTI compound potency are due to biological differences between the intracellular and extracellular parasites. For example, H3K9 is acetylated at the putative Pol II TSSs in *Leishmania* and *T. cruzi* but no PTMs of H3K9 have been mapped in *T. brucei*. Incubation with BIX-01294 and derivatives was shown to result in reduced methylation of both H3K9 and H3K4 in *P. falciparum*. It is therefore possible that the HKMTI compounds are ineffective against the intracellular protozoan parasites because they inhibit binding of histone methyltransferases rather than histone acetyltransferases to histone H3.

I observed no time dependent decrease of the H3K4me3 modification in *T. brucei* exposed to the HKMTI compounds (Figure 4.4). The immunoblot densitometry analysis assumes that the H3K4me3 modification is reduced by half every cell division (~8 hours) or the modification is being actively removed by a histone demethyltransferase (HDMT) and no functional redundancy exists for the H3K4me3 HKMT(s). The HKMT responsible for trimethylation of H3K4 in *T. brucei* has not yet been characterised (Wright et al. 2010) and the *T. brucei* genome encodes multiple SET-domain containing proteins which may be capable of H3K4 trimethylation. It is therefore possible that *T. brucei* utilises multiple SET domain containing proteins to trimethylated H3K4, as is the case for several higher eukaryotes (Ruthenburg et al. 2007) and the inhibitors do not target any or all these HKMTs. Despite these assay limitations a reduction in H3K4me3 levels was observed in *Plasmodium*

(Malmquist et al. 2012), and it is therefore unlikely that a similar reduction would not be detected in *T. brucei* if the HKMTI targeted the H3K4me3 HKMT or related pathway.

The HKMTI compound library was initially screened based on potency to rapidly identify trypanocidal compounds. The major disadvantage of this process is it selects for the most lethal chemicals rather than on-target compounds. The data in this chapter suggests the observed trypanosome cell death is most likely caused by inhibition of an alternative HKMT that is essential for extracellular trypanosome survival or has lethal off target effects. The HKMTI small molecule library may contain an inhibitor specific for targeting the HKMT(s) responsible for trimethylation of H3K4 but that this on-target compound has been overlooked due to its low potency.

All three of the HKMTI compounds have IC<sub>50</sub> values of less than 2 µg/ml in L-6 rat myoblast and are therefore classed as cytotoxic under the screening criteria outline by the Pan-Asian Screening Network (loset et al. 2009). Improved selectivity for the plasmodium parasites over human cells has already been accomplished (Sundriyal et al. 2017) and similar medical chemistry optimisation of the HKMTI compounds to improve cytotoxicity of host cells would be required for these inhibitors to proceed as anti-Kinetoplastids agents. However, the data presented in this chapter does demonstrate that with further optimisation the histone methyltransferase inhibitors may prove to be viable broad-spectrum chemotherapy against the causative agents of HAT and nagana.

## Chapter Five

### **Evaluation of RNA polymerase I inhibitors as potential anti-trypanosomal agents and as tools to investigate ESB assembly in BSF *T. brucei*.**

Parts of this chapter are published in PLoS Neglected Tropical Diseases (Kerry et al. 2017).

#### **5.1 - Introduction**

As an extracellular protozoan parasite, BSF *T. brucei* is vulnerable to the host immune system, but evades the host immune response using antigenic variation of a VSG coat (Rudenko 2010). Maintenance of the VSG coat is vital for trypanosome survival and blocking VSG synthesis triggers a pronounced cell cycle arrest *in vitro* and rapid clearance of the parasites *in vivo* (Shedder et al. 2005). Unusually, *T. brucei* utilises Pol I rather than Pol II to mediate transcription of the VSG genes (Günzl et al. 2003). Pol I is used for transcription of rDNA in trypanosomes and other eukaryotes (McStay & Grummt 2008) but the unorthodox use of Pol I to transcribe protein-coding genes is unique to trypanosomes (Günzl et al. 2003).

Pol I transcription of the active VSG ES does not occur within the subnuclear compartment of the nucleolus like the rDNA, but instead occupies an extranucleolar body, termed the Expression Site Body (ESB) (Navarro & Gull 2001). RPA2 is the second largest subunit of the Pol I complex in BSF *T. brucei*. Daniels and colleagues (2012) previously showed that N-terminal epitope-tagging of the RPA2 subunit gave a strong signal in the nucleolus corresponding to Pol I transcription of the rDNA. Additionally, an extranucleolar focus corresponding to the ESB was observed in  $67\% \pm 5\%$  of nonmitotic cells. More recently, the ESB associated protein VEX1 has been discovered to play a role in ES regulation. A single VEX1 focus was found in approximately 70% of nonmitotic cells with a increasing number of cells containing a second VEX1 focus following DNA replication (Glover et al. 2016). Epitope-tagged VEX1 and N-terminal tagged RPA2 serve as markers for the ESB and are used in this chapter to study the effect of Pol I transcription inhibition on this subnuclear structure.

Given the unique and vital role of Pol I in African trypanosomes it is perhaps surprising that such an appealing drug target has not resulted in the development of Pol I inhibitor based anti-trypanosomal chemotherapies. However, Pol I inhibitors have been extensively investigated and trialled as anti-cancer therapies (Quin et al. 2014; Hannan et al. 2013). In eukaryotic cells Pol I exclusively transcribes the rDNA, and accounts for over half of the transcription in proliferating cells (Warner 1999). The correlation between abnormal nucleoli and cancer was noted over a century ago and is now considered to be a hallmark of cancer (Pianese 1896). Abnormal nucleoli contribute to cancer by both increasing ribosome biogenesis, allowing for enhanced proliferation of cells and by interfering with the extra-ribosomal function of the nucleoli, such as regulation of tumour suppressor and oncogenes (Quin et al. 2014).

Quarfloxin (CX-3543) is one example of a chemical compound that inhibits Pol I transcription that is being investigated as a potential cancer treatment. Quarfloxin is a fluoroquinolone that specifically inhibits elongation of Pol I transcription by intercalating into guanine rich stretches of DNA. This intercalation prevents nucleolin from stabilising G-quadruplexes, which form in the guanine rich rDNA and telomeres, causing renaturation of the rDNA and rapid loss of Pol I transcription (Drygin et al. 2009). Preclinical data showed Quarfloxin that reduced cell proliferation in a large array of cancer cell lines, and had anti-cancer activity in mouse xenograft models for both pancreatic and breast cancer (Drygin et al. 2009). A phase I dose-escalation trial for solid tumours (Clinicaltrial.gov NCT00955786) (Papadopoulos et al. 2007) and a phase II trial in patients with neuroendocrine carcinoma (Clinicaltrial.gov NCT00780663) were successfully completed, but complications with bioavailability resulted in withdraw of a phase II trial in leukaemia patients (Clinicaltrial.gov NCT00485966) prior to patient enrolment (Balasubramanian et al. 2011).

Another example of a Pol I inhibitor being developed as an anti-cancer drug is CX-5461, which was identified as part of a small molecule screen to discover potential transcription inhibitors. This small molecule inhibits Pol I transcription initiation by interfering with binding of the

transcription factor SL-1 (selective factor 1) to the rDNA promoter. Akin to Quarfloxin, CX-5461 has been shown to prevent proliferation of cancer cells *in vitro* and has anti-tumour growth properties *in vivo* (Bywater et al. 2012). The CX-5461 compound is currently in phase I clinical trials against both breast cancer (Clinicaltrial.gov NCT02719977) and haematologic malignancies (Australia and New Zealand Clinical Trials Registry ACTRN12613001061729).

Similar to CX-5461, the Pol I inhibitor BMH-21 was also identified in a small molecule screen targeting the p53 tumour suppressor pathway (Peltonen et al. 2010). In eukaryotic cells the nucleoli are Pol I transcription seeded structures, as activation of the rDNA transcription machinery is required for nucleoli formation (Lam & Trinkle-Mulcahy 2015). BMH-21 intercalates into guanine-cytosine containing DNA sequences enriched in the rDNA. This blocks transcription of the rDNA and therefore results in disassembly of the nucleoli required for tumour growth (Peltonen et al. 2010; Peltonen et al. 2014). Similar to CX-5461 and Quarfloxin, BMH-21 has shown favourable selectivity and appears to discriminate between rapidly proliferating normal cells and cancer cells (Bywater et al. 2012; Drygin et al. 2009; Drygin et al. 2011). BMH-21 is currently in the preclinical stage of development as an anti-cancer therapy.

Repurposing of anti-cancer drugs as potential chemotherapies to treat parasitic diseases is well established. Eflornithine is one of the drugs routinely used to treat HAT, but was initially developed as an anti-cancer therapy (Sekhar et al. 2014). Tamoxifen is another example of an anti-cancer therapy being repurposed as an anti-parasitic agent. In this instance, Tamoxifen was developed as a hormone therapy to treat some breast cancers, but also has efficacy against several *Leishmania* species that cause the neglected tropical disease Leishmaniasis (Miguel et al. 2008a; Miguel et al. 2008b). In addition to repurposing drugs, target repurposing can also be used to exploit small molecule libraries developed against human targets. As previously discussed in chapter four, the BIX-01294 compound was originally identified in a screen for anti-cancer agents to target



human G9 histone methyltransferase, but has since shown promise as an anti-malarial agent (Malmquist et al. 2012; Malmquist et al. 2015).

## 5.2 - Aims and experimental outline

In this chapter I aimed to investigate if Pol I in BSF *T. brucei* is a druggable target by repurposing the anti-cancer Pol I inhibitors, CX-5461, Quarfloxin and BMH-21. To achieve this I conducted *in vitro* cytotoxicity assays, cell proliferation assays and wash out assays to assess the killing effect and reversibility of the Pol I inhibitors CX-5461, Quarfloxin and BMH-21 in BSF *T. brucei*. The specificity of the inhibitors in trypanosomes was investigated by RT-qPCR analysis of Pol I precursor transcript from the rDNA and 221 VSG ES, and precursor transcript of Pol II transcribed tubulin. *T. brucei* cell lines expressing either TY-YFP tagged RPA2 from the endogenous RPA2 locus or epitope-tagged VEX1 were stained with the L1C6 stain and DNA stain DAPI to visualise the nucleolus and extranucleolar ESB. Immunofluorescence microscopy analysis of the epitope tagged parasites was conducted to ascertain the effect of the Pol I inhibitors on the morphology of ESB and nucleolus in treated parasites. *In vitro* cytotoxicity assays of the Pol I inhibitors in mammalian cells were conducted by our collaborators in the Hannan laboratory (Australian National University) and our collaborators at the Drug Discovery Unit (University of Dundee) carried out initial *in vivo* studies of the CX-5461 compound. Another aim of this chapter was to investigate the hypothesis that the ESB is a transcription-seeded structure, similar to the nucleolus. This was investigated by monitoring precursor transcript and quantifying ESB reassembly in parasites immediately after removal of Pol I transcription inhibition.

### 5.3 - Efficacy of Pol I inhibitors against BSF *T. brucei* *in vitro*.

BSF *T. brucei* employs Pol I to transcribe not only the rDNA in the nucleolus, but also the single active VSG ES within the subnuclear ESB. Previous studies have shown that blocking VSG synthesis results in a precise precytokinesis cell cycle arrest *in vitro* and rapid clearance of the parasites *in vivo* (Shedder et al. 2005). This vital role of Pol I in African trypanosomes makes it an appealing drug target. The Pol I inhibitors CX-5461, BMH-21 and Quarfloxin have all been shown to prevent proliferation of cancer cells *in vitro* (Bywater et al. 2012; Drygin et al. 2009; Drygin et al. 2011). I performed cell proliferation assays to ascertain if the Pol I inhibitors had a lethal effect on BSF *T. brucei* *in vitro*, as had previously been shown for cancer cells.

In each proliferation assay *T. brucei* S16 cells were incubated with a range of concentrations of the Pol I inhibitors Quarfloxin (Figure 5.1A), BMH-21 (Figure 5.1B) and CX-5461 (Figure 5.1C). The anti-trypanosomal agent Suramin served as a lethality control (Figure 5.1D) and the cell density of all cultures was monitored over 48 hours. Parasite treatment with 300 nM Quarfloxin, 300 nM CX-5461 and 1  $\mu$ M BMH-21 resulted in suppressed proliferation over the 48 hours. No viable *T. brucei* were observed after 16 hours exposure to 1  $\mu$ M Quarfloxin, 3  $\mu$ M CX-5461 or 10  $\mu$ M BMH-21. No detrimental affect on parasite proliferation was observed in the untreated control cultures or those treated with the vehicle controls (DMSO or NaH<sub>2</sub>PO<sub>4</sub>).

In view of the lethal effect of the Pol I inhibitors, I next determined their potency against BSF *T. brucei* using an AlamarBlue® *in vitro* cytotoxicity assay. Evaluation of the dose response curves for the Pol I inhibitors Quarfloxin (Figure 5.2A), BMH-21 (Figure 5.2B), CX-5461 (Figure 5.2C) or the reference compound Suramin (Figure 5.2D) showed that *T. brucei* was sensitive to all compounds within the nanomolar range (Figure 5.2E). BMH-21 and Quarfloxin were the most efficacious inhibitors in BSF parasites with IC<sub>50</sub> values of 134  $\pm$  8 nM, and 155  $\pm$  9 nM, respectively. CX-5461 was less potent against *T. brucei* with an IC<sub>50</sub> of 279  $\pm$  16 nM. Suramin was used as a reference

compound and had an  $IC_{50}$  of  $63 \pm 5nM$ , comparable to previously published data (Gillingham & Munro 2007).

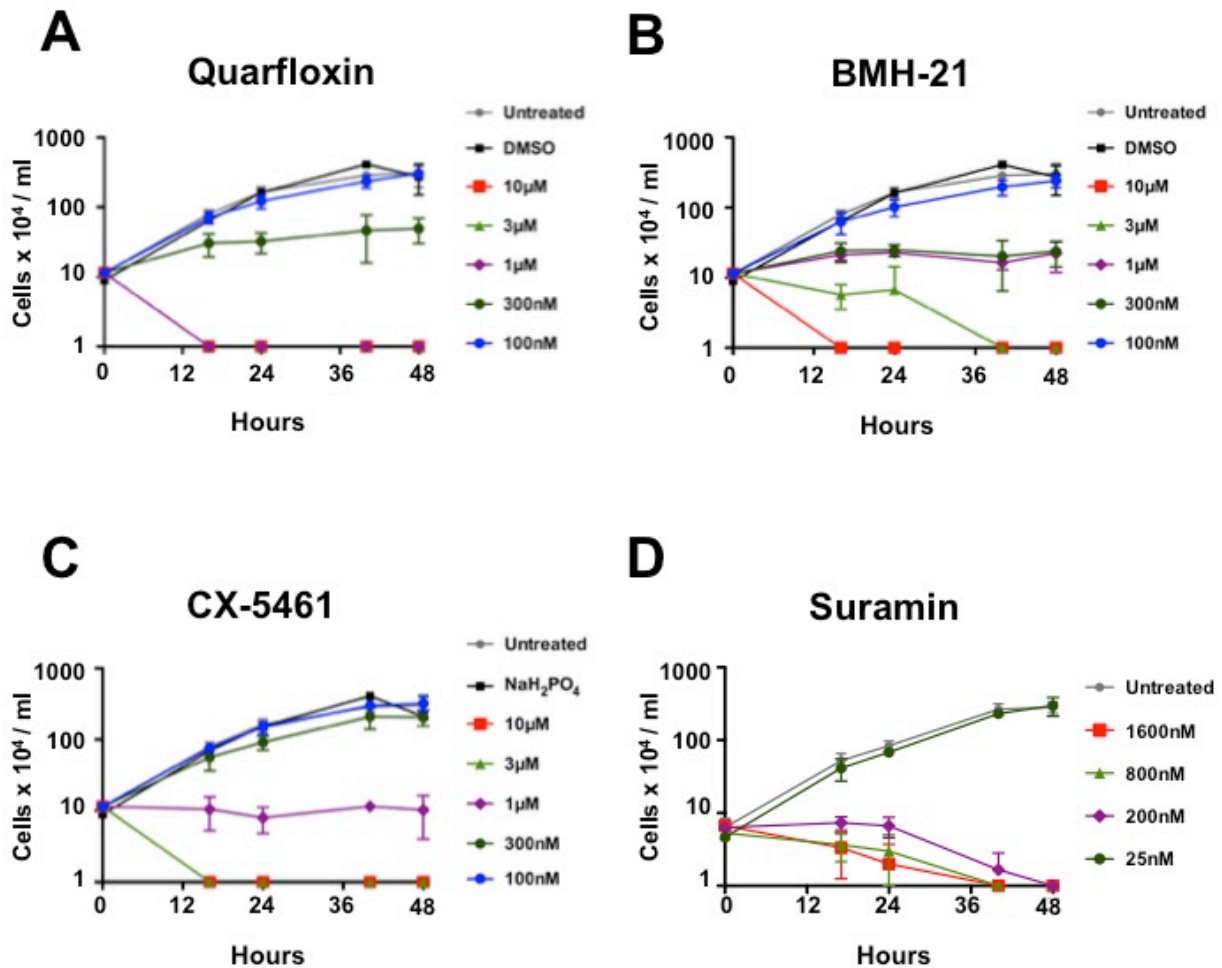


**Figure 5.1. RNA Polymerase I transcription inhibitors kill BSF *T. brucei* in a time- and dose-dependant manner.**

Cell proliferation assays were performed to determine the cell density of BSF *T. brucei* S16 cells incubated with a range of concentration of (A) Quarfloxin, (B) BMH-21, (C) CX-5461 or the anti-trypanosomal agent (D) Suramin. The cell density of untreated *T. brucei* and parasites exposed to the vehicles (DMSO or  $NaH_2PO_4$ ) are shown as controls. The mean of a minimum of three biological replicates is plotted with the standard deviation indicated with error bars.

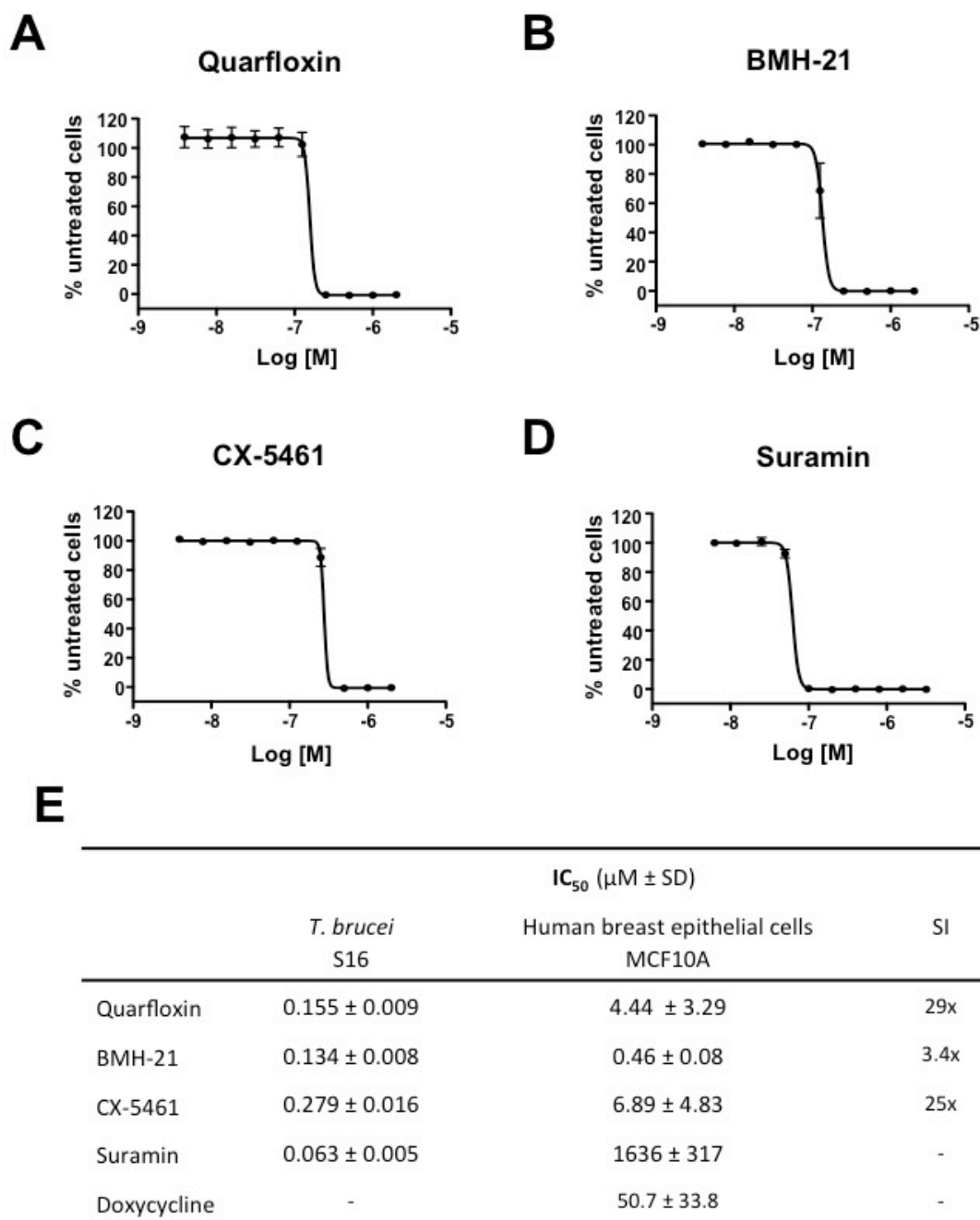


**Figure 5.2. Pol I inhibitors are potent and selective inhibitors of BSF *T. brucei* compared with human cells.**

An *in vitro* cytotoxicity assay was used to determine sigmoidal dose response curves of the Pol I inhibitors (A) Quarfloxin, (B) BMH-21, (C) CX-5461 and (D) Suramin as a reference control. The mean percentage of signal relative to the vehicle only control from three biological replicates of quadruplicate samples is plotted with the standard deviation indicated by error bars. (E) *T. brucei* IC<sub>50</sub> values were calculated from the sigmoidal dose response curves shown above. The human toxicity data was kindly provided by our collaborator Ross Hannan (Australian National University). The IC<sub>50</sub> concentrations of the Pol I inhibitors in human breast epithelial cells (MCF10A) were determined using an AlamarBlue® assay. All IC<sub>50</sub> data are shown as mean ± standard deviation of three biological replicates. – Indicates data is not available. SI is selectivity index.

To ascertain if the Pol I inhibitors had favourable selectivity against trypanosomes compared to mammalian cells, I collaborated with Ross Hannan and his colleagues in the Department of Cancer Biology and Therapeutics at the Australian National University. The Hannan laboratory tested the toxicity of the three Pol I inhibitors in the spontaneously immortalised human breast epithelial cell line (MCF10A) using an AlamarBlue® cytotoxicity assay (Figure 5.2E). Doxycycline was used as a toxicity control for the MCF10A cell line and had an  $IC_{50}$  comparable to published data (Song et al. 2014). The Pol I inhibitors Quarfloxin and CX-5461 had the most favourable selectivity index as parasites are 29-fold and 25-fold more sensitive to these compounds than the human cells. BMH-21 was the most potent inhibitor of *T. brucei* proliferation ( $IC_{50}$  134 nM), but was also toxic to human cells at nanomolar concentrations ( $IC_{50}$  460 nM) and therefore had a selectivity index of 3.4-fold. The  $IC_{50}$  data reveals which Pol I inhibitors have favourable toxicity, as they are more toxic to *T. brucei* than the human MCF10A cell line.

One of the issues with current treatments for HAT is the requirement for multiple doses over several days to be effective, as under therapeutic conditions the effective drug concentration in the blood declines over time (Büscher et al. 2017). An ideal anti-trypanosomal compound would cause irreversible commitment to cell death, as this would increase the likelihood that only a single dose would be required for HAT treatment. I therefore tested the reversibility of the Pol I inhibitors using a washout assay. BSF parasites were exposed to a range of concentrations of the Pol I inhibitors for 2 hours. Cells were subsequently washed and resuspended in inhibitor-free medium, and cell proliferation was monitored over 48 hours (Figure 5.3). Removal of Quarfloxin and CX-5461 from the cultures resulted in similar proliferation rates as previously observed in the proliferation assay in which the parasites were cultured in media containing the Pol I inhibitors (Figure 5.1 A&C). These data indicate that these Pol I inhibitors cause irreversible damage in *T. brucei*. In contrast, removal of BMH-21 at almost all concentrations resulted in restored parasite proliferation. This indicates that Pol I inhibition caused by BMH-21 is reversible. Unfortunately, this limits the therapeutic potential

of BMH-21, but the compound remains a useful biological tool to investigate the assembly kinetics of the ESB.

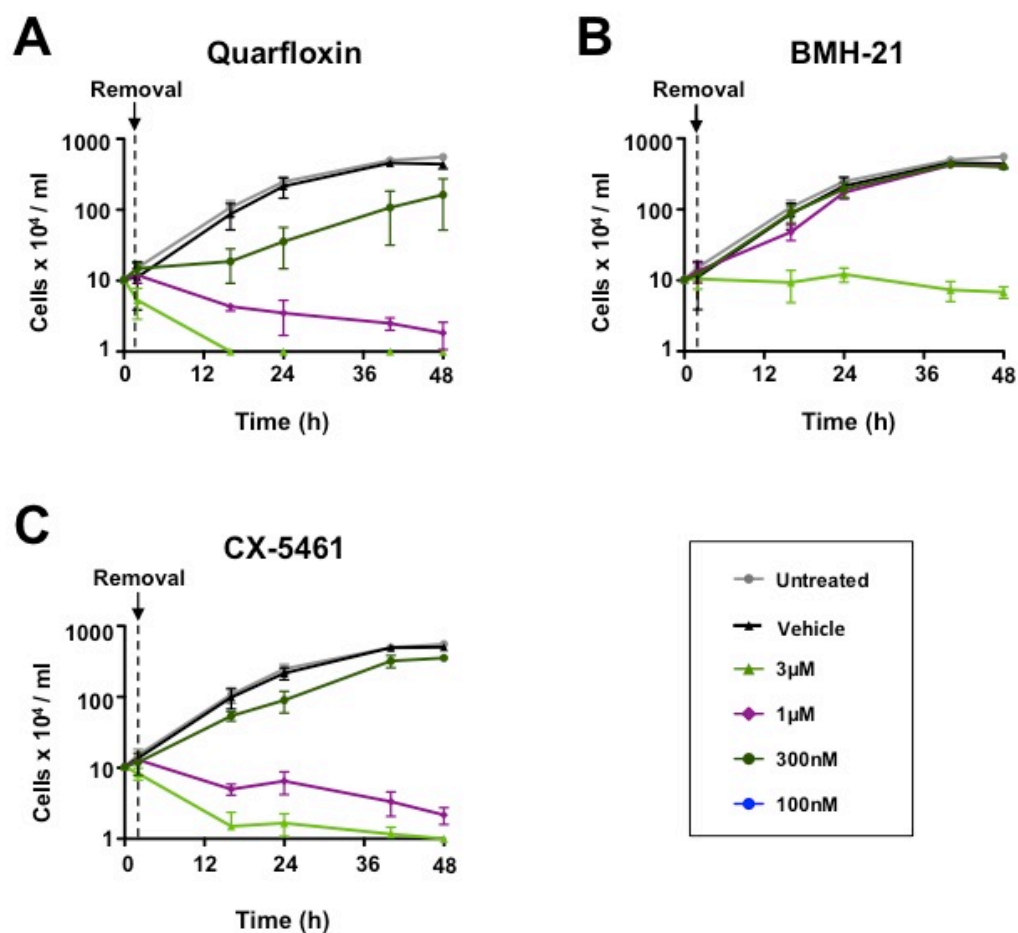


**Figure 5.3. Washout assay to determine the reversibility of Pol I inhibitors in *T. brucei*.**

*T. brucei* S16 cells were incubated with 100 nM – 3 µM (A) Quarfloxin, (B) BMH-21 and (C) CX-5461 for two hours. Parasites were then washed to remove the inhibitors prior to being cultured in inhibitor free media. The cell density of washed, untreated and the vehicle only controls (DMSO or NaH<sub>2</sub>PO<sub>4</sub>) cultures were monitored over 48 hours. The mean of three biological replicates is plotted and standard deviation indicated with error bars.

#### 5.4 – Specificity of Pol I inhibitors in BSF *T. brucei*

The inhibitors Quarfloxin, BMH-21 and CX-5461 all specifically inhibit Pol I transcription in cancer cells (Bywater et al. 2012; Drygin et al. 2009; Drygin et al. 2011). To ascertain if the inhibitors selectively target Pol I transcription in *T. brucei* I investigated transcription of the rDNA and VSG 221 ES in treated parasites. *T. brucei* precursor transcripts generated by Pol I transcription of the ten kilobase (kb) rDNA transcription units and 60 kb VSG 221 ES are rapidly processed. Pol I transcription of rDNA generates three unstable pre-rRNA precursors (Figure 5.4A) and transcription of the active VSG 221 ES also results in VSG 221 precursor transcript (White et al. 1986). The VSG 221 ES encodes a VSG pseudogene ( $\Psi$ ) approximately 4.7 kb upstream of the VSG gene (Figure 5.4B), which encodes a transcript that is rapidly degraded by nonsense mediated decay (Brojna et al. 2016). Primers previously published by Narayanan & Rudenko (2013) were used to analyse if these precursor transcripts were lost due to processing or degradation. In this chapter, these primers were used for RT-qPCR analysis to indirectly determine the level of transcription in BSF *T. brucei* treated with the Pol I inhibitors.

RNA was extracted from *T. brucei* S16\_221PureGFP cells at time zero and after 15 minutes treatment with 1  $\mu$ M of the Pol I inhibitors. RT-qPCR analysis using the primers designed against the precursor transcripts was conducted, and the RNA levels normalised to actin mRNA. The level of precursor RNA is shown as percentage relative expression compared with zero hours in figure 5.4. Incubation with 1  $\mu$ M Quarfloxin for 15 minutes caused a significant ( $P = <0.001$ ) decrease in pre-rRNA precursors detected in *T. brucei*. Pre-rRNA precursor transcript 1 was reduced by 98% with precursor transcripts 2 and 3 being reduced by 83-91% compared to zero hours (Figure 5.4D primers a-d). RT-qPCR analysis of the VSG 221 precursor transcript and unstable VSG pseudogene transcript revealed a significant ( $P = <0.001$ ) reduction of transcript in Quarfloxin treated parasites of 95% and 92%, respectively (Figure 5.4D primers  $\Psi$  and 221). Primers targeting the  $\alpha/\beta$ -tubulin precursor transcripts generated by Pol II transcription of the tubulin array, were used as a control for Pol II

transcription (Figure 5.4C). No reduction in the levels of Pol II derived tubulin precursor transcript was observed in *T. brucei* incubated with 1  $\mu$ M Quarfloxin for 15 minutes (Figure 5.4D primer tub).

This pronounced inhibition of Pol I transcription at 15 minutes was also observed in *T. brucei* exposed to 1  $\mu$ M of BMH-21 or CX-5461 when compared to the zero hours transcription. Pre-rRNA precursor transcript was reduced by up to 98% after treatment with BMH-21 (Figure 5.4E) and a reduction in transcript levels of 89-97% after exposure to CX-5461 were observed (Figure 5.4F). Pol I specific inhibition of transcription was noted for the *VSG 221* ES, but not the Pol II transcribed tubulin array in *T. brucei* treated with BMH-21 or CX-561 (Figure 5.4E-F).

In order to ensure that the selective reduction of Pol I derived precursor transcript was not simply an artefact of cell lethality induced by treatment with the Pol I inhibitors, RT-qPCR analysis of precursor transcript from parasites treated with the anti-trypanosomal agent Suramin was conducted in parallel (Figure 5.4G). No statistically significant reduction in the levels of Pol I or Pol II derived precursor transcript was observed after 15 minutes exposure to a lethal concentration (800nM) of Suramin. These data suggest that the loss of Pol I derived precursor transcript is not a consequence of cell death, but rather that all three Pol I inhibitors cause rapid and specific inhibition of Pol I transcription in *T. brucei*. The RT-qPCR analysis of precursor transcript from parasites treated with the Pol I inhibitors Quarfloxin, CX-5461 and BMH-21 confirms that these inhibitors specifically block Pol I transcription in BSF *T. brucei* but do not have an inhibitory effect on Pol II transcription.



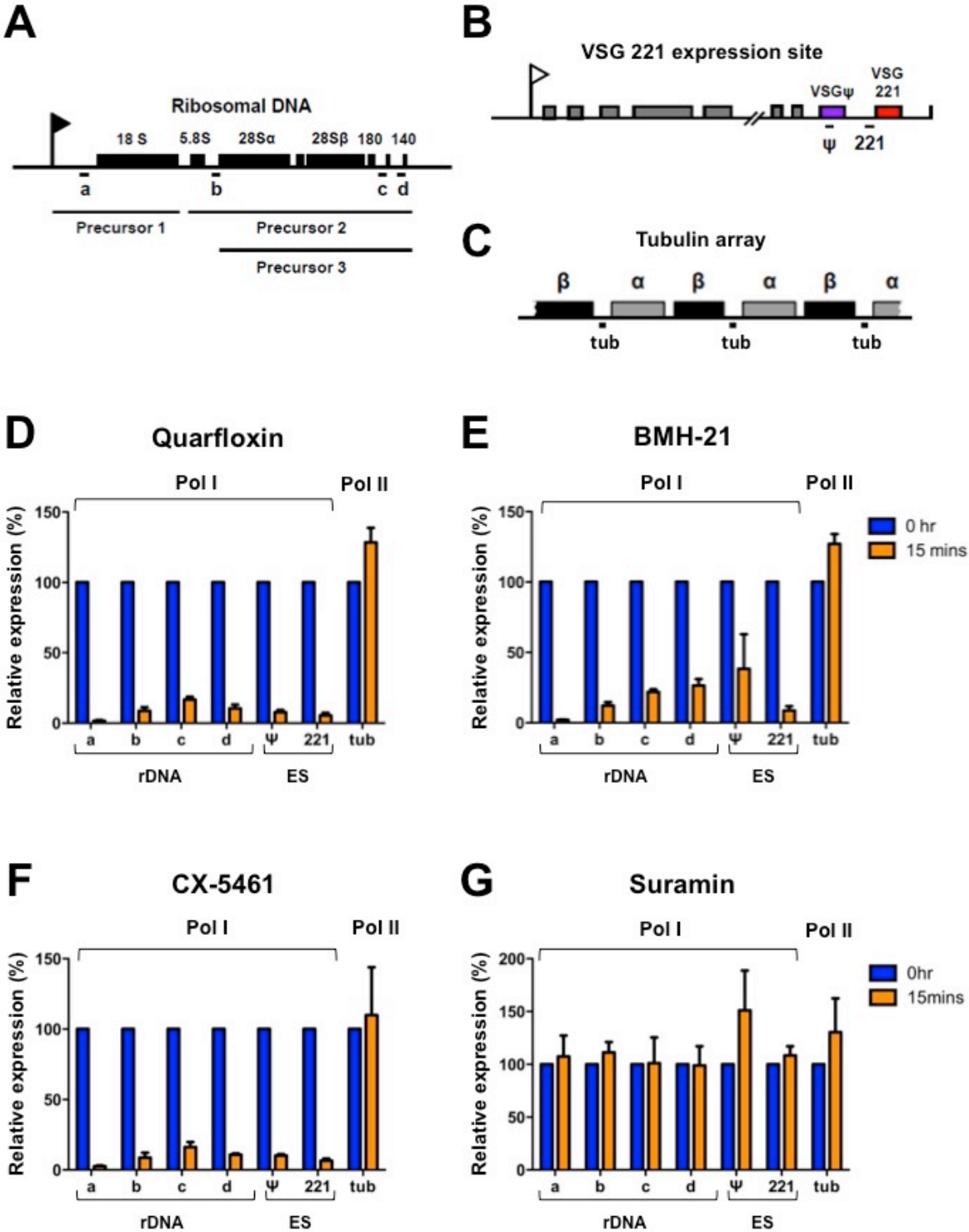


**Figure 5.4. Pol I inhibitors cause rapid and specific inhibition of BSF *T. brucei* Pol I transcription.** (A) Schematic of the *T. brucei* rDNA transcription unit. The promoter is shown as a flag, the rRNA genes are represented as black boxes and letters indicate the primers used to detect precursor transcript. (B) Schematic of the *VSG 221* ES. A flag indicates the promoter, the ESAGs are shown as grey boxes, the *VSG* pseudogene ( $\Psi$ ) is shown in purple and the *VSG* gene (221) is shown in red. (C) Schematic of the tubulin array composed of  $\alpha$ - and  $\beta$ -tubulin genes annotated with the intergenic regions used to assess the level of tubulin precursor transcript (tub). The *T. brucei* S16\_221PureGFP

cell line was exposed to 1  $\mu$ M (D) Quarfloxin, (E) BMH-21, (F) CX-5461 and (G) 800 nM Suramin for 15 minutes. RT-qPCR analysis was performed to quantify the levels of rDNA (a-d), ES ( $\Psi$  and 221) and  $\alpha/\beta$ -tubulin (tub) precursor transcript at zero hours and 15 minutes. RNA was normalised to actin mRNA levels, which are stable during Pol I inhibitor treatment. Data is shown as relative expression in treated parasites compared to untreated at zero hours and plotted as mean of three biological replicates  $\pm$  standard deviation.

### 5.5 - Effect of CX-5461 on parasitaemia in *T. brucei* infected mice.

Both the Pol I inhibitor Quarfloxin and CX-5461 are potent, selective inhibitors of *T. brucei* Pol I. Treatment of BSF *T. brucei* with these Pol I inhibitors *in vitro* results in irreversible parasite cell death at nanomolar concentrations. Cytotoxicity assays have shown favourable selectivity, as these compounds are more toxic to *T. brucei* than to mammalian cells *in vitro*. In view of this we sent samples of Quarfloxin and CX-5461 to our collaborators at the Drug Discovery Unit (University of Dundee) to assess the efficacy of the Pol I inhibitors in a stage I mouse model of Human African Trypanosomiasis. Unfortunately, the Quarfloxin sample was degraded during preparation of the stock solution resulting in the Quarfloxin *in vivo* study being abandoned. However, the *in vivo* study of CX-5461 efficacy against *T. brucei* infection was completed.

For the initial CX-5461 study, our collaborators at the Drug Discovery Unit infected ten female Balb/c mice with *T.b.brucei* 427 strain ( $1 \times 10^4$  parasites per mouse) and the level of parasitaemia was checked three days post-infection. The infected mice were dosed once daily commencing three days post-infection. Of the ten mice, five were treated orally with CX-5461 (40 mg/kg) and the remaining five mice were treated with the vehicle  $\text{NaH}_2\text{PO}_4$  as the control group. The increase in parasitaemia in the CX-5461 (40 mg/kg) treated group correlated to the parasite proliferation observed in the vehicle control group. By four days post infection, the level of parasitaemia had exceeded  $1 \times 10^8$  parasites/ml in one mouse in the CX-5461 group and one mouse in the vehicle group. As these mice would not survive a further 24 hours they were euthanized. After five days of infection, parasitaemia in the remaining mice treated with CX-5461 (40 mg/kg) or the

vehicle ( $\text{NaH}_2\text{PO}_4$ ) exceeded  $1 \times 10^8$  parasites/ml and consequently all remaining mice in this study were euthanized. A possible explanation for the lack of efficacy of CX-5461 is poor bioavailability. Pharmacokinetic data provided by our collaborators (Drug Discovery Unit) show that the concentration of CX-5461 exceeded the EC99 level shortly after oral dosing (~2 hours), however the CX-5461 concentration in the blood dropped below the EC99 after approximately 4 hours. It is therefore likely that the lack of efficacy observed is due to an insufficient concentration of CX-5461 in the blood over the period required to effectively kill *T. brucei*.

In light of the pharmacokinetics data, our collaborators at the Drug Discovery Unit conducted a second *in vivo* experiment using a higher dose of CX-5461. In this experiment a total of six mice were treated orally with either a single dose of CX-5461 (120 mg/ml) or the vehicle ( $\text{NaH}_2\text{PO}_4$ ) three days post-infection with *T.b.brucei* 427 strain. Unfortunately, all three mice in the CX-5461 (120 mg/kg) group and the three mice in the vehicle group had to be euthanized 24 hours after dosing as parasitaemia exceeded  $1 \times 10^8$  parasites/ml. Our collaborators did not collect pharmacokinetic data for this study.

The failure of CX-5461 to reduce or clear parasitaemia in *T. brucei* infected mice is most likely due to poor bioavailability of CX-5461 *in vivo*. However, one cannot rule out the possibility that the unfavourable efficacy observed in mice resulted from a biological mechanism activated in *T. brucei* during host infection, which bypasses or prevents CX-5461 induced Pol I inhibition *in vivo* but not *in vitro*. Pol I inhibitors are an intriguing drug lead but further investigation into the pharmacokinetics and mechanism of action in *T. brucei* is required for these inhibitors to progress as an anti-trypanosomal agent.

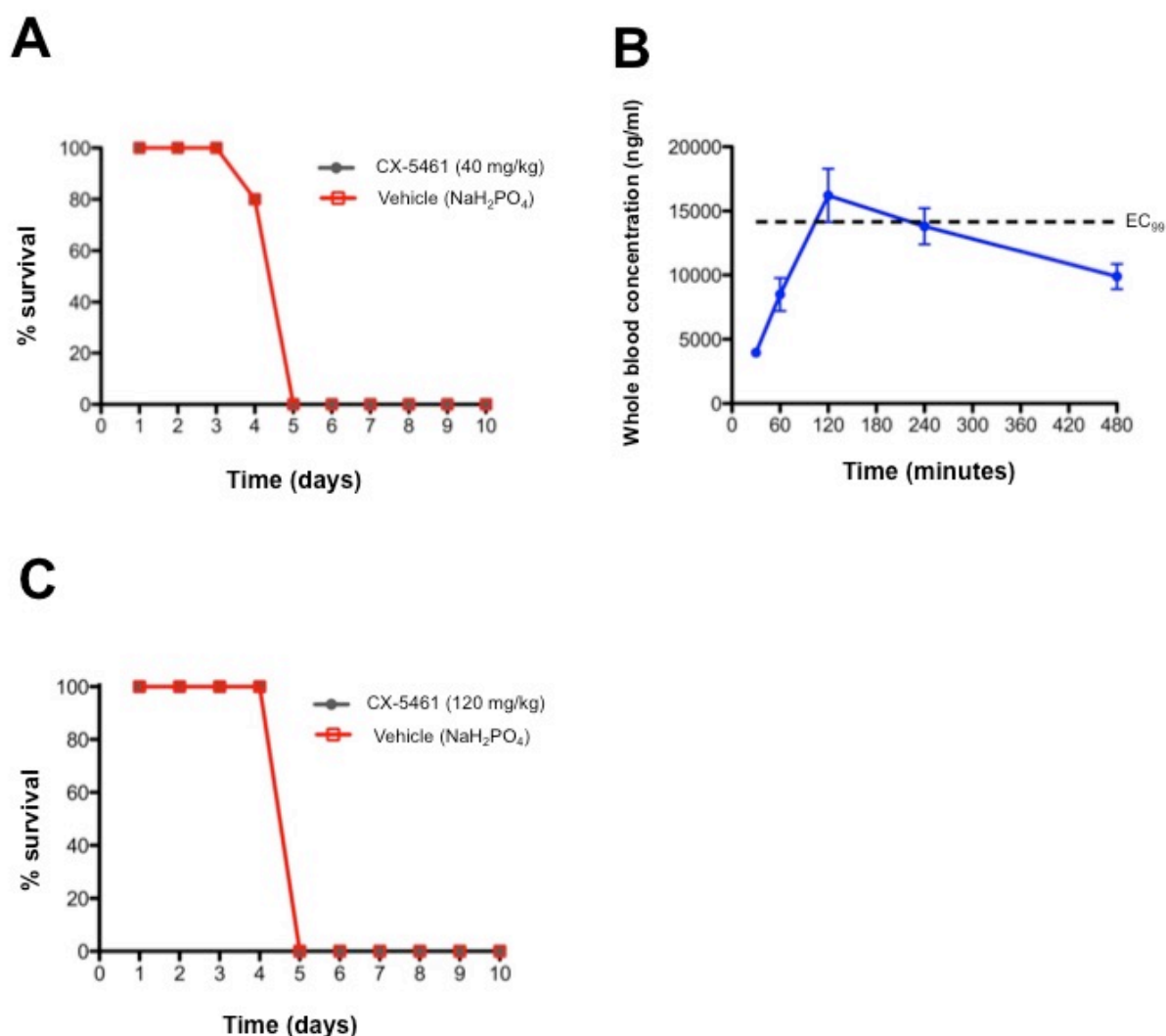


**Figure 5.5. Efficacy of CX-5461 in a stage I mouse model of Human African Trypanosomiasis and corresponding pharmacokinetic data.**

Mice were infected with *T.b.brucei* 427 at time zero and treated orally with either 40 mg/kg of CX-5461 daily, commencing three days post-infection or a single dose of 120 mg/kg three days post-infection. Parasite burden was assessed three days post-infection and (A) mouse survival after dosing with 40 mg/kg of CX-5461 was monitored thereafter. (B) Pharmacokinetic properties of CX-5461 compound delivered orally. The concentration of CX-5461 present in the blood was monitored over 480 minutes after dosing with 40 mg/kg CX-5461 3 days post-infection. The mean blood concentration of CX-5461 is shown and standard deviation indicated with error bars. The EC<sub>99</sub> value of CX-5461 is shown as a dotted line and was calculated from *in vitro* data using the EAnything algorithm in GraphPad Prism version 5. (C) Survival data for mice dosed with 120 mg/kg of CX-5461. The compound vehicle (NaH<sub>2</sub>PO<sub>4</sub>) was used to dose mice in the control groups. Our collaborators at the Drug Discovery Unit at the University of Dundee kindly provided the raw data for this figure.

## 5.6 - Effect of Pol I inhibitors on the ESB and nucleolus.

Although the therapeutic potential of the Pol I inhibitors Quarfloxin, CX-5461 and BMH-21 as anti-trypanosomal agents may be limited, these compounds have provided us with a useful tool to investigate the assembly kinetics of the ESB and nucleolus in *T. brucei*. In eukaryotes the nucleolus is a transcription-nucleated structure and its integrity relies on active rRNA synthesis. Consequently one of the indicators of inhibited Pol I transcription is nucleolar disassembly (Lam & Trinkle-Mulcahy 2015). In view of this I investigated the effect of Pol I inhibition on both the nucleolus and ESB using immunofluorescence microscopy analysis of BSF *T. brucei* treated with the Pol I inhibitors. Additionally, the reversibility of Pol I inhibition caused by BMH-21 treatment was exploited to ascertain if the ESB and nucleolus are transcription nucleated structures in *T. brucei*.

*T. brucei* Pol I is comprised of approximately 12 subunits of which RPA2 is the second largest (Schimanski et al. 2003). RPA2 has previously been endogenously tagged at the N-terminus with a TY-YFP epitope tag allowing for visualisation of signal corresponding to the nucleolus in all cells and the ESB in  $67 \pm 5\%$  of nonmitotic cells (Daniels et al. 2012). The Rudenko laboratory generated BSF *T. brucei* expressing TY-YFP tagged RPA2 from the endogenous RPA2 locus as previously described by (Daniels et al. 2012). The TY-YFP-RPA2 cell lines showed no growth defects and the tagged RPA2 subunit showed the expected Pol I localisation to the nucleolus and ESB.

In the following experiments I have used the TY-YFP-RPA2 cell line in conjunction with the DNA stain DAPI and L1C6 nucleolar marker to monitor the integrity of the nucleolus and ESB after treatment with the Pol I inhibitors. Figure 5.6 shows representative immunofluorescence microscopy panels of nonmitotic (G1 stage) *T. brucei* cells treated with 3  $\mu$ M Quarfloxin (A), BMH-21 (B), CX-5461 (C) and 800 nM Suramin (D) over a three hour period. Using DAPI staining, the *T. brucei* nucleus can be seen as a large stained focus, with the smaller focus indicating the kinetoplast (mitochondrial DNA). The nucleolus is visualised by YFP fluorescence from the tagged RPA2 subunit,

which co-localised with the L1C6 nucleolar marker (Figure 5.6 0 hour). The ESB is discernable by YFP fluorescence detected as an extranucleolar focus within the nucleus (Figure 5.6 white arrow heads).

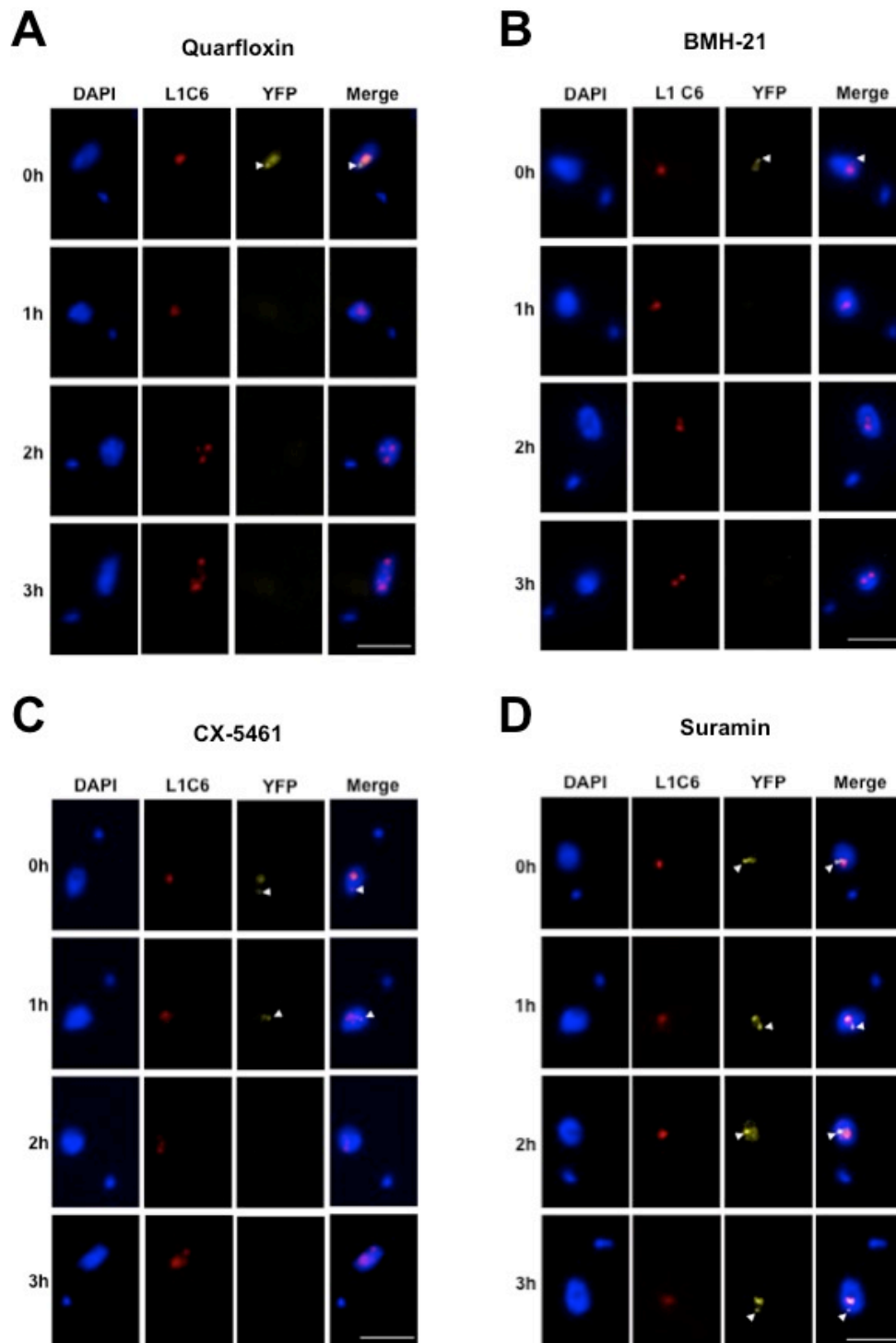


**Figure 5.6. Pol I inhibition causes disassembly of the nucleolus and loss of the ESB.**

Immunofluorescence microscopy panels of the TY-YFP-RPA2 cell line incubated with 3  $\mu$ M (A) Quarfloxin, (B) BMH-21 and (C) CX-5461 over a 3-hour period. (D) *T. brucei* cells were also treated with 800 nM of the trypanocidal agent Suramin. The panels show representative images of BSF *T.*

*brucei* cells in the G1 stage of the cell cycle. Cells are stained with DAPI (blue) and L1C6 (red) to visualise DNA and the nucleolus, respectively. Pol I is visualised by endogenous expression of YFP from the epitope-tagged RPA2 gene. YFP signal corresponds to Pol I within the nucleolus and the extranucleolar ESB is indicated with a white arrowhead. Scale bar is 5  $\mu\text{m}$ .

Immunofluorescence microscopy analysis of treated cells revealed incubation with 3  $\mu\text{M}$  of the Pol I inhibitors resulted in disassembly of the nucleolus into multiple L1C6 positive foci (Figure 5.6A-C). Quantification of the number of L1C6 positive foci within the nucleus of *T. brucei* showed an increase in the mean number of L1C6 dots from around one dot per cell at zero hours to three dots per cell after 3 hours incubation with 3  $\mu\text{M}$  Quarfloxin (Figure 5.7A). Treatment with 3  $\mu\text{M}$  BMH-21 and CX-5461 also resulted in the nucleoli fragmenting, observed by a 2 to 3-fold increase in the number of L1C6 positive foci from zero to three hours (Figure 5.7B-C). Similar nucleolar disassembly was recorded in *T. brucei* incubated with 300 nM and 1  $\mu\text{M}$  of the Pol I inhibitors (Supplementary Figure S2). In contrast, treatment with the trypanocidal agent Suramin (800 nM) resulted in no significant change to number or morphology of the nucleoli (Figure 5.6D & 5.7D). This suggests that nucleolar disassembly is not merely a consequence of cell death but rather a specific morphological change resulting from Pol I inhibition.

Next, in order to ascertain if the ESB is a transcription-nucleated structure, like the nucleolus, the number of extranucleolar YFP positive foci (ESB) present in *T. brucei* TY-YFP-RPA2 cells treated with a range of Pol I inhibitor concentrations and Suramin (800 nM) was quantified (Figure 5.6 white arrow head). The graph in Figure 5.8 shows this quantification as the percentage of cells in the G1 stage of the cell cycle with an ESB after exposure to the Pol I inhibitors. I observed  $64 \pm 17\%$  of untreated (0 hour) cells contained an ESB, which is comparable to the  $67 \pm 5\%$  previously published by (Daniels et al. 2012).

Inhibition of Pol I transcription caused by exposure to the Pol I inhibitors resulted in a decrease in the number of cells with a visible ESB. After 1-hour treatment with 300 nM Quarfloxin

the percentage of cells with an ESB had halved ( $64 \pm 17\%$  to  $30.5 \pm 5\%$ ) and by 3 hours only  $11.5 \pm 3.5\%$  of cells had a visible ESB (Figure 5.8A). After 3 hours Incubation with a higher concentration of  $1 \mu\text{M}$  Quarfloxin no cells contained an ESB. Loss of the ESB was even more rapid in cells incubated with  $3 \mu\text{M}$  Quarfloxin, as no ESBs were detected after 1 hour. A similar dose dependent loss of a visible ESB in cells cultured in media containing  $300\text{nM}$  to  $3 \mu\text{M}$  BMH-21 was observed (Figure 5.8B). Incubation with a range of concentrations of CX-5461 (Figure 5.8C) also resulted in a time- and dose-dependent decrease in the percentage of ESB positive cells. The percentage of cells containing an ESB after treatment with  $800 \text{ nM}$  Suramin was also monitored to ensure loss of the ESB was not simply a consequence of subnuclear architecture falling apart in dying cells. Despite treatment with a lethal concentration of Suramin, only a marginal reduction in the number of ESB positive cells was observed (Figure 5.8D).

To ensure that the loss of the extranucleolar YFP positive foci was representative of ESB disassembly, I epitope-tagged an endogenous copy of the ESB associated protein VEX1 in the S16\_221Pur *T. brucei* cell line with a triple myc tag as previously described by Glover et al. 2016 (Figure 5.9A). I then quantified the percentage of cells with 1 or 2 VEX1 foci after 3 hours incubation with  $3 \mu\text{M}$  of the Pol I inhibitor and  $800 \text{ nM}$  Suramin (Figure 5.9B). The percentage of cells with 1 or 2 VEX1 foci at zero hours is similar to the percentage of VEX1 positive G1 cells previously published by (Glover et al. 2016). The number of G1 cells containing a VEX1 signal was strikingly reduced after 3 hours exposure to BMH-21, CX-5461 and Quarfloxin suggesting disintegration of the ESB rather than just loss of the Pol I subunit RPA2. Similar to the results observed with the TY-YFP-RPA2 cells, incubation with  $800 \text{ nm}$  Suramin did not result in loss of the positive VEX1 signal suggesting that the ESB is lost due to Pol I inhibition rather than cell death.



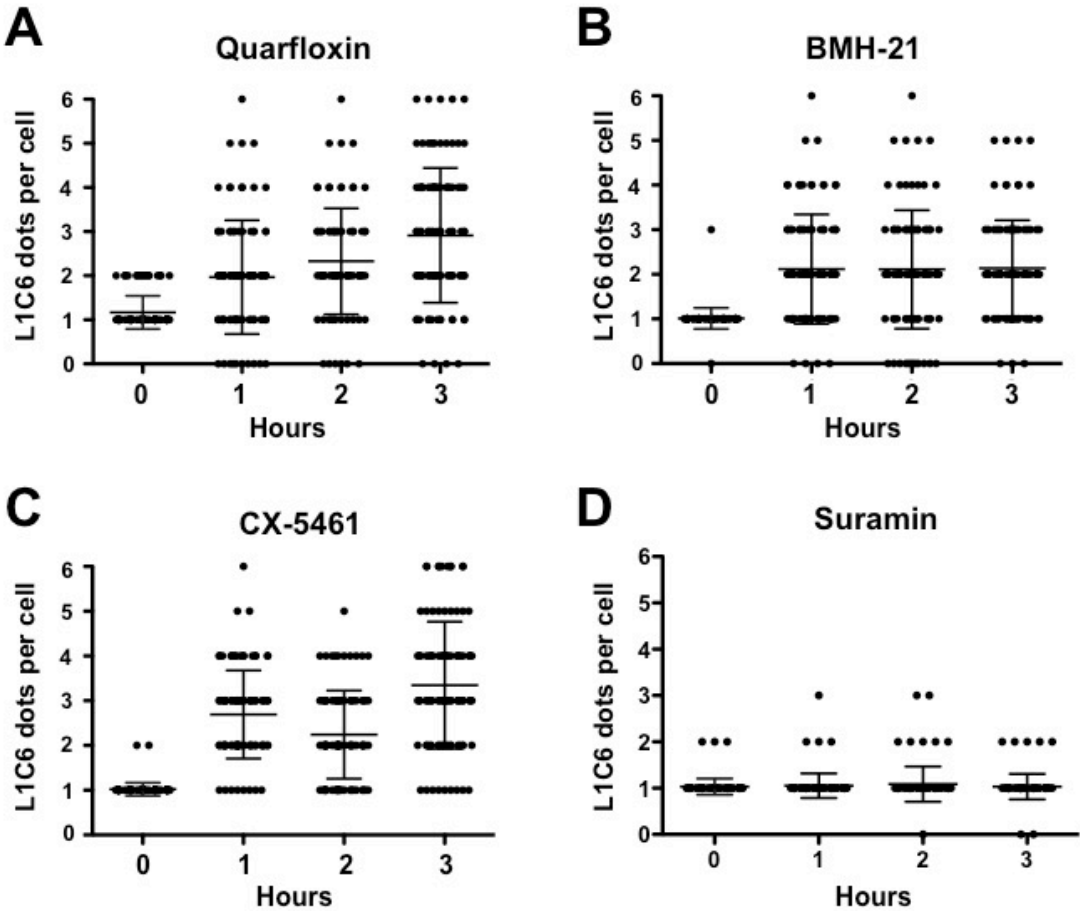


**Figure 5.7. Pol I inhibition in *T. brucei* results in rapid disassembly of the nucleolus.** *T. brucei* cells in the G1 stage of the cell cycle have a single nucleolus, which can be visualised by staining with the nucleolar marker L1C6. The number of L1C6 positive foci (Y-axis) per G1 cell (black dots) are shown after incubation of *T. brucei* with 3  $\mu$ M (A) Quarfloxin, (B) BMH-21, (C) CX-5461 or (D) the trypanocidal agent Suramin over a 3 hour period. The mean number of L1C6 dots from two biological replicates of  $\sim$  50 G1 cells is shown as a horizontal line and standard deviation is indicated with error bars.

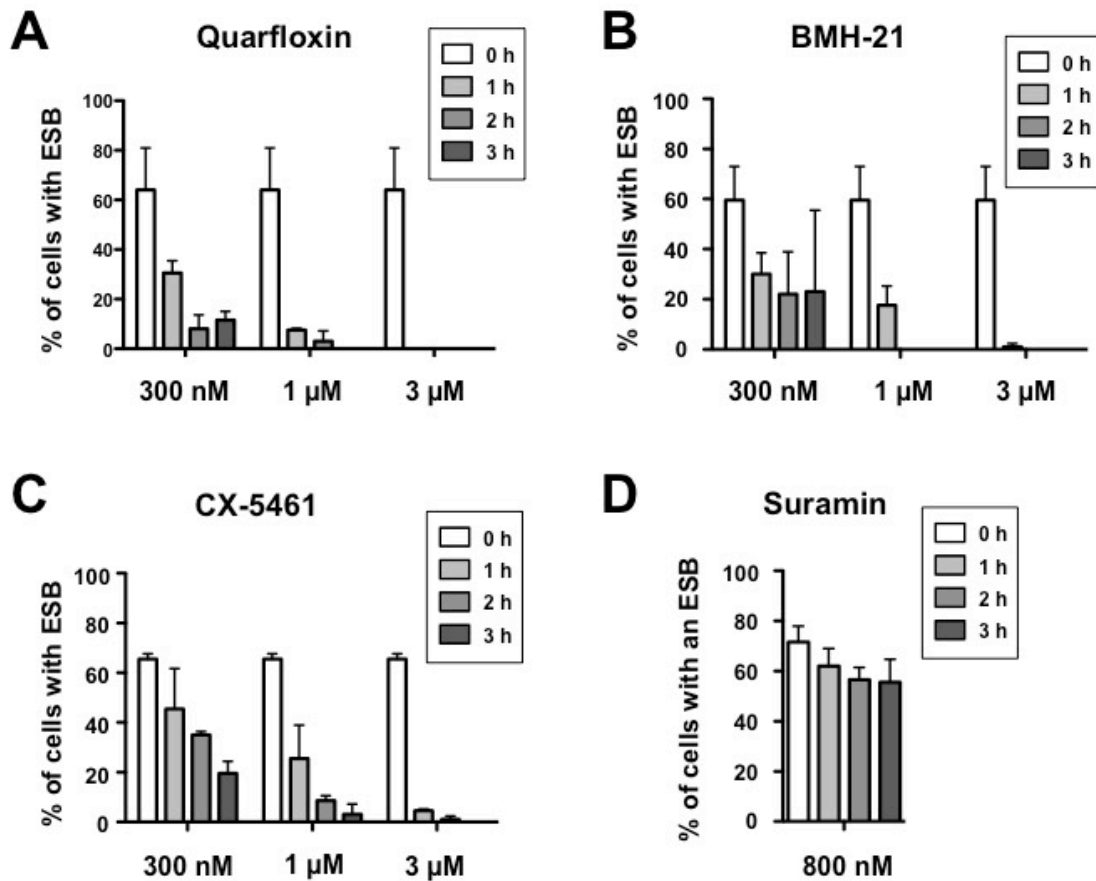


**Figure 5.8. Time- and dose-dependant decrease in the number of *T. brucei* with an ESB after Pol I inhibition.**

Quantitation of the percentage (%) of *T. brucei* TY-YFP-RPA2 cells that contain an extranucleolar YFP signal (ESB) after treatment with a range of concentrations of (A) Quarfloxin, (B) BMH-21, (C) CX-5461 and (D) the anti-trypanosomal agent Suramin. The mean percentage of cells with an ESB is plotted for each time point indicated in hours (h). The mean is of 100 cells from two biological replicates and the standard deviation is indicated with error bars.

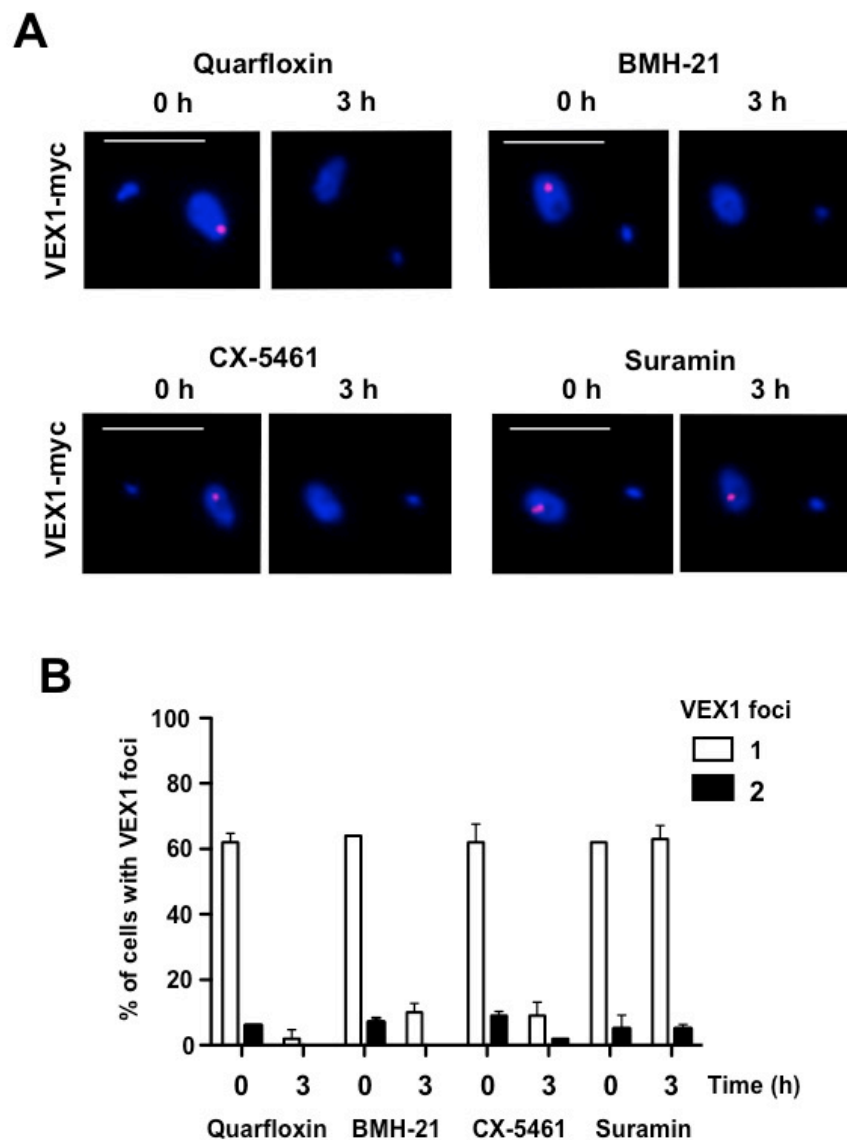


**Figure 5.9. Incubation of BSF *T. brucei* with Pol I inhibitors results in a striking loss of VEX1 foci.** (A) Immunofluorescence microscopy analysis of S16\_221Pur-VEX1:12myc cells exposed to 3  $\mu$ M of the Pol I inhibitors and 800 nM Suramin. The panels show representative images of VEX1-myc cells in the G1 stage of the cell cycle at 0 and 3 hours (h). Cells were stained with the DNA stain DAPI and probed with an anti-myc antibody and Alexa-594 secondary. Scale bar indicates 5  $\mu$ m. (B) Quantification of the percentage (%) of *T. brucei* in the G1 stage of the cell cycle positive for 1 or 2 VEX1 foci within the nuclei. The data shown is at 0 and 3 hours (h) after incubation with 3  $\mu$ M of the Pol I inhibitors and 800 nM of the trypanocidal agent Suramin. The mean percentage of 100 cells (two biological replicates) positive for 1 or 2 VEX1 foci is plotted with the standard deviation indicated with error bars.

In mammalian cells Pol I inhibition caused by BMH-21 exposure results in disintegration of the nucleolus and degradation of the Pol I large subunit (RPA194) (Peltonen et al. 2014). To ascertain if the disassembly of the nucleolus and loss of the ESB observed in *T. brucei* was accompanied by Pol I subunit degradation, I performed immunoblot analysis on cell protein lysate extracted from *T. brucei* cultures incubated with different concentrations of BMH-21 over a 60-minute period (Figure 5.10). Despite clear nucleolar disassembly (Figure 5.7B) and only 1% of cells retaining an ESB (Figure 5.8B), no evidence for the degradation of the *T. brucei* RPA2 Pol I subunit was observed even after 60 minutes exposure to 3  $\mu$ M BMH-21. In mammalian cells BMH-21 intercalates into guanine-cytosine DNA sequences enriched in the rDNA, preventing Pol I transcription, and resulting in apparent degradation of nucleolar subunits (Colis et al. 2014). The mechanism of Pol I inhibition by BMH-21 in *T. brucei* is not known. It is possible that BMH-21 intercalation disrupts Pol I transcription via a different mechanism in trypanosomes than in mammalian cells. Alternatively, as *T. brucei* has developed a unique role for Pol I in transcribing protein coding genes, it is therefore possible that *T. brucei* may have also evolved a way of disassembling Pol I nucleated structures while retaining some or all of the individual Pol I subunits.

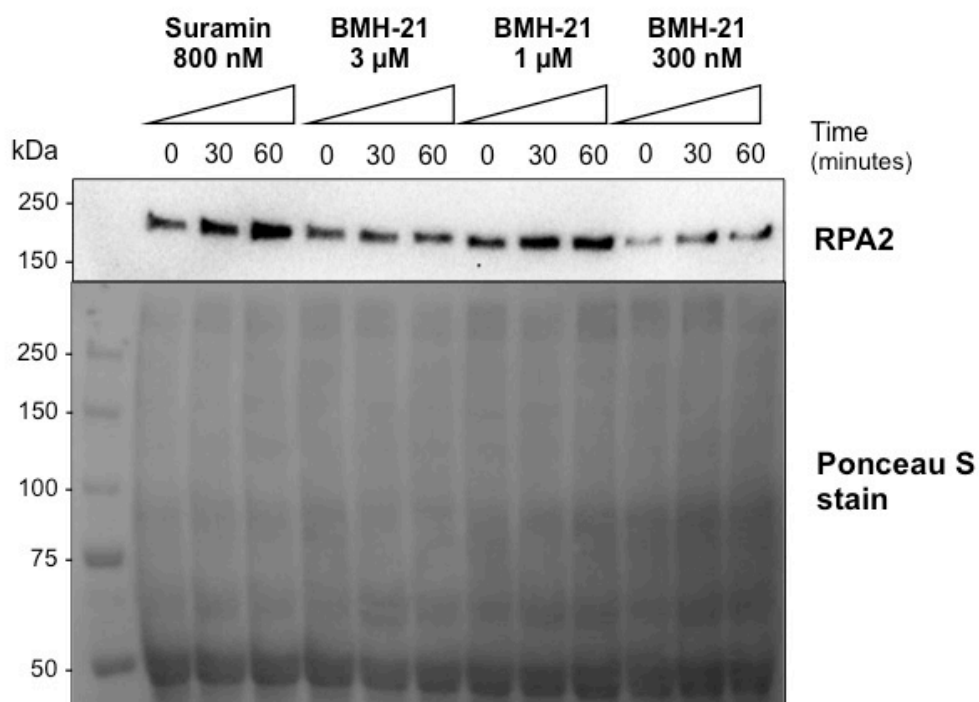


**Figure 5.10. The Pol I subunit RPA2 is not significantly degraded after Pol I inhibition caused by exposure to BMH-21 in BSF *T. brucei*.**

The *T. brucei* TY-YFP-RPA2 cell line was incubated with a range of concentrations of BMH-21. Cells were also exposed to 800 nM Suramin as a lethality control. Whole cell protein lysate from  $1 \times 10^7$  cell equivalents was analysed by immunoblot probed with the anti-TY (BB2) antibody. Signal corresponding to TY-YFP epitope-tagged RPA2 is shown in the top panel and Ponceau S stain of the blot is shown in the lower panel as a loading control. Size markers are annotated in kiloDaltons (kDa).

To further examine if the ESB and nucleolus are Pol I transcription nucleated structures in *T. brucei*, I monitored the reinitiation of Pol I transcription and status of the nucleolus and ESB using the reversible properties of the BMH-21 Pol I inhibitor (Figure 5.3B). BSF *T. brucei* cells were incubated with 1  $\mu$ M of BMH-21 for a two hour period, washed in warm media, and cultured in inhibitor free media prior to samples being extracted for RT-qPCR precursor transcript analysis and immunofluorescence microscopy. An untreated control was analysed in parallel, and all RT-qPCR precursor transcript was normalised to samples collected prior to treatment with BMH-21 (Figure 5.11B pre-treatment).

As expected, transcript levels within the rDNA transcription unit were significantly reduced based on RT-qPCR analysis of all three pre-rRNA precursors in *T. brucei* cells collected immediately after the two-hour treatment with BMH-21 (Figure 5.11B zero minutes post-wash). Interestingly, pre-rRNA precursor 1 transcript, amplified by primer a (Figure 5.11A), was significantly increased (compared to the untreated control) 15 minutes after removal of the BMH-21. These elevated levels of precursor 1 transcript were detected in the treated cells for the whole 120-minute post-wash period. This was not the case for primers b, c and d used for RT-qPCR analysis of pre-rRNA precursor transcript 2 and 3 (Figure 5.11A). The levels of precursor transcripts 2 and 3 in treated cells are significantly reduced compared to the control cells 15 minutes post-wash. A gradual increase in the levels of pre-rRNA precursor transcripts 2 and 3 is observed over time, and after 120 minutes recovery in Pol I inhibitor free media, no significant difference in precursor transcript levels were observed compared to the untreated control. This analysis of precursor transcripts suggests transcription re-initiation occurs rapidly after removal of BMH-21, however transcriptional elongation appears to lag.

The BMH-21 Pol I inhibitor has been shown to intercalate into G-C rich regions within the rDNA of mammalian cells (Colis et al. 2014). *T. brucei* rDNA is known to contain G-C enriched regions. It is therefore feasible that the lag in transcriptional elongation observed in *T. brucei* after

removal of the Pol I inhibitor is the result of uneven intercalation of BMH-21 within the rDNA transcription unit. To investigate if the distribution of G-C enriched regions within the rDNA transcription unit correlated with the location of the pre-rRNA primer binding sites, I mapped the percentage of G-C content along the length of the *T. brucei* rDNA transcription unit (Figure 5.11C). Interestingly, the percentage of G-C content within the rDNA promoter and region of precursor 1 (amplified by primer a) is relatively low (< 50% G-C content). In contrast the G-C content exceeds 50% in the region upstream of the primer b binding site in precursor 2 and the binding sites of primers c and d in precursors 2 and 3.

One possible model for the lag in transcription elongation in *T. brucei* after removal of BMH-21, is that BMH-21 intercalates with the G-C rich regions within the rDNA transcription units resulting in inhibition of Pol I transcription in *T. brucei*. Removal of the Pol I inhibitor from the media results in loss of DNA bound BMH-21 at a constant rate via an unknown mechanism. DNA regions enriched for guanine and cytosine nucleotides may contain more BMH-21 and therefore a longer recovery period (as observed in figure 5.11 for precursor transcripts 2 and 3) may be required for sufficient inhibitor loss to allow for Pol I transcription to proceed. Inhibition of Pol I transcription initiation at the rDNA promoter and transcription of the region immediately downstream (amplified by primer a) may be more rapidly reversed as fewer BMH-21 molecules are bound to the AT-rich DNA than bind the G-C enriched regions. Furthermore, the elevated levels of pre-rRNA precursor transcript 1 (Primer a) in treated cells may be caused by an increased rate of Pol I transcription initiation. Elevated levels of initiation could be caused by the BMH-21 molecules preventing Pol I transcribing the full length of the rDNA transcription unit, leading to elevated levels of unbound Pol I, which are then available to bind the Pol I promoter.

To ascertain the effect of Pol I transcription reinitiation on the fragmented nucleolus, I stained the cells with the nucleolar marker L1C6 and quantified the number of L1C6 positive foci observed after the removal of BMH-21 (Figure 5.12). At zero minutes post wash the fragmented

nucleolus was observed as multiple L1C6 positive foci in the treated *T. brucei* cells, whereas a single L1C6 positive focus was observed in the untreated control cells (Figure 5.12B). Interestingly, the multiple L1C6 foci observed in treated *T. brucei* at zero minutes, rapidly returns to an average of 1 focus per cell after 15 minutes recovery. This suggests that the disassembled nucleolus caused by inhibition of Pol I transcription is rapidly reassembled upon reinitiation of Pol I transcription. This data in conjunction with the RT-qPCR precursor analysis strongly suggests that the nucleolus is a transcription seeded structure, but that this nucleation is only reliant on Pol I transcription initiation but not on transcriptional elongation of the rDNA transcription unit.

The initial Pol I inhibitor experiments shown in this chapter showed loss of a visible ESB after Pol I inhibition of ES transcription. This led us to speculate that the ESB may be a transcription-nucleated structure similar to the nucleolus. To further explore this theory, I conducted RT-qPCR analysis of the *VSG* pseudogene ( $\Psi$ ) and *VSG 221* precursor transcript (Figure 5.13A) in the RNA extracted from *T. brucei* cells treated with BMH-21 for two hours compared with the untreated control. As previously shown for the rDNA, the ES precursor transcript levels were normalised to actin mRNA levels and the mean levels of transcript were expressed as a percentage relative to the pre-treatment samples.

As expected, ES precursor transcript levels in *T. brucei* cells treated with BMH-21 for two hours were significantly reduced in contrast to the untreated control, and only 0.7% of G1 stage cells contained an ESB (Figure 5.13B-C 0 minutes post-wash). The levels of *VSG* pseudogene and *VSG 221* precursor transcript rapidly increased to levels comparable with the untreated control at 15 and 30 minutes post-wash, respectively. Despite the levels of Pol I transcribed ES precursor transcript rapidly returning to normal 15-30 minutes after removal of BMH-21, only 48-55% of treated TY-YFP-RPA2 *T. brucei* cells had a visible ESB after 30-minutes recovery (Figure 5.13C). Only after 120 minutes recovery did the number of cells positive for an ESB return to the number observed in the untreated control. The rapid return of Pol I transcription to normal levels after removal of BMH-21,



compared with the relatively slow increase in the number of cells containing an ESB supports the model of the ESB being a transcription nucleated structure.

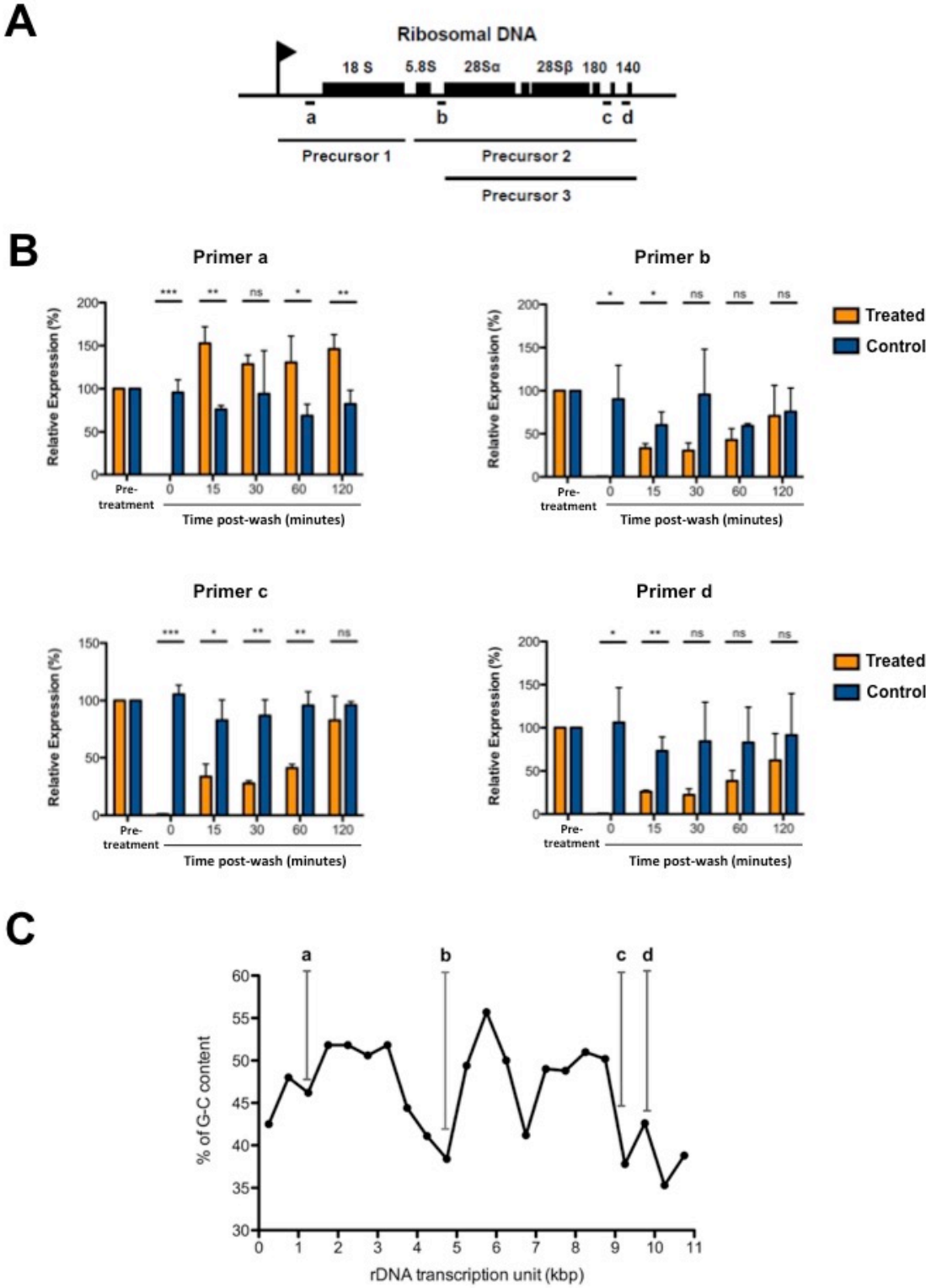


**Figure 5.11. Transcription reinitiation within the rDNA and nucleolar reassembly after removal of Pol I inhibitors in *T. brucei*.**

(A) Schematic of the *T. brucei* rDNA transcription unit with the promoter represented as a flag, the rRNA genes are denoted as black boxes and letters indicate the precursor transcript detected by qPCR primers a-d. (B) The percentage (%) relative expression of pre-rRNA precursor transcript determined by RT-qPCR analysis of TY-YFP-RPA2 *T. brucei*, previously incubated in 1  $\mu$ M of the Pol I inhibitor BMH-21 for two hours, then washed and cultured in inhibitor free media for a further 120 minutes. Precursor RNA was normalised to Actin mRNA levels and is shown as relative expression of treated (orange) or untreated control (blue) *T. brucei* compared to pre-treatment. Statistically significant differences between treated and control samples are indicated with asterisks (\*\* $p < 0.001$ , \*\* $p = 0.001-0.01$ , \* $p = 0.01-0.05$ , not significant (ns)  $p > 0.05$ ). The mean of three biological replicates is shown and the standard deviation is indicated with error bars. (C) Graph showing the abundance of guanine-cytosine (G-C) nucleotides calculated as a percentage (%) G-C content of 500bp windows. The rDNA transcription unit sequence from *T. brucei* chromosome 1 was analysed using Biologics International online GC content Calculator.

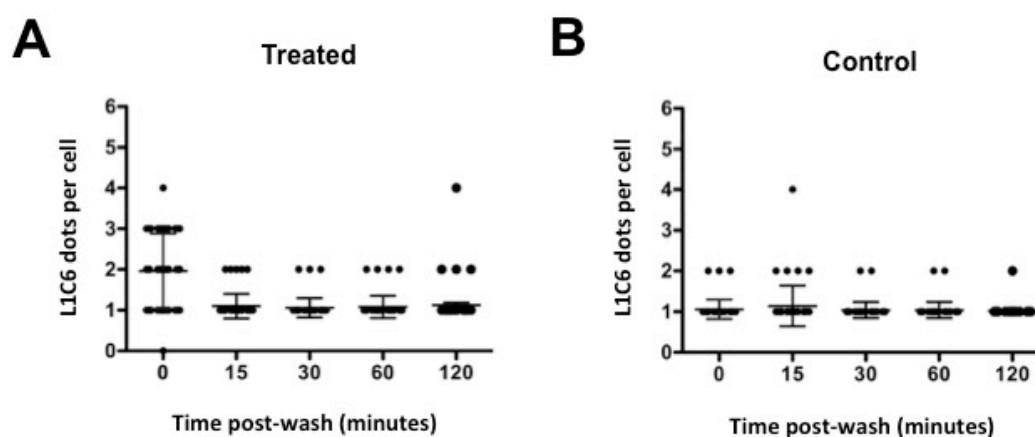


**Figure 5.12. Nucleolar reassembly after removal of BMH-21 from *T. brucei* media.**

Immunofluorescence microscopy analysis of cells stained with the DNA stain DAPI and the nucleolar marker L1C6 was used to quantify the number of L1C6 positive foci within the nucleus of (A) treated and (B) untreated control *T. brucei*. TY-YFP-RPA2 parasites were treated with 1  $\mu$ M BMH-21, washed to remove the Pol I inhibitor and then cultured in inhibitor free media. Samples for immunofluorescence microscopy analysis were taken immediately after the 2-hour incubation in BMH-21 (0 minutes post-wash) and at 15, 30, 60 and 120 minutes post-wash. Each dot represents a cell and the number of L1C6 dots is indicated on the Y-axis. A horizontal line indicates the mean number of L1C6 foci and standard deviation is indicated with error bars.

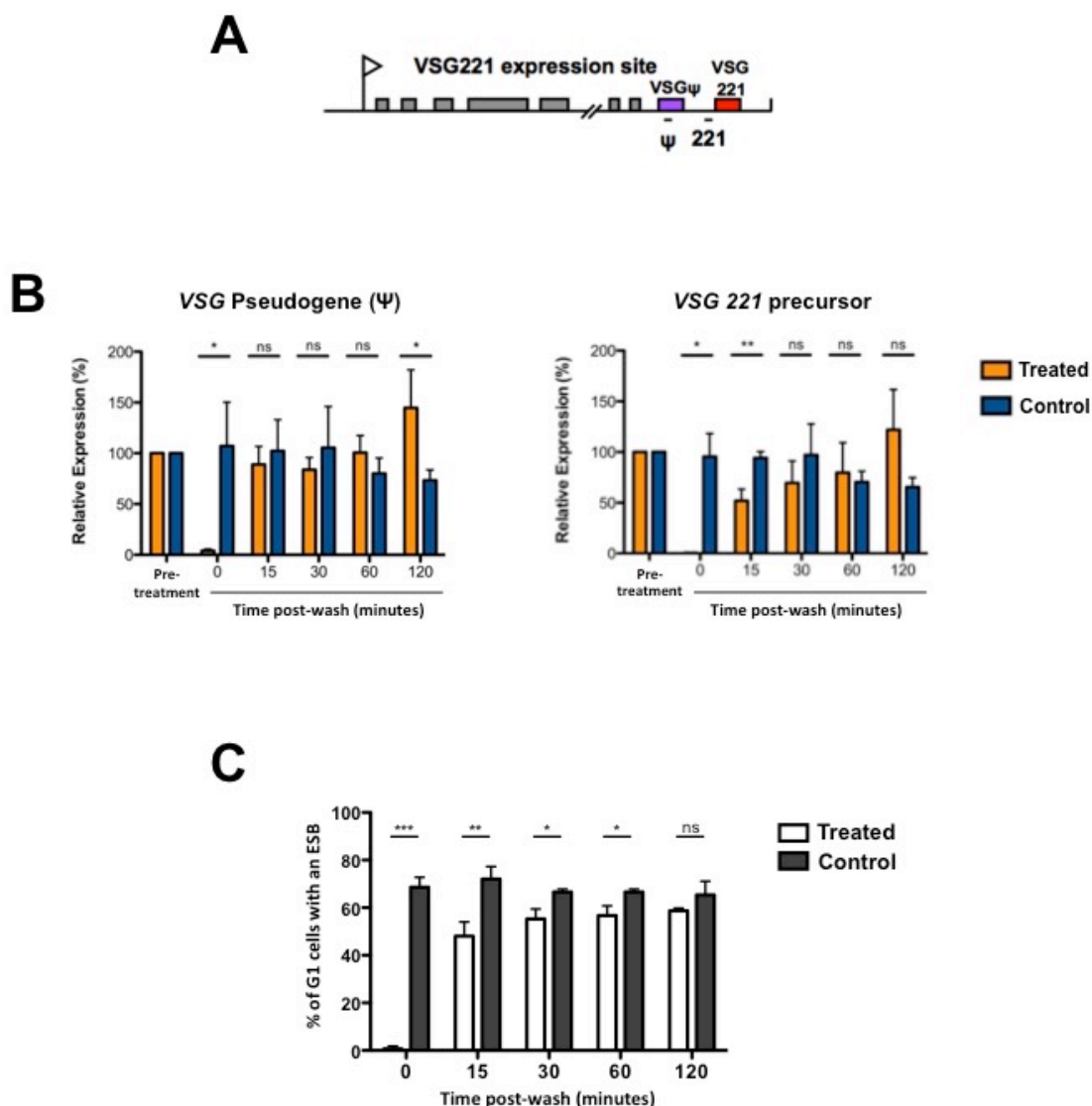


**Figure 5.13. Reinitiation of Pol I ES transcription and reappearance of an ESB in *T. brucei* after removal of the BMH-21 Pol I inhibitor.**

(A) Schematic of the *VSG 221* ES. The promoter is shown as a flag and the ESAGs are indicated with grey boxes. The *VSG* pseudogene (purple box) and *VSG 221* gene (red box) are annotated, as are the regions amplified by the pseudogene ( $\Psi$ ) and 221 precursor transcript primers. (B) Transcript levels for the *VSG* pseudogene and *VSG 221* precursor transcript determined by RT-qPCR analysis. Treated samples were exposed to 1  $\mu$ M of the Pol I inhibitor BMH-21 for two hours, washed and cultured in inhibitor free media for a further 120 minutes. Untreated samples was analysed in parallel as a control. Precursor RNA was normalised to Actin mRNA levels and is shown a percentage (%) of relative expression for treated (orange) or untreated control (blue) *T. brucei* compared to pre-treatment. (C) Quantification of immunofluorescence microscopy analysis showing the percentage (%) of *T. brucei* cells in the G1 stage of the cell cycle with an extra-nucleolar YFP positive foci (ESB) at various time point post-wash in treated and control cultures. For B and C statistically significant difference between treated and control samples are indicated with asterisks (\*\*\*)  $p < 0.001$ , \*\*  $p = 0.001-0.01$ , \*  $p = 0.01-0.05$ , not significant (ns)  $p > 0.05$  and the mean percentage  $\pm$  standard deviation of three biological replicates is plotted.

## 5.7 - Discussion

Unlike most eukaryotes, *T. brucei* utilises Pol I to transcribe not only the rDNA but also the essential *VSG* genes in a monoallelic fashion from one of multiple *VSG* ESs (Günzl et al. 2003). A very high transcription rate of the single active *VSG* ES is required to generate sufficient *VSG* transcript for *T. brucei* survival. Even minor disruption of *VSG* synthesis is catastrophic for *T. brucei* survival both *in vitro* and *in vivo* (Shedder et al. 2005). This *T. brucei* specific, essential role of Pol I make it an appealing drug target for the development of anti-trypanosomal chemotherapies. Interestingly, cancer cells are also highly sensitive to disruption of Pol I transcription, as elevated levels of rRNA transcript are needed to enable the rapid uncontrolled cell proliferation associated with tumour formation (Quin et al. 2014). Consequently, Pol I inhibitors have been developed as anti-tumour therapies to target rapid rDNA synthesis in cancer cells (Quin et al. 2014), while non-cancerous cells remain largely unaffected (Bywater et al. 2012). In this chapter, I investigated the Pol I inhibitors Quarfloxin, CX-5461 and BMH-21, previously developed as anti-cancer therapies, as potential trypanocidal agents and investigated the viability of Pol I as a druggable feature in BSF *T. brucei*. Additionally, I used these Pol I inhibitors to investigate if the *T. brucei* ESB is a transcription-nucleated structure similar to the nucleolus.

All three Pol I inhibitors perturb BSF *T. brucei* cell proliferation at nanomolar concentrations and were lethal to *T. brucei in vitro*. Cytotoxicity assays showed that BMH-21 was the most efficacious inhibitor in BSF parasites with an  $IC_{50}$  of  $134 \pm 8$  nM, Quarfloxin gave a similar  $IC_{50}$  to BMH-21 of  $155 \pm 9$  nM and CX-5461 was less potent against *T. brucei* with an  $IC_{50}$  of  $279 \pm 16$  nM. All three Pol I inhibitors are classed as “active” under the guidelines outlined by the Pan-Asian Screening Network (Ioset et al. 2009) with Quarfloxin and CX-5461 exceeding the recommended selectivity index ( $\geq 10$ -fold), being 29-fold and 25-fold more toxic to BSF *T. brucei* than the mammalian (MCF10A) cells, respectively.

RT-qPCR analysis of precursor transcript from the Pol I transcribed rDNA transcription units and VSG ES, in conjunction with analysis of precursor transcript from the Pol II transcribed tubulin array; showed Quarfloxin, CX-5461 and BMH-21 selectively and rapidly blocked Pol I transcription, while Pol II transcription was unaffected. It is intriguing that despite the inhibitors having different mechanisms of action in mammalian cells, all three of the Pol I inhibitors cause specific inhibition of Pol I transcription in *T. brucei*. For example, Quarfloxin is thought to bind G-rich regions that form G-quadruplexes within the rDNA and telomeres of mammalian cells (Brooks & Hurley 2010). *T. brucei* rDNA and telomeres also contain G-rich regions but it is unclear whether these form G-quadruplexes despite the conservation of the telomere repeat sequence (GGGTA) (Duan et al. 2001). It is therefore plausible that Quarfloxin binds these DNA features and prevents Pol I transcription elongation in a similar manner in both eukaryotes. In mammalian cells, CX-5461 prevents initiation of Pol I transcription by inhibiting binding of the transcription factor SL-1 to the rDNA promoter (Drygin et al. 2011). Although no obvious SL-1 homologue has been identified in *T. brucei*, the selective inhibition of Pol I by CX-5461 shown in this chapter does suggest an SL-1-like protein fulfils this function in *T. brucei*. The Pol I inhibitor BMH-21 intercalates with G-C rich regions of the rDNA in mammalian cells (Peltonen et al. 2014; Colis et al. 2014), and data presented in this chapter suggests a similar mechanism of inhibition occurs in *T. brucei*.

The reversibility of BMH-21 inhibition and poor selective toxicity (SI 3.4-fold) against *T. brucei* compared with mammalian cells limits the therapeutic potential of this compound as an anti-trypanosomal therapy. However, the *in vitro* data for CX-5461 and Quarfloxin was more promising, as both are irreversible specific inhibitors of Pol I transcription in BSF *T. brucei* with favourable selectivity compared to host cells. *In vivo* work was conducted by our collaborators at the Drug Discovery Unit (University of Dundee) to assess the efficacy of Quarfloxin and CX-5461 in a stage I mouse model of Human African Trypanosomiasis. Unfortunately, sample preparation issues resulted in the Quarfloxin arm of the study being aborted, and the CX-5461 arm showed no difference in survival of infected mice treated with CX-5461 (40 mg/kg or 120 mg/kg) compared with the vehicle

control group. CX-5461 was originally developed as an anti-cancer agent and was engineered to be stable and have favourable pharmacokinetics *in vivo* (Bywater et al. 2012). However, preliminary pharmacokinetics data from the *in vivo* work conducted by the Drug Discovery Unit suggests CX-5461 was ineffective at reducing parasitaemia due to poor bioavailability. Consequently, medical chemistry optimisation of this compound would be required prior to further development of CX-5461 as an anti-trypanosomal agent.

These Pol I specific inhibitors may have limited therapeutic potential in their current form but CX-5461, Quarfloxin and BMH-21 are ideal biological tools to investigate if the ESB is a Pol I transcription-nucleated structure in *T. brucei*. It has previously been demonstrated that the nucleolus is a Pol I specific transcription-seeded structure in higher eukaryotes (Lam & Trinkle-Mulcahy 2015). The rapid disassembly of the nucleoli observed in *T. brucei* treated with Pol I inhibitors strongly suggests that the Pol I specific transcription nucleated mechanism of nucleolar assembly is conserved in *T. brucei*. Furthermore, the elevated level of pre-rRNA precursor 1 transcript and nucleoli reassembly after removal of Pol I inhibition (induced by BMH-21) suggests that only Pol I transcription initiation and not transcriptional elongation within the rDNA is required to “seed” the nucleolus in *T. brucei*.

In *T. brucei* Pol I also localises to an extranucleolar body termed the ESB, in which Pol I transcribes a VSG ES in a monoallelic fashion (Navarro & Gull 2001). In this chapter, I have presented data that supports a transcription-nucleated model for the ordered assembly/disassembly of the ESB, similar to the nucleolus. Inhibition of Pol I transcription resulted in rapid disappearance of the ESB, as shown by loss of the extranucleolar Pol I positive foci and ESB associated protein VEX1 in *T. brucei*. In further support of a transcription-nucleated ESB, I also exploited the reversibility of the Pol I inhibitor BMH-21 to investigate ESB assembly after reinitiation of Pol I transcription. The level of Pol I precursor transcript from the active ES returns to normal within 30 minutes of the BMH-21 inhibitor being removed. However, the percentage of cells positive for an ESB did not return to the

levels observed in the uninhibited control for an additional 90 minutes. The observed lag between reinitiation of Pol I transcription and reappearance of an ESB strongly suggest that the ESB is a transcription nucleated structure. My findings are at odds with the previous suggestion that the ESB is a deterministic structure that is preassembled prior to transcription initiation of the active VSG ES. This was based on the observation that the ESB (extranucleolar Pol I positive focus) was retained in methanol fixed *T. brucei* cells treated with DNase I to destroy the active ES (Navarro & Gull 2001). However, this interpretation is complicated by the fact methanol fixation of the trypanosomes occurred prior to DNase I digestion, which may have inadvertently caused reduced motility of Pol I and related polymerase complexes, even after digestion of the DNA.

Repurposing of anti-cancer agents as anti-kinetoplastid chemotherapies to treat tropical neglected diseases, such as HAT, has previously been successful as drugs such as Tamoxifen (Miguel et al. 2008a; Miguel et al. 2008b) and Eflornithine (Sekhar et al. 2014) can attest. Despite some of the complications regarding toxicity, parasite specificity and bioavailability of the Pol I inhibitors Quarfloxin, BMH-21 and CX-5461, the data in this chapter does indicate Pol I is a druggable target in *T. brucei*. The development of Pol I inhibitory compounds as anti-cancer therapies will continue, and it is possible novel Pol I inhibitors will have favourable anti-parasitic properties leading to successfully repurposing as anti-trypanosomal agents. As I have demonstrated in this chapter, the limited therapeutic potential of these Pol I inhibitors does not negate their usefulness as specific inhibitors to investigate Pol I transcription in *T. brucei*. Here, they have proven to be a valuable experimental tool to investigate Pol I transcription and the resulting data presented in this chapter, provides strong evidence to support a transcription-nucleated model for the assembly of the ESB in *T. brucei*.

## Chapter Six

### The role of epigenetics and the ESB in the transcriptional control and monoallelic exclusion of ESs.

#### 6.1 - Introduction

As discussed previously, *T. brucei* evades the host immune response by periodically switching the VSG coat expressed on the cell surface, generating sufficient antigenic variation to ensure survival of the parasite population within the infected host. Monoallelic expression of a single VSG from one of multiple VSG ESs is key to maintaining a sufficient repertoire of VSGs to continuously remain one step ahead of the host immune system (Horn 2014; Rudenko 2010). This effective antigenic variation strategy requires a single VSG gene to be actively transcribed from one ES while the other ~20 very similar VSG ESs and VSG genes present in subtelomeric arrays are kept transcriptionally silent (Williams et al. 1982; Berriman 2005; Cross et al. 2014). As VSG constitutes ~10% of total cell protein, the single active VSG ES must be efficiently transcribed to ensure sufficient mRNA is generated from the single copy gene (Cross 1975). Additionally, the transcriptional state of the ESs must be reversible, to allow for *in situ* VSG switching in which the active ES is silenced and an alternative VSG is expressed from one of the other ~15 ESs (Hertz-Fowler et al. 2008; Aresta-Branco et al. 2016). The transcriptional state of the VSG ESs must also be inheritable, as the monoallelic choice of VSG ES must be acquired by the daughter cell during cell division (Navarro & Gull 2001; Landeira et al. 2009). Monoallelic expression has been extensively studied due to its importance for parasite survival in the host. These studies led to the discovery of the extranucleolar ESB (Navarro & Gull 2001) and a broad range of epigenetic factors believed to be important in regulating VSG gene transcription (Figueiredo & Cross 2010; Narayanan & Rudenko 2013; Stanne & Rudenko 2010).

The ESB is an extranucleolar structure where Pol I transcription of the single active VSG ES occurs and has previously been discussed in Chapter 5. Past studies have shown approximately 60-



70% of *T. brucei* cells in the G1 phase of the cell cycle contain an extranucleolar Pol I positive focus believed to correspond to the ESB (Navarro & Gull 2001; Daniels et al. 2012). However, the counting mechanism that ensures the singularity of the ESB and the ESB specific factors required for Pol I transcription of the active ES remain unknown.

Epigenetic studies have identified differences between the active and silent *VSG* ESs and demonstrated the role of various epigenetic factors in contributing to activation or repression of the *VSG* genes. For example, ChIP-qPCR experiments using antibodies specific for several of the *T. brucei* histones and Southern blot analysis of micrococcal nuclease digestion experiments, showed the active ES to be depleted of nucleosomes compared to the silent ESs. This led the authors to conclude that the relative lack of nucleosomes contributed to the more open chromatin composition within the active ES (Figueiredo & Cross 2010; Stanne & Rudenko 2010; Povelones et al. 2012). Conversely, the high mobility group box protein TDP1 has an inverse relationship with histones and is present along the length of the active *VSG* ES. TDP1 is believed to help retain the open chromatin structure during active transcription of the *VSG* ES (Narayanan & Rudenko 2013) but also appears to maintain the euchromatin conformation of the active ES if transcription is halted (Aresta-Branco et al. 2016).

The silent *VSG* ESs and DNA repeat sequences also contain an unusual DNA base modification, termed Base J (Gommers-Ampt et al. 1993). The silent ESs appear to have a gradient of this modified base, with base J being more abundant at the telomere than the ES promoter (Bernards et al. 1984). Base J is lost from the silent ES once transcription is activated, but is retained in the 50bp repeats and telomere repeat sequences of the active ES (van Leeuwen et al. 1997). Given the distribution of base J in the ESs and its conspicuous absence from the procyclic form of *T. brucei* (Pays et al. 1984), it has been implicated to play a role in monoallelic exclusion (Borst & Sabatini 2008). However, the precise function of base J in *T. brucei* remains unknown. Detailed

mapping of base J genomic distribution is currently lacking, but may help shed some light on the mechanism by which base J contributes to monoallelic exclusion in *T. brucei* (Borst & Sabatini 2008).

The histone methyltransferase DOT1B is responsible for trimethylation of H3K79 and knockdown of *DOT1B* results in the partial activation of the silent ESs, suggesting that this modification plays a role in repression of silent VSGs (Janzen et al. 2006a). Interestingly, depletion of DOT1B results in a mixed VSG coat present on the parasite surface for a longer period of time during an *in situ* switch, despite the activation of the new ES occurring at a similar rate to normal (Figueiredo et al. 2008). *In vivo*, rapid switching from expression of one VSG ES to expression of another functional ES is essential to minimise the amount of time the parasites present a mixed VSG coat, as this would increase the likelihood of the parasite being recognised by the host immune system. This is demonstrated by observations in *T. equiperdum*, which appeared to express two VSGs in a relatively stable manner in axenic culture (>90% with a mixed coat after 14 days *in vitro*), but these “double expressing” trypanosomes were rapidly cleared in mice (3% with a mixed coat after 3 days *in vivo*) (Baltz et al. 1986).

Expression of two VSGs from a single ES does not appear to have an adverse effect on parasite proliferation *in vivo* or *in vitro* (Muñoz-Jordán et al. 1996). This is perhaps unsurprising as the half life of the VSG protein is approximately 30-40 hours (Seyfang et al. 1990), so the trypanosome surface coat of switch variants will inevitably contain two VSGs for a short period. Previous experiments by Chaves and colleagues to generate *T. brucei* that express two VSGs from two separate ESs (selected for by drug resistance) resulted in the generation of unstable double expressers (Chaves et al. 1999). Upon removal of drug selection 82% of double drug resistant (DDR) cells reverted back to expressing a single VSG after 12 days. Interestingly, the switch rate between two ESs was dramatically increased from  $\sim 10^{-7}$ - $10^{-6}$  per doubling time in normal single expressers to  $<10^{-1}$  in the DDR cells. These observations lead the authors to propose the DDR cells are rapidly switching back and forth between the two ESs which are both in a “pre-active” state. The authors

suggest this pre-active state may be a natural intermediate in switching maintained epigenetically (Figure 6.1). However, the nature of the epigenetic state of these pre-active ESs has not been elucidated (Chaves et al. 1999).

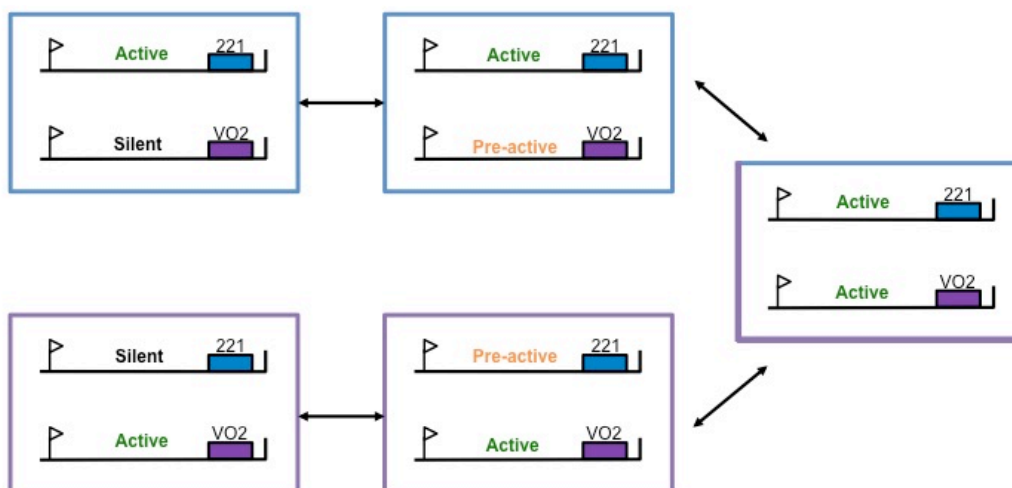


**Figure 6.1. Pre-active state model.**

Schematic adaptation of the model for *in situ* VSG expression site switching proposed by (Chaves et al. 1999). The box outlines represent the VSG coat expressed by the trypanosome. The box colour corresponds to the actively transcribed VSG gene either VSG 221 (blue) or VSG VO2 (purple), present in the representative ESs. The ES promoter is shown as a flag and the transcriptional state of each ES is indicated.

## 6.2 - Aims and experimental outline

The experiments presented in this chapter aim to investigate the unanswered questions regarding the epigenetic state of the pre-active ESs present in DDR cells and investigate the counting mechanism responsible for the singularity of the ESB. To achieve this we have generated our own DDR cell lines that express different fluorescent markers from both of the selected ESs. I used flow cytometry analysis to investigate switching and stability of the DDR (double expresser) cells and parental (single expresser) controls. CHIP-qPCR was performed to investigate the epigenetic state of the DDR pre-active ESs using antibodies against histone H1, histone H3, TDP1 and base J, as these epigenetic factors all play a role in either activation or repression of the VSG ESs. In addition I

determined the number of ESBs present in the double expresser cells by tagging RPA2 (Pol I subunit) in a DDR cell line.

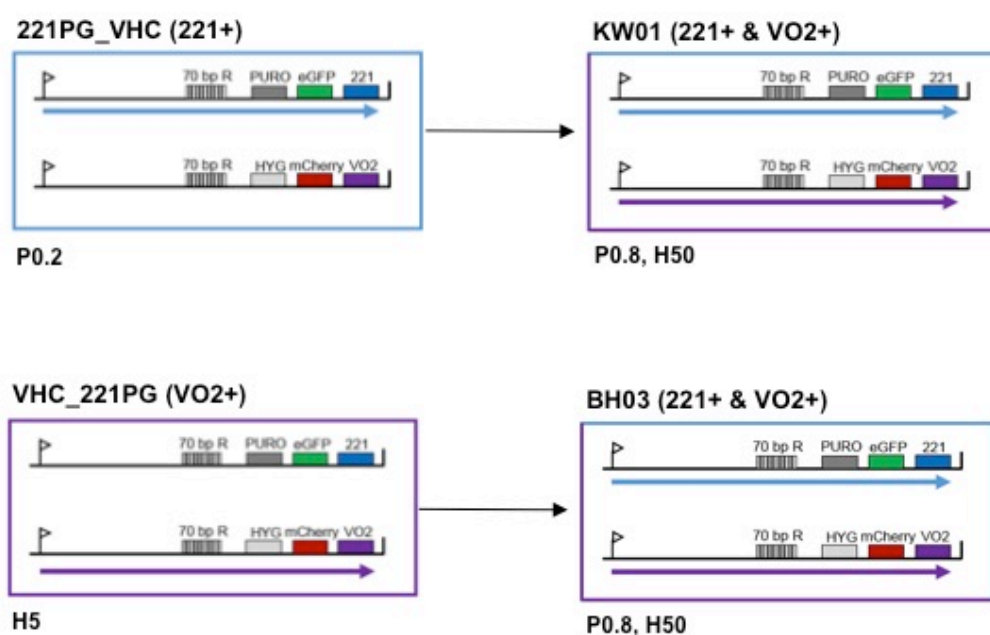
### **6.3 - Characterisation of Double Drug Resistant (DDR) BSF *T. brucei* that express two VSGs from two VSG ESs.**

In order to confirm the pre-active state model proposed by Chaves and colleagues (1999) and to further the understanding of the epigenetic state of the pre-active ESs, we generated double drug resistant (DDR) cells that express two VSGs from two different ESs. The DDR lines KW01 and BH03 were generated from the parental cell lines 221PG\_VHC and VHC\_221PG, respectively. 221PG\_VHC cell lines encodes a puromycin resistance gene and eGFP reporter gene downstream of the VSG 221 ES promoter and VHC\_221PG cell line contains a hygromycin resistance gene and mCherry reporter gene downstream of the VSG VO2 ES promoter (Figure 6.2A). Expression of the single active VSG expression site (VSG 221 or VSG VO2) is maintained by selection for resistance to either 5 µg/ml hygromycin (VSG VO2 ES) or 0.2 µg/ml puromycin (VSG 221 ES). The double expresser cell lines KW01 and BH03 were generated by selecting for 221PG\_VHC and VHC\_221PG cells resistant to both puromycin (0.8 µg/ml) and hygromycin (50 µg/ml) (Figure 6.2).

I monitored cell proliferation of the DDR and parental cell lines over a 96-hour period. The proliferation assay data showed a marginal growth defect in the BH03 cell line. The same proliferation rate was observed for the KW01 cells as the parental cell lines (Figure 6.3A). Culturing the parental cell lines in media containing higher concentrations of puromycin (0.8 µg/ml) and hygromycin (50 µg/ml), which are required to maintain the DDR cell line cultures, had no effect on cell proliferation (Figure 6.3B).

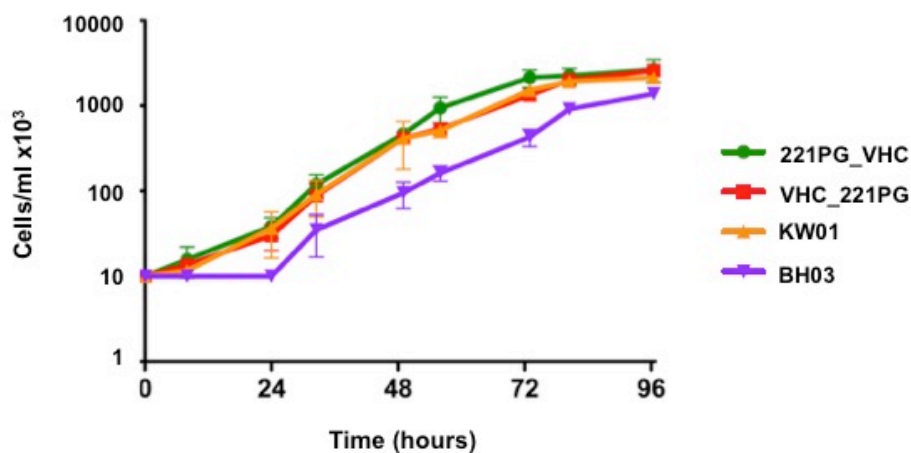
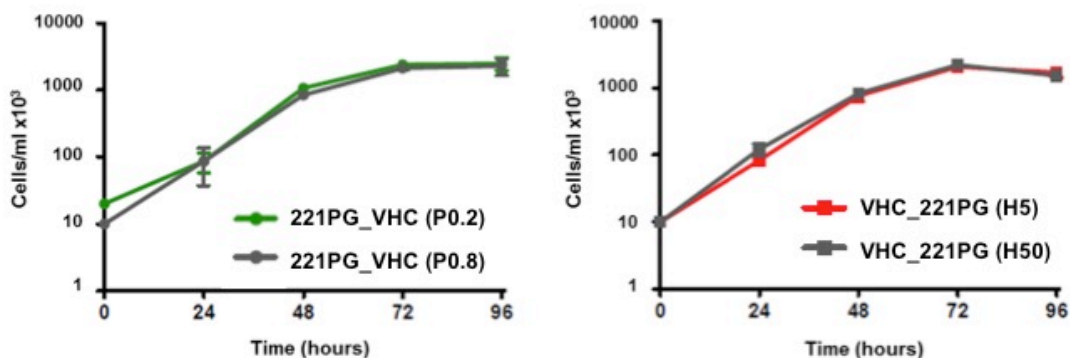
The endogenous fluorescence expressed from the VSG 221 and VSG VO2 ESs provided useful markers that indicate which ES is active in the BSF *T. brucei*. I conducted immunofluorescence analysis to confirm the endogenous fluorescence of individual cells, and that drug selection did not

appear to have an effect on cell morphology (Figure 6.4A). The population of the DDR cells that express both *eGFP* and *mCherry* genes were analysed by flow cytometry and representative flow cytometry traces for the parental and the DDR cell lines are shown in figure 6.4B. As expected, the 221PG\_VHC cells were eGFP positive and the VHC\_221PG cells were mCherry positive, with the DDR cells expressing both eGFP and mCherry.



**Figure 6.2. Schematic representation of the Double Drug Resistant (DDR) *T. brucei* cell lines.**

The parental cell lines 221PG\_VHC and VHC\_221PG that express a single VSG from one active ES are shown on the left. Black arrows indicate the parental cell line from which each DDR cell line was derived. The outer box is representative of the VSG coat being expressed by a single BSF trypanosome, within which two simplified VSG ES transcription units are shown. The VSG ES promoter is shown as a white flag, and active transcription indicated with an arrow. The 70bp repeats present in all VSG ESs are shown upstream of the *hygromycin* (HYG) and *puromycin* (PURO) drug resistance genes. The *eGFP* gene (green box) is located upstream of the VSG 221 gene (blue box) and the *mCherry* gene (red box) is upstream of the VSG VO2 gene (purple box). The concentration of puromycin (P) and/or hygromycin (H) required to maintain transcription of the active ES(s) is shown under each box in µg/ml.

**A****B**

**Figure 6.3. Growth curves of KW01, BH03 and the parental cell lines.**

(A) Proliferation assay to compare the growth rate of the DDR cell lines KW01 and BH03 with the parental cell lines over a 96-hour period. All cell lines were cultured in HMI-9 supplemented with the relevant drugs to maintain selection of the active ES (DDR cells 0.8  $\mu\text{g/ml}$  puro & 50  $\mu\text{g/ml}$  hygro, 221PG\_VHC 0.2  $\mu\text{g/ml}$  puro and VHC\_221PG 5  $\mu\text{g/ml}$  hygro). (B) Growth curves of parental cell lines 221PG\_VHC (left) and VHC\_221PG (right) show no alteration to growth rate when cells are cultured in the higher concentration of drug required to maintain the DDR phenotype.

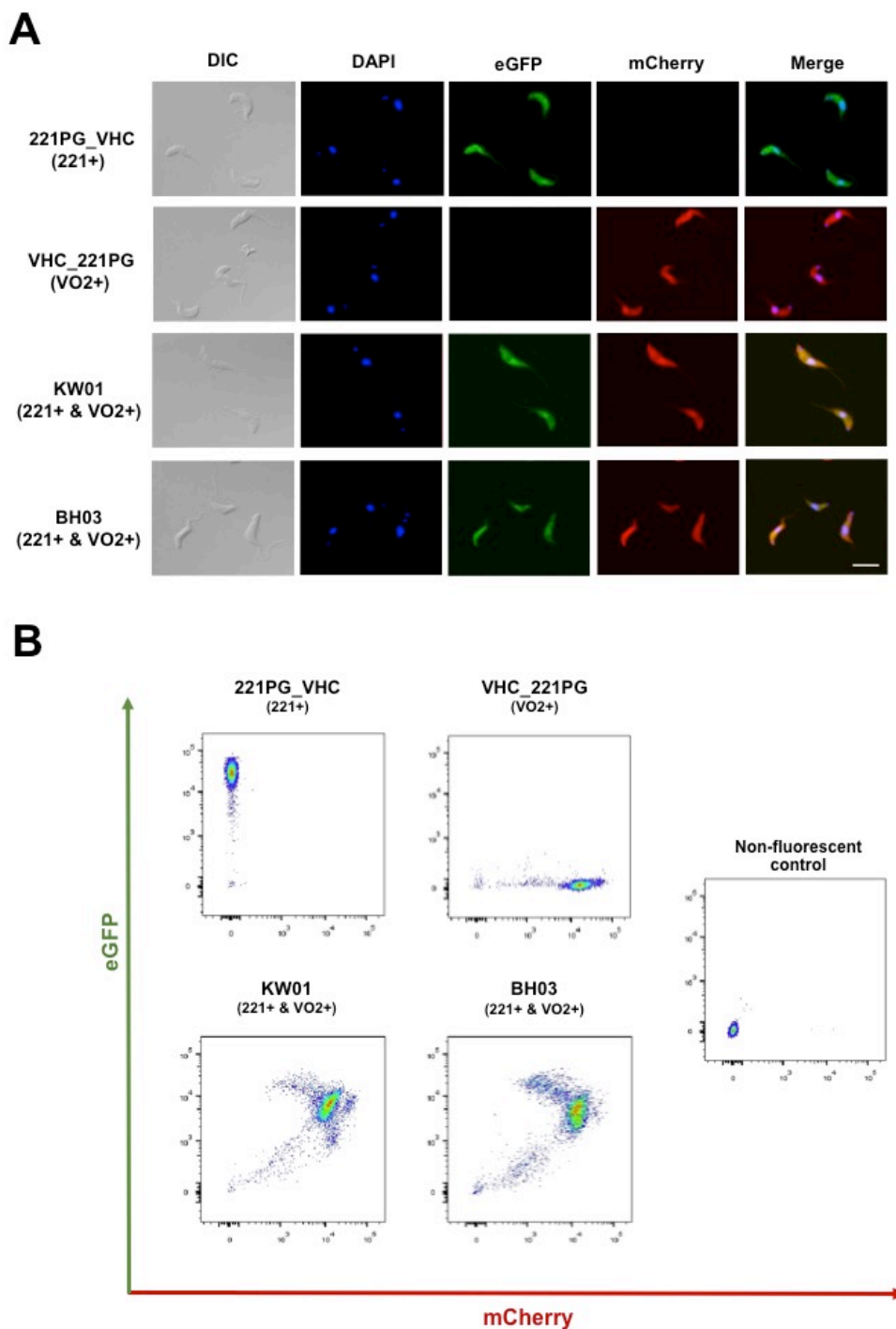


**Figure 6.4. Immunofluorescence images and flow cytometry capturing the endogenous fluorescence in the parental and DDR *T. brucei* cell lines.**

(A) The panel shows representative immunofluorescence images of 221PG\_VHC (221+), VHC\_221PG (VO2+), KW01 (221+ & VO2+) and BH03 (221+ & VO2+) *T. brucei* cell lines. Cells are stained with the DNA stain DAPI and endogenous expression of eGFP from the 221 ES or mCherry from the VO2 ES is visualised. Scale bar is 10  $\mu$ m. (B) Representative flow cytometry traces of 221PG\_VHC, VHC\_221PG, KW01 and BH03. The 1B2 cell line is shown as a non-fluorescent control. Endogenous fluorescence was monitored and eGFP fluorescence intensity (Y-axis) was plotted against mCherry fluorescence intensity (X-axis).

The fluorescent marker genes are located upstream of the *VSG* gene in the ESs. To ensure Pol I transcription in the DDR parasites extended the length of the ES including the *VSG* gene, immunoblot analysis was performed to confirm the DDR cell populations expressed both *VSG* 221 and *VSG* VO2. The immunoblot probed with antibodies against *VSG* VO2 and *VSG* 221 to detect the surface coat in cell protein lysate extracted from the two parental cell lines and the two DDR cell lines is shown in figure 6.5. Signal corresponding to both *VSG* 221 and *VSG* VO2 was detected in the KW01 and BH03 cell lines, with only a single band detected for *VSG* VO2 and *VSG* 221 in the VHC\_221PG and 221PG\_VHC cell lines, respectively. These data show that expression of both *VSG*s occurs within the DDR population.

To ensure the fluorescent markers accurately reflect the *VSG* surface coat being expressed, I probed all the cell lines with anti-221 conjugated to Alexa-647, and measured the fluorescence intensity of eGFP, mCherry and Alexa-647 (*VSG* 221) by flow cytometry. This experiment was next repeated using the anti-VO2 antibody conjugated to Alexa-647. The percentage of parental cells positive for eGFP and mCherry, and cells positive for Alexa-647 after probing with either antibodies against *VSG* 221 or *VSG* VO2 was determined using the gating outline in figure 2.2. The data from the parental cell line shows that the endogenous fluorescence from the active ES accurately corresponds to the *VSG* coat being expressed (Figure 6.6). For the 221PG\_VHC cells, 98% of eGFP positive cells were also positive for Alexa-647 when probed with the anti-221 antibody but no Alexa-647 signal was detected when the 221PG\_VHC cells were probed with an antibody against *VSG* VO2. The reverse is the case for the VHC\_221PG cell line that contains the *mCherry* fluorescent marker gene and *VSG* VO2 gene in the active ES.

Immunoblot analysis of surface coat proteins allows for detection of both *VSG*s in the DDR cells at a population level (Figure 6.5). In order to determine if the majority of individual DDR cells have a mixed surface coat, I conducted flow cytometry analysis on the DDR cell lines probed with either anti-221 or anti-VO2 antibodies, as described above for the parental cell lines (Figure 6.6A).



The flow cytometry analysis for KW01 shows that eGFP and mCherry positive cells are not only positive for VSG 221 and VSG VO2 respectively, but that the majority (>97%) of the DDR population has a mixed VSG coat. As 99% of KW01 cells that express mCherry (in the VSG VO2 ES) are VSG 221 positive, and 98% of KW01 cells that are eGFP positive (in VSG 221 ES) express VSG VO2. Similarly, a mixed VSG surface coat was detected for >95% of BH03 cells. Collectively, these data demonstrate that the DDR cell lines, BH03 and KW01 express two VSGs simultaneously, and that the fluorescence reporter genes within the ESs provide an accurate marker for the expressed surface coat.

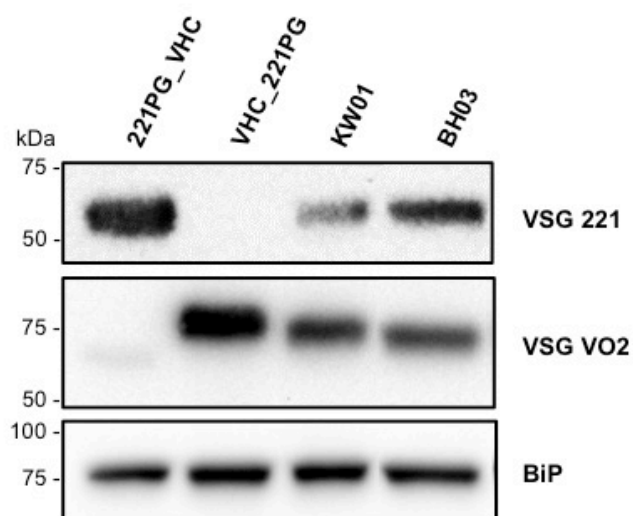


**Figure 6.5. *T. brucei* cell lines KW01 and BH03 simultaneously express VSG 221 and VSG VO2 surface coats.**

Immunoblot analysis of whole cell protein lysate extracted from parental (221PG\_VHC & VHC\_221PG) and DDR (KW01 & BH03) *T. brucei* probed with antibodies against VSG 221 and VSG VO2. The endoplasmic reticulum chaperone protein BiP was used as a loading control. Size markers are indicated in kiloDaltons (kDa).

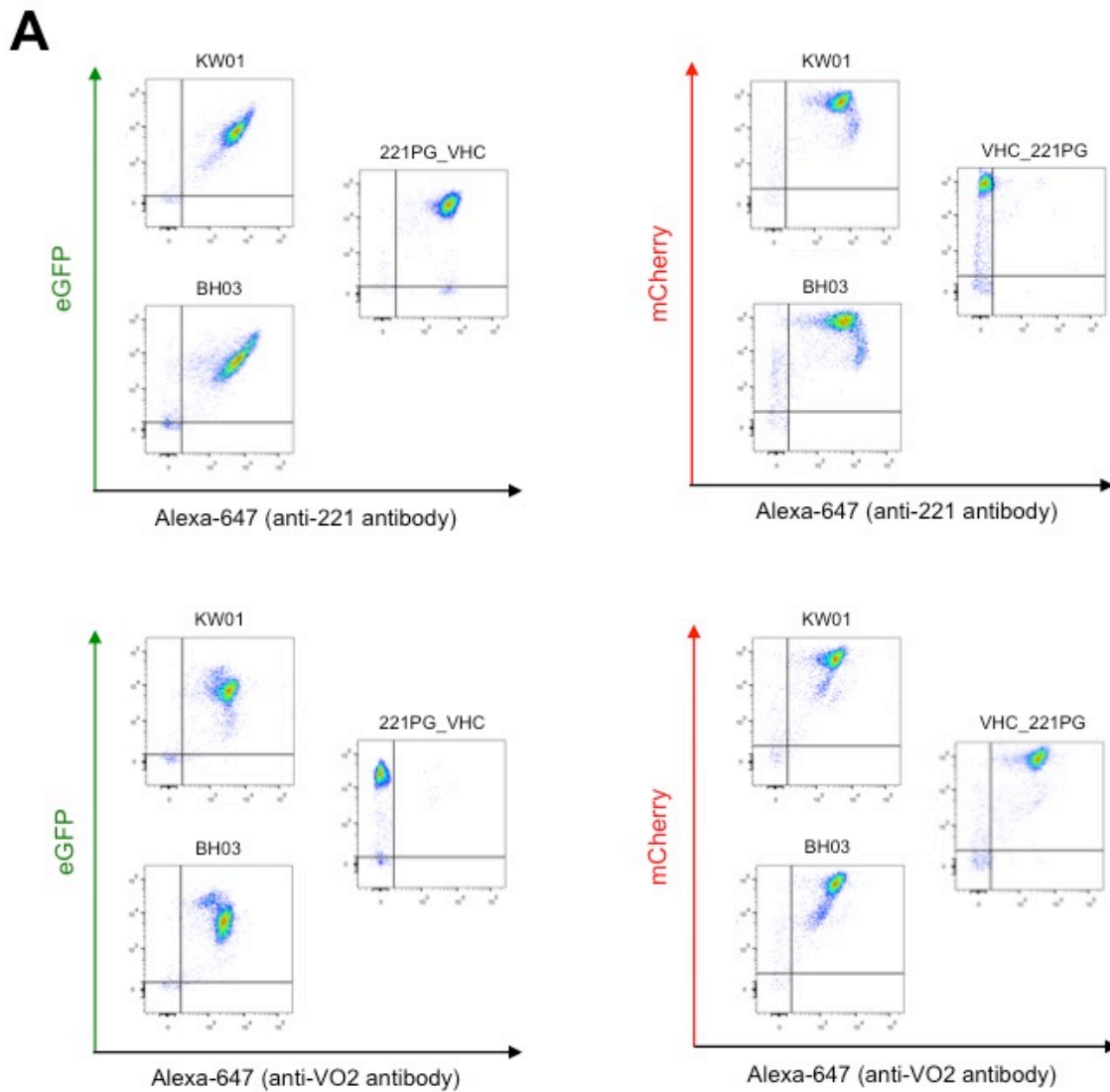


**Figure 6.6. Flow cytometry analysis of endogenous fluorescence in the DDR cell lines.**

(A) Flow cytometry traces of KW01, BH03, 221PG\_VHC and VHC\_221PG cells plotted as mCherry or eGFP against Alexa-647 conjugated to either anti-221 or anti-VO2 antibody. Gates were calculated using the 98<sup>th</sup> percentile of the appropriate control cell line. (B) The percentage of eGFP or mCherry positive cells also positive for Alexa-647 after probing with either anti-221 or anti-VO2 antibodies.

#### 6.4 - Heterogeneous DDR population or rapid switching phenotype?

The flow cytometry traces for the KW01 and BH03 cell lines clearly show a spectrum of fluorescence intensities (Figure 6.4B), with more eGFP and less mCherry detected in some cells compared with others within the DDR population or *visa versa*. In order to determine if this is the result of heterogeneous expression of the *eGFP* and *mCherry* genes within the DDR population, I conducted a dilution assay to obtain clonal KW01 and BH03 cells, and then analysed the fluorescence of the resulting clones. The KW01, BH03 and parental cell lines were analysed by flow cytometry, and the cultures were then diluted (<1 trypanosome per culture) to ensure the resulting populations were clonal. Five clones from each cell lines were subsequently analysed by flow cytometry and the fluorescence intensity of eGFP and mCherry was plotted as histograms with the flow traces shown on the right in Figure 6.7.

The flow cytometry traces of the KW01 cell line and the five KW01 derived clonal cell lines all appear relatively similar (Figure 6.7B). This similarity is even more evident in the histograms that show analogous frequency densities (peaks) for fluorescent intensity of eGFP and mCherry for the original KW01 cell line and the five clonal cell lines (Figure 6.7A). The data from the BH03 cell line is comparable to that obtained with the KW01 clones, as the histograms for the five BH03 clones appear to be very similar to the original BH03 cell line from which they were derived (Figure 6.7C). Flow cytometry analysis was also performed on the parental cell lines (221PG\_VHC and VHC\_221PG) and derived clones as a control (Figure 6.8). The fluorescence profiles of the clones from the parental cell lines remained similar to that obtained from the original parental lines pre-dilution. These data show that the spectrum of fluorescence observed in the DDR cell lines is not due to heterogeneity within the DDR population. The most likely explanation is that the DDR cells are rapidly switching back and forth between the two ESs, thus ensuring sufficient expression of the drug resistance genes to survive.

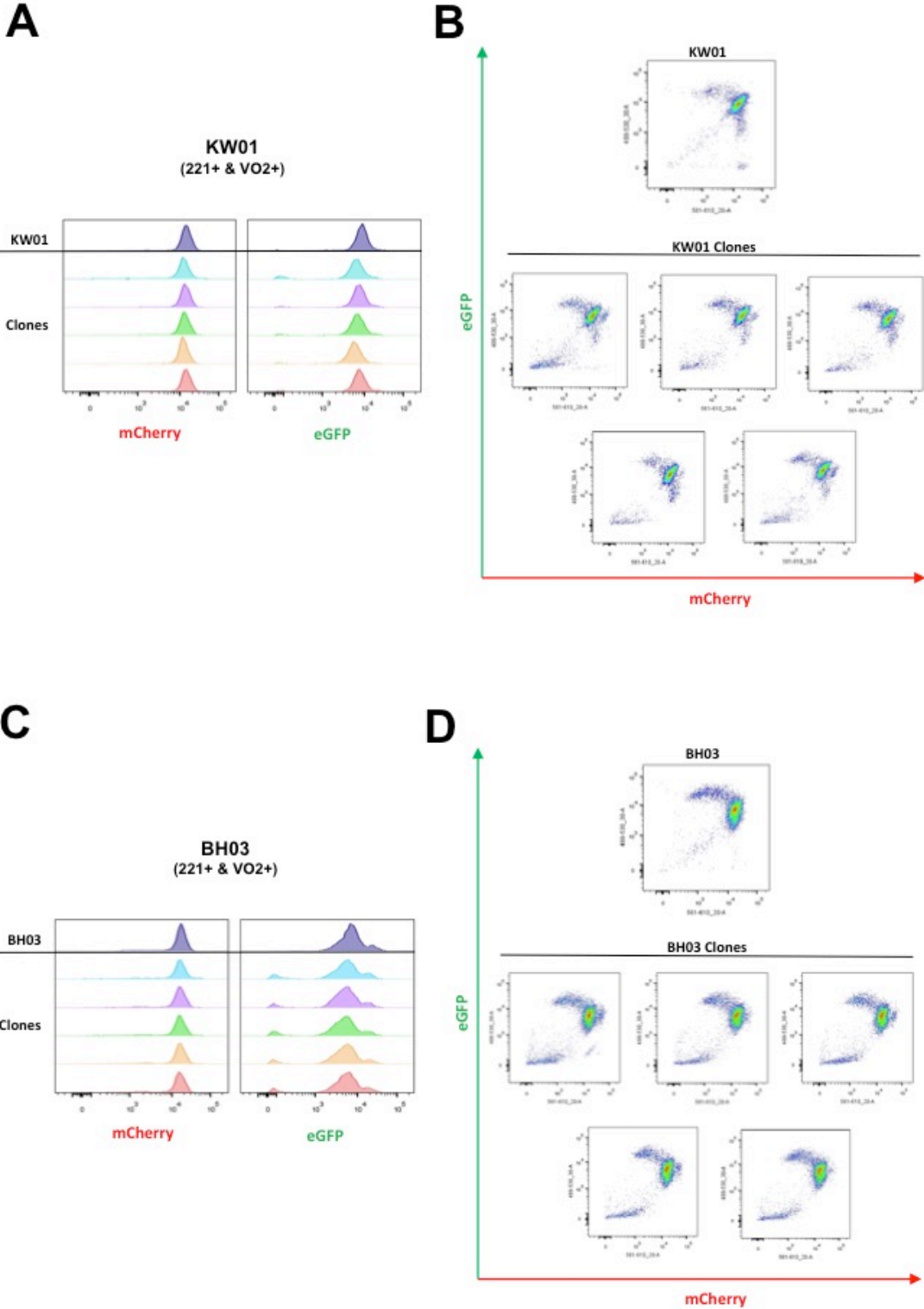


**Figure 6.7. Flow cytometry analysis of DDR clones obtained using a limiting dilution assay.** Histograms showing the eGFP and mCherry fluorescence intensity of **(A)** KW01 and **(C)** BH03 as well as the five clones obtained from the corresponding limiting dilution assays. The flow cytometry traces from which **(B)** KW01 and **(D)** histograms were derived are shown as eGFP fluorescence intensity (Y-axis) plotted against mCherry fluorescence intensity (X-axis).

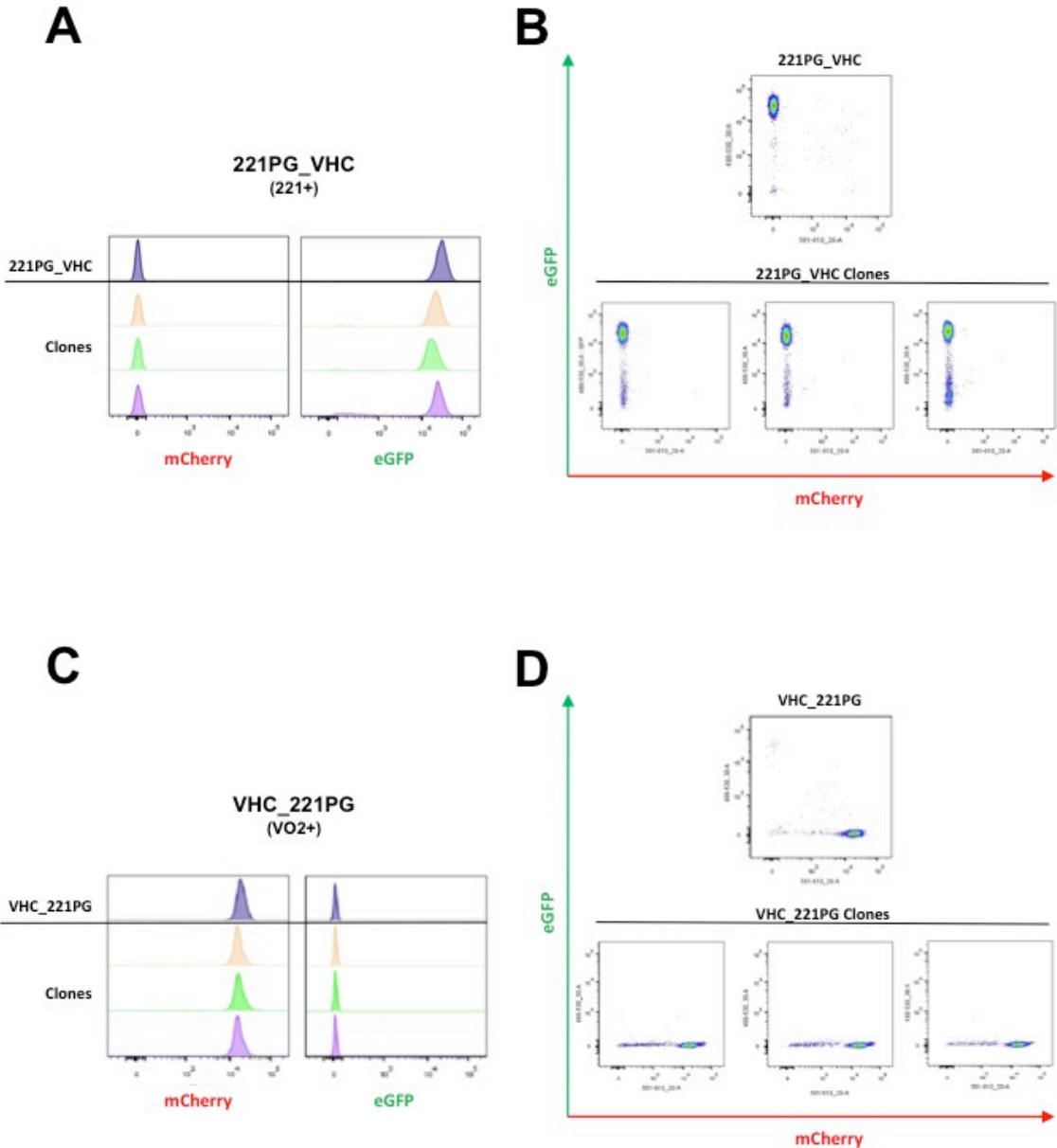


**Figure 6.8. Flow cytometry analysis of 221PG\_VHC and VHC\_221PG limiting dilution assay clones.** Histograms showing the flow cytometry analysis of the parental cell lines and three clonal populations obtained from the (A) 221PG\_VHC and (C) VHC\_221PG cultures. Flow cytometry traces corresponding to the histogram data for (B) 221PG\_VHC and (D) VHC\_221PG are shown. Endogenous eGFP fluorescence intensity (Y-axis) was plotted against mCherry fluorescence intensity (X-axis).

## 6.5 - Stability of the KW01 and BH03 cell lines

I next investigated the stability of the DDR cell lines once drug selection for the two active VSG ESs had been removed. If the DDR cells are rapidly switching between both ESs in order to maintain sufficient expression of the drug resistance genes to survive, then removal of the drug selection should result in a reduction in the percentage of double expresser cells in the DDR subpopulation (gates for subpopulations shown in figure 2.2). To test this hypothesis, both DDR cell lines (KW01 and BH03) were washed to remove the selection drugs and then cultured in the absence of puromycin and hygromycin. I conducted flow cytometry at regular intervals to monitor the fluorescence intensity of eGFP and mCherry to ascertain the percentage of DDR cells with a mixed coat. In parallel, I performed flow cytometry analysis of the DDR cell lines cultured in media containing hygromycin and puromycin (on drug) as well as analysis of the parental cell lines on and off drug selection as controls. Figure 6.9 shows the percentage of cells present in the DDR subpopulation (i.e. cells positive for both eGFP and mCherry), in the KW01, BH03 and parental cell lines cultured either on or off drug selection over a number of days.

Both the BH03 and KW01 cell lines cultured in the absence of drug selection (off drug) showed a reduction in the percentage of cells within the DDR subpopulation (eGFP and mCherry positive) over time compared with the on drug controls, which were cultured in the presence of hygromycin and puromycin. This suggests that the double expresser phenotype is not stable. Interestingly, the stability of the two DDR cell lines differs from one another. After 10 days off of drug selection, 55% of the KW01 population was still part of the DDR subpopulation (Figure 6.9A), and even after 25 days just over a quarter (26%) of the KW01 cell population were still double expressers. In contrast, only 1.5% of the BH03 cells cultured in the absence of drug selection still expressed both eGFP and mCherry after 10 days off drug selection. In the presence of drug selection (on drug) the percentage of the KW01 and BH03 cell lines regarded as DDR remained stable, with >93% of cells in these cultures expressing both eGFP and mCherry (Figure 6.9 A-B dotted line). The

percentage of DDR cells present in the parental cell lines was monitored as a negative control. Over the 25-day period no DDR cells were detected in the 221PG\_VHC (Figure 6.10C) or VHC\_21PG (Figure 6.9D) cell lines regardless of whether the parental cell lines were cultured in the presence or absence of the appropriate drug.

In addition to monitoring the DDR subpopulation, I also monitored the percentage of eGFP, mCherry and non-fluorescent cells (gates for subpopulations shown in figure 2.2) over a 96-hour period after removal of the selection drugs. This was in order to determine if the DDR cell lines would preferentially return to expressing the same VSG ES as the parental from which they were derived (Figure 6.10). After 96 hours off drug selection, the percentage of KW01 cells that had switched to expressing either eGFP (11.7%) or mCherry (9.5%) were relatively similar (Figure 6.9A). This suggests that the KW01 parasites are not biased towards the VSG 221 ES, which is active in the 221PG\_VHC parental cell lines from which KW01 was derived. The same is true of the BH03 cell line. After removal of drug selection for 96 hours, the BH03 cells did not preferentially revert back to expressing the VSG VO2 (mCherry positive) ES actively transcribed in the VHC\_221PG parental line (Figure 6.10B). No significant alteration in the percentage of eGFP or mCherry positive cells was observed in the cultures that were maintained on drug (Figure 6.10 dotted lines) or after removal of drug selection from the parental cell lines (Figure 6.10C-D).

Interestingly, when drug selection is removed, the KW01 and BH03 cell lines are significantly biased towards the VSG 221 or VSG VO2 ESs rather than any of the other VSG ESs. Switching to one of the ~15 other ESs would result in an increase in the percentage of non-fluorescent cells, as the DDR parasites do not encode a fluorescent marker genes in these ESs. No increase in non-fluorescent cells is observed in any of the cell lines over the 96-hour period (Figure 6.10). This suggests that the DDR parasites preferentially choose either the VSG 221 or VSG VO2 ESs over the other ESs. Presumably this is as these two ESs have a more open chromatin structure, whereas the other ~15 ESs are repressed.

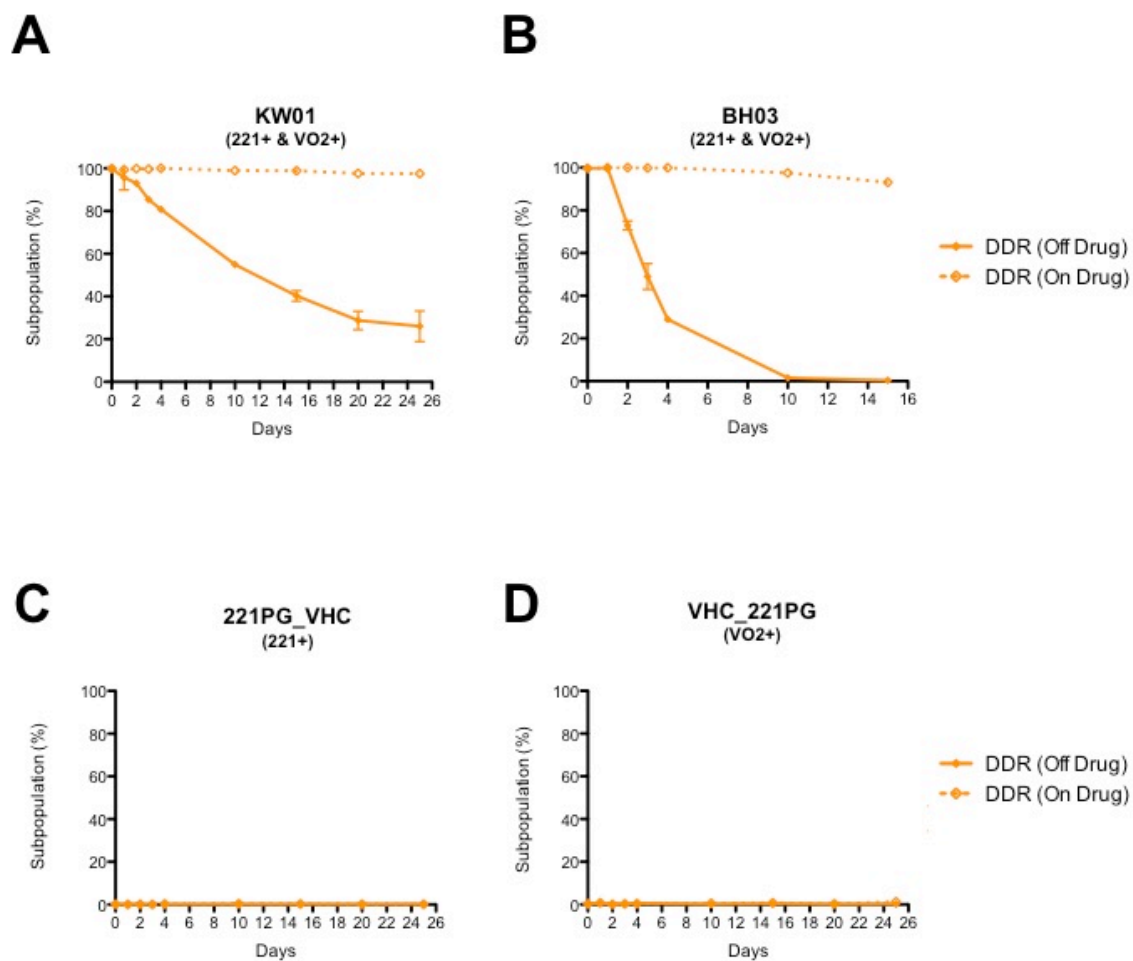


**Figure 6.9. Stability of the DDR subpopulation upon removal of drug selection.**

The endogenous mCherry and eGFP fluorescence was monitored at regular intervals after removal of drug selection (off drug) compared with the control, which was maintained on drug. The percentage of (A) KW01, (B) BH03, (C) 221PG\_VHC and (D) VHC\_221PG *T. brucei* cells within the DDR subpopulation gate (as defined in Section 2.11) are plotted as mean  $\pm$  standard deviation from two biological replicates. Block lines indicate the DDR subpopulation percentage (%) over time (days) for cultures kept off drug, and the dotted lines indicate the percentage of the DDR subpopulation in the on drug control.



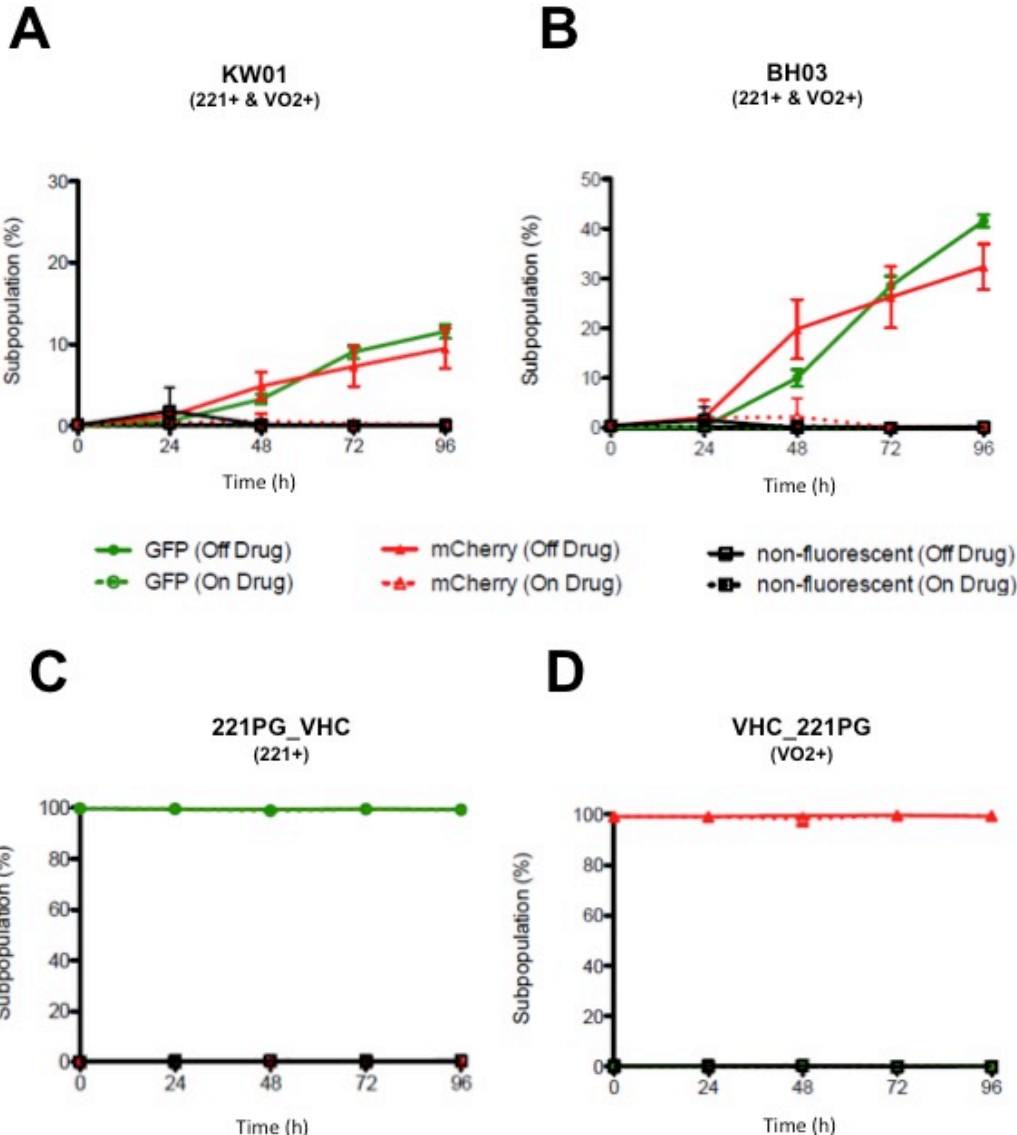


**Figure 6.10. Monitoring ESs in DDR cells maintained either on or off of drug selection.** The percentage of cells within the eGFP (green), mCherry (red) or non-fluorescent (black) subpopulations (see section 2.1) of the (A) KW01, (B) BH03, (C) 221PG\_VHC and (D) VHC\_221PG cell lines was monitored by flow cytometry over a 96-hour (h) period. The mean percentage of cells in each subpopulation from three biological replicates is plotted. Standard deviation is indicated with error bars.

## 6.6 - Epigenetic state of the pre-active VSG ESs in the KW01 and BH03 *T. brucei* cell lines

Chaves and colleagues (1999) previously speculated that the double expresser cells are the result of drug selection stabilising a natural intermediate switching state that is maintained epigenetically (Figure 6.1). However, the epigenetic factors responsible for the intermediate switch state were not identified (Chaves et al. 1999). Here, I have performed ChIP-qPCR using antibodies against histone H1, histone H3, the architectural protein TDP1 and the DNA modification base J in order to ascertain the epigenetic state of the DDR switch intermediate or pre-active ES. ChIP-qPCR experiments were performed on the two parental cell lines (221PG\_VHC and VHC\_221PG) and the DDR cell line KW01.

Analysis of the histone H3 ChIP-qPCR data (Figure 6.11A) showed that significant depletion of histone H3 was observed in the active ES of both parental cell lines for the regions amplified by qPCR primers specific for *VSG 221* and the drug resistance genes. This is in agreement with previously published data that showed histone H3 to be depleted at the active expression site compared to the silent ESs (Figueiredo & Cross 2010; Stanne & Rudenko 2010). Unfortunately, *T. brucei* encodes two copies of the *VSG VO2* gene, one in the active ES and a second *VO2* gene located in a non-ES locus. The elevated levels of histone H3 observed for *VSG VO2* were due to the qPCR primer pair amplifying an additional copy of the *VSG VO2* gene not present in the ES.

The level of histone H3 present in the pre-active *VSG* ESs of the KW01 cell line was 5 to 10-fold less compared with the percentage of histone H3 observed in the silent ESs of the parental cell lines. However, it was still marginally higher than the histone H3 levels observed in the active ES of the parental cell lines (Figure 6.11A). This data indicates that the unstably active *VSG* ESs have a more open chromatin structure than the silent ESs, but not at the level observed in the single active *VSG* ESs of the parental cell lines. I also conducted qPCR analysis using primers that recognise sequences within a silent *VSG* (*VSG 14*), the rDNA transcription unit, and Pol II transcribed genes (Actin, Pol I and Y-tubulin) as controls. Comparison between the KW01 cell line and the parental cell

lines showed no significant differences in the percentage of histone H3 immunoprecipitated in regions amplified by qPCR primers specific for *VSG* 14 (Figure 6.11A), the Pol I transcribed rDNA transcription unit (Figure 6.11B) nor the Pol II transcribed genes (Figure 6.11C). This suggests that the reduced histone H3 levels are not universal, but restricted to the pre-active *VSG* ESs in the KW01 cells.

In agreement with previously published data (Povelones et al. 2012), qPCR analysis of ChIP material immunoprecipitated using an anti-histone H1 antibody showed that the active ES is depleted of histone H1 in the parental cell lines (Figure 6.12A). Similar to histone H3, an intermediate level of histone H1 was observed in the pre-active ESs of the DDR parasites (Figure 6.12A). The level of histone H1 immunoprecipitated in the KW01 cell line appears elevated (although not significantly) compared to the parental control cell lines in the silent *VSG* (Figure 6.12A *VSG*14), in the rDNA transcription unit (Figure 6.11B), as well as the Pol II transcribed genes (Figure 6.12C). Immunoblot analyses of protein lysates from the DDR and parental cell lines ( $1 \times 10^6$ ,  $5 \times 10^5$  and  $2.5 \times 10^5$  cell equivalence per cell line per lane) showed similar levels of signal corresponding to histone H1 were detected for all three cell lines (Figure 6.12D). This suggests that the increased amount of histone H1 immunoprecipitated was not due to a universal upregulation of histone H1 in DDR parasites.

TDP1 is an architectural protein enriched at the Pol I transcribed rDNA transcription units and *VSG* ESs, and has an inverse distribution with histones (Narayanan & Rudenko 2013). I performed ChIP-qPCR analysis to determine the distribution of TDP1 at the pre-active ESs in the DDR cell. An enrichment of TDP1 on the active ES compared to the silent ES was seen in the 221PG\_VHC cells and the level of TDP1 was marginally elevated in the active ES of the VHC\_221PG cell line (Figure 6.13A). TDP1 is present in the pre-active *VSG* ESs (Figure 6.13A) and the Pol I transcribed rDNA transcription unit (Figure 6.13B) of the KW01 cells at comparable levels to the active ESs and rDNA of the parental cell lines. This is consistent with a previously proposed model that TDP1

replaces histones in active Pol I transcription units in order to help retain an open chromatin structure (Narayanan & Rudenko 2013). The percentage of TDP1 immunoprecipitated at the silent *VSG* (Figure 6.13A) and Pol II transcribed genes (Figure 6.13C) was less than the actively transcribed Pol I transcription units, but comparable levels of TDP1 were immunoprecipitated between the KW01 and parental cell lines.

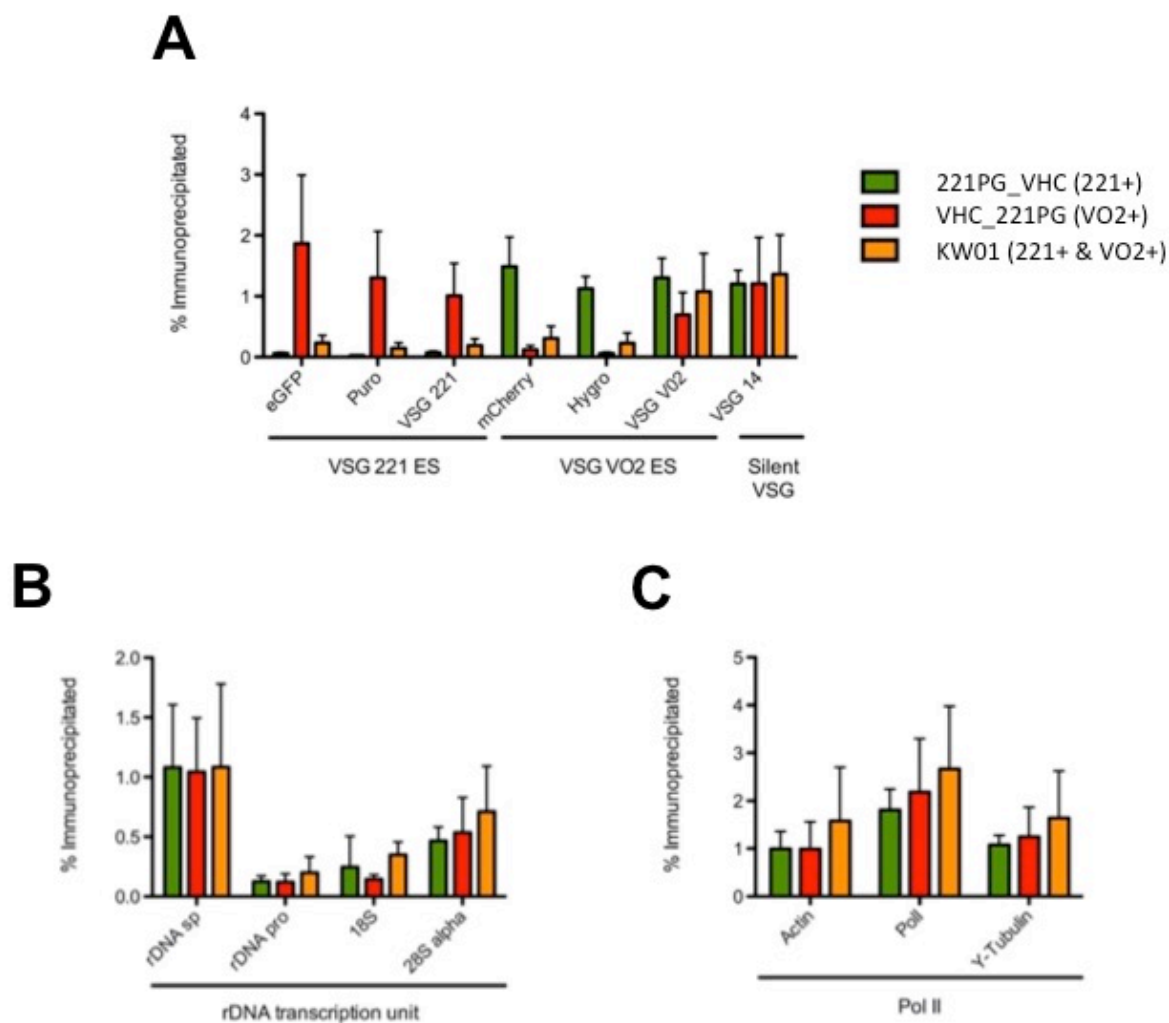


**Figure 6.11. Distribution of histone H3 in the Pol I transcribed VSG ESs, rDNA transcription units and Pol II transcribed gene loci in DDR parasites.**

The levels of histone H3 were determined by ChIP using an antibody against histone H3 in the 221PG\_VHC (green), VHC\_221PG (red) and KW01 (orange) *T. brucei* cell lines. (A) qPCR analysis using primers designed to amplify regions within the fluorescent marker genes (*eGFP* and *mCherry*), the *hygromycin* (*hygro*) and *puromycin* (*puro*) resistance genes, the *VSG* genes located within the marked ESs and silent *VSG* gene (*VSG 14*) was conducted. ChIP-qPCR analysis using primers to amplify regions within (B) the Pol I transcribed rDNA transcription units and (C) Pol II transcribed *actin*, *RNA polymerase I* (Pol I) and *gamma-tubulin* ( $\gamma$ -Tubulin) gene loci was also performed. Results are presented as the percentage of input immunoprecipitated after subtraction of the no antibody control. The data plotted is the mean of three independent ChIP-qPCR experiments with the standard deviation indicated with error bars.

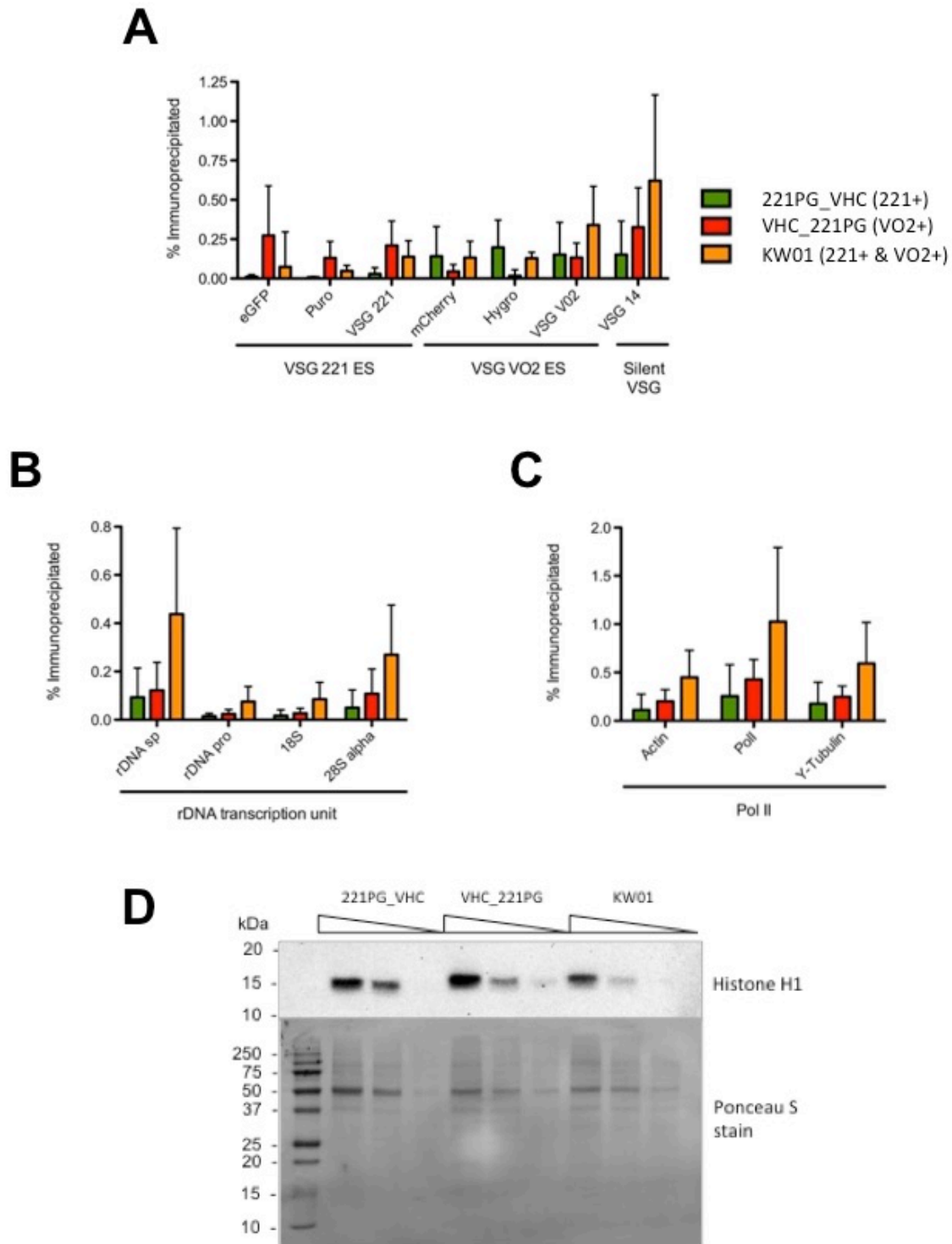


**Figure 6.12. Distribution of histone H1 in the Pol I transcribed VSG ESs, rDNA transcription unit and Pol II transcribed gene loci in DDR parasites.**

(A-C) as in figure 6.11 A-C, only ChIP-qPCR analysis of material immunoprecipitated using an antibody against histone H1. (D) Immunoblot analysis of the levels of histone H1 present in the *T. brucei* 221PG\_VHC, VHC\_221PG and KW01 cell lines. Whole protein lysate from  $1 \times 10^6$ ,  $5 \times 10^5$  and  $2.5 \times 10^5$  cell equivalence were blotted and probed with anti-histone H1 antibody. Bands corresponding to histone H1 are shown and a Ponceau S stain of the blot serves as a loading control. Size markers are shown in kiloDaltons (kDa).

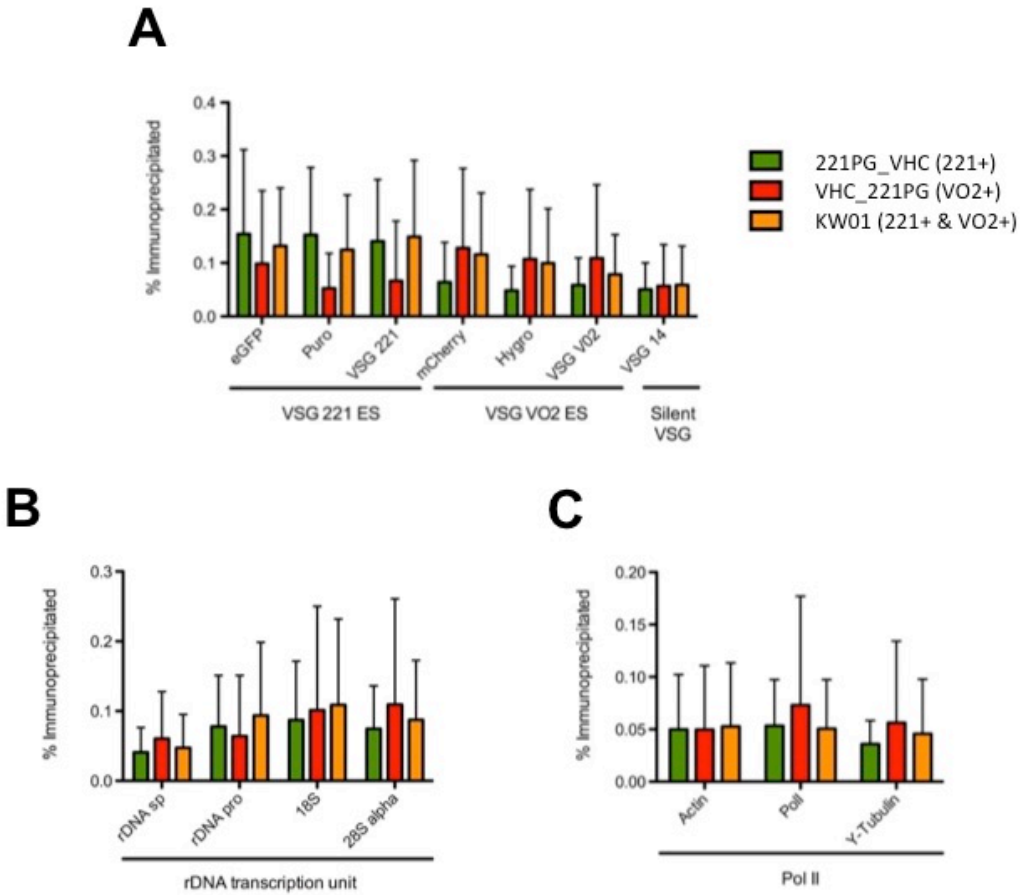


**Figure 6.13. Distribution of TDP1 in the Pol I transcribed VSG ESs, rDNA transcription unit and Pol II transcribed gene loci in DDR parasites.** (A-C) as in figure 6.11 A-C, only ChIP-qPCR analysis of material immunoprecipitated using an antibody against *T. brucei* TDP1.

### **6.7 - Optimisation and troubleshooting of chromatin immunoprecipitation using antisera against base J in BSF *T. brucei*.**

Base J is a novel DNA modification found in the repeat sequences of the *VSG* ESs and is present in a gradient extending from the telomeres into the ESs of silent *VSG* transcription units in BSF *T. brucei* but not procyclic (PCF) *T. brucei*. Although the precise function of base J remains to be elucidated, its distribution suggests a role in suppressing transcriptional elongation in the silent *VSG* ESs (Borst & Sabatini 2008). In 1997, an initial endeavour to generate an antiserum specific for *T. brucei* base J was successful (van Leeuwen et al. 1997). However, subsequent attempts to generate more rabbit polyclonal antisera and a mouse monoclonal antibody have failed (Borst & Sabatini 2008).

In order to investigate the distribution of base J in the DDR parasites, I attempted to optimise ChIP using various concentrations of the original base J antisera (gift from Professor Borst, Netherland Cancer Institute) and an anti-histone H3 antibody as a control in the 221PG\_VHC BSF *T. brucei* cell line. qPCR analysis, using primers specific for sequences within the *VSG* genes, drug resistance genes and fluorescent marker genes, showed no PCR amplification using the ChIP material immunoprecipitated with any of the base J antisera concentrations (Figure 6.14A). However, ChIP-qPCR analysis showed the distribution and level of histone H3 was as expected, thus suggesting that the ChIP-qPCR experiment was further successful (Figure 6.14A).

To check the specificity of the base J antiserum, I performed an immunofluorescence assay on BSF *T. brucei* and PCF *T. brucei*. Signal was detected in the nucleus, kinetoplast and cytoplasm of both the bloodstream and procyclic form *T. brucei* (Figure 6.14B). This signal is most likely due to non-specific binding of rabbit serum components in the antisera. These data suggests that the antiserum may have degraded and no longer recognises the base J epitopes. Unfortunately, the Rudenko lab does not have any additional aliquots of the antisera to test, and given the scarcity of



remaining aliquots from 1997 I was unable to continue to investigate the distribution of base J in the DDR parasites.

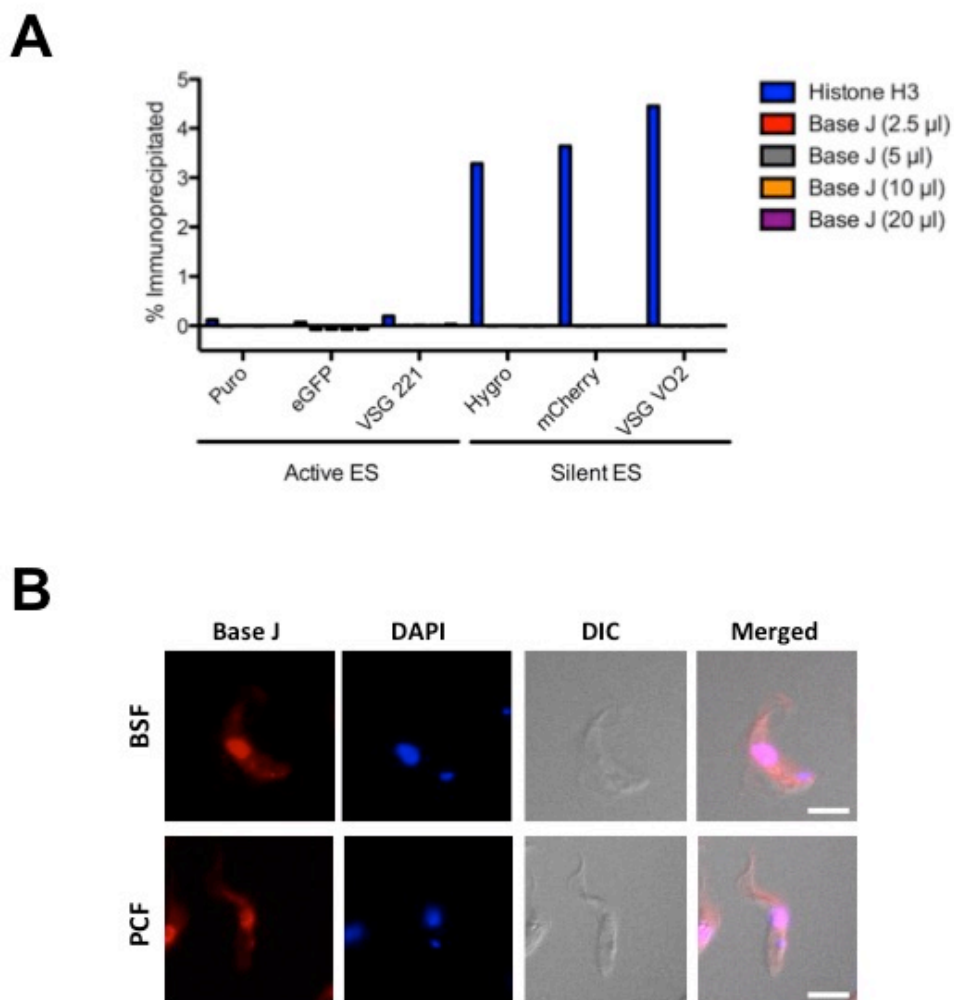


**Figure 6.14. Optimisation of ChIP using an antibody against the DNA modification base J.**

(A) ChIP was performed using a range of concentrations of the anti-base J antisera using the anti-H3 antibody as a positive control. ChIP-qPCR data monitoring the single copy marker genes within the active and silent ESs from a single ChIP experiment is shown as the percentage of input immunoprecipitated after subtraction of the no antibody control. The distribution of histone H3 is consistent with previously published data (Stanne & Rudenko 2010) but no base J was detected by qPCR amplification of the ChIP material for any of the antisera concentrations used. (B) Representative immunofluorescence microscopy images of bloodstream form (BSF) or procyclic form (PCF) *T. brucei* stained with the DNA stain DAPI and probed with the anti-Base J antisera and an anti-rabbit alexa-594 secondary antibody. Differential interference contract (DIC) and merged images are shown for each panel. Scale bar is 5µm.

### 6.8 - Number of ESBs present in the DDR *T. brucei* cell line KW01

Here, I investigated if the rapid switching between ES observed in the DDR cells is a consequence of the singularity of the ESB. In order to quantify the number of ESBs present in the KW01 cell line, I generated a construct to epitope tag the N-terminus of RPA2. RPA2 is the second largest subunit of the Pol I complex and has previously been used as a marker for the ESB (Daniels et al. 2012; Kerry et al. 2017). The resulting pEnt5B-3xHA:RPA2 construct was used to generate *T. brucei* expressing 3xHA tagged RPA2 from the endogenous RPA2 locus in the KW01 cell line. RPA2 was visualised in the 3xHA:RPA2 tagged cell lines using an antibody against HA with Alexa Fluor 647 secondary antibody. Endogenous fluorescence from expression of the *eGFP* and *mCherry* fluorescent marker genes and DNA stained DAPI was also monitored. The tagged cell lines did not exhibit any reduction in growth, and the localisation of RPA2 signal in cells probed with anti-HA corresponded to the nucleolus and the extranucleolar ESB.

Previous studies have shown approximately 60-70% of G1 *T. brucei* cells contain an extranucleolar Pol I positive focus corresponding to the ESB (Navarro & Gull 2001; Daniels et al. 2012). Our preliminary Immunofluorescence microscopy analysis showed that 62% of the KW01 cells in the G1 stage of the cell cycle contained an extranucleolar focus corresponding to an ESB, but a further 10% of G1 cells contained a second RPA2 positive focus (Figure 6.15). Chaves and colleagues previously showed a similar percentage (13-14%) of double expresser cells contained two fluorescent signals corresponding to expression site nuclear transcript (Chaves et al. 1999).

The observation that only 10% of the KW01 cells contain a second extranucleolar RPA2 positive focus may help explain why the DDR cell lines are forced to rapidly switch between the two ESs in order to generate sufficient drug resistance to survive selection. The ESB complex may contain a limited component(s) that ensure only a single ESB can be assembled and fully active. It is possible the second RPA2 positive focus is a simplified pre-ESB complex recruited to probe the pre-active ES ensuring it is functional prior to committing to the *in situ* switch. This natural intermediate may only

be visible in the DDR cells due to their extremely rapid switch rate, which would increase the likelihood of capturing this transient stage during an *in situ* switch.

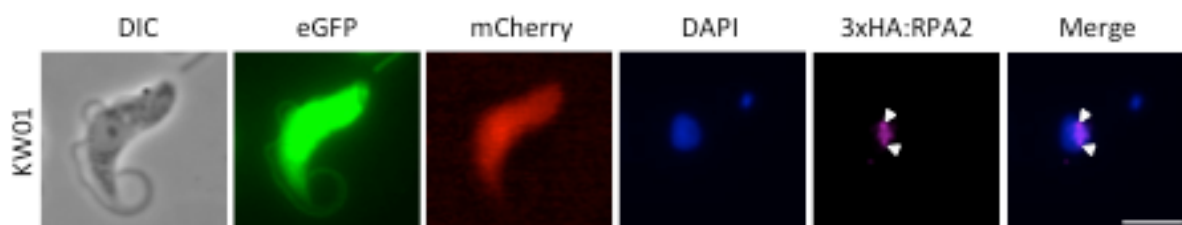


**Figure 6.15. Representative immunofluorescence microscopy panels of a KW01 cell containing two ESBs.**

Immunofluorescence panel showing images representative of the KW01-3xHA:RPA2 cells in the G1 stage of the cell cycle. Cell morphology was visualised using differential interference contrast (DIC) and DNA content was visualised by DAPI staining (blue). Endogenous expression of eGFP (green) from the 221 ES and mCherry (red) from the VO2 ES is shown. KW01-3xHA:RPA2 cells were probed with anti-HA antibody and an Alexa-647 secondary antibody to visualise expression of the HA tagged RPA2 gene (purple). Foci corresponding to the two ESBs are indicated with white arrowheads. Imaged by J.Budzak. Scale bar is 5  $\mu$ m.

## 6.9 - Discussion

Monoallelic expression of a single *VSG* gene from one of ~20 very similar *VSG* ESs is essential for *T. brucei* to maintain sufficient levels of antigenic variation to prolong host infection (Hertz-Fowler et al. 2008). Given the importance of this monoallelic *VSG* expression for parasite survival (Pays et al. 2014); numerous studies have investigated the mechanism that enables *T. brucei* to express a single *VSG* in a reversible and heritable manner (Aresta-Branco et al. 2016; Landeira et al. 2009). Importantly, *T. brucei* must be able to rapidly switch from expression of one *VSG* to another, with this switch resulting in the rapid activation of a new fully functional *VSG* ES and repression of the previously active ES.

Chaves and colleagues (1999) previously studied this mechanism of silencing and switching by generating double drug resistant (DDR) *T. brucei* with two drug resistance genes in two different ESs. After drug selection the parasites were thought to be rapidly switching back and forth between the marked ESs. Given the 30-40 hour half-life of the *VSG* protein (Seyfang et al. 1990), the rapid switching explained the mixed *VSG* surface coat observed. The authors proposed that drug selection resulted in stabilisation of a natural switch intermediate ES, and this poised pre-active state (Figure 6.1) was likely maintained by an unknown epigenetic mechanism (Chaves et al. 1999). In this chapter I have validated and characterised new DDR cell lines, investigated the epigenetic state of the pre-active ESs, and completed preliminary analysis of the role of the ESB in monoallelic exclusion.

Here, flow cytometry analysis of the endogenous fluorescent marker genes present in the ESs of KW01 and BH03 clones has shown that the heterogeneity of fluorescence observed in the DDR populations was the result of the double expresser cells rapidly switching between the *VSG* 221 and *VSG* VO2 ESs (Figure 6.7). Interestingly, upon removal of drug selection the DDR cell lines do not immediately revert to single expressers and the stability of the DDR phenotype differs between the two cell lines. After 10 days off drug, almost no DDR subpopulation exists in the BH03 cultures

whereas, 26% of the KW01 cells retain the DDR phenotype after 25 days off drug selection. Additionally, the DDR cells preferentially switched to the *VSG VO2* or *VSG 221* ES rather than any of the other ~15 ESs after drug removal. The lag in loss of the DDR phenotype and preference for the marked ESs, suggest an open chromatin composition of the *VSG 221* and *VSG VO2* ESs compared to the unmarked ESs.

The data presented in this chapter show that the epigenetic status of the *VSG 221* and *VSG VO2* ESs in the DDR cell line KW01 appear to be identical to one another, and similar to the active ES of the parental cell lines (Section 6.6). This pre-active or intermediate state is characterised by a depletion of histones (H1 and H3) and an enrichment of TDP1 within the *VSG VO2* and *VSG 221* ESs of the KW01 cell line. In the pre-active state this open chromatin structure, stabilised by TDP1, could allow for “probing” of a new ES prior to fully committing to the switch. If the “probed” ES was found to be non-functional, the cell could rapidly reactivate the original ES from the pre-active state. My data regarding the pre-active state is in agreement with two other studies both of which propose an intermediate switch state regulated by TDP1 (Aresta-Branco et al. 2016) and DOT1B (Batram et al. 2014). Despite using different experimental approaches these studies provide supportive evidence for a pre-active ES state.

The DNA modification base J is enriched in a gradient increasing towards the telomeres of silent ES, and it would therefore be fascinating to determine the status of this DNA modification in the pre-active ES. Unfortunately, my attempts to immunoprecipitate base J were not successful as the base J antiserum appeared to have degraded and no alternative base J antiserum was available (Figure 6.14). However, gDNA samples from the KW01, BH03 and parental cell lines have since been collected and sent to our collaborator Professor Peter Myler and colleagues (University of Washington). They will perform ChIP-Seq analysis to map the distribution of base J in the DDR and single expresser parental *T. brucei* cell lines. It is hoped that this comprehensive mapping of the

---

distribution of base J in *T. brucei* may provide clues as to the role of base J, as well as shed light on the status of base J at pre-active ESs.

Here, I have shown that the DDR cells rapidly switch between the *VSG 221* and *VSG VO2* ESs rather than transcribing both ESs simultaneously. CHIP-qPCR analysis has shown that both DDR ESs retain an open chromatin composition (pre-active state) similar to the active ES of the single expresser *T. brucei*. Consequently, an additional mechanism must be operating in BSF *T. brucei* that ensures that only a single *VSG* ES is actively transcribed at once. This restrictive mechanism would need to be able to rapidly activate and repress the ESs in order to maintain the fast switch rate observed in the DDR cells.

The ESB is an obvious candidate to play an important role in ensuring monoallelic expression in *T. brucei*. Preliminary investigation into the number of Pol I (3xHA:RPA2) positive foci in the DDR cells revealed 62% of G1 cells contain a single ESB and a further 10% of G1 cells were positive for a second ESB. It has previously been shown that low levels of transcription occur at silent *VSG* ESs, which suggest that Pol I can be recruited to the promoters of silent ESs (Günzl et al. 2003). The epigenetic data in this chapter and from previous studies (Chaves et al. 1999; Batram et al. 2014; Aresta-Branco et al. 2016) strongly suggests that a pre-active ES is epigenetically distinct from the other silent ESs, and in a pre-active state prior to switching. Additionally, the observed lag in loss of the DDR phenotype after removal of drug selection suggests that the open chromatin state of the previously active ES is retained for some time before becoming repressed (Figure 6.9)

One possible model to explain these data is that the ESB complex contains a limiting factor(s) required for assembly of a single fully active ESB but a pre-active ES could be transcribed at low levels by a simple 'pre-ESB' complex. The relatively open chromatin structure of the pre-active ES may allow for not only the recruitment of low levels of Pol I, but also additional ESB factors to form a 'pre-ESB' complex. This basic 'pre-ESB' would lack the limiting component(s) required for fully active transcription and contain a much lower concentration of Pol I than the ESB, but would

provided sufficient transcription to test the pre-active ES. Provided the pre-active ES is found to be functional, the limited ESB component(s) would disassemble from the active ES and re-assemble on the pre-active ES to form a fully active ESB, thereby completing the *in situ* switch. This fail-safe mechanism would allow the trypanosome to rapidly reactivate the previously active ES (as it is in the pre-active state) if the new ES proves faulty. Evidence supporting the ability of the ESB to rapidly disassemble and reassemble upon inhibition or reinitiation of Pol I transcription was previously discussed in chapter 5.

In the context of the pre-ESB model, the 10% of KW01 cells that contain two ESBs would result from capturing the assembly of the new ESB on the pre-active ES and disassembly of the old ESB on the previously active ES. During nucleation of the new ESB and disassembly of the old ESB the abundance of RPA2 (Pol I) is sufficient at both ESs to be detected by immunofluorescence microscopy. The transitional state may only be visible in the KW01 cell line because of the rapid switch rate. As this would result in an increased chance of capturing the disassembly of the old ESB and completion of a fully functional new ESB from the pre-ESB complex during the *in situ* switch.

This proposed pre-ESB model is based on preliminary data, and further investigation of additional factors contributing to the epigenetic status of the pre-active ESs is required. In collaboration with Professor Terry Smith (University of St. Andrews) we plan to perform SWATH analysis with the aim of identifying differences in the proteome of the DDR cell lines compared to the parental. This may shed light on the epigenetic factors contributing to the double expresser phenotype. Additionally, determining the number of VEX1 foci present in the DDR cells may provide clarity on the maintenance of a single ESB in G1 *T. brucei*, as VEX1 has been proposed as a limiting factor for establishment of ESB associated transcription (Glover et al. 2013).

## Chapter Seven

### Final discussion and conclusions

#### 7.1 - Scope and goals of this thesis

HAT is endemic to sub-Saharan Africa resulting in human mortality and socio-economic hardship (WHO 2017c). Regarded as a NTD, current treatments for HAT are problematic; chemotherapies are difficult to administer, often ineffective in eradicating the parasites from the central nervous system, and highly toxic with treatment related mortality rates of up to 10% (Büscher et al. 2017). *T. brucei* subspecies are the etiological agent of HAT and evade the host immune system through antigenic variation of its surface coat proteins. Uniquely, *T. brucei* utilises Pol I to transcribe not only the rDNA transcription units but also the *VSG* surface coat genes from an extranucleolar ESB (Günzl et al. 2003). These *VSG* genes are expressed in a monoallelic manner with a single *VSG* gene transcribed at a time from one of approximately 15 very similar *VSG* ESs (Hertz-Fowler et al. 2008). This monoallelic expression is essential, as switching between a repertoire of hundreds of *VSG* genes and pseudogenes provides the parasites with sufficient antigenic variation to prolong host infection (Taylor & Rudenko 2006). Chromatin structure, chromatin-remodelling proteins and the histone methyltransferase DOT1B have been shown to contribute to the regulation of the Pol I transcribed *VSG* ESs (Povelones et al. 2012; Figueiredo & Cross 2010; Narayanan & Rudenko 2013).

Despite these numerous studies, the epigenetic mechanisms that maintain maximal activation of a single *VSG* ES and repression of the other ESs are not fully understood. The goal of my PhD research was to advance our understanding of the epigenetic factors that contribute to regulation of Pol I transcription in *T. brucei* and to evaluate epigenetic drug targets as novel anti-parasitic agents.



## 7.2 - Distribution of H3K4me3 in Pol I transcribed loci in BSF *T. brucei*

The *T. brucei* genome is organised into long polycistronic transcription units that are constitutively transcribed by Pol II and are regulated almost exclusively post-transcriptionally (Berriman 2005). Histone modifications, histone variants and chromatin-remodelling proteins play a role in the regulation of Pol II transcribed gene expression in trypanosomes (Siegel et al. 2009; Wright et al. 2010; Talbert & Henikoff 2009). Additionally, the histone modifications H3K4me3 and H4K10ac are enriched at the putative Pol II TSSs in *T. brucei* (Wright et al. 2010). This demonstrates that like higher eukaryotes trypanosomes utilise histone modifications to regulate gene expression. In higher eukaryotes, trimethylation of H3K4 is associated with the 5' end of genes actively transcribed by Pol II or Pol I (Barski et al. 2007; McStay & Grummt 2008). This suggests that the distribution of the H3K4me3 modification may be universally conserved in eukaryotes.

Given the importance of maintaining monoallelic expression of the *VSG* ES to prolong parasite survival in the host, perturbing this process would be a possible drug target. The histone modification H3K4me3 is enriched at putative Pol II TSSs in *T. brucei* (Wright et al. 2010) and at Pol I transcribed RNA promoters in higher eukaryotes (McStay & Grummt 2008). Therefore I investigated the distribution of the H3K4me3 modification at Pol I transcribed loci in BSF *T. brucei*. I validated two commercially available anti-H3K4me3 antibodies (M04-745 and ab8580) and confirmed H3K4me3 to be enriched at Pol II TSSs, which is in agreement with ChIP-Seq data previously published by Wright and colleagues (2010). I did not find any evidence of H3K4me3 enrichment in the Pol I transcribed rDNA transcription units in *T. brucei* (Figure 3.5). The histone modification was also only detectable at very low levels within the *VSG* ESs, regardless of whether the ES was active or silent (Figure 3.6). These results suggest that enrichment of trimethylated H3K4 is not correlated with active Pol I transcription in BSF *T. brucei*, as it is in higher eukaryotes (McStay & Grummt 2008).

These results may be explained by the fact that trypanosomes diverged early in the eukaryotic lineage. Consequently, core histone sequences and some of the PTMs are divergent from

other eukaryotes. This is also the case with the role of Pol I, which transcribes the surface coat protein coding genes in *T. brucei* instead of exclusively the rDNA as is found in other eukaryotes (Thatcher & Gorovsky 1994; Mandava et al. 2007; Janzen et al. 2006b; Günzl et al. 2003). It is therefore plausible that *T. brucei* has evolved to utilise an alternative epigenetic modification to denote the promoters of Pol I transcribed genes. Several histone modifications have already been mapped to putative Pol II promoters in *T. brucei* providing evidence that histone modifications and TSSs are correlated in *T. brucei*, thus suggesting the parasites use PTMs to modulate gene expression (Wright et al. 2010). My data suggests trimethylation of H3K4 does not modulate transcription of Pol I promoters in *T. brucei*. Leaving the intriguing questions as to which alternative modification is used, and if the modification is trypanosome specific, whether it could be a viable drug target for anti-kinetoplastid chemotherapies.

### **7.3 - Repurposing of chemical inhibitors, originally developed against cancer, as potential anti-kinetoplastid agents.**

Repurposing drugs and target compounds is an appealing option for the development of new chemotherapies to treat neglected tropical diseases, such as HAT. The increased success rate, shortened drug development time and reduced cost are particularly important (Nosengo 2016). NTDs tend to affect less economically developed countries (WHO 2017a; WHO 2017c), so pharmaceutical companies would therefore struggle to financially recoup the cost of *de novo* drug development (Andrews et al. 2014). In this study, I have found several novel and commercially available chemical compounds, originally developed as anti-cancer therapies, to have potential as anti-kinetoplastid agents.

BIX-01294 was originally designed to selectively inhibit the histone methyltransferase G9a in human cells as an anti-cancer therapy (Kubicek et al. 2007), and was later shown to have an anti-parasitic effect on *P. falciparum* (Malmquist et al. 2012). The HKMTI chemical compounds (HKMTI-1-014, HKMTI-1-017 and HKMTI-1-251) identified from *T. brucei* lethality screening of BIX-01294

derivatives, caused *T. brucei* cell death in a time and dose dependant manner *in vitro* (Section 4.3). All three compounds had IC<sub>50</sub> values in the nanomolar range and favourable selectivity compared to the mammalian L-6 rat myoblasts. BIX-01294 is known to inhibit methylation of H3K9 and H3K4 in *P. falciparum* (Malmquist et al. 2012; Sundriyal et al. 2014), however trimethylation of H3K4 did not appear to be reduced after exposure of BSF *T. brucei* to an inhibitory concentration of the HKMTI compounds (Section 4.4). This may be a result of functional redundancy of the HKMT(s) responsible for trimethylation of H3K4 with the observed lethality due to off target effects of the HKMTI compounds.

Identification of drugs that target a broad spectrum of disease causing kinetoplastid species would be advantageous. Although biological differences exist between kinetoplastids, epigenetic factors are important in regulating expression of surface coat proteins linked to immune evasion, virulence and pathogenicity in the etiological agents of HAT, Chagas and leishmaniasis (Lopez-Rubio et al. 2007). Efficacy data obtained in collaboration with the Swiss TPH institute and GALVmed showed that the compounds HKMTI-1-014, HKMTI-1-017 and HKMTI-1-251 were active against the *T. brucei* subspecies *T. b. rhodesiense* and related trypanosomatids, *T. congolense* and *T. vivax* (Table 4.1). Additionally, all three HKMTI compounds were 10 to 124-fold more toxic to the trypanosomatids than to mammalian cells, exceeding the minimum SI outlined by the Pan-Asian Screening Network criteria of  $\geq 10$ -fold (loset et al. 2009).

Interestingly, the HKMTI compounds had unfavourable SIs, and were only moderately active or inactive against the intracellular kinetoplastids *T. cruzi* and *L. donovani*, respectively. It is possible the HKMTI compounds were ineffective against *T. cruzi* and *L. donovani* as H3K9 is acetylated not methylated in *T. cruzi* and Leishmania (Thomas et al. 2009; Respuela et al. 2008). Despite this, our data suggests that the HKMT inhibitors may prove to be a viable cross species chemotherapy against extracellular kinetoplastids (Section 4.3). However, significant further optimisation and screening

for more BIX-01294 derivatives is required to overcome the host cytotoxicity issues and ensure lethality results from inhibition of the desired HKMT.

VSG expression is essential for *T. brucei* survival both *in vitro* and *in vivo* (Sheader et al. 2005). Given the unique and essential role of Pol I in transcribing the VSG genes, I evaluated the use of commercially available Pol I specific inhibitors Quarfloxin, CX-5461 and BMH-21 as potential anti-trypanosomal agents. Quarfloxin, BMH-21 and CX-5461 were all originally developed as anti-cancer therapies and have been shown to inhibit Pol I transcription in mammalian cell lines (Bywater et al. 2012; Drygin et al. 2009; Drygin et al. 2011). *In vitro* cytotoxicity assay and cell proliferation assay data (Section 5.3) showed all three Pol I inhibitors to be classed as active, under Pan-Asian Screening Network criteria (Ioset et al. 2009), causing parasite cell death in a time- and dose-dependent manner with IC<sub>50</sub> values within the nanomolar range. *T. brucei* Pol I inhibition was reversible in parasites treated with BMH-21. Although this, in conjunction with unfavourable selectivity (SI 3.4-fold), limits the therapeutic potential of BMH-21, it has provided a valuable biological tool to investigate the assembly kinetics of the ESB in BSF *T. brucei*.

Quarfloxin and CX-5461 were the more promising compounds, having favourable selectivity ( $\geq 10$ -fold) when compared to the human MCF10A cell line, and inhibition of *T. brucei* Pol I was irreversible even after removal of the inhibitors from the trypanosome growth media (Figure 5.3). However, the efficacy of CX-5461 in a stage I mouse model of human African Trypanosomiasis was disappointing, as no difference in survival of infected mice treated with CX-5461 (40 mg/kg or 120 mg/kg) was observed compared with the vehicle control group (Section 5.5). Preliminary pharmacokinetic data suggested that this lack of efficacy was most likely due to poor bioavailability. In this study, I have provided evidence that Pol I is a druggable target in BSF *T. brucei*, and despite some of the complications regarding bioavailability and potential toxicity, repurposing of Pol I inhibitors could potentially function as new chemical weapons against HAT.

#### **7.4 - The ESB and nucleolus are transcription nucleated in BSF *T. brucei*.**

The nucleolus has previously been shown to be a Pol I transcription seeded structure in eukaryotes (Názer et al. 2011; Lam & Trinkle-Mulcahy 2015). The Pol I specific inhibitors Quarfloxin, CX-5461 and BMH-21 proved to be ideal biological tools to determine if the ESB and nucleolus are Pol I transcription nucleated structures in BSF *T. brucei*. Inhibition of Pol I transcription caused rapid disassembly of the nucleolus and loss of the ESB in *T. brucei*. However, immunoblot analysis of the tagged Pol I subunit, RPA2, showed that the disassembly of these structures was not accompanied by degradation of the Pol I subunit (Section 5.6). This lack of degradation may explain the rapid reappearance of the single nucleoli (L1C6 positive foci) in each cell within 15 minutes of Pol I transcription reinitiation, as reassembly of existing proteins would likely be faster than resynthesizing degraded components. Interestingly, a lag of over a hundred minutes was observed between the recovery of pre-rRNA precursor transcript 1 to the levels of the untreated control and that of pre-rRNA precursor transcripts 2 and 3. These data suggest that the nucleolus is a transcription-seeded structure in BSF *T. brucei* and indicates that the nucleation may only require Pol I transcription initiation not elongation at the rDNA transcription units.

In chapter five, I have shown that the ESB and ESB associated protein VEX1 can be rapidly lost upon inhibition of Pol I transcription (Section 5.6). Analysis of the *VSG* pseudogene and *VSG 221* precursor transcript showed that transcription was reinitiated within 30 minutes after removal of Pol I inhibition, but the percentage of cells containing an ESB did not return to the number observed in the untreated control until 120 minutes after removal of Pol I inhibition (Figure 5.13). This ordered reinitiation of Pol I transcription followed by a relatively slow increase in the number of cells containing an ESB supports the hypothesis that the ESB is a Pol I transcription seeded structure.

## 7.5 - Epigenetic status and the ESB play a role in the monoallelic exclusion of VSG ESs

As previously discussed, monoallelic expression of a single VSG gene from a repertoire of hundreds of VSG genes is essential for parasite survival in the host (Section 6.1). This monoallelic expression must also be inheritable and reversible to allow for *in situ* VSG switches to occur and antigenic variants to arise within the parasite population (Taylor & Rudenko 2006). Several studies into the regulation of VSG expression have led to the discovery of the ESB (Navarro & Gull 2001) and identification of numerous epigenetic factors that contribute to maintaining as single active ES and repress transcription of the remaining silent ESs (Figueiredo & Cross 2010; Narayanan & Rudenko 2013; Stanne & Rudenko 2010). The challenge now is to understand how these multiple layers of epigenetic regulation and the unique extranucleolar location of VSG transcription contribute to ES control.

Chaves and colleagues (1999) previously investigated the mechanism of silencing and switching using trypanosomes with two ESs tagged with different drug resistance genes and selected for double drug resistant (DDR) *T. brucei*. The resulting DDR cells had a mixed surface coat as a result of rapid switching between two VSG ESs. The authors proposed that the two ESs were both in a natural “pre-active” switching state maintained by unknown epigenetic factors, with a brief transient state in which both ES were selected to be simultaneously active due to the drug selection pressure (Figure 6.1) (Chaves et al. 1999).

In chapter six, I validated and characterised two new DDR cell lines KW01 and BH03. These cell lines are rapidly switching back and forth between the two pre-active ESs, resulting in a mixed surface coat of VSG 221 and VSG VO2 (Section 6.3-6.4). Here, I have shown that the epigenetic state of the pre-active ESs are similar to each other. The distribution of TDP1, histone H3 and histone H1 resemble the chromatin state of an active VSG ES (Section 6.6). These findings are in agreement with other published studies that propose *T. brucei* has an epigenetically regulated intermediate or pre-active ES state (Batram et al. 2014; Aresta-Branco et al. 2016). The open chromatin structure of

this pre-active state presumably allows *T. brucei* to test the new ES to ensure it is functional before fully committing to an *in situ* switch.

The open chromatin composition appears to be identical for both pre-active ESs in the DDR cell lines, suggesting that an additional restrictive mechanism acts to maintain monoallelic expression of the single *VSG*. Here, I have presented preliminary data that suggest that the singularity of the ESB may be the limiting factor that causes rapid switching between the two pre-active *VSG* ESs in the DDR cells. In support of this, preliminary analysis showed that 62% of KW01 (DDR) cells contained a single ESB and only 10% of KW01 cells had two ESBs (Section 6.8).

It has previously been proposed that the ESB is a self-organised structure, and monoallelic exclusion is achieved by the restricted association of one ES with the ESB at any one time (Navarro & Gull 2001). However, this model is based on the ESB being a predetermined structure and does not satisfactorily address the observation that not all BSF *T. brucei* G1 cells contain a visible ESB (Daniels et al. 2012; Navarro & Gull 2001). In chapter six, I suggest an alternative model based on the evidence that the ESB is a transcription-nucleated structure, which can be rapidly assembled and disassembled and the DDR data. This model proposes that the ESB complex contains a limiting factor(s) required for assembly of a single fully functional ESB, but that a pre-active ES could be transcribed at low levels by a 'pre-ESB' complex. The relatively open chromatin structure of the pre-active ES would allow for recruitment of low levels of Pol I and some additional factors to form a pre-ESB complex. This pre-ESB complex lacks the limiting factor(s) required for the rapid processing of *VSG* transcript and only recruits enough Pol I for sufficient transcription to probe the pre-active ES. Provided that the pre-active ES is found to be functional, the trypanosome can commit to the *in situ* switch, and the limiting ESB component(s) rapidly disassembles from the active ES and reassembles on the pre-active ES to form a fully functional ESB complex. The previously active expression site would now be in the pre-active state for a short time, allowing the trypanosome to rapidly revert back to this ES should the new ES prove faulty.

This model is based on very preliminary data regarding the number of ESBs present in the DDR cells. However, it does imply that the 10% of DDR cells with two ESB results from capturing the nucleation of the new ESB and disassembly of the previously active ESB, which is only observable due to the rapid switch rate present in the DDR cells. More extensive immunofluorescence microscopy experiments are required to obtain robust data regarding the number of ESBs (TY-RPA2 positive foci) present in the DDR cell lines. Additionally, it would be extremely interesting to determine the number of VEX1 foci in the DDR cells to ascertain if the two ESBs are each associated with a VEX1 focus. The data presented here supports the existence of an epigenetically regulated pre-active ES and tentatively suggests that an unknown limiting factor(s), which prevents nucleation of multiple ESB complexes in BSF *T. brucei*, achieves the singularity of the ESB.



---

## Chapter Eight

### References

- Acosta-Serrano, A. et al., 2001. The surface coat of procyclic *Trypanosoma brucei*: Programmed expression and proteolytic cleavage of procyclin in the tsetse fly. *Proceedings of the National Academy of Sciences of the United States of America*, 98(4), pp.1513-1518.
- Alsford, S. & Horn, D., 2012. Cell-cycle-regulated control of VSG expression site silencing by histones and histone chaperones ASF1A and CAF-1b in *Trypanosoma brucei*. *Nucleic acids research*, 40(20), pp.10150–10160.
- Alsford, S. & Horn, D., 2004. Trypanosomatid histones. *Molecular microbiology*, 53(2), pp.365–72.
- Andrews, K.T., Fisher, G. & Skinner-Adams, T.S., 2014. Drug repurposing and human parasitic protozoan diseases. *International journal for parasitology. Drugs and drug resistance*, 4(2), pp.95–111.
- Aresta-Branco, F., Pimenta, S. & Figueiredo, L.M., 2016. A transcription-independent epigenetic mechanism is associated with antigenic switching in *Trypanosoma brucei*. *Nucleic acids research*.
- Babokhov, P. et al., 2013. A current analysis of chemotherapy strategies for the treatment of human African trypanosomiasis. *Pathogens and global health*, 107(5), pp.242–52.
- Baker, N. et al., 2013. Drug resistance in African trypanosomiasis: the melarsoprol and pentamidine story. *Trends in Parasitology*, 29(3), pp.110–118.
- Balasegaram, M. et al., 2006. Treatment outcomes and risk factors for relapse in patients with early-stage human African trypanosomiasis (HAT) in the Re. *Bulletin of the World Health Organization*, 84(8410).
- Balasubramanian, S., Hurley, L.H. & Neidle, S., 2011. Targeting G-quadruplexes in gene promoters: a novel anticancer strategy? *Nature reviews. Drug discovery*, 10(4), pp.261–75.
- Baltz, T. et al., 1986. Stable expression of two variable surface glycoproteins by cloned *Trypanosoma equiperdum*. *Nature*, 319(6054), pp.602–604.
- Barratt, M.J. & Frail, D., 2012. *Drug repositioning : bringing new life to shelved assets and existing drugs*, Wiley.
- Barrett, M.P. et al., 2011. Drug resistance in human African trypanosomiasis. *Future Microbiology*, 6(9), pp.1037–1047.
- Barrett, M.P. et al., 2003. The trypanosomiases. *The Lancet*, 362, pp.1469–1480.
- Barry, J.D. & McCulloch, R., 2001. Antigenic variation in trypanosomes: enhanced phenotypic variation in a eukaryotic parasite. *Advances in parasitology*, 49, pp.1–70.
- Barski, A. et al., 2007. High-resolution profiling of histone methylations in the human genome. *Cell*, 129(4), pp.823–37.
- Bastin, P. et al., 1996. A novel epitope tag system to study protein targeting and organelle biogenesis in *Trypanosoma brucei*. *Molecular and biochemical parasitology*, 77(2), pp.235–9.

- Batram, C. et al., 2014. Expression site attenuation mechanistically links antigenic variation and development in *Trypanosoma brucei*. *eLife*, 3, p.e02324.
- Bernards, A. et al., 1981. Activation of trypanosome surface glycoprotein genes involves a duplication-transposition leading to an altered 3' end. *Cell*, 27(3 Pt 2), pp.497–505.
- Bernards, A., van Harten-Loosbroek, N. & Borst, P., 1984. Modification of telomeric DNA in *Trypanosoma brucei*; a role in antigenic variation? *Nucleic acids research*, 12(10), pp.4153–70.
- Berriman, M., 2005. The Genome of the African Trypanosome *Trypanosoma brucei*. *Science*, 309(5733), pp.416–422.
- Biebinger, S. et al., 1996. The PARP promoter of *Trypanosoma brucei* is developmentally regulated in a chromosomal context. *Nucleic acids research*, 24(7), pp.1202–11.
- Böhme, U. & Cross, G.A.M., 2002. Mutational analysis of the variant surface glycoprotein GPI-anchor signal sequence in *Trypanosoma brucei*. *Journal of cell science*, 115(Pt 4), pp.805–16.
- Borst, P., 2002. Antigenic variation and allelic exclusion. *Cell*, 109(1), pp.5–8.
- Borst, P. & Sabatini, R., 2008. Base J: Discovery, Biosynthesis, and Possible Functions. *Annual Review of Microbiology*, 62(1), pp.235–251.
- Briggs, S.D. et al., 2001. Histone H3 lysine 4 methylation is mediated by Set1 and required for cell growth and rDNA silencing in *Saccharomyces cerevisiae*. *Genes & development*, 15(24), pp.3286–95.
- Brogna, S., McLeod, T. & Petric, M., 2016. The Meaning of NMD: Translate or Perish. *Trends in Genetics*, 32(7), pp.395–407.
- Brooks, T.A. & Hurley, L.H., 2010. Targeting MYC Expression through G-Quadruplexes. *Genes & cancer*, 1(6), pp.641–649.
- Brun, R. et al., 2010. Human African trypanosomiasis. *Lancet*, 375(9709), pp.148–59.
- Büscher, P. et al., 2017. Human African trypanosomiasis. *The Lancet*. 390(10110), pp.2397–2409.
- Bywater, M. et al., 2012. Inhibition of RNA Polymerase I as a Therapeutic Strategy to Promote Cancer-Specific Activation of p53. *Cancer Cell*, 22(1), pp.51–65.
- Capewell, P. et al., 2016. The skin is a significant but overlooked anatomical reservoir for vector-borne African trypanosomes. *eLife*, 5, p.e17716.
- Chang, Y. et al., 2009. Structural basis for G9a-like protein lysine methyltransferase inhibition by BIX-01294. *Nature structural & molecular biology*, 16(3), pp.312–7.
- Chappuis, F. et al., 2005. Eflornithine Is Safer than Melarsoprol for the Treatment of Second-Stage *Trypanosoma brucei gambiense* Human African Trypanosomiasis. *Clinical Infectious Diseases*, 41(5), pp.748–751.
- Chaves, I. et al., 1999. Control of variant surface glycoprotein gene-expression sites in *Trypanosoma brucei*. *The EMBO Journal*, 18(17), pp.4846–4855.
- Cherblanc, F.L. et al., 2013. Chaetocin is a nonspecific inhibitor of histone lysine methyltransferases. *Nature Chemical Biology*, 9(3), pp.136–137.

- Cliffe, L.J. et al., 2009. JBP1 and JBP2 are two distinct thymidine hydroxylases involved in J biosynthesis in genomic DNA of African trypanosomes. *Nucleic acids research*, 37(5), pp.1452–62.
- Colis, L. et al., 2014. DNA intercalator BMH-21 inhibits RNA polymerase I independent of DNA damage response. *Oncotarget*, 5(12), pp.4361–9.
- Conconi, A. et al., 1989. Two different chromatin structures coexist in ribosomal RNA genes throughout the cell cycle. *Cell*, 57(5), pp.753–61.
- Cross, G.A., 1975. Identification, purification and properties of clone-specific glycoprotein antigens constituting the surface coat of *Trypanosoma brucei*. *Parasitology*, 71(3), pp.393–417.
- Cross, G.A.M., 1990. Cellular and Genetic Aspects of Antigenic Variation in Trypanosomes. *Annual Review of Immunology*, 8(1), pp.83–110.
- Cross, G.A.M., Kim, H.-S. & Wickstead, B., 2014. Capturing the variant surface glycoprotein repertoire (the VSGnome) of *Trypanosoma brucei* Lister 427. *Molecular and biochemical parasitology*, 195(1), pp.59–73.
- Daniels, J.-P., Gull, K. & Wickstead, B., 2010. Cell Biology of the Trypanosome Genome. *Microbiology and Molecular Biology Reviews*, 74(4), pp.552–569.
- Daniels, J.-P., Gull, K. & Wickstead, B., 2012. The trypanosomatid-specific N terminus of RPA2 is required for RNA polymerase I assembly, localization, and function. *Eukaryotic cell*, 11(5), pp.662–72.
- Dehé, P.-M. & Géli, V., 2006. The multiple faces of Set1This paper is one of a selection of papers published in this Special Issue, entitled 27th International West Coast Chromatin and Chromosome Conference, and has undergone the Journal's usual peer review process. *Biochemistry and Cell Biology*, 84(4), pp.536–548.
- Devaux, S. et al., 2007. Diversification of function by different isoforms of conventionally shared RNA polymerase subunits. *Molecular biology of the cell*, 18(4), pp.1293–301.
- DNDi, 2017. DNDi Achievements – DNDi. Available at: <https://www.dndi.org/achievements/> [Accessed October 23, 2017].
- Doyle, J.J. et al., 1980. Antigenic variation in clones of animal-infective *Trypanosoma brucei* derived and maintained in vitro. *Parasitology*, 80(2), p.359.
- Drygin, D. et al., 2009. Anticancer activity of CX-3543: a direct inhibitor of rRNA biogenesis. *Cancer research*, 69(19), pp.7653–61.
- Drygin, D. et al., 2011. Targeting RNA polymerase I with an oral small molecule CX-5461 inhibits ribosomal RNA synthesis and solid tumor growth. *Cancer research*, 71(4), pp.1418–30.
- Duan, W. et al., 2001. Design and synthesis of fluoroquinophenoxazines that interact with human telomeric G-quadruplexes and their biological effects. *Molecular cancer therapeutics*, 1(2), pp.103–20.
- Dunbar, D.A. et al., 2000. The genes for small nucleolar RNAs in *Trypanosoma brucei* are organized in clusters and are transcribed as a polycistronic RNA. *Nucleic acids research*, 28(15), pp.2855–61.
- Embley, T.M. & Martin, W., 2006. Eukaryotic evolution, changes and challenges. *Nature*, 440(7084), pp.623–30.

- Ersfeld, K., 2011. Nuclear architecture, genome and chromatin organisation in *Trypanosoma brucei*. *Research in microbiology*, 162(6), pp.626–36.
- Etzioni, S. et al., 2005. Homodimeric MyoD preferentially binds tetraplex structures of regulatory sequences of muscle-specific genes. *The Journal of biological chemistry*, 280(29), pp.26805–12.
- Fenn, K. & Matthews, K.R., 2007. The cell biology of *Trypanosoma brucei* differentiation. *Current opinion in microbiology*, 10(6), pp.539–46.
- Ferrins, L., Rahmani, R. & Baell, J.B., 2013. Drug discovery and human African trypanosomiasis: a disease less neglected? *Future Med Chem*, 5, pp.1801–1841.
- Fèvre, E. et al., 2006. Human African Trypanosomiasis: Epidemiology and Control. *Advances in parasitology*, 61, pp.167–221.
- Field, M.C. et al., 2017. Anti-trypanosomatid drug discovery: an ongoing challenge and a continuing need. *Nature Reviews Microbiology*. 15(4). pp217-231.
- Figueiredo, L.M. & Cross, G.A., 2010. Nucleosomes are depleted at the VSG expression site transcribed by RNA polymerase I in African trypanosomes. *Eukaryot Cell*, 9, pp.148–154.
- Figueiredo, L.M., Cross, G.A. & Janzen, C.J., 2009. Epigenetic regulation in African trypanosomes: a new kid on the block. *Nat Rev Microbiol*, 7, pp.504–513.
- Figueiredo, L.M., Janzen, C.J. & Cross, G.A., 2008. A histone methyltransferase modulates antigenic variation in African trypanosomes. *PLoS Biol*, 6, p.e161.
- Fingerman, I.M. et al., 2005. Global loss of Set1-mediated H3 Lys4 trimethylation is associated with silencing defects in *Saccharomyces cerevisiae*. *The Journal of biological chemistry*, 280(31), pp.28761–5.
- Franco, J.R. et al., 2012. Monitoring the use of nifurtimox-eflornithine combination therapy (NECT) in the treatment of second stage gambiense human African trypanosomiasis. *Research and Reports in Tropical Medicine*, 3, pp.93–101.
- Gibson, W., 2003. Species concepts for trypanosomes: from morphological to molecular definitions? *Kinetoplastid Biology and Disease*, 2(1), p.10.
- Gillingham, A.K. & Munro, S., 2007. The small G proteins of the Arf family and their regulators. *Annu Rev Cell Dev Biol*, 23, pp.579–611.
- Giordani, F. et al., 2016. The animal trypanosomiasis and their chemotherapy: a review. *Parasitology*, 143(14), pp.1862–1889.
- Glover, L. et al., 2013. Antigenic variation in African trypanosomes: the importance of chromosomal and nuclear context in VSG expression control. *Cellular microbiology*, 15(12), pp.1984–93.
- Glover, L. et al., 2016. VEX1 controls the allelic exclusion required for antigenic variation in trypanosomes. *Proceedings of the National Academy of Sciences*, 113(26), pp.7225–7230.
- Gommers-Ampt, J.H. et al., 1993. beta-D-glucosyl-hydroxymethyluracil: a novel modified base present in the DNA of the parasitic protozoan *T. brucei*. *Cell*, 75(6), pp.1129–36.
- La Greca, F. & Magez, S., 2011. Vaccination against trypanosomiasis. *Human Vaccines*, 7(11), pp.1225–1233.

- Guenther, M.G. et al., 2007. A Chromatin Landmark and Transcription Initiation at Most Promoters in Human Cells. *Cell*, 130(1), pp.77–88.
- Günzl, A. et al., 2003. RNA polymerase I transcribes procyclin genes and variant surface glycoprotein gene expression sites in *Trypanosoma brucei*. *Eukaryot Cell*, 2, pp.542–551.
- Haddach, M. et al., 2012. Discovery of CX-5461, the First Direct and Selective Inhibitor of RNA Polymerase I, for Cancer Therapeutics. *ACS Medicinal Chemistry Letters*, 3(7), pp.602–606.
- Hammarton, T.C., 2007. Cell cycle regulation in *Trypanosoma brucei*. *Molecular and biochemical parasitology*, 153(1), pp.1–8.
- Hannan, R.D., Drygin, D. & Pearson, R.B., 2013. Targeting RNA polymerase I transcription and the nucleolus for cancer therapy. *Expert Opinion on Therapeutic Targets*, 17(8), pp.873–878.
- Haring, M. et al., 2007. Chromatin immunoprecipitation: optimization, quantitative analysis and data normalization. *Plant methods*, 3(11), pp. 11-27.
- Hecker, H. et al., 1994. The chromatin of trypanosomes. *International journal for parasitology*, 24(6), pp.809–19.
- Hecker, H. & Gander, E.S., 1985. The compaction pattern of the chromatin of trypanosomes. *Biology of the cell*, 53(3), pp.199–208.
- Hee Lee, S., Stephens, J.L. & Englund, P.T., 2007. A fatty-acid synthesis mechanism specialized for parasitism. *Nature Reviews Microbiology*, 5(4), pp.287–297.
- Helin, K. & Dhanak, D., 2013. Chromatin proteins and modifications as drug targets. *Nature*, 502, pp.480–488.
- Hertz-Fowler, C. et al., 2008. Telomeric expression sites are highly conserved in *Trypanosoma brucei*. *PloS one*, 3(10), p.e3527.
- Hirumi, H. & Hirumi, K., 1989. Continuous cultivation of *Trypanosoma brucei* blood stream forms in a medium containing a low concentration of serum protein without feeder cell layers. *J Parasitol*, 75, pp.985–989.
- Horn, D., 2014. Antigenic variation in African trypanosomes. *Molecular and Biochemical Parasitology*, 195(2), pp.123–129.
- Horn, D., 2007. Introducing histone modification in trypanosomes. *Trends in parasitology*, 23(6), pp.239–42.
- Horn, D. & Duraisingh, M.T., 2014. Antiparasitic Chemotherapy: From Genomes to Mechanisms. *Annual Review of Pharmacology and Toxicology*, 54(1), pp.71–94.
- Horn, D. & McCulloch, R., 2010. Molecular mechanisms underlying the control of antigenic variation in African trypanosomes. *Current Opinion in Microbiology*, 13(6), pp.700–705.
- Howe, F.S. et al., 2017. Is H3K4me3 instructive for transcription activation? *BioEssays*, 39(1), p.e201600095.
- Huang, R. et al., 2011. The NCGC pharmaceutical collection: a comprehensive resource of clinically approved drugs enabling repurposing and chemical genomics. *Science translational medicine*, 3(80), p.80ps16.

- Hughes, K. et al., 2007. A novel ISWI is involved in VSG expression site downregulation in African trypanosomes. *EMBO J*, 26, pp.2400–2410.
- Ingram, A.K. & Horn, D., 2002. Histone deacetylases in *Trypanosoma brucei*: two are essential and another is required for normal cell cycle progression. *Mol Microbiol*, 45, pp.89–97.
- Ioset, J.-R., Kaiser, M. & Yardley, V., 2009. Drug Screening for Kinetoplastids Diseases The Pan-Asian Screening Network.
- Ivens, A.C. et al., 2005. The genome of the kinetoplastid parasite, *Leishmania major*. *Science (New York, N.Y.)*, 309(5733), pp.436–42.
- Iyer, L.M. et al., 2008. Comparative genomics of transcription factors and chromatin proteins in parasitic protists and other eukaryotes. *International journal for parasitology*, 38(1), pp.1–31.
- Jamonneau, V. et al., 2012. Untreated Human Infections by *Trypanosoma brucei gambiense* Are Not 100% Fatal J. M. Ndung'u, ed. *PLoS Neglected Tropical Diseases*, 6(6), p.e1691.
- Janzen, C.J., et al., 2006a. Selective Di- or Trimethylation of Histone H3 Lysine 76 by Two DOT1 Homologs Is Important for Cell Cycle Regulation in *Trypanosoma brucei*. *Molecular Cell*, 23(4), pp.497–507.
- Janzen, C.J., et al., 2006b. Unusual histone modifications in *Trypanosoma brucei*. *FEBS Letters*, 580(9), pp.2306–2310.
- Jenuwein, T. & Allis, C.D., 2001. Translating the histone code. *Science (New York, N.Y.)*, 293(5532), pp.1074–80.
- Kagira, J.M. et al., 2011. Prevalence and types of coinfections in sleeping sickness patients in kenya (2000/2009). *Journal of tropical medicine*, 2011, p.248914.
- Kennedy, P.G., 2013. Clinical features, diagnosis, and treatment of human African trypanosomiasis (sleeping sickness). *The Lancet. Neurology*, 12(2), pp.186–94.
- Kerry, L.E. et al., 2017. Selective inhibition of RNA polymerase I transcription as a potential approach to treat African trypanosomiasis. J. Raper, ed. *PLoS neglected tropical diseases*, 11(3), p.e0005432.
- Kibona, S.N. et al., 2006. Drug-resistance of *Trypanosoma b. rhodesiense* isolates from Tanzania. *Tropical Medicine and International Health*, 11(2), pp.144–155.
- Klug, D.M., Gelb, M.H. & Pollastri, M.P., 2016. Repurposing strategies for tropical disease drug discovery. *Bioorganic & Medicinal Chemistry Letters*, 26(11), pp.2569–2576.
- Kondo, Y. et al., 2008. Downregulation of histone H3 lysine 9 methyltransferase G9a induces centrosome disruption and chromosome instability in cancer cells. *PLoS one*, 3(4), p.e2037.
- Korber, P. & Hörz, W., 2004. SWRred not shaken; mixing the histones. *Cell*, 117(1), pp.5–7.
- Kratochwil, C.F. & Meyer, A., 2015. Mapping active promoters by ChIP-seq profiling of H3K4me3 in cichlid fish - a first step to uncover cis-regulatory elements in ecological model teleosts. *Molecular Ecology Resources*, 15(4), pp.761–771.
- Kubicek, S. et al., 2007. Reversal of H3K9me2 by a small-molecule inhibitor for the G9a histone methyltransferase. *Mol Cell*, 25, pp.473–481.

- Lam, Y.W. & Trinkle-Mulcahy, L., 2015. New insights into nucleolar structure and function. *F1000prime reports*, 7, p.48.
- Landeira, D. et al., 2009. Cohesin regulates VSG monoallelic expression in trypanosomes. *The Journal of Cell Biology*, 186(2), pp.243–254.
- Landeira, D. & Navarro, M., 2007. Nuclear repositioning of the VSG promoter during developmental silencing in *Trypanosoma brucei*. *The Journal of Cell Biology*, 176(2).
- van Leeuwen, F. et al., 1997. Localization of the modified base J in telomeric VSG gene expression sites of *Trypanosoma brucei*. *Genes & development*, 11(23), pp.3232–41.
- van Leeuwen, F. et al., 1996. The telomeric GGGTTA repeats of *Trypanosoma brucei* contain the hypermodified base J in both strands. *Nucleic acids research*, 24(13), pp.2476–82.
- Van Leeuwen, F. et al., 1998. The modified DNA base beta-D-glucosyl-hydroxymethyluracil is not found in the tsetse fly stages of *Trypanosoma brucei*. *Molecular and Biochemical Parasitology*, 94.
- Leung, K.F. et al., 2014. *Trypanosomes and trypanosomiasis Chapter 1 Cell Biology for Immune Evasion: Organizing Antigenic Variation, Surfaces, Trafficking, and Cellular Structures in Trypanosoma brucei* S. Magez & M. Radwanska, eds., Springer-Verlag Wien.
- Li, X. et al., 2008. High-Resolution Mapping of Epigenetic Modifications of the Rice Genome Uncovers Interplay between DNA Methylation, Histone Methylation, and Gene Expression. *THE PLANT CELL ONLINE*, 20(2), pp.259–276.
- Liang, X. et al., 2003. trans and cis splicing in trypanosomatids: mechanism, factors, and regulation. *Eukaryotic cell*, 2(5), pp.830–40.
- Lips, S., Revelard, P. & Pays, E., 1993. Identification of a new expression site-associated gene in the complete 30.5 kb sequence from the AnTat 1.3A variant surface protein gene expression site of *Trypanosoma brucei*. *Molecular and biochemical parasitology*, 62(1), pp.135–7.
- Liu, C.L. et al., 2005. Single-nucleosome mapping of histone modifications in *S. cerevisiae*. *PLoS biology*, 3(10), p.e328.
- Lo, H.J., Huang, H.K. & Donahue, T.F., 1998. RNA polymerase I-promoted HIS4 expression yields uncapped, polyadenylated mRNA that is unstable and inefficiently translated in *Saccharomyces cerevisiae*. *Molecular and cellular biology*, 18(2), pp.665–75.
- López-Farfán, D. et al., 2014. SUMOylation by the E3 Ligase TbSIZ1/PIAS1 Positively Regulates VSG Expression in *Trypanosoma brucei* K. L. Hill, ed. *PLoS Pathogens*, 10(12), p.e1004545.
- Lopez-Rubio, J.J., Riviere, L. & Scherf, A., 2007. Shared epigenetic mechanisms control virulence factors in protozoan parasites. *Current Opinion in Microbiology*, 10(6), pp.560–568.
- Lowell, J.E. et al., 2005. Histone H2AZ dimerizes with a novel variant H2B and is enriched at repetitive DNA in *Trypanosoma brucei*. *Journal of cell science*, 118(Pt 24), pp.5721–30.
- Lowell, J.E. & Cross, G.A.M., 2004. A variant histone H3 is enriched at telomeres in *Trypanosoma brucei*. *Journal of cell science*, 117(Pt 24), pp.5937–47.
- Magez, S. et al., 2008. The Role of B-cells and IgM Antibodies in Parasitemia, Anemia, and VSG Switching in *Trypanosoma brucei*-Infected Mice S. Black, ed. *PLoS Pathogens*, 4(8), p.e1000122.

- Malmquist, N.A. et al., 2015. Histone methyltransferase inhibitors are orally bioavailable, fast-acting molecules with activity against different species causing malaria in humans. *Antimicrobial agents and chemotherapy*, 59(2), pp.950–9.
- Malmquist, N.A. et al., 2012. Small-molecule histone methyltransferase inhibitors display rapid antimalarial activity against all blood stage forms in *Plasmodium falciparum*. *Proc Natl Acad Sci U S A*, 109, pp.16708–16713.
- Malvy, D. & Chappuis, F., 2011. Sleeping sickness. *Clinical Microbiology & Infection*, 17, pp.986–995.
- Mandava, V. et al., 2007. Histone modifications in *Trypanosoma brucei*. *Molecular and biochemical parasitology*, 156(1), pp.41–50.
- Maree, J.P. & Patterton, H.G., 2014. The epigenome of *Trypanosoma brucei*: a regulatory interface to an unconventional transcriptional machine. *Biochim Biophys Acta*, 1839, pp.743–750.
- Marks, P.A. & Xu, W.-S., 2009. Histone deacetylase inhibitors: Potential in cancer therapy. *Journal of Cellular Biochemistry*, 107(4), pp.600–608.
- Le Martelot, G. et al., 2012. Genome-Wide RNA Polymerase II Profiles and RNA Accumulation Reveal Kinetics of Transcription and Associated Epigenetic Changes During Diurnal Cycles A. Kramer, ed. *PLoS Biology*, 10(11), p.e1001442.
- Matthews, K.R., 2005. The developmental cell biology of *Trypanosoma brucei*. *J Cell Sci*, 118, pp.283–290.
- Matthews, K.R., Ellis, J.R. & Paterou, A., 2004. Molecular regulation of the life cycle of African trypanosomes. *Trends in Parasitology*, 20(1), pp.40–47.
- McStay, B. & Grummt, I., 2008. The epigenetics of rRNA genes: from molecular to chromosome biology. *Annual review of cell and developmental biology*, 24, pp.131–57.
- Miguel, D.C. et al., 2009. Tamoxifen as a potential antileishmanial agent: efficacy in the treatment of *Leishmania braziliensis* and *Leishmania chagasi* infections. *Journal of Antimicrobial Chemotherapy*, 63(2), pp.365–368.
- Miguel, D.C. et al., 2008. Tamoxifen Is Effective in the Treatment of *Leishmania amazonensis* Infections in Mice C. Jaffe, ed. *PLoS Neglected Tropical Diseases*, 2(6), p.e249.
- Mikkelsen, T.S. et al., 2007. Genome-wide maps of chromatin state in pluripotent and lineage-committed cells. *Nature*, 448(7153), pp.553–60.
- Miller, T. et al., 2001. COMPASS: A complex of proteins associated with a trithorax-related SET domain protein. *Proceedings of the National Academy of Sciences*, 98(23), pp.12902–12907.
- Muñoz-Jordán, J.L., Davies, K.P. & Cross, G.A., 1996. Stable expression of mosaic coats of variant surface glycoproteins in *Trypanosoma brucei*. *Science (New York, N.Y.)*, 272(5269), pp.1795–7.
- Myler, P.J. et al., 1985. Antigenic variation in clones of *Trypanosoma brucei* grown in immune-deficient mice. *Infection and immunity*, 47(3), pp.684–90.
- Narayanan, M.S. et al., 2011. NLP is a novel transcription regulator involved in VSG expression site control in *Trypanosoma brucei*. *Nucleic acids research*, 39(6), pp.2018–31.
- Narayanan, M.S. & Rudenko, G., 2013. TDP1 is an HMG chromatin protein facilitating RNA polymerase I transcription in African trypanosomes. *Nucleic acids research*, 41(5), pp.2981–92.



- Navarro, M. & Gull, K., 2001. A pol I transcriptional body associated with VSG mono-allelic expression in *Trypanosoma brucei*. *Nature*, 414(6865), pp.759–763.
- Názer, E. et al., 2011. Nucleolar Accumulation of RNA Binding Proteins Induced by ActinomycinD Is Functional in *Trypanosoma cruzi* and *Leishmania mexicana* but Not in *T. brucei*. S. N. Moreno, ed. *PLoS ONE*, 6(8), p.e24184.
- Nosengo, N., 2016. Can you teach old drugs new tricks? *Nature*, 534(7607), pp.314–316.
- O'Connor, O.A. et al., 2015. Belinostat in Patients With Relapsed or Refractory Peripheral T-Cell Lymphoma: Results of the Pivotal Phase II BELIEF (CLN-19) Study. *Journal of clinical oncology : official journal of the American Society of Clinical Oncology*, 33(23), pp.2492–9.
- Papadopoulos, K.P. et al., 2007. Phase I clinical trial of CX-3543, a protein-rDNA quadruplex inhibitor. *Journal of Clinical Oncology*, 25(18), pp.3585–3585.
- Patil, V. et al., 2010. Antimalarial and antileishmanial activities of histone deacetylase inhibitors with triazole-linked cap group. *Bioorganic & medicinal chemistry*, 18(1), pp.415–25.
- Pays, E. et al., 1983. Gene conversion as a mechanism for antigenic variation in trypanosomes. *Cell*, 34(2), pp.371–81.
- Pays, E. et al., 1984. Possible DNA modification in GC dinucleotides of *Trypanosoma brucei* telomeric sequences; relationship with antigen gene transcription. *Nucleic acids research*, 12(13), pp.5235–47.
- Pays, E. et al., 2014. The molecular arms race between African trypanosomes and humans. *Nature Reviews Microbiology*, 12(8), pp.575–584.
- Pays, E. et al., 2001. The VSG expression sites of *Trypanosoma brucei*: multipurpose tools for the adaptation of the parasite to mammalian hosts. *Molecular and biochemical parasitology*, 114(1), pp.1–16.
- Pedrique, B. et al., 2013. The drug and vaccine landscape for neglected diseases (2000–11): a systematic assessment. *The Lancet Global Health*, 1(6), pp.e371–e379.
- Peltonen, K. et al., 2014. A targeting modality for destruction of RNA polymerase I that possesses anticancer activity. *Cancer cell*, 25(1), pp.77–90.
- Peltonen, K. et al., 2010. Identification of novel p53 pathway activating small-molecule compounds reveals unexpected similarities with known therapeutic agents. *PloS one*, 5(9), p.e12996.
- Pena, A.C. et al., 2014. *Trypanosoma brucei* histone H1 inhibits RNA polymerase I transcription and is important for parasite fitness *in vivo*. *Molecular Microbiology*, 93(4), pp.645–663.
- Pena, A.C., Aresta-Branco, F. & Figueiredo, L.M., 2016. Epigenetic Regulation in *T. brucei*: Changing Coats Is a Chance to Survive. In W. Doerfler & J. Casadesus, eds. *Epigenetics of Infectious Diseases*. Springer, pp. 443–458.
- Pianese, G., 1896. Beitrag zur histologie und aetiologie der carcinoma. histoloische und experimentelle untersuchungen. (Contribution to the histology and etiology of carcinoma. Histological and experimental studies). *beitr. Pathol. Anat. Allgen. Pathol*, 142, pp.1–193.
- Picchi, G.F.A. et al., 2017. Post-translational Modifications of *Trypanosoma cruzi* Canonical and Variant Histones. *Journal of Proteome Research*, 16(3), pp.1167–1179.

- Pillus, L., 2008. MYSTs mark chromatin for chromosomal functions. *Current opinion in cell biology*, 20(3), pp.326–33.
- Pohlig, G. et al., 2016. Efficacy and Safety of Pafuramidine versus Pentamidine Maleate for Treatment of First Stage Sleeping Sickness in a Randomized, Comparator-Controlled, International Phase 3 Clinical Trial C. Franco-Paredes, ed. *PLOS Neglected Tropical Diseases*, 10(2), p.e0004363.
- Pollastri, M.P. & Campbell, R.K., 2011. Target repurposing for neglected diseases. *Future Medicinal Chemistry*, 3(10), pp.1307–1315.
- Ponte-Sucre, A., 2016. An Overview of Trypanosoma brucei Infections: An Intense Host-Parasite Interaction. *Frontiers in microbiology*, 7, p.2126.
- Povelones, M.L. et al., 2012. Histone H1 plays a role in heterochromatin formation and VSG expression site silencing in Trypanosoma brucei. *PLoS pathogens*, 8(11), p.e1003010.
- Priotto, G. et al., 2009. Nifurtimox-eflornithine combination therapy for second-stage African Trypanosoma brucei gambiense trypanosomiasis: a multicentre, randomised, phase III, non-inferiority trial. *The Lancet*, 374(9683), pp.56–64.
- Quin, J.E. et al., 2014. Targeting the nucleolus for cancer intervention. *Biochimica et Biophysica Acta (BBA) - Molecular Basis of Disease*, 1842(6), pp.802–816.
- Respuela, P. et al., 2008. Histone acetylation and methylation at sites initiating divergent polycistronic transcription in Trypanosoma cruzi. *The Journal of biological chemistry*, 283(23), pp.15884–92.
- Robinson, N.P. et al., 1999. Predominance of duplicative VSG gene conversion in antigenic variation in African trypanosomes. *Molecular and cellular biology*, 19(9), pp.5839–46.
- Rudenko, G., 2010. Epigenetics and transcriptional control in African trypanosomes. *Essays Biochem*, 48, pp.201–219.
- Rudenko, G., 1998. Selection for activation of a new variant surface glycoprotein gene expression site in Trypanosoma brucei can result in deletion of the old one. *Molecular and Biochemical Parasitology*, 95(1), pp.97–109.
- Rudenko, G. et al., 1994. VSG gene expression site control in insect form Trypanosoma brucei. *The EMBO journal*, 13(22), pp.5470–82.
- Ruthenburg, A.J., Allis, C.D. & Wysocka, J., 2007. Methylation of lysine 4 on histone H3: intricacy of writing and reading a single epigenetic mark. *Molecular cell*, 25(1), pp.15–30.
- Sambrook, J., Fritsch, E.F. & Maniatis, T., 1989. *Molecular cloning: a laboratory manual* 2nd ed., Cold Spring Harbour, N.Y: Cold Spring Harbour Laboratory.
- Santos-Rosa, H. et al., 2002. Active genes are tri-methylated at K4 of histone H3. *Nature*, 419(6905), pp.407–11.
- Saulnier Sholler, G.L. et al., 2011. A Phase 1 Study of Nifurtimox in Patients With Relapsed/Refractory Neuroblastoma. *Journal of Pediatric Hematology/Oncology*, 33(1), pp.25–30.
- Schimanski, B. et al., 2003. The second largest subunit of Trypanosoma brucei's multifunctional RNA polymerase I has a unique N-terminal extension domain. *Molecular and Biochemical Parasitology*, 126(2), pp.193–200.

- Schimanski, B., Nguyen, T.N. & Günzl, A., 2005. Characterization of a multisubunit transcription factor complex essential for spliced-leader RNA gene transcription in *Trypanosoma brucei*. *Molecular and cellular biology*, 25(16), pp.7303–13.
- Schlimme, W. et al., 1993. *Trypanosoma brucei brucei*: differences in the nuclear chromatin of bloodstream forms and procyclic culture forms. *Parasitology*, 107 ( Pt 3), pp.237–47.
- Schulz, D. et al., 2015. Bromodomain Proteins Contribute to Maintenance of Bloodstream Form Stage Identity in the African Trypanosome. *PLoS biology*, 13(12), p.e1002316.
- Sekhar, G.N. et al., 2014. Delivery of Antihuman African Trypanosomiasis Drugs Across the Blood–Brain and Blood–CSF Barriers. In *Advances in pharmacology (San Diego, Calif.)*. pp. 245–275.
- Seyfang, A., Mecke, D. & Duszenko, M., 1990. Degradation, recycling, and shedding of *Trypanosoma brucei* variant surface glycoprotein. *The Journal of protozoology*, 37(6), pp.546–52.
- Shedden, K. et al., 2005. Variant surface glycoprotein RNA interference triggers a precytokinesis cell cycle arrest in African trypanosomes. *Proceedings of the National Academy of Sciences of the United States of America*, 102(24), pp.8716–21.
- Shedden, K., de Vruyte, D. & Rudenko, G., 2004. Bloodstream Form-specific Up-regulation of Silent VSG Expression Sites and Procyclin in *Trypanosoma brucei* after Inhibition of DNA Synthesis or DNA Damage. *Journal of Biological Chemistry*, 279(14), pp.13363–13374.
- Siegel, T.N. et al., 2008. Acetylation of histone H4K4 is cell cycle regulated and mediated by HAT3 in *Trypanosoma brucei*. *Molecular microbiology*, 67(4), pp.762–71.
- Siegel, T.N. et al., 2009. Four histone variants mark the boundaries of polycistronic transcription units in *Trypanosoma brucei*. *Genes Dev*, 23, pp.1063–1076.
- Simarro, P.P. et al., 2012. Estimating and Mapping the Population at Risk of Sleeping Sickness. *Food and Agriculture Organization of the United Nations Regional Office for Africa World Health Organization*, 6(10).
- Smith, T.K. et al., 2009. Blocking variant surface glycoprotein synthesis in *Trypanosoma brucei* triggers a general arrest in translation initiation. *PLoS one*, 4(10), p.e7532.
- Sollier, J. et al., 2004. Set1 is required for meiotic S-phase onset, double-strand break formation and middle gene expression. *The EMBO journal*, 23(9), pp.1957–67.
- Song, H. et al., 2014. Cytotoxic Effects of Tetracycline Analogues (Doxycycline, Minocycline and COL-3) in Acute Myeloid Leukemia HL-60 Cells Z. Wang, ed. *PLoS ONE*, 9(12), p.e114457.
- Stanne, T.M. et al., 2015. Identification of the ISWI Chromatin Remodeling Complex of the Early Branching Eukaryote *Trypanosoma brucei*. *The Journal of biological chemistry*, 290(45), pp.26954–67.
- Stanne, T.M. & Rudenko, G., 2010. Active VSG expression sites in *Trypanosoma brucei* are depleted of nucleosomes. *Eukaryotic cell*, 9(1), pp.136–47.
- Steverding, D., 2000. The transferrin receptor of *Trypanosoma brucei*. *Parasitology international*, 48(3), pp.191–8.
- Sudarshi, D. et al., 2014. Human African Trypanosomiasis Presenting at Least 29 Years after Infection—What Can This Teach Us about the Pathogenesis and Control of This Neglected Tropical Disease? C. Franco-Paredes, ed. *PLoS Neglected Tropical Diseases*, 8(12), p.e3349.

- Sundriyal, S. et al., 2014. Development of diaminoquinazoline histone lysine methyltransferase inhibitors as potent blood-stage antimalarial compounds. *ChemMedChem*, 9, pp.2360–2373.
- Sundriyal, S. et al., 2017. Histone lysine methyltransferase structure activity relationships that allow for segregation of G9a inhibition and anti-Plasmodium activity. *Med. Chem. Commun.*, 8(5), pp.1069–1092.
- Talbert, P.B. & Henikoff, S., 2009. Chromatin-based transcriptional punctuation. *Genes & Development*, 23(9), pp.1037–1041.
- Taylor, J.E. & Rudenko, G., 2006. Switching trypanosome coats: what's in the wardrobe? *Trends Genet*, 22, pp.614–620.
- Thatcher, T.H. & Gorovsky, M.A., 1994. Phylogenetic analysis of the core histones H2A, H2B, H3, and H4. *Nucleic Acids Res*, 22, pp.174–179.
- Thomas, S. et al., 2009. Histone acetylations mark origins of polycistronic transcription in *Leishmania major*. *BMC Genomics*, 10(1), p.152.
- Tornaletti, S., Park-Snyder, S. & Hanawalt, P.C., 2008. G4-forming sequences in the non-transcribed DNA strand pose blocks to T7 RNA polymerase and mammalian RNA polymerase II. *The Journal of biological chemistry*, 283(19), pp.12756–62.
- Ulbert, S., Chaves, I. & Borst, P., 2002. Expression site activation in *Trypanosoma brucei* with three marked variant surface glycoprotein gene expression sites. *Molecular and Biochemical Parasitology*, 120(2), pp.225–235.
- Vanhamme, L. et al., 2001. An update on antigenic variation in African trypanosomes. *Trends in parasitology*, 17(7), pp.338–43.
- Vanhamme, L. et al., 2000. Differential RNA elongation controls the variant surface glycoprotein gene expression sites of *Trypanosoma brucei*. *Molecular microbiology*, 36(2), pp.328–40.
- Vastenhouw, N.L. et al., 2010. Chromatin signature of embryonic pluripotency is established during genome activation. *Nature*, 464(7290), pp.922–6.
- Warner, J.R., 1999. The economics of ribosome biosynthesis in yeast. *Trends in biochemical sciences*, 24(11), pp.437–40.
- White, T.C., Rudenko, G. & Borst, P., 1986. Three small RNAs within the 10 kb trypanosome rRNA transcription unit are analogous to domain VII of other eukaryotic 28S rRNAs. *Nucleic acids research*, 14(23), pp.9471–89.
- WHO, 2017a. WHO | Chagas disease (American trypanosomiasis). *WHO*. Available at: <http://www.who.int/mediacentre/factsheets/fs340/en/> [Accessed August 17, 2017].
- WHO, 2017b. WHO | Leishmaniasis. *WHO*. Available at: <http://www.who.int/mediacentre/factsheets/fs375/en/> [Accessed August 17, 2017].
- WHO, 2017c. WHO | Trypanosomiasis, human African (sleeping sickness). *WHO*. Available at: <http://www.who.int/mediacentre/factsheets/fs259/en/> [Accessed October 5, 2017].
- Williams, R.O., Young, J.R. & Majiwa, P.A., 1982. Genomic environment of *T. brucei* VSG genes: presence of a minichromosome. *Nature*, 299(5882), pp.417–21.
- Wirtz, E. et al., 1999. A tightly regulated inducible expression system for conditional gene knock-outs

and dominant-negative genetics in *Trypanosoma brucei*. *Molecular and biochemical parasitology*, 99(1), pp.89–101.

Wright, J.R., Siegel, T.N. & Cross, G.A., 2010. Histone H3 trimethylated at lysine 4 is enriched at probable transcription start sites in *Trypanosoma brucei*. *Mol Biochem Parasitol*, 172, pp.141–144.

Yang, X. et al., 2009. RAP1 is essential for silencing telomeric variant surface glycoprotein genes in *Trypanosoma brucei*. *Cell*, 137, pp.99–109.

Zhou, M.-M. et al., 1999. Structure and ligand of a histone acetyltransferase bromodomain. *Nature*, 399(6735), pp.491–496.

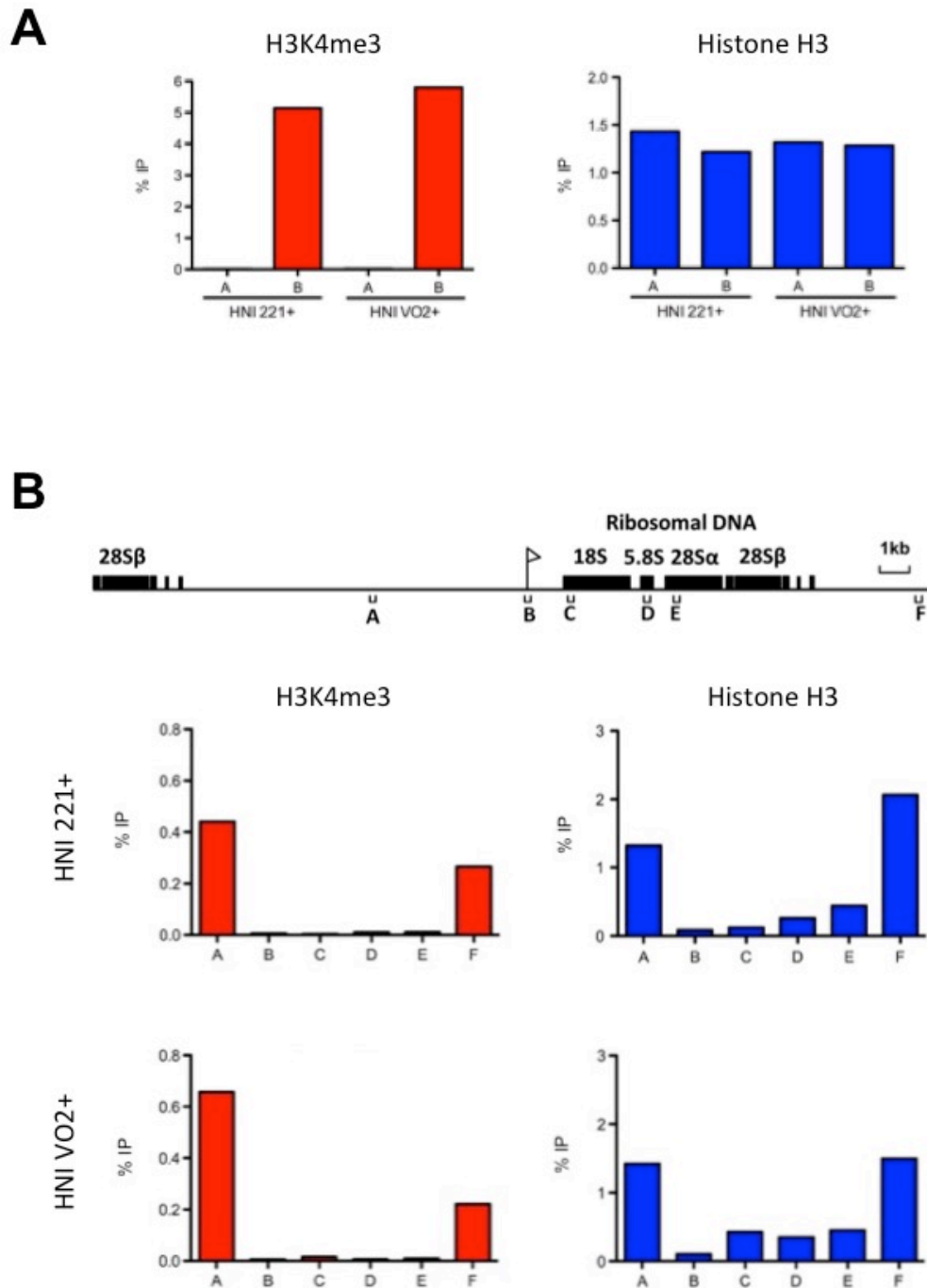
Ziegelbauer, K. & Overath, P., 1993. Organization of two invariant surface glycoproteins in the surface coat of *Trypanosoma brucei*. *Infection and immunity*, 61(11), pp.4540–5.

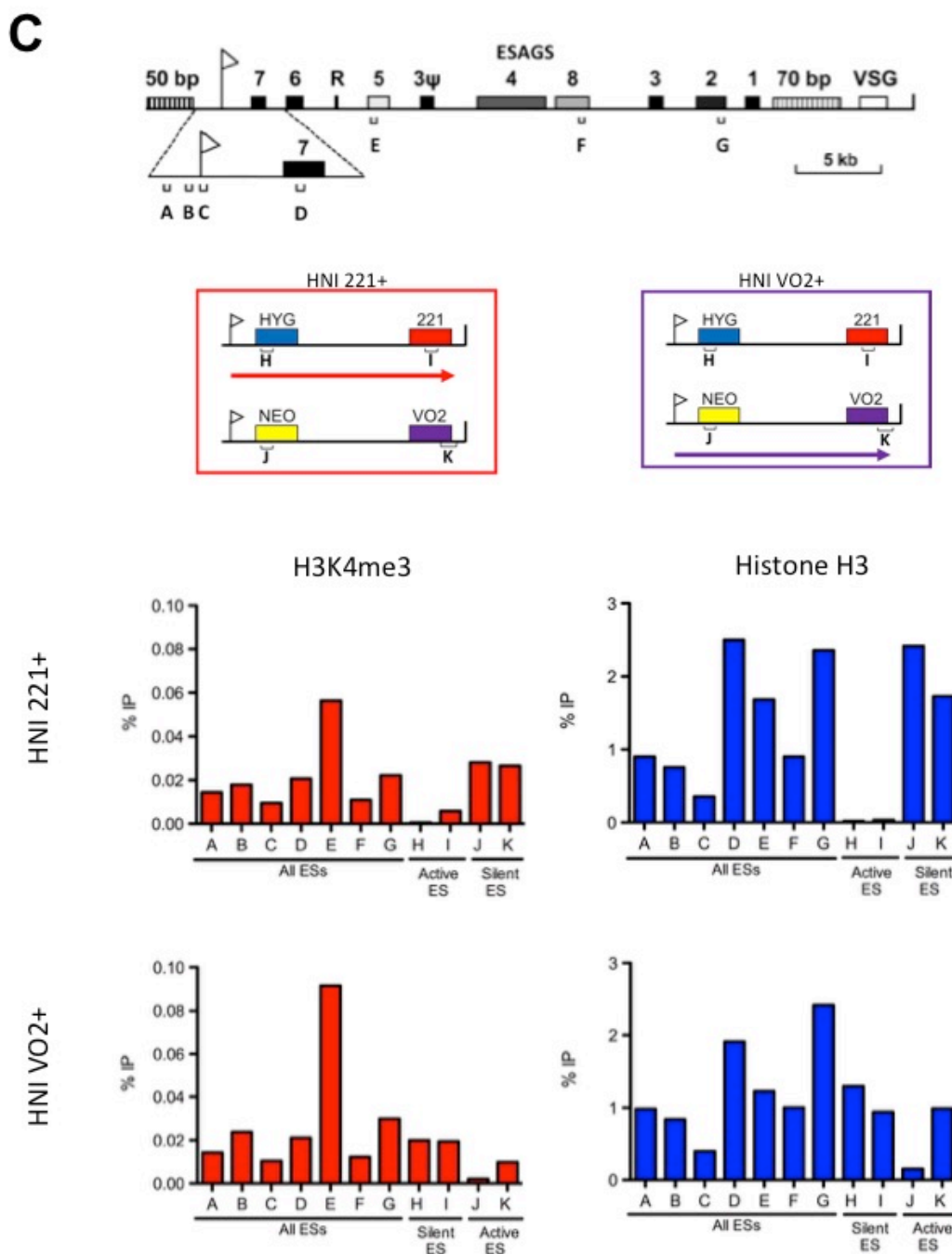
Zuma, A.A. et al., 2017. Chaetocin—A histone methyltransferase inhibitor—Impairs proliferation, arrests cell cycle and induces nucleolar disassembly in *Trypanosoma cruzi*. *Acta Tropica*, 170, pp.149–160.

## Chapter Nine

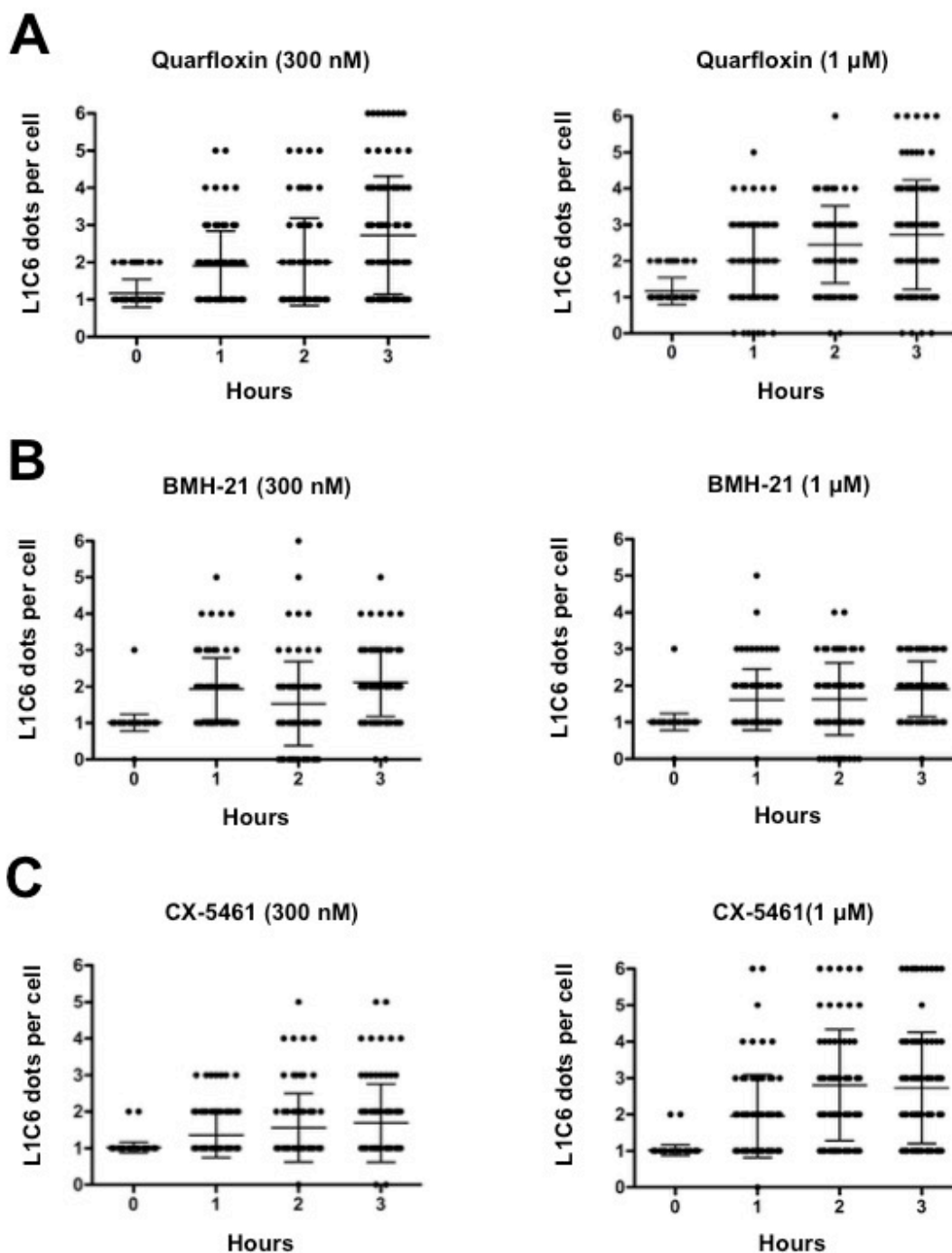
### Appendices

#### 9.1 - Supplementary material





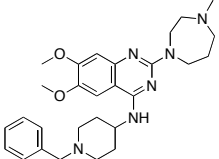
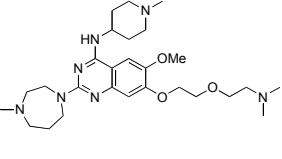
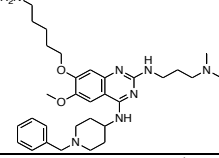
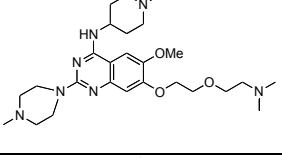
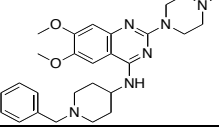
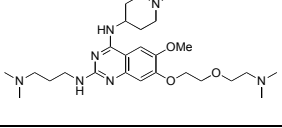
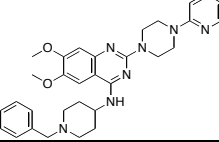
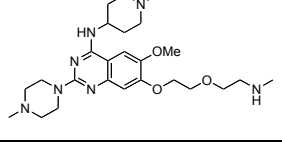
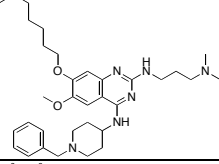
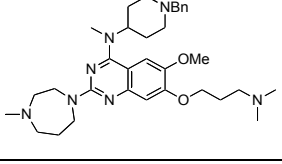
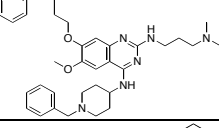
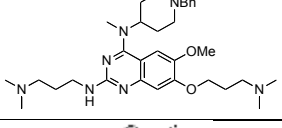
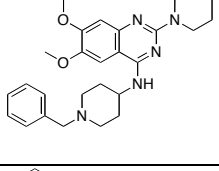
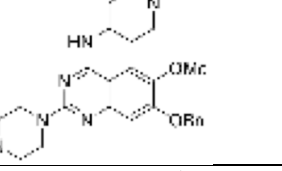
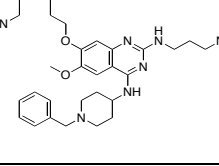
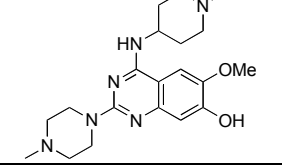
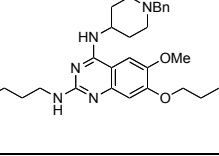
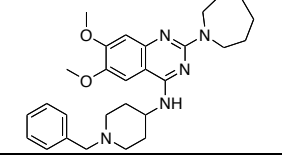
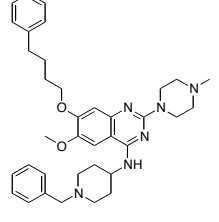
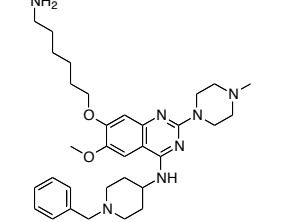
**Figure S.1. Native H3K4me3 and Histone H3 ChIP signal normalised to percentage input.** The levels of trimethylated H3K4 (Red) and histone H3 (Blue) as determined by ChIP using anti-H3K4me3 and anti-H3 antibodies. The data are shown as the percentage of input immunoprecipitated (% IP) after subtraction of the no antibody control from the H3 and H3K4me3 ChIP-qPCR signals. (A) Native ChIP-qPCR data of H3K4me3 and histone H3 levels at the SSR (primers A (C3DN\_185s/C3DN\_300as) and B (Dive2\_SSR\_3108s/Dive2\_SSR\_3229as)). (B) Native ChIP-qPCR data of the rDNA transcription unit. (C) Native ChIP-qPCR data showing the distribution of H3K4me3 and histone H3 at VSG ESs in the HNI 221+ and HNI VO2+ cell lines. Results are from qPCR analysis of ChIP material from a single immunoprecipitation experiment.



**Figure S.2. Exposure to 300 nM and 1  $\mu$ M of Pol I inhibitors results in disintegration of the nucleolus in BSF *T. brucei*.**

BSF parasites (TY-YFP-RPA2 cell line) were incubated with 300 nM and 1  $\mu$ M of Quarfloxin (A), BMH-21 (B) and CX-5461 (C). Cells were stained with DNA stain DAPI and nucleolar marker L1C6 to visualise the morphology of the nucleoli. Each dot represents a nonmitotic (G1) cell and the number of L1C6 positive foci (dots) within the each nucleolus is shown on the Y-axis. The mean number of L1C6 dots per cell from two biological replicates is shown as a horizontal line  $\pm$  standard deviation.



Compound	Compound
HKMTI-1-001 (BIX-01294) 	HKMTI-1-044 
HKMTI-1-003 	HKMTI-1-045 
HKMTI-1-005 	HKMTI-1-046 
HKMTI-1-011 	HKMTI-1-047 
HKMTI-1-014 	HKMTI-1-048 
HKMTI-1-015 	HKMTI-1-049 
HKMTI-1-022 	HKMTI-1-050 
HKMTI-1-030 	HKMTI-1-051 
HKMTI-1-032 	HKMTI-1-053 
HKMTI-1-060 	HKMTI-1-054 

HKMTI-1-034		HKMTI-1-055	
HKMTI-1-035		HKMTI-1-056	
HKMTI-1-036		HKMTI-1-058	
HKMTI-1-037		HKMTI-1-059	
HKMTI-1-039		HKMTI-1-033	
HKMTI-1-040		HKMTI-1-061	
HKMTI-1-041		HKMTI-1-062	
HKMTI-1-042		HKMTI-1-017	
HKMTI-1-043		HKMTI-1-251	

**Table S.1. Library of small molecules derived from BIX-01294 screened for anti-trypanosomal activity.**

The compound name and chemical structure for all BIX-01294 derived HKMT inhibitors synthesised by the Fuchter laboratory.

## 9.2 - Publication

**L. E. Kerry**, et al., 2017. Selective inhibition of RNA polymerase I transcription as a potential approach to treat African Trypanosomiasis. J. Raper, ed. *PLoS neglected tropical diseases*, 11(3), p.e0005432.

(Open access article under a Creative Commons attribution licence)

## 9.3 - Conference presentations

**L. E. Kerry**, E. E. Pegg, D. Cameron, J. Budzak, G. Poortinga, K. Hannan, R. D. Hannan, G. Rudenko. "Selective inhibition of RNA polymerase I transcription as a potential approach to treat African Trypanosomiasis." Oral presentation - Kinetoplastid Molecular Cell Biology Meeting, Woods Hole, Massachusetts, USA. April 2017.

**L. E. Kerry**, C. Davis, J. Budzak, E. E. Pegg, K. Witmer, B. Hall, M. Kushwaha, S. D'Archivio, B. Wickstead, G. Rudenko. "Characterisation of three independent *T. brucei* 'double-expressers' strains showing simultaneous activation of two VSG expression sites." Poster - Kinetoplastid Molecular Cell Biology Meeting, Woods Hole, Massachusetts, USA. April 2017.

**L. E. Kerry**, E. E. Pegg, D. Cameron, J. Budzak, R. D. Hannan, G. Rudenko. "The African trypanosome *Trypanosoma brucei* is susceptible to therapeutic concentrations of RNA polymerase I inhibitors." Poster - British Society for Parasitology (BSP), Trypanosomiasis & Leishmaniasis Seminar. Czech Republic. September 2016.

## 9.4 - Awards

First prize for best third year PhD research presentation. "Epigenetic control of transcription in the African trypanosome, *Trypanosoma brucei*." Postgraduate Research Day. Imperial College London. March 2017.

RESEARCH ARTICLE

# Selective inhibition of RNA polymerase I transcription as a potential approach to treat African trypanosomiasis

Louise E. Kerry<sup>1</sup>, Elaine E. Pegg<sup>1</sup>, Donald P. Cameron<sup>2,3</sup>, James Budzak<sup>1</sup>, Gretchen Poortinga<sup>2,3</sup>, Katherine M. Hannan<sup>2,3</sup>, Ross D. Hannan<sup>2,3</sup>, Gloria Rudenko<sup>1\*</sup>

**1** Department of Life Sciences, Sir Alexander Fleming Building, Imperial College London, London, United Kingdom, **2** ACRF Department of Cancer Biology and Therapeutics, The John Curtin School of Medical Research, The Australian National University, Canberra, Australia, **3** Oncogenic Signalling and Growth Control Program, Peter MacCallum Cancer Centre, Melbourne, Australia

\* [gloria.rudenko@imperial.ac.uk](mailto:gloria.rudenko@imperial.ac.uk)



 OPEN ACCESS

**Citation:** Kerry LE, Pegg EE, Cameron DP, Budzak J, Poortinga G, Hannan KM, et al. (2017) Selective inhibition of RNA polymerase I transcription as a potential approach to treat African trypanosomiasis. *PLoS Negl Trop Dis* 11(3): e0005432. doi:10.1371/journal.pntd.0005432

**Editor:** Jayne Raper, Hunter College, CUNY, UNITED STATES

**Received:** September 14, 2016

**Accepted:** February 23, 2017

**Published:** March 6, 2017

**Copyright:** © 2017 Kerry et al. This is an open access article distributed under the terms of the [Creative Commons Attribution License](https://creativecommons.org/licenses/by/4.0/), which permits unrestricted use, distribution, and reproduction in any medium, provided the original author and source are credited.

**Data Availability Statement:** All relevant data are within the paper and its Supporting Information files.

**Funding:** LEK is funded by a BBSRC DTP PhD studentship (<http://www.bbsrc.ac.uk>), GR is a Wellcome Senior Fellow in the Basic Biomedical Sciences (<https://wellcome.ac.uk>). Research in the Hannan lab is supported by a National Health and Medical Research Council (NHMRC) of Australia project grant (1100654) and program grant (1053792) (<https://www.nhmrc.gov.au>). RDH was

## Abstract

*Trypanosoma brucei* relies on an essential Variant Surface Glycoprotein (VSG) coat for survival in the mammalian bloodstream. High VSG expression within an expression site body (ESB) is mediated by RNA polymerase I (Pol I), which in other eukaryotes exclusively transcribes ribosomal RNA genes (rDNA). As *T. brucei* is reliant on Pol I for VSG transcription, we investigated Pol I transcription inhibitors for selective anti-trypanosomal activity. The Pol I inhibitors quarfloxin (CX-3543), CX-5461, and BMH-21 are currently under investigation for treating cancer, as rapidly dividing cancer cells are particularly dependent on high levels of Pol I transcription compared with nontransformed cells. In *T. brucei* all three Pol I inhibitors have IC50 concentrations for cell proliferation in the nanomolar range: quarfloxin (155 nM), CX-5461 (279 nM) or BMH-21 (134 nM) compared with IC50 concentrations in the MCF10A human breast epithelial cell line (4.44 μM, 6.89 μM or 460 nM, respectively). *T. brucei* was therefore 29-fold more sensitive to quarfloxin, 25-fold more sensitive to CX-5461 and 3.4-fold more sensitive to BMH-21. Cell death in *T. brucei* was due to rapid inhibition of Pol I transcription, as within 15 minutes treatment with the inhibitors rRNA precursor transcript was reduced 97-98% and VSG precursor transcript 91-94%. Incubation with Pol I transcription inhibitors also resulted in disintegration of the ESB as well as the nucleolus subnuclear structures, within one hour. Rapid ESB loss following the block in Pol I transcription argues that the ESB is a Pol I transcription nucleated structure, similar to the nucleolus. In addition to providing insight into Pol I transcription and ESB control, Pol I transcription inhibitors potentially also provide new approaches to treat trypanosomiasis.

## Author summary

*Trypanosoma brucei* is protected by an essential Variant Surface Glycoprotein (VSG) coat in the mammalian bloodstream. The active VSG gene is transcribed by RNA polymerase I (Pol I), which typically only transcribes rDNA. Pol I transcription inhibitors are under

funded by an NHMRC Fellowship (1022402). This research is funded by the Wellcome Trust. The funders had no role in the study design, data collection and analysis, decision to publish, or preparation of the manuscript.

**Competing interests:** The authors have declared that no competing interests exist.

clinical trials for cancer chemotherapy. As *T. brucei* relies on Pol I for VSG transcription, we investigated its susceptibility to these drugs. We show that quarfloxin (CX-3543), CX-5461, and BMH-21 are effective against *T. brucei* at nanomolar concentrations. *T. brucei* death was due to rapid and specific inhibition of Pol I transcription. Incubation with Pol I transcription inhibitors also resulted in disappearance of Pol I subnuclear structures like the nucleolus and the VSG expression site body (ESB). Rapid ESB loss followed the Pol I transcription block, arguing that the ESB is nucleated by Pol I transcription. Pol I transcription inhibitors could therefore potentially function as novel drugs against trypanosomiasis.

## Introduction

Human African Trypanosomiasis (HAT) or African Sleeping Sickness is endemic to sub-Saharan Africa, with distribution restricted by the tsetse fly insect vector [1]. Most of the HAT disease burden (98%) is the chronic form of the disease caused by *Trypanosoma brucei gambiense*. The remainder of the HAT cases are the acute form of the disease caused by *Trypanosoma brucei rhodesiense* [2]. Although there has been a progressive decline in the annual number of HAT cases, 1.8 million Africans are still thought to be living in high or very high risk areas, with 11.3 million people at moderate risk of contracting HAT [3]. Vaccines are ineffective against *T. brucei*, as it uses a highly sophisticated strategy of antigenic variation of a surface Variant Surface Glycoprotein (VSG) coat allowing effective escape from the mammalian immune system [4, 5]. As individual trypanosomes have thousands of different VSG genes and pseudogenes, and new chimeric VSG variants are continuously being generated [6], treatment of HAT has relied on drug treatment rather than immunisation.

Only a limited number of drugs are effective against HAT, of which many are toxic, expensive, or difficult to administer in the field [7]. Pentamidine is used against early stage infection of *T. brucei gambiense*, with eflornithine (DFMO) or NECT (nifurtimox-eflornithine combination treatment) also effective against later stages of *T. brucei gambiense* infection [8, 9]. Suramin has been used since 1922 against early stage *T. brucei rhodesiense*, with the highly toxic arsenical drug melarsoprol effective against the later stages of the disease once parasites have penetrated the blood-brain barrier [8]. A constant concern with this limited number of treatment options is human drug toxicity, as well as the development of parasite resistance. Drug resistant *T. brucei* strains are easily generated in the laboratory and have been found in the field [10, 11]. While there is a clear need for new treatments for HAT, the decreasing number of HAT cases has reduced the incentive to develop new drugs.

This increases the attractiveness of ‘repurposing’ drugs which have already undergone clinical trials for use against other human diseases [12–14]. The anti-trypanosomal drug eflornithine is a good example of drug “repurposing”. Originally developed as a drug against cancer, it was subsequently repurposed for use against *T. brucei gambiense*, as well as female hirsutism [15]. Similarly the drug tamoxifen, which is effective against estrogen receptor-positive breast cancer, also has efficacy against *Leishmania* [16, 17]. In addition to repurposing drugs, target repurposing can also be used to exploit libraries of small molecules developed against human target molecules. For example, an extensive panel of human kinase inhibitors are currently being investigated for their selective potential against essential *T. brucei* kinases [18].

Here, we investigate the efficacy of RNA polymerase I (Pol I) transcription inhibitors as treatment against *T. brucei*. Pol I transcribes the ribosomal RNA genes (rDNA), which

accounts for up to 60% of transcription in proliferating cells [19]. Tumour cells are highly sensitive to disruption of Pol I transcription [20], while normal cells remain largely unaffected [21]. Tumour cell death upon Pol I transcription inhibition is not due to ribosome depletion, but due to cell “checkpoint” activation [20–22], explaining why in particular tumour cells undergoing uncontrolled cell proliferation are exquisitely sensitive to inhibition of Pol I transcription. Chemical inhibitors of Pol I are therefore currently being investigated for treatment against cancer [20, 23, 24].

African trypanosomes are unicellular eukaryotes which proliferate at high rates within the mammalian bloodstream. They have a particularly high dependency on Pol I transcription, as they transcribe the gene encoding their VSG coat from a Pol I transcribed VSG expression site (ES) transcription unit [25, 26]. VSG is highly essential in *T. brucei* both *in vitro* and *in vivo*, and perturbation of VSG synthesis *in vivo* results in very rapid trypanosome clearance within hours [27]. We therefore hypothesised that Pol I transcription inhibitors might represent useful drug leads against *T. brucei*.

A number of compounds have been shown to selectively impact on Pol I transcription (referred to here as Pol I inhibitors), including quarfloxin, CX-5461 and BMH-21. Quarfloxin has anti-cancer activity, and using a mouse xenograft model system, a large range of cancer cell lines were shown to be sensitive to it *in vivo* [28]. Quarfloxin was subsequently investigated for its therapeutic potential [28–30], and reached Phase II clinical trials before withdrawal due to problems with bioavailability [31]. The Pol I inhibitor CX-5461 was identified in a small molecule screen of compounds inhibiting transcription [32]. Similar to quarfloxin, CX-5461 prevented proliferation of a broad range of cancer cell lines *in vitro* or solid tumours *in vivo* [21, 33, 34]. This led to its investigation as an anti-cancer therapy, and it is currently in Phase I clinical trials against breast cancer (Clinicaltrials.gov NCT02719977) and hematologic cancer (ANZCTR ACTRN12613001061729)[23, 35]. The small molecule BMH-21 was identified in a small molecule screen targeting the p53 tumour suppressor pathway, and is also considered to have possible therapeutic potential against cancer [36, 37].

Here we show selective sensitivity of *T. brucei* compared with human breast epithelial or fibroblast cell lines for the Pol I inhibitors quarfloxin, CX-5461 and BMH-21. Trypanosome sensitivity for these drugs is within the nanomolar range, and at concentrations which are therapeutic against cancer. We show that these Pol I inhibitors specifically target Pol I transcription in *T. brucei*, as incubation results in very rapid and specific disappearance of Pol I derived RNA precursor transcripts. In addition, incubation with these compounds leads to Pol I subnuclear structures including the VSG expression site body (ESB) and the nucleolus disassembling. These chemical inhibitors demonstrate that the ESB, like the nucleolus, is a Pol I transcription-seeded subnuclear structure. In addition, these data argue that repurposing these potential cancer chemotherapy agents could potentially provide therapeutic potential against African trypanosomes.

## Materials and methods

### Ethics statement

No patient material was used. No animal experiments were performed. All experiments were performed *in vitro* with the established laboratory strain *Trypanosoma brucei* 427.

### Trypanosome strains and culturing

The laboratory bloodstream form strain *Trypanosoma brucei* 427 was cultured *in vitro* according to [38]. The *T. brucei* SM or “single marker” cell line [39] or the SM derived S16\_221Pur cell line (containing a construct with a puromycin resistance gene inserted behind the active

VSG221 ES promoter) were used for all *in vitro* cytotoxicity and proliferation assays, and were cultured in drug free media for at least 48 hours prior to treatment. The *T. brucei* S16221Pur-oGFP cell line was used for RNA precursor transcript analysis [40, 41]. Selection on puromycin maintained active transcription of the VSG221 ES in these cell lines. For the immunofluorescence analyses, the *T. brucei* TY-YFP-RPA2 cell line was generated through transfection of pEnT5H-Y:NLS:RPA2 (gift of the Gull lab) into *T. brucei* SM cells [42]. This resulted in a single RPA2 allele (second largest Pol I subunit) endogenously tagged with Yellow Fluorescence Protein (YFP) at the N-terminus. For analysis of VEX1 foci, the *T. brucei* S16\_221Pur cell line was transfected with the pNATVEX1<sup>x12myc</sup> construct (gift of the Horn lab) [43]. This resulted in the addition of a 12x myc C-terminal epitope tag to VEX1.

### Pol I inhibitors and proliferation, wash-out and cytotoxicity assays

RNA polymerase I inhibitors used were CX-5461 (Ross Hannan, ANU, Australia) [32], quarfloxin (CX-3543) (Adooq Bioscience) [28] or BMH-21 (Sigma) [36], with suramin (Sigma) used as a lethality control. Stock solutions of CX-5461 (10mM) were made up in 50 mM NaH<sub>2</sub>PO<sub>4</sub> (pH 7.0). Quarfloxin (1 mM) and BMH-21 (1 mM) were dissolved in DMSO (dimethyl sulfoxide) (Sigma ≥99.9%). A 10 mM solution of suramin was made in nuclease free water immediately prior to use. All compounds were diluted directly in HMI-9 media immediately before use.

For proliferation assays, *T. brucei* SM was treated with inhibitors, and densities were determined using a Neubauer haemocytometer. Growth curves were repeated minimally in triplicate. For wash-out assays, *T. brucei* SM was treated with various concentrations of inhibitors. After two hours the cells were washed, resuspended in drug free HMI-9 medium, and cell proliferation was monitored using a haemocytometer. For the Alamar Blue *in vitro* cytotoxicity assay [44], 200 µl samples of *T. brucei* SM cells (2 x 10<sup>3</sup> cells ml<sup>-1</sup>) were plated in 96 well plates, and incubated for 72 hours with two fold serial dilutions of the inhibitors. At 72 hours, 20 µl of Resazurin (0.125 mg ml<sup>-1</sup>) (Sigma) was added, and the parasites were incubated for a further 18 hours. Fluorescence was measured using a Tecan infinite plate reader (excitation at 530 nm, emission at 585 nm). The change in fluorescence (minus the chemical only control) was plotted as a function of the concentration of chemical compound using the sigmoidal dose-response (variable slope) algorithm using GraphPad Prism version 5.

For the mammalian cell toxicity assays, either the spontaneously immortalised Michigan Cancer foundation (MCF10A) human breast epithelial cell line was used [45], or the BJ3 cell line, which is a human foreskin fibroblast cell line immortalized with the h-Tert catalytic subunit of telomerase [46]. Cells were seeded in 96-well plates, and after 48 hours each well was treated in quintuplicate using ten different concentrations of CX-5461, quarfloxin, BMH-21 or suramin. After incubation for 48 hours, the cells were imaged and cell confluence was calculated using an IncuCyte ZOOM (Essen Biosciences). Cell confluence was normalised to a drug vehicle only control which was set to 100%. An Alamar Blue assay was also performed on the MCF10A cell line in the presence of the different Pol I transcription inhibitors. Here the Alamar Blue readout was also normalised to the vehicle only control. Experiments were performed as three biological replicates with the exception of the IncuCyte data for MCF10A in the presence of BMH-21 and doxycycline which were obtained in duplicate. The dose response curves and IC50s were calculated using GraphPad Prism.

### Immunofluorescence microscopy

Trypanosomes were fixed in 2% paraformaldehyde, permeabilised with 0.1% NP-40 for 5 minutes at room temperature before incubation for one hour with an antibody against the

nucleolar marker LIC6 [47] or anti-myc tag antibody (clone 4A6, EMD Millipore). Slides were subsequently incubated with a goat anti-mouse secondary antibody coupled to Alexa-594 (Molecular Probes), before mounting in Vectashield containing DAPI (Vector Laboratories). Microscopy was performed using a Zeiss Imager.M1 microscope equipped with a Zeiss AxioCam MRm camera and Axio Vision Rel 4.8 software. A Z-stack of images was taken at 200 nm intervals, and the images from the individual channels were processed using Image J software. For quantitation of ESB signal using YFP, VEX1 signal using the anti-myc tag antibody or nucleolar signal using the LIC6 antibody, the exposure time and contrast was uniformly adjusted across all conditions. Quantification of ESB and nucleolar signal was carried out using compressed stacks of all appropriate channels in which the images acquired on the Z-axis were analysed. The ESB and nucleolar status was recorded for a total of approximately 100 cells in G1 (two biological replicates of approximately 50 cells) for each condition.

### Transcript analysis

RNA transcript analysis was performed using quantitative reverse transcription PCR (qRT-PCR). Total RNA was isolated using the RNeasy kit (Qiagen) and DNase treated with TURBO DNA-free kit (Invitrogen). Reverse transcription was performed using 100 ng RNA as a template for cDNA synthesis using random hexamer primers (Promega) and the Omniscript RT kit (Qiagen). qPCR was performed on the 7500 Fast Real-Time PCR system (Life Technologies) using Brilliant II SYBR Green QPCR Low ROX Master Mix (Agilent Technologies). DNase treated RNA without reverse transcriptase was used as a control. The amplification conditions for each primer pair were optimised, and the primer sequences are listed in [S1 Table](#). Transcript levels were normalised against actin mRNA, and plotted as relative change relative to the zero hour time point.

### Statistical analysis

Where indicated, the data was analysed using the Student's t-test (paired, two-tailed) (Graph-Pad Prism version 5). Data was considered 'significant' where  $P = 0.01-0.05$  (\*), 'very significant' where  $P = 0.001-0.01$  (\*\*) or 'extremely significant' where  $P = <0.001$  (\*\*).

## Results

### Efficacy of RNA polymerase I inhibitors against bloodstream form *Trypanosoma brucei*

Bloodstream form *T. brucei* utilises RNA polymerase I (Pol I) to transcribe rRNA within the nucleolus, as well as the active VSG ES in the ESB [48–50]. Blocking VSG synthesis triggers a pre-cytokinesis arrest within one cell division, and very rapid trypanosome clearance *in vivo* [27]. The vital role of this multi-functional RNA polymerase I in African trypanosomes therefore makes it an appealing drug target. In light of this, we tested the RNA Pol I inhibitors quarfloxin (CX-3543), BMH-21 and CX-5461 for their efficacy against bloodstream form *Trypanosoma brucei*. We generated dose response curves using an Alamar Blue *in vitro* cytotoxicity assay, with the anti-trypanosomal agent suramin as a lethality control ([Fig 1A–1D](#)) [28, 32, 36, 51]. We found that *T. brucei* showed susceptibility to each of these Pol I inhibitors in the nanomolar range. *T. brucei* was most sensitive to BMH-21 with an IC50 for proliferation of  $134 \pm 8$  nM ([Table 1](#)). Next most effective were quarfloxin with an IC50 of  $155 \pm 9$  nM and CX-5461 with an IC50 of  $279 \pm 16$  nM. As expected, *T. brucei* was susceptible to suramin with an IC50 of  $63 \pm 5$  nM, comparable to the value of 53.0 nM found for *T. b. rhodesiense* using a similar Alamar Blue assay [51].



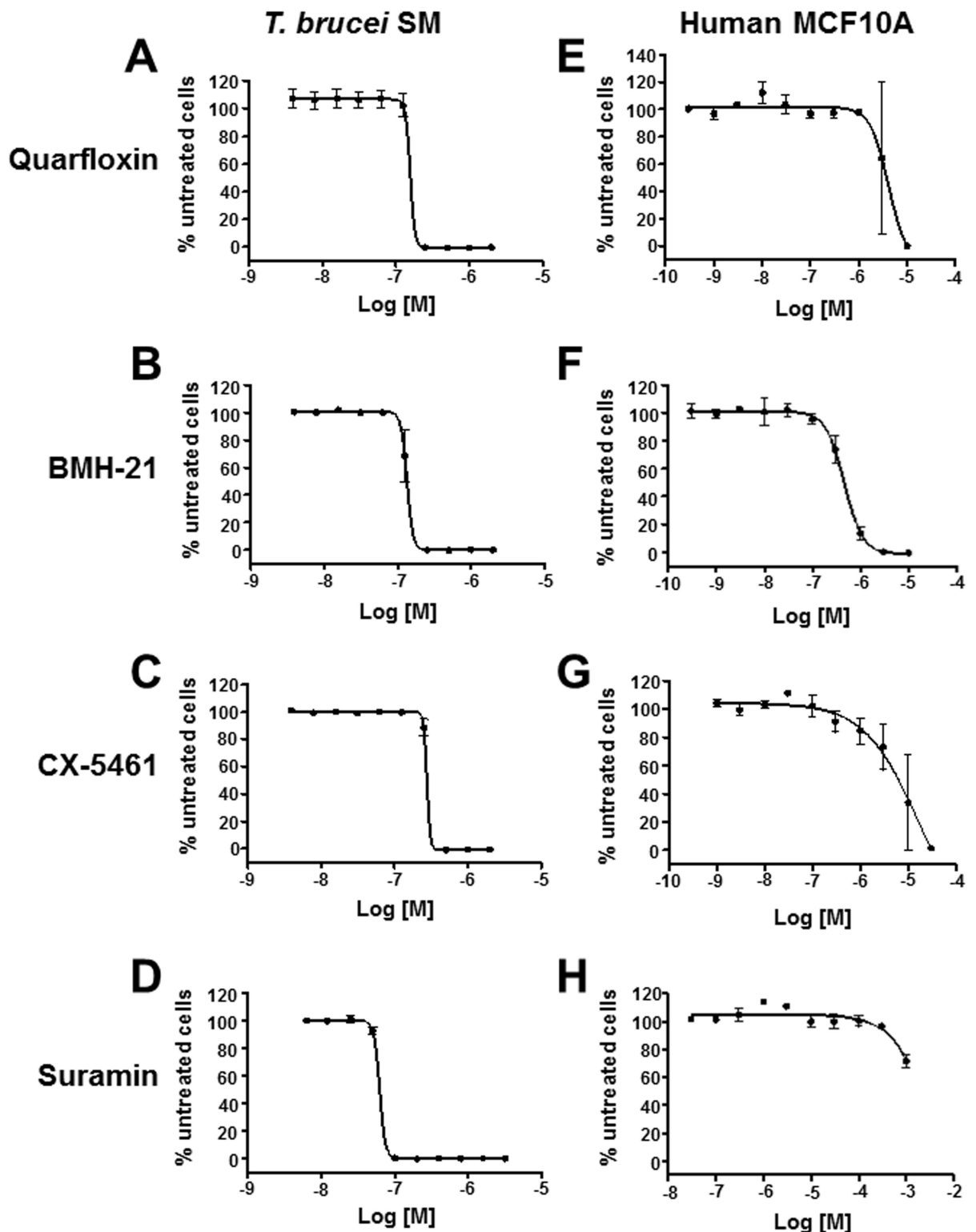


**Fig 1. RNA polymerase I (Pol I) transcription inhibitors selectively inhibit proliferation of bloodstream form *Trypanosoma brucei*.** An Alamar Blue *in vitro* cytotoxicity assay was used to determine sigmoidal dose response curves of *T. brucei* SM (A-D) or the MCF10A human breast epithelial cell line (E-H) incubated with the Pol I inhibitors quarfloxin (A, E), BMH-21 (B, F), CX-5461 (C, G) or the anti-trypanosomal agent suramin (D, H) [44]. The mean percentage of signal relative to the negative control (vehicle without drug) from three biological replicates is plotted with the standard deviation indicated with error bars.

doi:10.1371/journal.pntd.0005432.g001

**Table 1. Relative toxicity of Pol I inhibitors in *T. brucei* compared with human breast epithelial or fibroblast cells expressed as IC<sub>50</sub> (μM ± SD)<sup>a</sup>.** The selectivity index for *T. brucei* is indicated in brackets.

Compound	Alamar blue		Incucyte assay	
	<i>T. brucei</i>	MCF10A Human breast epithelial cells	BJ3 human fibroblasts	MCF10A Human breast epithelial cells
Quarfloxin	0.155 ± 0.009	4.44 ± 3.29 (29x)	2.72 ± 0.17 (18x)	6.24 ± 3.87 (40x)
BMH-21	0.134 ± 0.008	0.46 ± 0.08 (3.4x)	1.36 ± 0.22 (10x)	0.622 ± 0.34 (4.6x)
CX-5461	0.279 ± 0.016	6.89 ± 4.83 (25x)	9.78 ± 0.79 (35x)	7.84 ± 9.8 (28x)
Suramin	0.063 ± 0.005	1636 ± 317	890 ± 127	1260 ± 90
Doxycycline		50.7 ± 33.8		

<sup>a</sup> *T. brucei* cell proliferation was determined using a 72 hour Alamar Blue based cytotoxicity assay, with the IC<sub>50</sub> values presented as the mean ± standard deviation (SD) for three biological replicates of quadruplicate samples after subtraction of fluorescence from the inhibitor only control. Suramin served as a positive control. Proliferation of the MCF10A human breast epithelial cell line was determined using either a 72 hour Alamar Blue or a 48 hour IncuCyte cell proliferation assay. Doxycycline served as a positive control. Growth inhibition of the Tert immortalised BJ3 human fibroblast cell line was determined using an IncuCyte assay. The IC<sub>50</sub> values are presented as the mean ± SD.

doi:10.1371/journal.pntd.0005432.t001

Toxicity of these compounds was also determined in mammalian cells using an Alamar Blue cytotoxicity assay in a spontaneously immortalised breast epithelial cell line (MCF10A) [45] (Fig 1E–1H). The compound doxycycline was used as a positive control for toxicity. These human epithelial cells were the least susceptible to CX-5461 (IC<sub>50</sub> of 6.89 ± 4.83 μM), followed by quarfloxin (4.44 ± 3.29 μM) and BMH-21 (460 ± 80 nM). In parallel, proliferation of these human cells in the presence of Pol I inhibitors was monitored by assessing cell confluence using an IncuCyte ZOOM. This automated system allows monitoring of cells in real-time using live cell imaging, and produced comparable results to the Alamar Blue assay (S1 Fig) (Table 1).

In parallel, the BJ3 human foreskin fibroblast cell line that had been immortalised with hTert (the catalytic subunit of telomerase) was also tested for sensitivity to these compounds [46] (S2 Fig)(S3 Fig). The IC<sub>50</sub> values corresponding to either growth arrest or cell death shown in S2 Fig were obtained by observing the cell images (S3 Fig) and determining the point where the specific dose curve plateaus at the higher concentrations. If the cells were morphologically sound, then the dose curve represented growth arrest of the cells. If the cells were dead, then the dose curve represented cell death. The IC<sub>50</sub> values for cell death were used to calculate the selectivity index scores. This was done as the mammalian cells used in the dose response assays were intended to approximate normal quiescent human cells, hence the IC<sub>50</sub> values for growth arrest are not relevant.

Similar to the breast cancer cells, these human fibroblasts were the least susceptible to CX-5461 (IC<sub>50</sub> of 9.78 ± 0.79 μM), followed by quarfloxin (2.72 ± 0.17 μM) and BMH-21 (1.36 ± 0.22 μM) (Table 1). If one therefore compares the relative selectivity of these compounds for *T. brucei*, CX-5461 is the most effective compound, with *T. brucei* 25–35 fold more sensitive than human cells. *T. brucei* is 18–40 fold more sensitive to quarfloxin and 3–10 fold more sensitive to BMH-21. As expected, the trypanocide suramin showed minimal toxicity to mammalian cells (IC<sub>50</sub> of 1636 ± 317 μM).

We next investigated the effect of these Pol I inhibitors on *T. brucei* proliferative growth over 48 hours (Fig 2). The drug concentrations of quarfloxin, BMH-21 or CX-5461 that resulted in suppression of proliferative growth in *T. brucei* were 300 nM, 300 nM and 1 μM

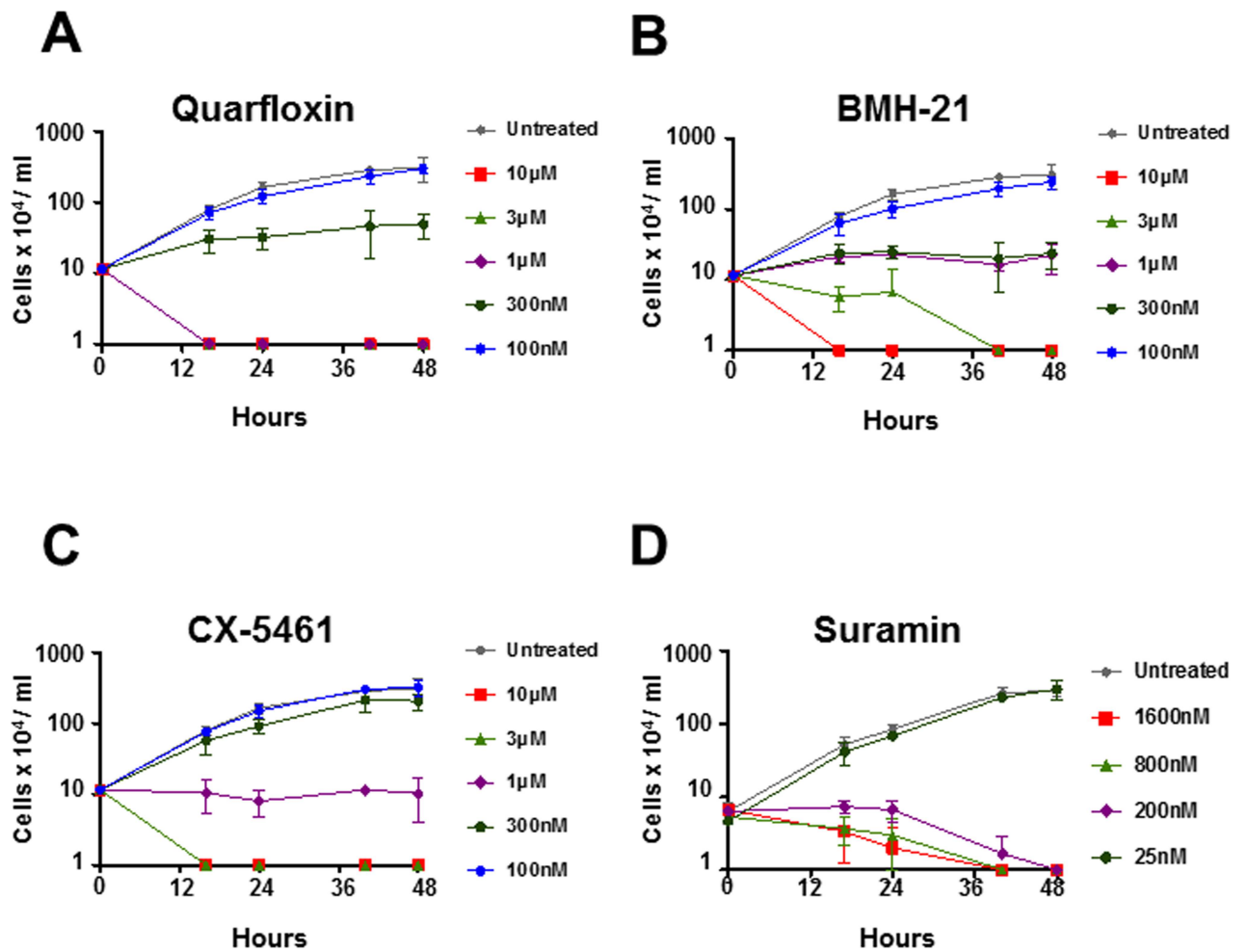


**Fig 2. Pol I transcription inhibitors kill bloodstream form *Trypanosoma brucei* in a time and dose dependent manner.** Cell proliferation assays were performed in which *T. brucei* SM cells were exposed to a range of concentrations of Pol I inhibitors including quarfloxin (A), BMH-21 (B) or CX-5461 (C) using the anti-trypanosomal agent suramin (D) as a control. The graph shows the cell density of treated parasites in comparison with the untreated *T. brucei* SM line at 0, 16, 24, 40 and 48 hours. The mean of four biological replicate experiments for the Pol I inhibitors, or three replicates for the suramin control are shown with standard deviation indicated with error bars.

doi:10.1371/journal.pntd.0005432.g002

respectively (Fig 2A–2C), with suramin serving as a positive control (Fig 2D). The impact of these Pol I inhibitors on *T. brucei* cell growth was rapid, and evident within two cell divisions.

Under therapeutic conditions effective drug concentrations in the blood typically fluctuate through time. We therefore tested the reversibility of these Pol I transcription inhibitors on the inhibition of *T. brucei* proliferation using wash-out assays. *T. brucei* was incubated with various concentrations of these inhibitors for two hours. Cells were subsequently washed and resuspended in drug-free medium, before cell proliferation was monitored (Fig 3). Incubation of *T. brucei* with quarfloxin and CX-5461 for two hours still resulted in significantly reduced proliferation at similar concentrations of drug (1 μM) even after the wash-out was performed. This indicates that quarfloxin and CX-5461 were working irreversibly. In contrast, wash-out of the BMH-21 inhibitor at all except for the highest concentration (3 μM) resulted in restored *T. brucei* growth. This indicates reversibility in how this compound is inhibiting trypanosome growth, which could potentially limit its use as a therapeutic agent.

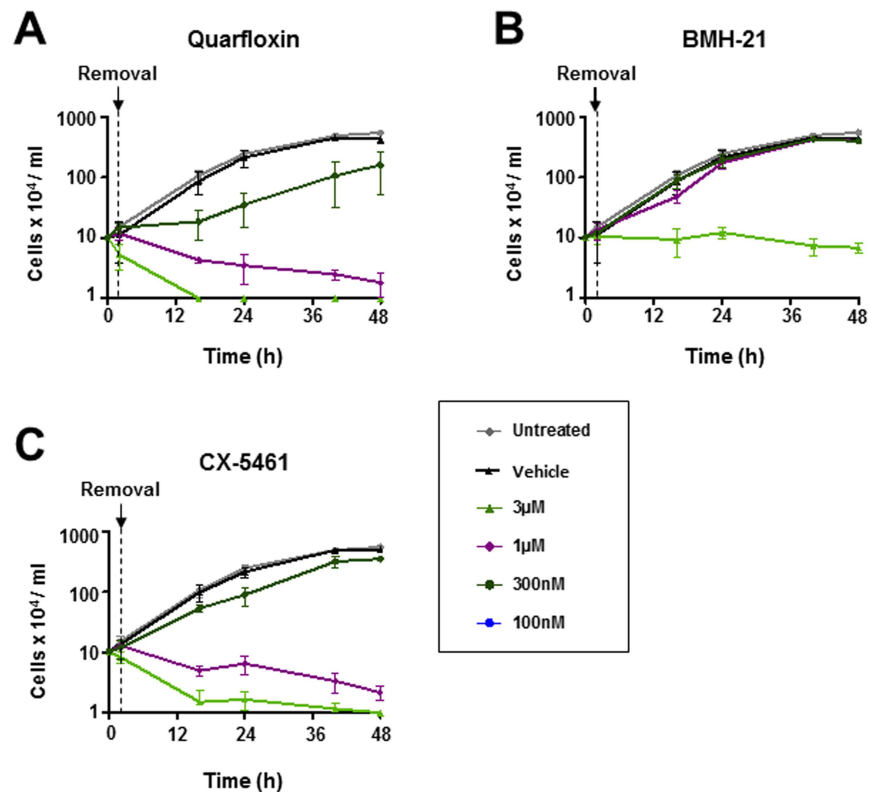


**Fig 3. Irreversible inhibition of *T. brucei* growth after incubation with quarfloxin or CX-5461 as determined using wash-out assays.** *T. brucei* SM cells were treated with various concentrations of quarfloxin (A), BMH-21 (B) or CX-5461 (C) for two hours, washed, diluted into fresh media and cell growth was monitored. Untreated cells, and parasites incubated with the appropriate drug vehicle (DMSO for quarfloxin and BMH-21) or  $\text{NaH}_2\text{PO}_4$  (for CX-5461) were used as controls. The mean of three biological replicates is plotted with the standard deviation indicated with error bars.

doi:10.1371/journal.pntd.0005432.g003

### Treatment with Pol I inhibitors leads to selective reduction in Pol I transcription

As these Pol I inhibitors dramatically affected *T. brucei* proliferation, we next investigated if Pol I transcription of the rDNA or VSG ES was selectively inhibited (Fig 4A and 4B). The rDNA in *T. brucei* is transcribed as an approximately ten kilobase transcription unit, with the pre-rRNA precursor transcripts subsequently undergoing rapid processing reactions (Fig 4A) [52]. After incubation of *T. brucei* with the Pol I inhibitors, we determined the abundance of these unstable rRNA precursors using qRT-PCR as an indirect method of rRNA synthesis rates as performed previously [53]. Incubation with 1  $\mu\text{M}$  quarfloxin, resulted in a dramatic reduction in pre-rRNA precursors within 15 minutes (Fig 4C), and pre-rRNA Precursor 1 transcript levels were reduced by  $98.5 \pm 0.66\%$  (primer a), and rRNA Precursor 2 decreased by  $91.3 \pm 2.6\%$  (primer b). Comparable degrees of repression of rDNA transcription were seen using primer pairs c and d, which detect both rRNA Precursors 2 and 3, where levels were also drastically reduced within fifteen minutes by  $83.4 \pm 2.1\%$  or  $89.5 \pm 2.7\%$  respectively.

The VSG221 ES is a highly active Pol I transcription unit in the bloodstream form of *T. brucei*. We investigated the repression of transcripts derived from regions of the ES which could be expected to be unstable, as they are encoded by intergenic regions or pseudogenes. We monitored the presence of a VSG221 precursor transcript using a primer pair 520 bp upstream

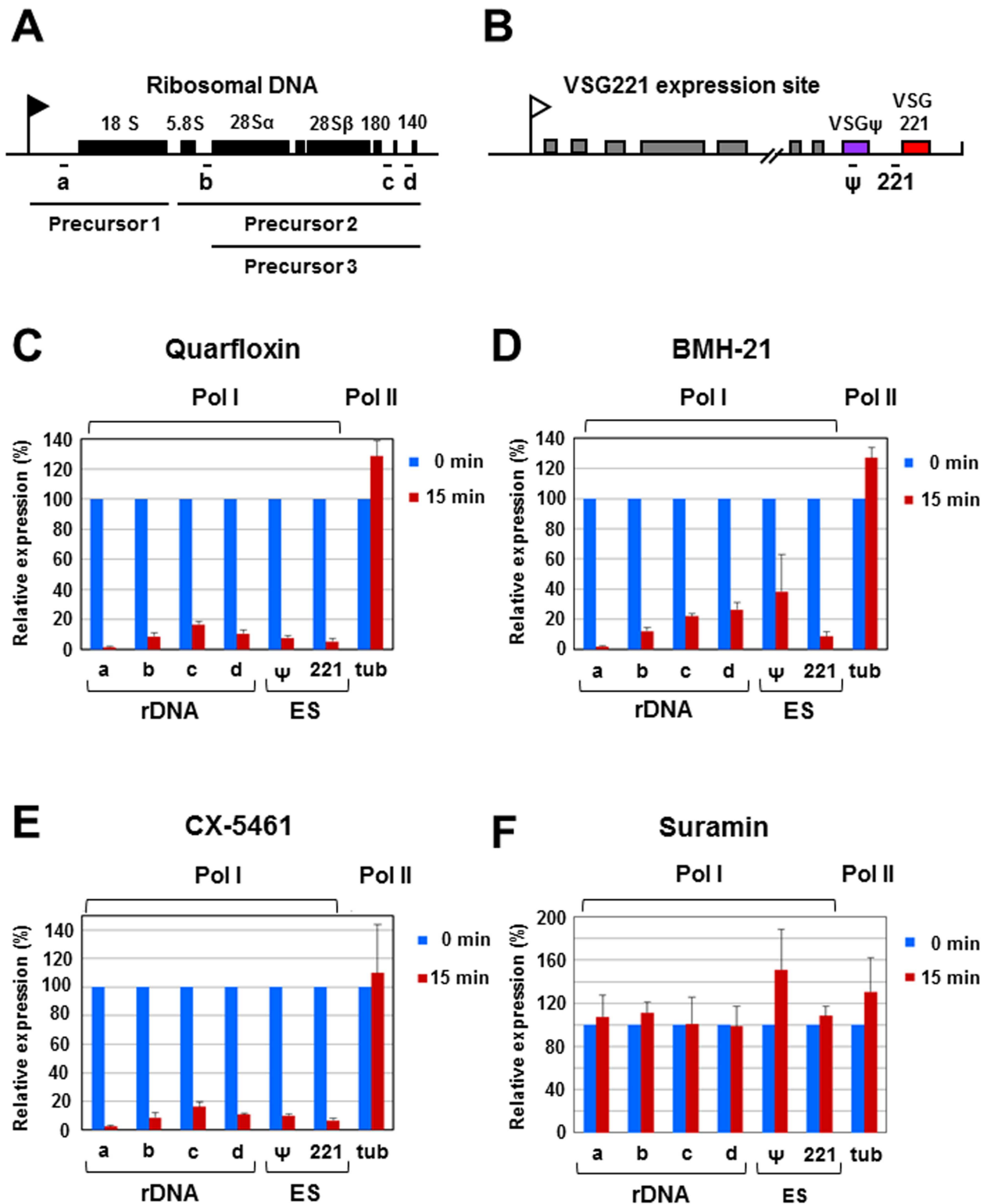


**Fig 4. Rapid and specific inhibition of Pol I transcription by Pol I inhibitors in bloodstream form *T. brucei*.** (A) Schematic of the ten kilobase pair *T. brucei* ribosomal DNA (rDNA) transcription unit with the rDNA promoter indicated with a black flag, and the rRNA genes with black boxes. Different rRNA precursor transcripts are shown below according to [52], with the qPCR primers used indicated with letters. The first rRNA cleavage produces rRNA Precursor 1 (3.4 kb) and Precursor 2 (5.6 kb) transcripts. Subsequently, Precursor 2 is cleaved to

generate Precursor 3 (5.0 kb) [52]. (B) Schematic of the sixty kilobase pair *VSG221* expression site with the promoter indicated with a white flag. Various expression site associated genes are indicated with grey boxes, and the telomeric *VSG* pseudogene ( $\psi$ ) and the *VSG221* gene indicated with coloured boxes with relevant primers indicated below. These transcription units are not drawn according to scale. (C) Rapid and specific inhibition of Pol I transcription in the presence of quarfloxin. The *T. brucei* S16221PuroGFP cell line was incubated with 1  $\mu$ M quarfloxin for 15 minutes. RNA precursor transcripts analysed were either from the Pol I transcribed rDNA (primer pairs a-d) or the active *VSG221* ES. ES transcripts analysed corresponded to a *VSG* pseudogene ( $\psi$ ) or a *VSG221* precursor transcript (221). In comparison, levels of precursor transcript from the Pol II transcribed alpha-beta tubulin locus (*tub*) remained unaffected. RNA was normalised against actin mRNA, levels of which remained unchanged by the different Pol I inhibitors. Results shown are the mean of three biological replicates with standard deviation indicated with error bars. (D) As in (C), only cells were incubated in 1  $\mu$ M BMH-21. (E) As in (C), only cells were incubated in 1  $\mu$ M CX-5461. (F) As in (C), only cells were incubated with 800 nM suramin.

doi:10.1371/journal.pntd.0005432.g004

of the *VSG221* gene (Fig 4B). This *VSG221* precursor transcript was reduced by  $94.5 \pm 1.9\%$  after 15 minutes incubation with quarfloxin (Fig 4C). A single copy *VSG* pseudogene ( $\psi$ ) is located approximately 4.7 kb upstream of the telomeric *VSG221* in the approximately 60 kilobase *VSG221* expression site [49]. Even when the *VSG221* expression site is transcriptionally active, only very low levels of this *VSG* pseudogene transcript are present, presumably as a consequence of rapid degradation by nonsense mediated decay [54]. After incubation of *T. brucei* with quarfloxin for 15 minutes, levels of *VSG* pseudogene transcript were reduced by  $92.3 \pm 1.6\%$ .

The rapid disappearance of these RNA precursors indicates that both the Pol I derived pre-rRNA as well as the Pol I derived *VSG* expression site encoded RNA precursor transcripts for *VSG221* and the *VSG* pseudogene have very short half-lives of approximately three or four minutes. Precursor transcripts from the tubulin gene cluster are also highly unstable, and have been estimated to have a half-life of about one minute [55, 56]. However, treatment with quarfloxin for fifteen minutes did not result in a reduction in the levels of Pol II derived tubulin precursor transcript ( $129 \pm 10.3\%$  normal). Actin mRNA has been estimated to have a half-life of about 30 minutes in bloodstream form *T. brucei* [57]. We did not find that actin mRNA levels were affected by any of the inhibitors used in this study, and therefore the qPCR results were normalised using this transcript. These experiments therefore provide evidence for the selective inhibition of Pol I transcription in *T. brucei* with quarfloxin, which was highly significant (\*\* $P = <0.001$ ) in all cases.

Similar striking repression of Pol I transcription was observed after incubation of *T. brucei* with 1  $\mu$ M BMH-21 for fifteen minutes (\*\* $P = <0.001$ ) (Fig 4D). In addition, incubation with 1  $\mu$ M CX-5461 inhibitor for 15 minutes produced similar results to the other two inhibitors with specific knockdown of Pol I transcripts (\*\* $P = <0.001$  in all cases) (Fig 4E). To confirm that the selective reduction in Pol I derived precursor transcripts was not simply a consequence of cell lethality following treatment with the Pol I inhibitors, cells were treated for 15 minutes with 800 nM suramin (Fig 4F). Despite eventually causing cell death, this suramin treatment did not lead to reduced levels of any of these transcripts. In summary, these data show that incubation of *T. brucei* with all three Pol I inhibitors results in robust and rapid inhibition of Pol I transcription.

### Incubation with Pol I inhibitors leads to loss of the ESB and disassembly of the nucleolus

One of the hallmarks of blocking Pol I transcription is disassembly of the nucleolus as its integrity is dependent on rRNA synthesis [58]. We therefore monitored the disappearance of intact nucleoli as well as the ESB using immunofluorescence microscopy after incubation of *T. brucei* with the different Pol I inhibitors. The *T. brucei* RNA polymerase I complex contains at least twelve subunits, of which RPA2 is the second largest subunit [59, 60]. RPA2 has previously been endogenously tagged at the N-terminus with Yellow Fluorescence Protein (YFP) in



bloodstream form *T. brucei*, allowing visualisation of the Pol I complex in both the nucleolus and the ESB [42]. In these experiments the ESB was visible in  $67\% \pm 5\%$  of nonmitotic cells [42]. We generated *T. brucei* expressing YFP tagged RPA2 from the endogenous RPA2 locus in the bloodstream form of the parasite, as described previously by Daniels *et al* [42]. As expected, there was no growth reduction in these cell lines, and the YFP-RPA2 subunit showed the expected subnuclear location for a Pol I subunit.

Using the DNA stain DAPI, the *T. brucei* nucleus can be visualised as a large stained focus, with a smaller focus indicating the kinetoplast (mitochondrial) DNA. The Pol I subunit RPA2 was visualised using YFP fluorescence, and the location of the nucleolus was confirmed using the L1C6 nucleolar marker [47]. As expected, YFP-RPA2 was enriched in the nucleolus in all of the cells, and in a small extra-nucleolar ESB structure in  $64 \pm 17\%$  of the cells (Fig 5, Fig 6) as shown earlier [42]. We next investigated the effect of the Pol I inhibitors on the presence of the Pol I complex. As one of the hallmarks of blocking rRNA transcription is disintegration of the nucleolus [58], an antibody against the nucleolar marker protein L1C6 was used to visualise this. *T. brucei* cells in the G1 stage of the cell cycle have one nucleolus, and incubation of *T. brucei* with quarfloxin (3  $\mu$ M) resulted in disintegration of this nucleolus into multiple L1C6 containing spots. In addition, there was loss of Pol I signal from the ESB, as well as from the nucleolar remnants (Fig 5). Incubation with 3  $\mu$ M BMH-21 and CX-5461 also resulted in similar ESB loss and nucleolar disintegration (although not complete loss) in *T. brucei* (Fig 5). In contrast, incubation with lethal concentrations of the trypanocide suramin (800 nM) did not impact on distribution of Pol I or result in changes in ESB or nucleolar morphology.

We next quantitated the effect of different concentrations of quarfloxin on the presence of the ESB. Incubation with 300 nM quarfloxin for one hour resulted in a reduction in ESB positive cells from  $64 \pm 17\%$  to  $30.5 \pm 5\%$ , while in 1  $\mu$ M quarfloxin only  $7.5 \pm 0.7\%$  of the cells were ESB positive after one hour (Fig 6A). No cells contained an ESB after one hour of incubation with 3  $\mu$ M quarfloxin. A similar analysis was performed with BMH-21, where very similar results were obtained (Fig 6B). Incubation with a range of concentrations of CX-5461 also resulted in a time and dose dependent decrease in presence of the ESB (Fig 6C). We used suramin in order to establish that the observed loss of the ESB in these experiments was not simply a consequence of subnuclear architecture falling apart in dying cells. Suramin rapidly kills *T. brucei* at a concentration of 800 nM (Fig 2). After one to three hours incubation with 800 nM suramin, there was only a marginal reduction in ESB positive cells (Fig 6D).

Recently, the VEX1 protein has been discovered to play a role in ES regulation in bloodstream form *T. brucei*, although how this operates mechanistically remains unclear [43]. In bloodstream form *T. brucei* VEX1 associates with the ESB, serving as a marker for this subnuclear structure. We investigated the effect of incubation with Pol I transcription inhibitors on VEX1 localisation. We incubated bloodstream form *T. brucei*, which had an endogenous copy of VEX1 epitope tagged with myc, with 3  $\mu$ M quarfloxin, BMH-21 or CX-5461 (Fig 7). Similar to as observed with YFP tagged RPA2, VEX1 signal was drastically reduced after incubation of the cells with all three Pol I transcription inhibitors. In contrast, although incubation with the trypanocide suramin resulted in severe reduction in trypanosome growth no specific disintegration of the ESB was observed as visualised using epitope tagged VEX1 (Fig 7). These results support the observation that the ESB (as visualised using VEX1) is a transcription nucleated structure.

Similar to the Pol I ESB body, the structure of the Pol I nucleolar structures rapidly disintegrated (but did not disappear entirely) within one hour in cells incubated with these Pol I inhibitors. Incubation with 3  $\mu$ M quarfloxin, BMH-21 and CX-5461 universally resulted in nucleoli fragmenting into multiple foci as monitored using the nucleolar marker L1C6 (Fig 8). Again, incubation with suramin did not lead to significant changes in structure of the nucleoli.

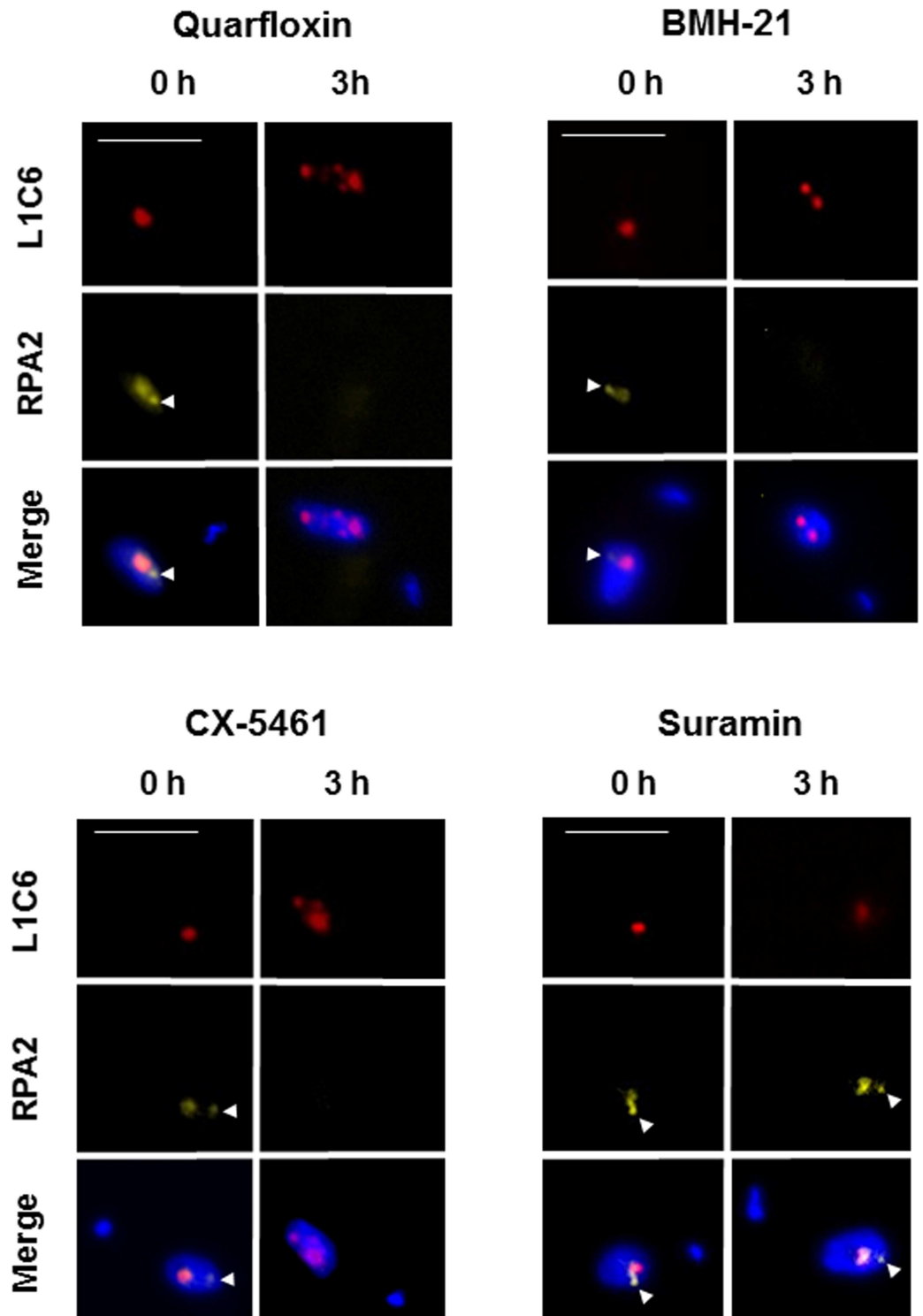


**Fig 5. Incubation of *T. brucei* with Pol I transcription inhibitors leads to rapid disappearance of the Pol I Expression Site Body (ESB) and fragmentation of the nucleolus.** Immunofluorescence analysis of *T. brucei* TY-YFP-RPA2 incubated with 3  $\mu$ M quarflorin, BMH-21, CX-5461 or 800nM suramin for three hours (h). The panels show representative *T. brucei* cells in the G1 cell cycle stage with DNA visualised with the DNA stain DAPI, and the nucleolus with the L1C6 nucleolar marker. The Pol I complex can be visualised using Yellow Fluorescence Protein



(YFP), as one allele of the RPA2 gene (second largest Pol I subunit) is epitope tagged. Signal corresponding to the extra-nucleolar ESB is indicated with a white arrow head. Scale bar indicates 5  $\mu$ m.

doi:10.1371/journal.pntd.0005432.g005

We do not know if these Pol I transcription inhibitors operate mechanistically in a similar fashion in *T. brucei* compared with mammalian cells. In the case of BMH-21, in human cells BMH-21 blocks Pol I transcription, resulting in degradation of the Pol I large subunit [37]. We investigated if incubation of *T. brucei* with increasing concentrations of BMH-21 resulted in similar degradation of the *T. brucei* RPA2 Pol I subunit. However even after incubation of *T. brucei* TY-YFP-RPA2 with 3  $\mu$ M BMH-21 for one hour, we did not see evidence for degradation of the RPA2 Pol I subunit (S4 Fig). As BMH-21 intercalates with DNA, it is possible that this DNA binding activity disrupts Pol I transcription in *T. brucei* in a different fashion to mammals.

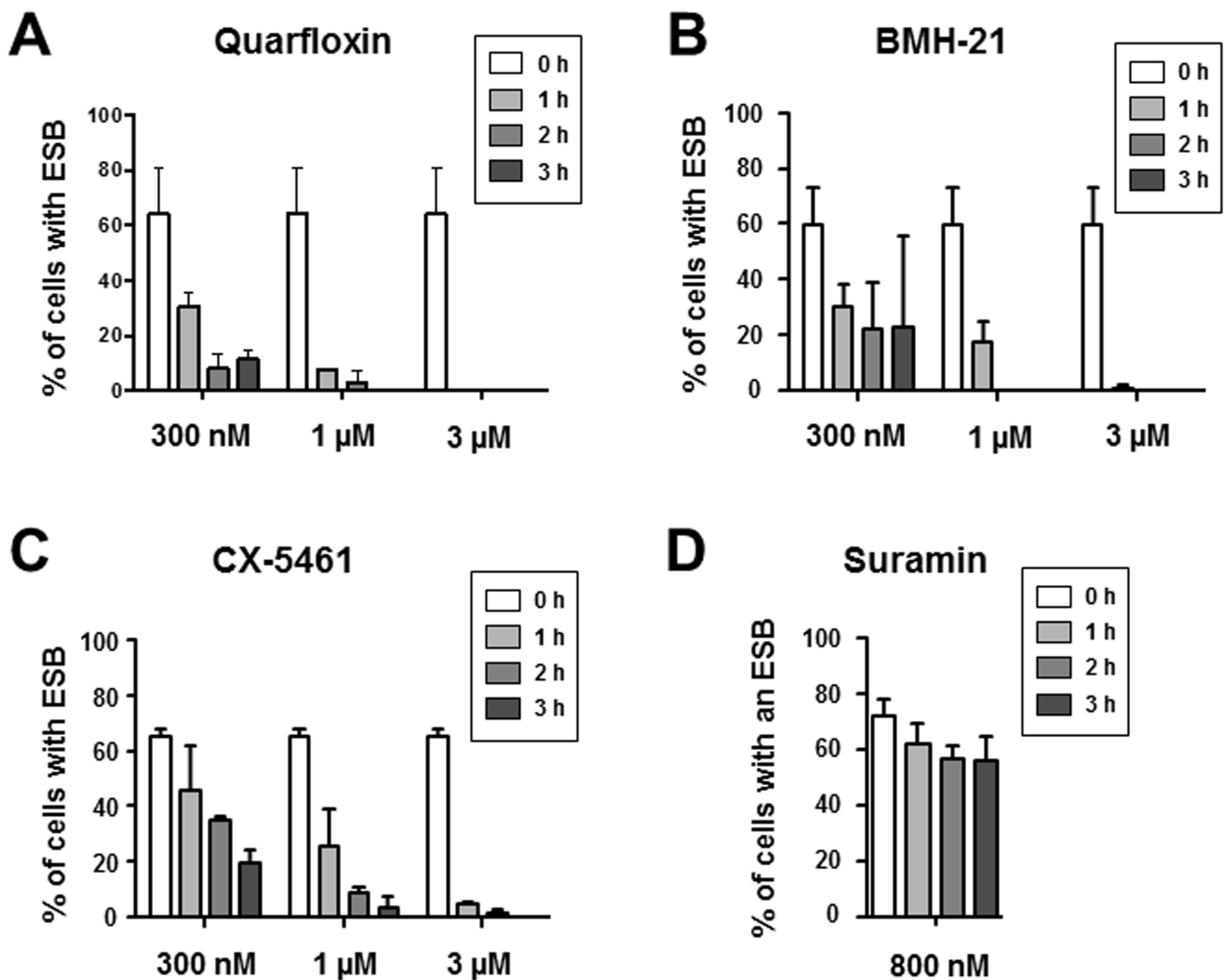


**Fig 6. Time dependent disappearance of the Pol I Expression Site Body (ESB) in *T. brucei* incubated with Pol I transcription inhibitors.** Quantitation of ESB presence in *T. brucei* cells in the G1 cell cycle stage incubated with various concentrations of quarfloxin (A), BMH-21 (B), CX-5461 (C) or 800 nM suramin (D). The percentage (%) of cells with an ESB after incubation for the time indicated in hours (h) is shown. A total of 100 cells (two biological replicates of ~50 cells) was analysed with the standard deviation indicated with error bars.

doi:10.1371/journal.pntd.0005432.g006

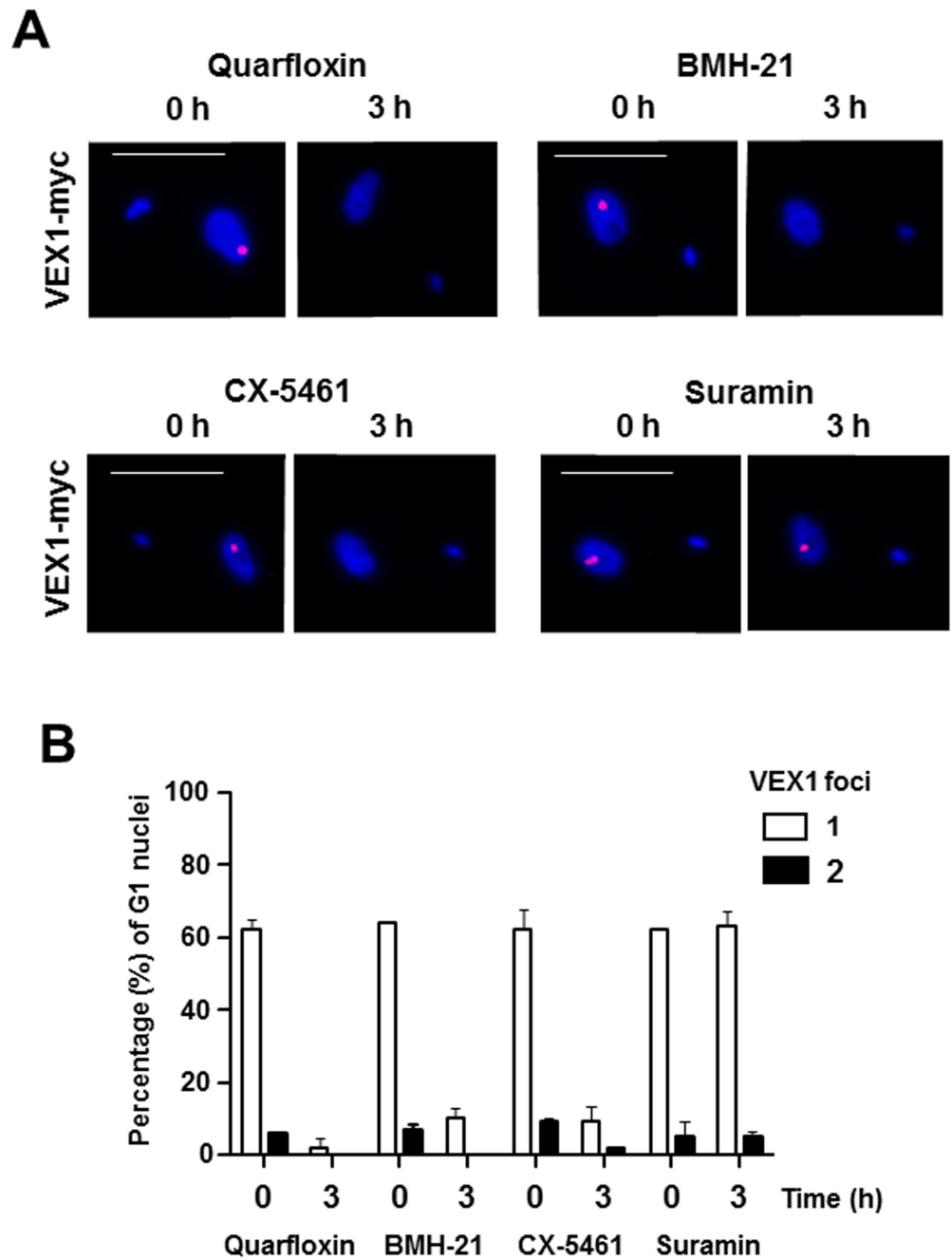


**Fig 7. Incubation of *T. brucei* with Pol I transcription inhibitors results in a dramatic decrease in VEX1 foci.** (A) Immunofluorescence analysis of *T. brucei* S16\_221PurVEX1x12myc incubated with 3  $\mu$ M quarflorin, BMH-21, CX-5461 or 800 nM suramin for three hours (h). The panels show representative cells in the G1 cell cycle stage. DNA is stained with DAPI and the myc-epitope tagged VEX1 protein visualised with an anti-myc antibody and Alexa954 secondary. Scale bar indicates 5  $\mu$ M. (B) Quantification of VEX1 foci present in nuclei of *T. brucei* in the G1 cell cycle stage (1K1N) at 0 hours or after a three hour incubation with 3  $\mu$ M quarflorin, BMH-21, CX-5461 or 800 nM suramin. The mean percentage (%) of G1 cells with either one or two VEX1 foci per nucleus (two biological replicates of 50 cells) is plotted with the standard deviation indicated with error bars.

doi:10.1371/journal.pntd.0005432.g007

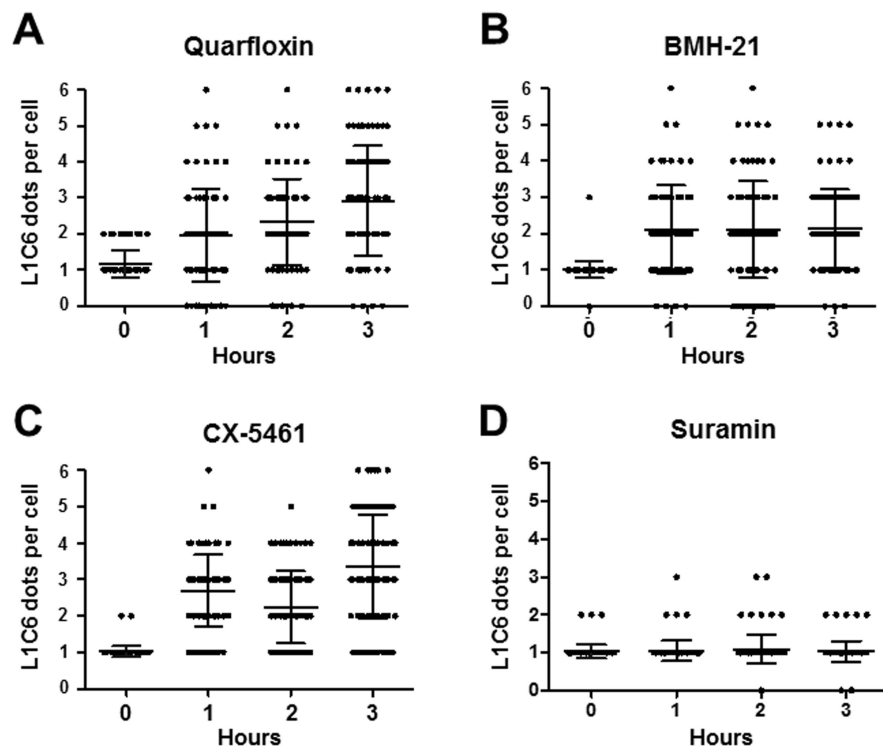


**Fig 8. Incubation of *T. brucei* with Pol I transcription inhibitors leads to rapid disintegration of nucleoli.** The nucleolus can be visualised with the L1C6 nucleolar marker as one spot in *T. brucei* in the G1 cell cycle stage. Nucleoli rapidly disintegrate into multiple L1C6 positive spots after incubation of cells with 3  $\mu$ M quarfloxin (A), BMH-21 (B), CX-5461 (C) or 800 nM suramin (D). Each dot indicates a cell, where the number of L1C6 positive spots is indicated. The mean indicated with a line, and standard deviation with error bars. A total of 100 cells was analysed (two biological replicates of ~50 cells).

doi:10.1371/journal.pntd.0005432.g008

Collectively, these data show that bloodstream form *T. brucei* is highly sensitive to Pol I inhibitors compared with the human host. Moreover, Pol I inhibitors rapidly and selectively inhibit Pol I transcription in *T. brucei*, leading to loss of the ESB and fragmentation of the nucleolus. Together, these experiments provide evidence that the ESB within *T. brucei* is fundamentally a Pol I transcription nucleated structure.

## Discussion

Rapidly proliferating cells require high levels of transcription of the Pol I transcribed rDNA, and chemical inhibitors of this Pol I transcription are effective against cancer [20, 21, 28, 33, 37]. Pol I not only transcribes the rDNA in bloodstream form *T. brucei*, but also the highly essential VSG gene. *T. brucei* is therefore particularly reliant on high levels of Pol I transcription, as even minor perturbations of VSG synthesis would be disastrous for parasite survival *in vivo* [27].

Here, we show that three established mammalian Pol I transcription inhibitors including CX-5461, quarfloxin and BMH-1 are selectively toxic for *T. brucei*. The most selective Pol I inhibitors against *T. brucei* are CX-5461 with an IC<sub>50</sub> of 279 nM and quarfloxin with an IC<sub>50</sub> of 155 nM. *T. brucei* is therefore 25–35 fold more susceptible to CX-5461 or 18–40 fold more susceptible to quarfloxin compared with the spontaneously immortalised MCF10A human breast epithelial cell line or the immortalised BJ3 human fibroblast cell line. This differential

sensitivity could potentially provide a “therapeutic window” to treat a human trypanosome infection using these compounds. Although in *T. brucei* BMH-21 has a lower IC<sub>50</sub> concentration (134 nM) compared with CX-5461 or quarfloxin, BMH-21 is also more toxic to human cells and there is only 3–10 fold selectivity for *T. brucei*. The selective toxicity of 25–35 fold for CX-5461 and 18–40 fold for quarfloxin in *T. brucei* compared with human cells meets DNDI criteria for drug screening for Kinetoplastid diseases where the minimum selectivity index is  $\geq 10$  (Ioset *et al* at: [www.dndi.org/2009/media-centre/scientific](http://www.dndi.org/2009/media-centre/scientific) articles). This makes Pol I inhibitors intriguing drug leads. However, further studies including structure-activity relationship (SAR) studies would clearly be required to optimise both their potency and their selectivity against *T. brucei*.

We show that all three Pol I inhibitors selectively and rapidly block Pol I transcription, with rRNA precursor transcripts in some cases reduced by 98%, and VSG expression site derived precursor transcripts reduced by 94%. In contrast, we saw no reduction in levels of precursor transcript from the Pol II transcribed tubulin transcription unit. Incubation of *T. brucei* with these three Pol I inhibitors lead to disappearance of Pol I signal within the nuclei within one hour. In addition, within one hour there was disappearance of the ESB (as visualised using RPA2 or VEX1) and rapid disintegration of the nucleolus, which shattered into small dots as visualised using an antibody for the nucleolar protein LIC6.

It has been demonstrated that nucleoli are ‘Pol I transcription-seeded’ structures which require active transcription for maintenance of their structure [58, 61]. This transcription needs to be specifically mediated by Pol I, as nucleoli do not form if rDNA is transcribed by Pol II [62]. The fact that the nucleoli in *T. brucei* rapidly disassemble after incubation of the cells with specific Pol I inhibitors, argues that nucleoli are also Pol I transcription-nucleated structures in African trypanosomes. As well as disintegration of the nucleoli, incubation with all three Pol I inhibitors also leads to a very striking and rapid disappearance of the ESB. After one hour incubation with 3  $\mu$ M BMH-21 or CX-5461, only  $1 \pm 1.4\%$  or  $4.5 \pm 0.7\%$  of the cells respectively still had an ESB. After a one hour incubation with 3  $\mu$ M quarfloxin, none of the cells had an ESB. Similar rapid disappearance of the ESB in the presence of Pol I inhibitors was observed if the ESB was visualised using VEX1. These results would therefore suggest that the *T. brucei* ESB similar to the nucleolus, requires active Pol I transcription for its maintenance.

The active VSG gene is transcribed at a high rate from a single active telomeric VSG expression site locus, allowing the cell to produce vast amounts of VSG transcript (approximately 10% total mRNA) from a single copy VSG gene. This highly efficient VSG transcription, as well as rapid processing of the abundant VSG mRNA is presumably facilitated by the presence of the VSG expression site within the ESB subnuclear structure. The ESB has been proposed to function as a specialised factory assembled on the active VSG expression site, containing high concentrations of Pol I transcription factors as well as the RNA processing machinery necessary for efficient expression of VSG [50].

It has been postulated that the ESB is a coherent architectural structure, rather than simply a consequence of resident Pol I on the active ES DNA. This is based on the observation that removal of the DNA in DNase I treated methanol fixed cells, still resulted in concentrated localisation of Pol I in an ESB [50]. However, a potential complication in interpreting these experiments could be a possible reduction in motility in Pol I and associated transcription complexes after the methanol precipitation needed for fixation, even in the absence of DNA. Is the ESB a ‘Pol I transcription-seeded’ structure as has been proposed for the nucleolus? Our results would agree with this, and suggest that the ESB is a subnuclear structure which is nucleated around sites of active Pol I transcription, as the ESB rapidly disappears after Pol I transcription is blocked.

The ESB shares some, but not all components with nucleoli. Key Pol I transcription factors including CITFA-7 and the architectural chromatin protein TDP are located in both Pol I subnuclear structures [53, 63]. However, other nucleolar components including fibrillarin as well as the L1C6 nucleolar protein are found in the nucleolus but not the ESB [47, 50]. The only factor that has yet been proposed to be ESB specific is VEX1, although its mode of action in VSG control is yet to be determined [43]. Our experiments using Pol I inhibitors show that these two types of Pol I transcription complexes at either the rDNA or the active ES are inhibited in a similar fashion, although there are clearly significant differences in their control.

It is striking that all three of these mammalian Pol I inhibitors appear to specifically inhibit Pol I transcription in *T. brucei* despite having differences in their modes of action in mammalian cells. BMH-21 is a DNA intercalator, which binds GC-rich sequences present at high frequency in ribosomal DNA genes [37, 64]. In human cells BMH-21 blocks Pol I transcription elongation, leading to proteasome dependent destruction of RPA194 (largest Pol I subunit), which is correlated with cancer cell killing [37]. In *T. brucei*, although there is also rapid disappearance of Pol I subnuclear structures like the nucleoli and the ESB after one hour incubation with 1  $\mu$ M BMH-21, we did not see evidence for significant reduction in levels of YFP2-RPA2 as monitored by Western blot analysis (S4 Fig). However, despite the presence of unreduced amounts of YFP-RPA2 protein, intercalation of BMH-21 with DNA could still potentially result in disassociation of Pol I complex from the DNA.

In mammalian cells, CX-5461 inhibits Pol I mediated initiation of transcription at the rDNA through interference of SL1 transcription factor binding to the rDNA promoter [33]. *T. brucei* does not have an obvious SL1 homologue, and it is still unclear which protein fulfils its function in trypanosomes. It is therefore, not straightforward to test if the mode of action of CX-5461 in *T. brucei* is indeed similar to that in mammalian cells. Quarfloxin is a fluoroquinolone which intercalates with DNA, and is thought to preferentially bind G-rich stretches forming G-quadruplexes within the rDNA and at telomeres [29, 30, 65]. Quarfloxin accumulates in the nucleoli, where it selectively interferes with rRNA synthesis at the level of Pol I elongation, leading to reduced levels of rRNA precursor transcript [28]. Although *T. brucei* rDNA has G-rich regions, it is unclear if these indeed form G-quadruplexes. *T. brucei* telomere repeats have the same sequence (GGGTTA) as those in mammalian cells, and could therefore also be expected to form G-quadruplex structures [65]. As well as interfering with Pol I transcription of the rDNA in *T. brucei*, it is possible that quarfloxin also interferes with telomere function as well. A similarity between BMH-21 and quarfloxin is that they intercalate with DNA, particularly in G-rich regions, and it is presumably this feature that is behind their efficacy in *T. brucei*. These Pol I inhibitors could therefore provide a new tool for specifically blocking Pol I transcription in African trypanosomes, which should help us dissect how the regulated Pol I mediated transcription of the VSG variant antigen genes is controlled.

Pol I inhibitors are currently being investigated for their suitability for treating cancer. The inhibitor quarfloxin progressed to Phase II clinical trials, but was withdrawn due to problems regarding bioavailability [31]. However, CX-5461 is still under investigation for cancer treatment, and is currently in Phase I clinical trials against breast cancer (Clinicaltrials.gov NCT02719977) and haematologic cancer (ACTRN12613001061729). Could these Pol I inhibitors indeed be used to treat human African trypanosomiasis? Pol I is of particular importance for bloodstream form *T. brucei* as very high levels of transcription of the single active VSG gene are essential to provide the huge amount of VSG protein required to coat this extracellular parasite. As blocking VSG synthesis results in very rapid parasite clearance in infected mice [27], we would predict that targeting VSG transcription should allow us to target this particularly vulnerable feature of the parasite. It is likely that even minor perturbation of VSG synthesis would result in rapid trypanosome

clearance *in vivo*. This could potentially allow the repurposing of a potential anti-cancer agent for treatment of a tropical parasite.

As clinical trials are the main cost in developing a pharmaceutical treatment, one could envisage that repurposing an existing drug could provide an economical means to increase the number of substances that can be used to treat trypanosomiasis [13, 14]. This is particularly an issue as the current relatively small number of annual human African trypanosomiasis cases make the cost of developing new drugs problematic. However, despite some of the complications that would need to be considered regarding potential toxicity of these compounds, our data indicate that these Pol I inhibitors could potentially function as new chemical weapons against human African trypanosomiasis.

## Supporting information

**S1 Fig. Dose response curves of MCH10A human breast epithelial cells incubated with Pol I transcription inhibitors.** (A-D) An Incucyte assay was used to determine dose response curves of MCF10A human breast epithelial cells incubated for 48 hours with a range of concentrations of Pol I transcription inhibitors or the trypanocidal agent Suramin. Dose response curves for quarfloxin (A), BMH-21 (B), CX-5461 (C) or suramin (D) are shown. The mean percentage (%) of cell confluence from three biological replicates is plotted, except in the case of BMH-21, where the results of two biological replicates are shown. The standard deviation is indicated with error bars. (E) Comparison of the IC50 values for Pol I transcription inhibitors determined using either an Incucyte cell confluence proliferation assay or a Resazurin based assay (Alamar Blue).

(TIF)

**S2 Fig. Dose response curves of immortalised BJ3 human foreskin fibroblasts incubated with Pol I transcription inhibitors.** (A-D) Dose response curves of human foreskin fibroblasts immortalised by the addition of h-Tert and incubated for 48 hours with various doses of (A) quarfloxin, (B) BMH-21, (C) CX-5461 or (D) suramin. The mean percentage (%) of cell confluence is plotted from five biological replicates with the standard deviation indicated with error bars. (E) Summary of IC50 values for growth inhibition (where the higher doses prevent cell growth) and the cell death (where the higher doses cause cell death) (n = 5, error bars represent standard deviation).

(TIF)

**S3 Fig. Representative images of Incucyte assay of immortalised BJ3 human fibroblasts treated with various Pol I inhibitors.** Cells were treated with various doses of quarfloxin, BMH-21, CX-5461 or suramin for 48 hours. Cells before treatment are shown (T = 0). Cells were imaged and cell confluence established using an IncuCyte ZOOM. Scale bars correspond to 100 μm.

(TIF)

**S4 Fig. Incubation of *T. brucei* with the Pol I transcription inhibitor BMH-21 does not lead to significant degradation of the RPA2 Pol I subunit.** (A) The *T. brucei* TY-YFP-RPA2 cell line was incubated with various concentrations of BMH-21 for the time indicated in hours. As a control, *T. brucei* was also incubated with 800 nM of suramin. Lysate from 1 x 10<sup>7</sup> cell equivalents was blotted and probed with anti-TY (BB2) antibody. A band corresponding to *T. brucei* RPA2 is shown, as well as a Ponceau S stain of the blot to serve as a loading control. Size markers in kiloDaltons (kDa) are indicated.

(TIF)

**S1 Table. List of the primers used in the qPCR experiments.** The gene location of the primers is shown, as well as the primer names and their DNA sequence (5'-3').  
(PDF)

## Acknowledgments

We are indebted to Prof. Piet Borst (Netherlands Cancer Institute, Amsterdam) for encouraging this investigation and for illuminating discussions and comments on the manuscript. We are grateful to Bill Wickstead (University of Nottingham, UK) for discussions, and Bill Wickstead, Steve Kelly (University of Oxford, UK) and Keith Gull (University of Oxford, UK) for the Pol I epitope tagging construct. We thank David Horn and Seb Hutchison (University of Dundee) for providing the VEX1 epitope tagging construct. We are grateful to Keith Gull and laboratory and Jay Bangs (SUNY Buffalo, US) for providing antibodies, and Jake Baum (Imperial College London, UK) for use of the fluorescence plate reader. We thank Cher-Pheng Ooi, Georgios Sioutas, Selina Fecht and Barnabas Hegedus for comments on the manuscript.

## Author Contributions

**Conceptualization:** LEK DPC RDH GR.

**Formal analysis:** LEK EEP DPC JB.

**Funding acquisition:** GR RDH.

**Investigation:** LEK EEP DPC JB GP KMH.

**Methodology:** JB DPC LEK.

**Project administration:** GR RDH.

**Resources:** DPC RDH.

**Supervision:** GR RDH.

**Visualization:** LEK EEP DPC JB GR.

**Writing – original draft:** GR LEK DPC RDH.

**Writing – review & editing:** GR LEK EEP DPC JB RDH.

## References

1. Welburn SC, Molyneux DH, Maudlin I. Beyond Tsetse - Implications for Research and Control of Human African Trypanosomiasis Epidemics. *Trends Parasitol.* 2016; 32(3):230–41. doi: [10.1016/j.pt.2015.11.008](https://doi.org/10.1016/j.pt.2015.11.008) PMID: [26826783](https://pubmed.ncbi.nlm.nih.gov/26826783/)
2. Franco JR, Simarro PP, Diarra A, Jannin JG. Epidemiology of human African trypanosomiasis. *Clinical epidemiology.* 2014; 6:257–75. PubMed Central PMCID: PMC4130665. doi: [10.2147/CLEP.S39728](https://doi.org/10.2147/CLEP.S39728) PMID: [25125985](https://pubmed.ncbi.nlm.nih.gov/25125985/)
3. Simarro PP, Cecchi G, Franco JR, Paone M, Diarra A, Priotto G, et al. Monitoring the Progress towards the Elimination of Gambiense Human African Trypanosomiasis. *PLoS neglected tropical diseases.* 2015; 9(6):e0003785. PubMed Central PMCID: PMC4461311. doi: [10.1371/journal.pntd.0003785](https://doi.org/10.1371/journal.pntd.0003785) PMID: [26056823](https://pubmed.ncbi.nlm.nih.gov/26056823/)
4. Glover L, Hutchinson S, Alsford S, McCulloch R, Field MC, Horn D. Antigenic variation in African trypanosomes: the importance of chromosomal and nuclear context in VSG expression control. *Cell Microbiol.* 2013; 15(12):1984–93. PubMed Central PMCID: PMC3963442. doi: [10.1111/cmi.12215](https://doi.org/10.1111/cmi.12215) PMID: [24047558](https://pubmed.ncbi.nlm.nih.gov/24047558/)
5. Taylor JE, Rudenko G. Switching trypanosome coats: what's in the wardrobe? *Trends Genet.* 2006; 22(11):614–20. doi: [10.1016/j.tig.2006.08.003](https://doi.org/10.1016/j.tig.2006.08.003) PMID: [16908087](https://pubmed.ncbi.nlm.nih.gov/16908087/)



6. McCulloch R, Morrison LJ, Hall JP. DNA Recombination Strategies During Antigenic Variation in the African Trypanosome. *Microbiol Spectr*. 2015; 3(2):MDNA3-0016-2014.
7. Jones AJ, Avery VM. Future treatment options for human African trypanosomiasis. *Expert Rev Anti Infect Ther*. 2015; 13(12):1429–32. doi: [10.1586/14787210.2015.1094374](https://doi.org/10.1586/14787210.2015.1094374) PMID: [26414688](https://pubmed.ncbi.nlm.nih.gov/26414688/)
8. Babokhov P, Sanyaolu AO, Oyibo WA, Fagbenro-Beyioku AF, Iriemenam NC. A current analysis of chemotherapy strategies for the treatment of human African trypanosomiasis. *Pathog Glob Health*. 2013; 107(5):242–52. PubMed Central PMCID: [PMCPMC4001453](https://pubmed.ncbi.nlm.nih.gov/PMC4001453/). doi: [10.1179/2047773213Y.000000105](https://doi.org/10.1179/2047773213Y.000000105) PMID: [23916333](https://pubmed.ncbi.nlm.nih.gov/23916333/)
9. Eperon G, Balasegaram M, Potet J, Mowbray C, Valverde O, Chappuis F. Treatment options for second-stage gambiense human African trypanosomiasis. *Expert Rev Anti Infect Ther*. 2014; 12(11):1407–17. PubMed Central PMCID: [PMCPMC4743611](https://pubmed.ncbi.nlm.nih.gov/PMC4743611/). doi: [10.1586/14787210.2014.959496](https://doi.org/10.1586/14787210.2014.959496) PMID: [25204360](https://pubmed.ncbi.nlm.nih.gov/25204360/)
10. Barrett MP, Vincent IM, Burchmore RJ, Kazibwe AJ, Matovu E. Drug resistance in human African trypanosomiasis. *Future Microbiol*. 2011; 6(9):1037–47. doi: [10.2217/fmb.11.88](https://doi.org/10.2217/fmb.11.88) PMID: [21958143](https://pubmed.ncbi.nlm.nih.gov/21958143/)
11. Alsford S, Kelly JM, Baker N, Horn D. Genetic dissection of drug resistance in trypanosomes. *Parasitology*. 2013; 140(12):1478–91. PubMed Central PMCID: [PMCPMC3759293](https://pubmed.ncbi.nlm.nih.gov/PMC3759293/). doi: [10.1017/S003118201300022X](https://doi.org/10.1017/S003118201300022X) PMID: [23552488](https://pubmed.ncbi.nlm.nih.gov/23552488/)
12. Andrews KT, Fisher G, Skinner-Adams TS. Drug repurposing and human parasitic protozoan diseases. *Int J Parasitol Drugs Drug Resist*. 2014; 4(2):95–111. PubMed Central PMCID: [PMCPMC4095053](https://pubmed.ncbi.nlm.nih.gov/PMC4095053/). doi: [10.1016/j.ijpddr.2014.02.002](https://doi.org/10.1016/j.ijpddr.2014.02.002) PMID: [25057459](https://pubmed.ncbi.nlm.nih.gov/25057459/)
13. Klug DM, Gelb MH, Pollastri MP. Repurposing strategies for tropical disease drug discovery. *Bioorg Med Chem Lett*. 2016; 26(11):2569–76. PubMed Central PMCID: [PMCPMC4853260](https://pubmed.ncbi.nlm.nih.gov/PMC4853260/). doi: [10.1016/j.bmcl.2016.03.103](https://doi.org/10.1016/j.bmcl.2016.03.103) PMID: [27080183](https://pubmed.ncbi.nlm.nih.gov/27080183/)
14. Pollastri MP, Campbell RK. Target repurposing for neglected diseases. *Future Med Chem*. 2011; 3(10):1307–15. PubMed Central PMCID: [PMCPMC3160716](https://pubmed.ncbi.nlm.nih.gov/PMC3160716/). doi: [10.4155/fmc.11.92](https://doi.org/10.4155/fmc.11.92) PMID: [21859304](https://pubmed.ncbi.nlm.nih.gov/21859304/)
15. Sekhar GN, Watson CP, Fidanboyu M, Sanderson L, Thomas SA. Delivery of antihuman African trypanosomiasis drugs across the blood-brain and blood-CSF barriers. *Adv Pharmacol*. 2014; 71:245–75. doi: [10.1016/bs.apha.2014.06.003](https://doi.org/10.1016/bs.apha.2014.06.003) PMID: [25307219](https://pubmed.ncbi.nlm.nih.gov/25307219/)
16. Miguel DC, Zauli-Nascimento RC, Yokoyama-Yasunaka JK, Katz S, Barbieri CL, Uliana SR. Tamoxifen as a potential antileishmanial agent: efficacy in the treatment of *Leishmania braziliensis* and *Leishmania chagasi* infections. *J Antimicrob Chemother*. 2009; 63(2):365–8. doi: [10.1093/jac/dkn509](https://doi.org/10.1093/jac/dkn509) PMID: [19095684](https://pubmed.ncbi.nlm.nih.gov/19095684/)
17. Coelho AC, Trinconi CT, Senra L, Yokoyama-Yasunaka JK, Uliana SR. *Leishmania* is not prone to develop resistance to tamoxifen. *Int J Parasitol Drugs Drug Resist*. 2015; 5(3):77–83. PubMed Central PMCID: [PMCPMC4486464](https://pubmed.ncbi.nlm.nih.gov/PMC4486464/). doi: [10.1016/j.ijpddr.2015.05.006](https://doi.org/10.1016/j.ijpddr.2015.05.006) PMID: [26150922](https://pubmed.ncbi.nlm.nih.gov/26150922/)
18. Amata E, Xi H, Colmenarejo G, Gonzalez-Diaz R, Cordon-Obras C, Berlanga M, et al. Identification of "Preferred" Human Kinase Inhibitors for Sleeping Sickness Lead Discovery. Are Some Kinases Better than Others for Inhibitor Repurposing? *ACS Infect Dis*. 2016; 2(3):180–6. PubMed Central PMCID: [PMCPMC4791575](https://pubmed.ncbi.nlm.nih.gov/PMC4791575/). doi: [10.1021/acsinfecdis.5b00136](https://doi.org/10.1021/acsinfecdis.5b00136) PMID: [26998514](https://pubmed.ncbi.nlm.nih.gov/26998514/)
19. Warner JR. The economics of ribosome biosynthesis in yeast. *Trends Biochem Sci*. 1999; 24(11):437–40. PMID: [10542411](https://pubmed.ncbi.nlm.nih.gov/10542411/)
20. Quin JE, Devlin JR, Cameron D, Hannan KM, Pearson RB, Hannan RD. Targeting the nucleolus for cancer intervention. *Biochim Biophys Acta*. 2014; 1842(6):802–16. doi: [10.1016/j.bbadis.2013.12.009](https://doi.org/10.1016/j.bbadis.2013.12.009) PMID: [24389329](https://pubmed.ncbi.nlm.nih.gov/24389329/)
21. Bywater MJ, Poortinga G, Sanij E, Hein N, Peck A, Cullinane C, et al. Inhibition of RNA polymerase I as a therapeutic strategy to promote cancer-specific activation of p53. *Cancer Cell*. 2012; 22(1):51–65. PubMed Central PMCID: [PMCPMC3749732](https://pubmed.ncbi.nlm.nih.gov/PMC3749732/). doi: [10.1016/j.ccr.2012.05.019](https://doi.org/10.1016/j.ccr.2012.05.019) PMID: [22789538](https://pubmed.ncbi.nlm.nih.gov/22789538/)
22. Quin J, Chan KT, Devlin JR, Cameron DP, Diesch J, Cullinane C, et al. Inhibition of RNA polymerase I transcription initiation by CX-5461 activates non-canonical ATM/ATR signaling. *Oncotarget*. 2016.
23. Hannan RD, Drygin D, Pearson RB. Targeting RNA polymerase I transcription and the nucleolus for cancer therapy. *Expert Opin Ther Targets*. 2013; 17(8):873–8. doi: [10.1517/14728222.2013.818658](https://doi.org/10.1517/14728222.2013.818658) PMID: [23862680](https://pubmed.ncbi.nlm.nih.gov/23862680/)
24. Drygin D, Rice WG, Grummt I. The RNA polymerase I transcription machinery: an emerging target for the treatment of cancer. *Annu Rev Pharmacol Toxicol*. 2010; 50:131–56. doi: [10.1146/annurev.pharmtox.010909.105844](https://doi.org/10.1146/annurev.pharmtox.010909.105844) PMID: [20055700](https://pubmed.ncbi.nlm.nih.gov/20055700/)
25. Kooter JM, van der Spek HJ, Wagter R, d'Oliveira CE, van der Hoeven F, Johnson PJ, et al. The anatomy and transcription of a telomeric expression site for variant-specific surface antigens in *T. brucei*. *Cell*. 1987; 51(2):261–72. PMID: [2444341](https://pubmed.ncbi.nlm.nih.gov/2444341/)



26. Gunzl A, Kirkham JK, Nguyen TN, Badjatia N, Park SH. Mono-allelic VSG expression by RNA polymerase I in *Trypanosoma brucei*: expression site control from both ends? *Gene*. 2015; 556(1):68–73. PubMed Central PMCID: PMC4272636. doi: [10.1016/j.gene.2014.09.047](https://doi.org/10.1016/j.gene.2014.09.047) PMID: [25261847](https://pubmed.ncbi.nlm.nih.gov/25261847/)
27. Sheader K, Vaughan S, Minchin J, Hughes K, Gull K, Rudenko G. Variant surface glycoprotein RNA interference triggers a precytokinesis cell cycle arrest in African trypanosomes. *Proc Natl Acad Sci U S A*. 2005; 102(24):8716–21. doi: [10.1073/pnas.0501886102](https://doi.org/10.1073/pnas.0501886102) PMID: [15937117](https://pubmed.ncbi.nlm.nih.gov/15937117/)
28. Drygin D, Siddiqui-Jain A, O'Brien S, Schwaebe M, Lin A, Bliesath J, et al. Anticancer activity of CX-3543: a direct inhibitor of rRNA biogenesis. *Cancer Res*. 2009; 69(19):7653–61. doi: [10.1158/0008-5472.CAN-09-1304](https://doi.org/10.1158/0008-5472.CAN-09-1304) PMID: [19738048](https://pubmed.ncbi.nlm.nih.gov/19738048/)
29. Brooks TA, Hurley LH. Targeting MYC Expression through G-Quadruplexes. *Genes Cancer*. 2010; 1(6):641–9. PubMed Central PMCID: PMCPCMC2992328. doi: [10.1177/1947601910377493](https://doi.org/10.1177/1947601910377493) PMID: [21113409](https://pubmed.ncbi.nlm.nih.gov/21113409/)
30. Bidzinska J, Cimino-Reale G, Zaffaroni N, Folini M. G-quadruplex structures in the human genome as novel therapeutic targets. *Molecules*. 2013; 18(10):12368–95. doi: [10.3390/molecules181012368](https://doi.org/10.3390/molecules181012368) PMID: [24108400](https://pubmed.ncbi.nlm.nih.gov/24108400/)
31. Balasubramanian S, Hurley LH, Neidle S. Targeting G-quadruplexes in gene promoters: a novel anticancer strategy? *Nat Rev Drug Discov*. 2011; 10(4):261–75. PubMed Central PMCID: PMCPCMC3119469. doi: [10.1038/nrd3428](https://doi.org/10.1038/nrd3428) PMID: [21455236](https://pubmed.ncbi.nlm.nih.gov/21455236/)
32. Haddach M, Schwaebe MK, Michaux J, Nagasawa J, O'Brien SE, Whitten JP, et al. Discovery of CX-5461, the First Direct and Selective Inhibitor of RNA Polymerase I, for Cancer Therapeutics. *ACS Med Chem Lett*. 2012; 3(7):602–6. PubMed Central PMCID: PMCPCMC4025669. doi: [10.1021/ml300110s](https://doi.org/10.1021/ml300110s) PMID: [24900516](https://pubmed.ncbi.nlm.nih.gov/24900516/)
33. Drygin D, Lin A, Bliesath J, Ho CB, O'Brien SE, Proffitt C, et al. Targeting RNA polymerase I with an oral small molecule CX-5461 inhibits ribosomal RNA synthesis and solid tumor growth. *Cancer Res*. 2011; 71(4):1418–30. doi: [10.1158/0008-5472.CAN-10-1728](https://doi.org/10.1158/0008-5472.CAN-10-1728) PMID: [21159662](https://pubmed.ncbi.nlm.nih.gov/21159662/)
34. Devlin JR, Hannan KM, Hein N, Cullinane C, Kusnadi E, Ng PY, et al. Combination Therapy Targeting Ribosome Biogenesis and mRNA Translation Synergistically Extends Survival in MYC-Driven Lymphoma. *Cancer Discov*. 2016; 6(1):59–70. doi: [10.1158/2159-8290.CD-14-0673](https://doi.org/10.1158/2159-8290.CD-14-0673) PMID: [26490423](https://pubmed.ncbi.nlm.nih.gov/26490423/)
35. Woods SJ, Hannan KM, Pearson RB, Hannan RD. The nucleolus as a fundamental regulator of the p53 response and a new target for cancer therapy. *Biochim Biophys Acta*. 2015; 1849(7):821–9. doi: [10.1016/j.bbagr.2014.10.007](https://doi.org/10.1016/j.bbagr.2014.10.007) PMID: [25464032](https://pubmed.ncbi.nlm.nih.gov/25464032/)
36. Peltonen K, Colis L, Liu H, Jaamaa S, Moore HM, Enback J, et al. Identification of novel p53 pathway activating small-molecule compounds reveals unexpected similarities with known therapeutic agents. *PLoS One*. 2010; 5(9):e12996. PubMed Central PMCID: PMCPCMC2946317. doi: [10.1371/journal.pone.0012996](https://doi.org/10.1371/journal.pone.0012996) PMID: [20885994](https://pubmed.ncbi.nlm.nih.gov/20885994/)
37. Peltonen K, Colis L, Liu H, Trivedi R, Moubarek MS, Moore HM, et al. A targeting modality for destruction of RNA polymerase I that possesses anticancer activity. *Cancer Cell*. 2014; 25(1):77–90. PubMed Central PMCID: PMCPCMC3930145. doi: [10.1016/j.ccr.2013.12.009](https://doi.org/10.1016/j.ccr.2013.12.009) PMID: [24434211](https://pubmed.ncbi.nlm.nih.gov/24434211/)
38. Stanne TM, Narayanan MS, Ridewood S, Ling A, Witmer K, Kushwaha M, et al. Identification of the ISWI Chromatin Remodeling Complex of the Early Branching Eukaryote *Trypanosoma brucei*. *J Biol Chem*. 2015; 290(45):26954–67. PubMed Central PMCID: PMCPCMC4646403. doi: [10.1074/jbc.M115.679019](https://doi.org/10.1074/jbc.M115.679019) PMID: [26378228](https://pubmed.ncbi.nlm.nih.gov/26378228/)
39. Wirtz E, Leal S, Ochatt C, Cross GA. A tightly regulated inducible expression system for conditional gene knock-outs and dominant-negative genetics in *Trypanosoma brucei*. *Mol Biochem Parasitol*. 1999; 99(1):89–101. PMID: [10215027](https://pubmed.ncbi.nlm.nih.gov/10215027/)
40. Sheader K, te Vrugte D, Rudenko G. Bloodstream form-specific up-regulation of silent vsg expression sites and procyclin in *Trypanosoma brucei* after inhibition of DNA synthesis or DNA damage. *J Biol Chem*. 2004; 279(14):13363–74. doi: [10.1074/jbc.M312307200](https://doi.org/10.1074/jbc.M312307200) PMID: [14726511](https://pubmed.ncbi.nlm.nih.gov/14726511/)
41. Povelones ML, Gluenz E, Dembek M, Gull K, Rudenko G. Histone H1 plays a role in heterochromatin formation and VSG expression site silencing in *Trypanosoma brucei*. *PLoS Pathog*. 2012; 8(11):e1003010. PubMed Central PMCID: PMC3486875. doi: [10.1371/journal.ppat.1003010](https://doi.org/10.1371/journal.ppat.1003010) PMID: [23133390](https://pubmed.ncbi.nlm.nih.gov/23133390/)
42. Daniels JP, Gull K, Wickstead B. The trypanosomatid-specific N terminus of RPA2 is required for RNA polymerase I assembly, localization, and function. *Eukaryot Cell*. 2012; 11(5):662–72. PubMed Central PMCID: PMCPCMC3346432. doi: [10.1128/EC.00036-12](https://doi.org/10.1128/EC.00036-12) PMID: [22389385](https://pubmed.ncbi.nlm.nih.gov/22389385/)
43. Glover L, Hutchinson S, Alford S, Horn D. VEX1 controls the allelic exclusion required for antigenic variation in trypanosomes. *Proc Natl Acad Sci U S A*. 2016; 113(26):7225–30. doi: [10.1073/pnas.1600344113](https://doi.org/10.1073/pnas.1600344113) PMID: [27226299](https://pubmed.ncbi.nlm.nih.gov/27226299/)

44. Raz B, Iten M, Grether-Buhler Y, Kaminsky R, Brun R. The Alamar Blue assay to determine drug sensitivity of African trypanosomes (*T. b. rhodesiense* and *T. b. gambiense*) in vitro. *Acta Trop.* 1997; 68(2):139–47. PMID: [9386789](#)
45. Soule HD, Maloney TM, Wolman SR, Peterson WD Jr., Brenz R, McGrath CM, et al. Isolation and characterization of a spontaneously immortalized human breast epithelial cell line, MCF-10. *Cancer Res.* 1990; 50(18):6075–86. PMID: [1975513](#)
46. Hahn WC, Counter CM, Lundberg AS, Beijersbergen RL, Brooks MW, Weinberg RA. Creation of human tumour cells with defined genetic elements. *Nature.* 1999; 400(6743):464–8. doi: [10.1038/22780](#) PMID: [10440377](#)
47. Devaux S, Kelly S, Lecordier L, Wickstead B, Perez-Morga D, Pays E, et al. Diversification of function by different isoforms of conventionally shared RNA polymerase subunits. *Mol Biol Cell.* 2007; 18(4):1293–301. PubMed Central PMCID: PMC1838988. doi: [10.1091/mbc.E06-09-0841](#) PMID: [17267688](#)
48. Gunzl A, Bruderer T, Laufer G, Schimanski B, Tu LC, Chung HM, et al. RNA polymerase I transcribes procyclin genes and variant surface glycoprotein gene expression sites in *Trypanosoma brucei*. *Eukaryot Cell.* 2003; 2(3):542–51. doi: [10.1128/EC.2.3.542-551.2003](#) PMID: [12796299](#)
49. Hertz-Fowler C, Figueiredo LM, Quail MA, Becker M, Jackson A, Bason N, et al. Telomeric expression sites are highly conserved in *Trypanosoma brucei*. *PLoS One.* 2008; 3(10):e3527. Epub 2008/10/28. PubMed Central PMCID: PMC2567434. doi: [10.1371/journal.pone.0003527](#) PMID: [18953401](#)
50. Navarro M, Gull K. A pol I transcriptional body associated with VSG mono-allelic expression in *Trypanosoma brucei*. *Nature.* 2001; 414(6865):759–63. doi: [10.1038/414759a](#) PMID: [11742402](#)
51. Gillingwater K, Kumar A, Ismail MA, Arafa RK, Stephens CE, Boykin DW, et al. In vitro activity and preliminary toxicity of various diamidine compounds against *Trypanosoma evansi*. *Vet Parasitol.* 2010; 169(3-4):264–72. doi: [10.1016/j.vetpar.2010.01.019](#) PMID: [20149544](#)
52. White TC, Rudenko G, Borst P. Three small RNAs within the 10 kb trypanosome rRNA transcription unit are analogous to domain VII of other eukaryotic 28S rRNAs. *NucleicAcidsRes.* 1986; 14(23):9471–89.
53. Narayanan MS, Rudenko G. TDP1 is an HMG chromatin protein facilitating RNA polymerase I transcription in African trypanosomes. *Nucleic Acids Res.* 2013; 41(5):2981–92. PubMed Central PMCID: PMC3597664. doi: [10.1093/nar/gks1469](#) PMID: [23361461](#)
54. Brogna S, McLeod T, Petric M. The Meaning of NMD: Translate or Perish. *Trends Genet.* 2016.
55. Imboden MA, Laird PW, Affolter M, Seebeck T. Transcription of the intergenic regions of the tubulin gene cluster of *Trypanosoma brucei*: evidence for a polycistronic transcription unit in a eukaryote. *Nucleic Acids Res.* 1987; 15(18):7357–68. PubMed Central PMCID: PMC306253. PMID: [3658696](#)
56. Ullu E, Matthews KR, Tschudi C. Temporal order of RNA-processing reactions in trypanosomes: rapid trans splicing precedes polyadenylation of newly synthesized tubulin transcripts. *Mol Cell Biol.* 1993; 13(1):720–5. PubMed Central PMCID: PMC358950. PMID: [8417363](#)
57. Li CH, Irmer H, Gudjonsdottir-Planck D, Freese S, Salm H, Haile S, et al. Roles of a *Trypanosoma brucei* 5'→3' exoribonuclease homolog in mRNA degradation. *RNA.* 2006; 12(12):2171–86. PubMed Central PMCID: PMC1664730. doi: [10.1261/rna.291506](#) PMID: [17077271](#)
58. Lam YW, Trinkle-Mulcahy L. New insights into nucleolar structure and function. *F1000Prime Rep.* 2015; 7:48. PubMed Central PMCID: PMC4447046. doi: [10.12703/P7-48](#) PMID: [26097721](#)
59. Schimanski B, Klumpp B, Laufer G, Marhofer RJ, Selzer PM, Gunzl A. The second largest subunit of *Trypanosoma brucei*'s multifunctional RNA polymerase I has a unique N-terminal extension domain. *Mol Biochem Parasitol.* 2003; 126(2):193–200. PMID: [12615318](#)
60. Nguyen TN, Schimanski B, Zahn A, Klumpp B, Gunzl A. Purification of an eight subunit RNA polymerase I complex in *Trypanosoma brucei*. *Mol Biochem Parasitol.* 2006; 149(1):27–37. doi: [10.1016/j.molbiopara.2006.02.023](#) PMID: [16730080](#)
61. Diesch J, Hannan RD, Sanij E. Perturbations at the ribosomal genes loci are at the centre of cellular dysfunction and human disease. *Cell Biosci.* 2014; 4:43. PubMed Central PMCID: PMC4422213. doi: [10.1186/2045-3701-4-43](#) PMID: [25949792](#)
62. Oakes M, Nogi Y, Clark MW, Nomura M. Structural alterations of the nucleolus in mutants of *Saccharomyces cerevisiae* defective in RNA polymerase I. *Mol Cell Biol.* 1993; 13(4):2441–55. PubMed Central PMCID: PMC359565. PMID: [8455621](#)
63. Nguyen TN, Muller LS, Park SH, Siegel TN, Gunzl A. Promoter occupancy of the basal class I transcription factor A differs strongly between active and silent VSG expression sites in *Trypanosoma brucei*. *Nucleic Acids Res.* 2014; 42(5):3164–76. PubMed Central PMCID: PMC3950698. doi: [10.1093/nar/gkt1301](#) PMID: [24353315](#)

64. Colis L, Peltonen K, Sirajuddin P, Liu H, Sanders S, Ernst G, et al. DNA intercalator BMH-21 inhibits RNA polymerase I independent of DNA damage response. *Oncotarget*. 2014; 5(12):4361–9. PubMed Central PMCID: PMC4147329. doi: [10.18632/oncotarget.2020](https://doi.org/10.18632/oncotarget.2020) PMID: [24952786](https://pubmed.ncbi.nlm.nih.gov/24952786/)
65. Duan W, Rangan A, Vankayalapati H, Kim MY, Zeng Q, Sun D, et al. Design and synthesis of fluoroquinophenoxazines that interact with human telomeric G-quadruplexes and their biological effects. *Mol Cancer Ther*. 2001; 1(2):103–20. PMID: [12467228](https://pubmed.ncbi.nlm.nih.gov/12467228/)